THE UNIVERSITY *of* EDINBURGH

An Investigation of Synaptic Dysfunction in Alzheimer's Disease

Rosemary Joan Jackson

The University of Edinburgh

2017

Declaration

I declare that this thesis has been composed by me, and that the work is either my own, or, where I have been a member of a research group, that I have made a substantial contribution to the work, such contribution being clearly indicated, and that the work has not been submitted for any other degree or professional qualification.

The work presented in Chapter 3 was previously published in The European Journal of Neuroscience as Human tau increases amyloid β plaque size but not amyloid β-mediated synapse loss in a novel mouse model of Alzheimer's disease by **Jackson RJ**, Rudinskiy N, Herrmann AG, Croft S, Kim JM, Petrova V, Ramos-Rodriguez JJ, Pitstick R, Wegmann S, Garcia-Alloza M, Carlson GA, Hyman BT, Spires-Jones TL. The first author is the student and author of the declaration and the primary supervisor is the last author. This study was conceived by all of the authors. My contribution involved the data collection and analysis of synapses by array tomography (Figures 5 and 6). I also contributed to Figure 3 by increasing the n for the neurite curvature experiments and performed the western blots for Figure 4. All other data was collected by the co-authors and analysed by me. The manuscript was written by me with input from co-authors most particularly Prof. Tara Spires-Jones.

14/12/17

Rosemary Joan Jackson Date

Acknowledgements

First and foremost, I would like to thank Tara for being a fantastic PhD supervisor, mentor, and role model. I appreciate the support, feedback, opportunities, and encouragement I have received throughout my PhD all delivered with a smile. I am particularly grateful for all the help and reassurance when experiments did not work and excitement and enthusiasm when they did. I hope you remain not only a colleague and mentor but also a friend.

Thank you to Ellie for always being there; they say that a journey is made better by the company you keep and I can't imagine a better partner in crime to have taken this journey with. Thank you to Abi for always making me laugh at myself and for reminding me that if you put rubbish in you will get rubbish out, which I believe was a life lesson as well as a proteomics one. Thank you to Chris for the innumerable things you have taught me, to Raphael for always being amused at my cheerful greetings, to Jamie for making three solid days of synaptoneurosome processing good fun, and to Jane for always being up for a chat. Thank you as well to all the students that have passed through the lab; Shaun, Monica, Vessy, Sanzi, Sadaf, Dimitri, Emily, Pooja, Maria, Leo, Will, Makis, Jackie, Anna, Sally, and Claudia. You've made the last three years great fun and very productive.

Thank you to the Wishart lab and the Chandran lab for being kind, patient, and great fun to work with and for teaching me the intricacies of proteomics and stem cell culture respectively. Thank you as well to Tom and Siddharthan themselves for being so welcoming and willing to help me out. Thank to my second supervisors Tilo and Ollie and my thesis committee chair Tom for all their input and help. Thank you must also go to the University of Edinburgh and the Edinburgh Global Fund for financially supporting this PhD.

Thank you to the members of 1 George square and HRB that made it such a fun place to work: Daisy, Antonis, Tizzy, Richard, Anna, Liv, Ros, Lisa and more. The intriguing and entertaining conversations we have shared have been a highlight and I will never forget the tiny tiny tent.

Thank you to my friends and family for listening, getting me outside when I needed it, and for reminding me that there is a life outside the lab. Thank you especially to Izzy and Bridget for putting up with me and for making me both jealous and proud of the lives you lead. I can't wait to see what you do next and am honoured to be your big sister.

Thank you to Daniel for being there through thick and thin, for celebrating the highs and supporting the lows, for keeping me sane and for making me many many cups of tea. Your unwavering support and encouragement is more than I deserve and I am so grateful for it. Thank you as well to Dan's family for being my home away from home and for making sure Daniel looked after me properly.

Finally, thank you to my parents for the enthusiasm for science, inspiration to pursue it, and the encouragement to continue when the going got tough. For all the advice you've given and all your support through out the years, I couldn't have done it without you both.

Abstract

Alzheimer's disease (AD) is characterized by the presence of aggregates of amyloid beta (Aβ) in senile plaques and tau in neurofibrillary tangles, as well as marked neuron and synapse loss. Of these pathological changes, synapse loss correlates most strongly with cognitive decline. Understanding the contributions of different risk factors, toxic proteins, and protein networks to synaptic dysfunction and loss is essential to understanding and one day curing this disease.

Oligomeric species of both Aβ and tau are implicated in synapse, however the interaction between them requires further exploration. The first aim of this thesis was to investigate the interaction of Aβ and tau in a novel mouse model AD. In this model APP/PS1 mice were crossed with mice expressing full length wild type human tau (hTau). Expression of hTau in APP/PS1 mice increased plaque size by~50% and increased plaque-associated dystrophic neurites. However, no increase in neurite curvature, neuron loss, or synapse loss was observed in the hTau APP/PS1 animals compared with APP/PS1 alone.

The underlying cause of most cases of AD is not known, however genetic risk factors have been identified, the strongest of which is the *APOE* ε4 allele. *APOE* ε4 is associated with increased risk of developing AD and increased rates of cognitive decline compared to the more common *APOE* ε3 allele. The second aim of this thesis was to detect differences in the AD synaptic proteome compared with controls and to also investigate the effect of an *APOE* ε4 allele on those changes. Unbiased label free LC-MS/MS based proteomics of synapses isolated from human AD and control post-mortem brains of known *APOE* genotypes was used. Of the 1043 proteins detected in 20 synaptic preparations 17% (173) were found to differ significantly ($p<0.05$, fold change >1.2) in AD compared with control. A significant sub-set of these proteins were affected by *APOE* ε4 allele genotype. One of these was Clusterin which was not only increased in the AD synapse but further increased in cases with an *APOE* ε4 allele. Clusterin is closely related to ApoE has also been genetically linked to AD in genome-wide association studies.

Aim three was to further investigate the involvement of Clusterin at the synapse and the interaction of ApoE with Clusterin using array tomography. Array tomography confirmed an increase in Clusterin co-localization with presynapses and postsynapses in AD cases compared with controls and found a further increase in cases with an *APOE* ε4 allele. Array tomography also found an increase in synapses which co-localized with Clusterin and Aβ together in cases with an *APOE* ε4 allele. This implies that Clusterin is important in Aβ mediated synapse loss in AD.

To further investigate the role of synapse loss in AD aim 4 of this thesis was to develop a novel human based model of Aβ mediated synapse loss. This model uses cortical neurons derived from induced pluripotent stem cells from a control individual that are challenged with Aβ extracted from brains from AD and control individuals. This model shows a significant and concentration dependent reduction in the number of synapses in response Aβ from AD brain but not to control brain extract or AD brain extract immunodepleted of Aβ.

The work presented in this thesis has investigated two novel models of AD to assess the effect of known toxic proteins in AD related synapse degeneration. This work also shows that profound protein changes occur at the synapse in AD and that many of these are affected by *APOE* genotype. Many of these changes potentially cause or contribute to synaptic dysfunction in AD and therefore could be important for therapeutic interventions.

Lay summary

Alzheimer's Disease (AD) is a neurodegenerative disease that is the most common cause of dementia in older people. It is currently one of the leading causes of death in the UK and current treatments only cause small improvement in some of the symptoms of disease but do not prevent the progression of dementia. Central to the loss of cognitive function in AD are the loss of synapses, the connections between neurons, which are known to be crucial for the making, losing, and keeping of memory. In this thesis I have used a number of methods to investigate the effects of AD on synaptic dysfunction and loss.

Using a high resolution microscopy technique I found that one of the proteins known to be toxic in AD, amyloid beta (Aβ), causes synapse loss in a mouse model but that the synapse loss is not affected by the presence of another of the toxic proteins in AD, tau.

To further understand what effect these toxic proteins were having at the synapse, I used the powerful technique of proteomics. This allowed me to investigate the effects of AD on the entire protein contents of synapses from brains donated by individuals with and without AD. I found that many proteins in the synapse were affected by AD and that many but not all of these proteins were involved in systems previously shown to be important in AD or in other neurodegenerative diseases. I also used proteomics to assess the impact that genetic risk factors played on the effect of AD on the synapse.

The greatest genetic risk factor for AD, *APOE* ε4, increases the risk of AD by 3 times if inherited from one parent and 12 times if inherited from both. The effect of *APOE* ε4 at synapses in AD is not yet fully understood. Here I have shown that *APOE* ε4 affects many of the protein changes that AD has on the synapse. I investigated one of these, Clusterin, by high resolution microscopy and found that it was increased in the synapse of AD cases and was frequently found in the same synapses as Aβ. This indicates that it plays a role in the effects of Aβ on the synapse. However, it is still

unknown what that role might be as reduction of Clusterin in a model of AD did not change synapse loss.

Here I have shown that AD causes many changes to the synapse many of which are important for the disease and some of which may be crucial in one day finding a cure for this disease.

Contents

List of Figures

List of Tables

List of Appendices

List of Abbreviations

2D	2 dimensional
3D	3 dimensional
3R	3 repeat
4R	4 repeat
ABCA1	ATP-binding cassette transporter A1
aCSF	Artificial cerebrospinal fluid
ACTS	Astrocytic component of a tripartite synapse
AD	Alzheimer's Disease
AICD	APP intracellular domain
AMPAR	α-amino-3-hydroxy-5-methyl-4-isoxazolepropionic acid receptor
ANXA1	Annexin A1
ANXA2	Annexin A2
ApoA1	Apolipoprotein A1
ApoE	The protein Apolipoprotein E
Apoe	The gene encoding for Apolipoprotein E (murine)
APOE	The gene encoding for Apolipoprotein E (human)
APOE e2	An APOE 2 allele
APOE e3	An APOE 3 allele
APOE e4	An APOE 4 allele
ApoE2	The protein encoded for by an APOE e2 allele
ApoE3	The protein encoded for by an APOE e4 allele
APOE3	Human Post-mortem cases which have a APOE 3/3 genotype
ApoE4	The protein encoded for by the APOE e3 allele
APOE4	Human Post-mortem cases which have a APOE 4/x genotype
ApoER2	Apolipoprotein E receptor 2
ApoJ	Apolipoprotein J
APP	Amyloid precusor protein
Arg	Arginine
Aβ	Amyloid beta
$A\beta_{40}$	Amyloid beta that is 40 amino acids long
$A\beta_{42}$	Amyloid beta that is 42 amino acids long
BBB	Blood Brain Barrier
BCA	Bicinchoninic acid
BDNF	Brain-derived neurotrophic factor
C_{13}	Carbon 13
Ca^{2+}	Calcium
CaMKII	Ca2+ /calmodulin-dependent protein kinase II
cAMP	Cyclic adenosine monophosphate
CAPNS1	calpain small subunit 1
Cb	Cerebellum
cGy	Cingulate gyrus
Clu	Clusterin
CNS	Central nervous system
CRISPR/CAS9	Clustered Regularly Interspaced Short Palindromic Repeats/CRISPR associated protein 9

CSF	Cerebrospinal fluid
Cys	Cysteine
DAVID	Database for Annotation, Visualization and Integrated Discovery
dH_2O	Deionized H2O
DLPC	Dorsolateral prefrontal cortex
DMEM	Dulbecco's Modified Eagle's medium
DMSO	Dimethyl sulfoxide
DNA	Deoxyribonucleic acid
DS	Down syndrome
DTT	Dithiothreitol
EAAT 1/2	Excitatory amino acid transporter 1/2
EC	Entorhinal Cortex
EDTA	Ethylenediaminetetraacetic acid
ELISA	Enzyme-linked immunosorbent assay
EM	Electron Microscopy
EOAD	Early onset Alzheimer's Disease
ER	Endoplasmic eticulum
ERK1/2	Extracellular signal–regulated kinases
ESI-QTOF-MS/MS	Electrospray ionisation and quadrupole time-of-flight tandem mass spectrometry
fAD	Familial Alzheimer's Disease
fCx	Frontal cortex
FGF2	Fibroblast growth factor 2
FLOT1	Flotillin 1
FLOT2	Flotillin 2
FTD	Frontotemporal dementia
GABA	γ–αμινοβυτψριχ αχιδ
$GABA_AR$	$GABA_A$ receptor
$GABA_BR$	$GABA_B$ receptors
GAPDH	Glyceraldehyde 3-phosphate dehydrogenase
GDNF	Glial cell-derived neurotrophic factor
Glu	Glutamic acid
GO	Gene ontology
GPCRs	G-protein coupled receptors
GSK-3β	Glycogen synthase kinase-3β
GWAS	Genome wide association studies
HDL	Higher density lipoproteins
HEPES	4-(2-hydroxyethyl)-1-piperazineethanesulfonic acid)
HLA	Human leukocyte antigen
HLA-A	Major histocompatibility complex class I A
HP	Hippocampus
HPLC	High-performance liquid chromatography
HRP	Horseradish peroxidase
HSP70	Heat shock protein 70
hTau	Human tau
ID	Immunodepletion
IgG	Immunoglobulin G

iGluR	Ionic glutamate receptors
IPA	Ingenuity Pathway Analysis
iPSC	Induced pluripotent stem cell
ITGAV	Integrin alpha V
iTRAQ	Isobaric tags for relative and absolute quantitation
KO	Knock out
L1CAM	L1 cell adhesion molecule
LC	Liquid chromatography
LC-MS	Liquid chromatography–mass spectrometry
LC-MS/MS	Liquid chromatography–tandem mass spectrometry
LDL	Lower density lipoproteins
LDLR	Low-density lipoprotein receptor family
LOAD	Load onset Alzheimer's Disease
LRP1	Lipoprotein receptor-related protein 1
LTD	Long term depression
LTP	Long term potentiation
MALDI TOF	Matrix-assisted laser desorption/ionization time-of-flight
MAP2	Microtubule-associated protein 2
MCI	Mild Cognitive Impairment
mGluR	Metabotropic glutamate receptors
MID	Mock immunodepletion
MRC BBN	Medical research council brain bank number
NDC	Non-demented Control
NFT	Neurofibrillary tangles
NMDAR	N-methyl-D-aspartate receptor
NMDAR2B	N-methyl D- aspartate receptor subtype 2B
NPC	Neuronal precursor cells
O_{18}	Oxygen 18
oAβ	oligomeric Amyloid Beta
OC	Old controls
PB	Phosphate buffer
PBS	Phosphate buffered saline
PCR	Polymerase chain reaction
pCx	Parietal cortex
PICK1	Protein Interacting with C Kinase - 1
PITRM1	Pitrilysin metallopeptidase 1
PLA2G16	Phospholipase A2 group XVI
PLC	phospholipase C
PLCL1	Phospholipase C
PP1	Protein phosphatase 1
PrA	Protein A
PrPc	Cellular prion protein
PS1	Presenillin 1
PS2	Presenillin 2
PSAP	Prosaposin
PSD	Postsynaptic density
PSD95	Postsynaptic density protein 95

RNA	Ribonucleic acid
sAD	Sporadic Alzheimer's Disease
sCx	Sensorimotor cortex
SDS	Sodium dodecyl sulfate
SDS-PAGE	Sodium dodecyl sulfate polyacrylamide gel electrophoresis
SEPT10	Septin 10
SEPT2	Septin 2
SEPT7	Septin 7
siRNA	Small interfering RNA
SN	Substania Nigra
SNAP-25	Synaptosomal-associated protein 25
SNARE	Soluble NSF attachment protein receptor
SP	Senile plaques
TBE	Tris/Borate/EDTA
TBS	Tris buffered saline
tCx	Temporal cortex
Tg	Transgenic
TMB	3,3’,5,5’-Tetramethylbenzidine
TREM2	Triggering receptor expressed on myeloid cells 2
Tris-HCl	2-Amino-2-(hydroxymethyl)-1,3-propanediol hydrochloride
UV	Ultraviolet
VAMP-1/-2	Vesicle-associated membrane protein 1/2
vGAT	Vesicular GABA transporter
VGLUT	Vesicular glutamate transporter
VLDL	Very low-density lipoprotein
VLDLR	Low-density lipoprotein receptors
YC	Young controls
α7nAChR	α7-nicotinic acetylcholine receptor

1 Introduction

1.1 Alzheimer's Disease

Dementia describes a state of progressive cognitive decline, which often manifests itself as memory loss, difficulty concentrating, and problems with visuospatial skills, among other signs and symptoms. Alzheimer's disease (AD) is currently the most common cause of dementia which affects an estimated 850,000 people in the UK alone (Prince *et al.*, 2015; Dementia Statistics Hub, 2017) (Figure 1.1A). The greatest risk factor for AD is age, with the risk of developing AD doubling every 5 years after an individual turns 65. This is especially worrying as the average life expectancy of both the UK and the world is rising and it is predicted that if the incidence of AD continues to rise at its current rate the number of affected individuals in the UK will increase to 1 million by 2025 (Alzheimer's Association 2014) (Figure 1.1C). This is compounded by the fact that there are currently no disease modifying treatments for AD, making AD the only condition in the top 10 causes of death in the UK without a treatment to slow or prevent progression (Dementia Statistics Hub, 2017). The current financial burden of dementia in the UK is £26.3 billion with almost half of this cost provided by family and friends who also shoulder an enormous responsibility of care and the stress that goes along with it. Unfortunately, these numbers are only expected to increase, however treatment which could delay the onset or reduce progression of AD would have an enormous impact both on the financial burden of AD but also on the quality of life for both affected individuals and carers (Dementia Statistics Hub, 2017) (Figure 1.1B).

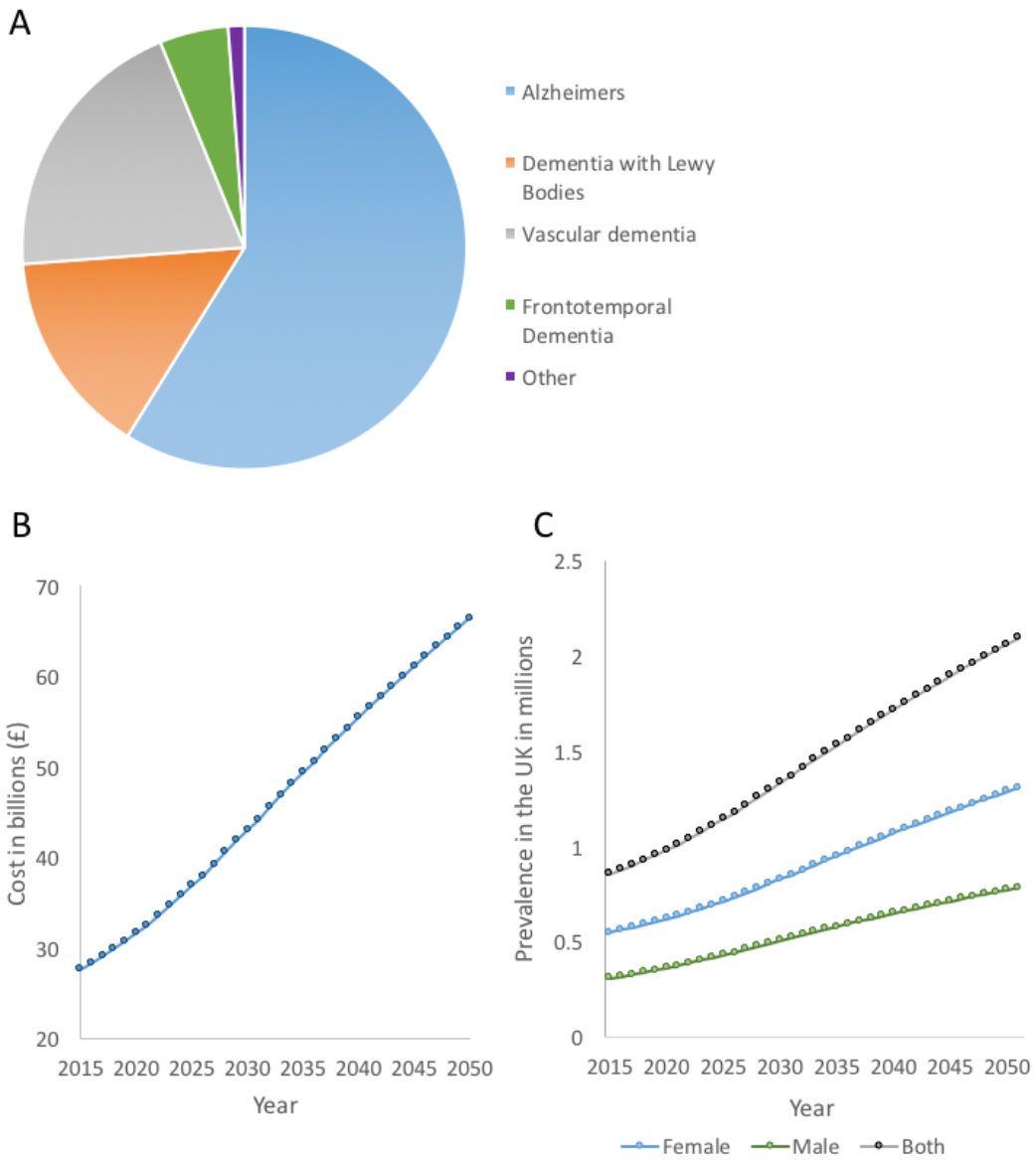

Figure 1.1: The effect and projected effect of AD within the UK population. AD makes up about 2/3rds of dementia diagnoses (A) which currently costs the UK economy £26 billion (B) due to a prevalence of about 850,000 which disproportionately effects females (C). Unfortunately both of these numbers are expected to rise in the coming years due in part to the increased life expectancy among other reasons. Source: (Dementia Statistics Hub, 2017).

Alzheimer's disease was first described over 100 years ago by Alois Alzheimer. It is characterized in part by the occurrence of senile plaques (SP) which are extracellular deposits made of misfolded and aggregated forms of amyloid beta (Aβ) (Alzheimer *et al.*, 1907, 1995). Alzheimer also described intracellular deposits termed neurofibrillary tangles (NFTs) that are made of hyperphosphorylated and aggregated tau. Both of

these aggregates can be stained using a silver stain or thioflavin S and Alzheimer noted how these silver stained deposits appeared to correlate with neuron death. He commented that cells with only one or two fibrils appeared normal but cells with large "tangles" appeared to be dead or dying (Alzheimer *et al.*, 1907). It is now well established that NFTs and Aβ plaques appear not only in individuals with Alzheimer's disease but also in the brains of most cognitively normal elderly people, however the degree to which they occur is often much less (Spires-Jones *et al.*, 2017).

The brains of AD patients also show brain atrophy particularly in the cerebral cortex and the hippocampus due to neuron loss that is, in part, associated with these misfolded proteins (Alzheimer *et al.*, 1907; Perl, 2010). More recently it has been shown that synapses are heavily affected in Alzheimer's disease with some cases showing a loss of 45% of synaptic elements. This is of great importance as it is the loss of synapses that provides the strongest pathological correlate to cognitive ability, with plaques exhibiting only a weak correlation and tangles and neuron loss a stronger correlation (Masliah *et al.*, 1989; Terry *et al.*, 1991). Although Alzheimer's disease was first described 110 years ago the complexity of both the disease and the brain mean that we are only now beginning to understand some of the interactions between the genetic, epigenetic, and lifestyle factors that influence the disease and we of course still have much to learn.

1.1.1 Amyloid Beta and the Amyloid Cascade Hypothesis

The senile plaques observed by Alzheimer in 1907 were found to be comprised of Aβ in the 1980s (Glenner and Wong, 1984; Allsop *et al.*, 1986). Aβ is produced when the amyloid precursor protein (APP) is cleaved first by β-secretase and then by γ-secretase to generate an internal fragment (APP intracellular domain) and a small ~39-43 amino acid long molecule (Aβ), which oligomerizes and eventually forms aggregates of β-pleated sheets (Sun *et al.*, 2015) (Figure 1.2). Although all isoforms of Aβ are produced in the healthy brain the major isoform of Aβ produced by this sequential cleavage is $A\beta_{40}$ and in the Alzheimer's brain, $A\beta_{42}$ is more abundant. All forms of Aβ

aggregate, however $A\beta_{42}$ is more insoluble and is more prone to aggregation than $A\beta_{40}$ due to its slightly longer hydrophobic carboxyl terminus (Burdick *et al.*, 1992). It is predominantly $A\beta_{42}$ that accumulates into plaques in the AD brain and it is thought that other isoforms of Aβ including $A\beta_{40}$ may even be protective against AD by preventing the accumulation of $A\beta_{42}$ (Kim *et al.*, 2007). APP can also be cleaved by α-secretase which cleaves the APP molecule in the middle of the Aβ domain and thus produces non-amyloidogenic fragments (Gandy *et al.*, 1994). Evidence suggests that in development, APP plays an important role in neurite outgrowth and synapse formation and later in life it regulates synaptic function by regulating synaptic structure and acting as a cell adhesion molecule (Soldano and Hassan, 2014; Montagna *et al.*, 2017)

Aβ has been well studied throughout the history of Alzheimer's research in particular due to its genetic link with the disease and its proposed place as the initiating factor of AD. Although mutations in both tau and Aβ are associated with dementia, tau related mutations have been found to cause rare familial forms of Frontotemporal Dementia (FTD), while Aβ related mutations have been found to cause very rare forms of familial AD (fAD) (Goedert and Jakes, 2005; Sun *et al.*, 2015). Most AD cases are sporadic (sAD), in that they occur in the absence of disease causing genetic mutations, yet the rare genetic forms have the same signature plaques and tangles. The age of onset of fAD is often less than 60 years of age placing most familial cases of AD in the bracket of Early Onset Alzheimer's Disease (EOAD). EOAD is very rare and is mainly associated of fAD while over 95% of AD cases fall into the alternative bracket, Late Onset Alzheimer's Disease (LOAD) which is associated mainly with sAD (Tanzi, 2012).

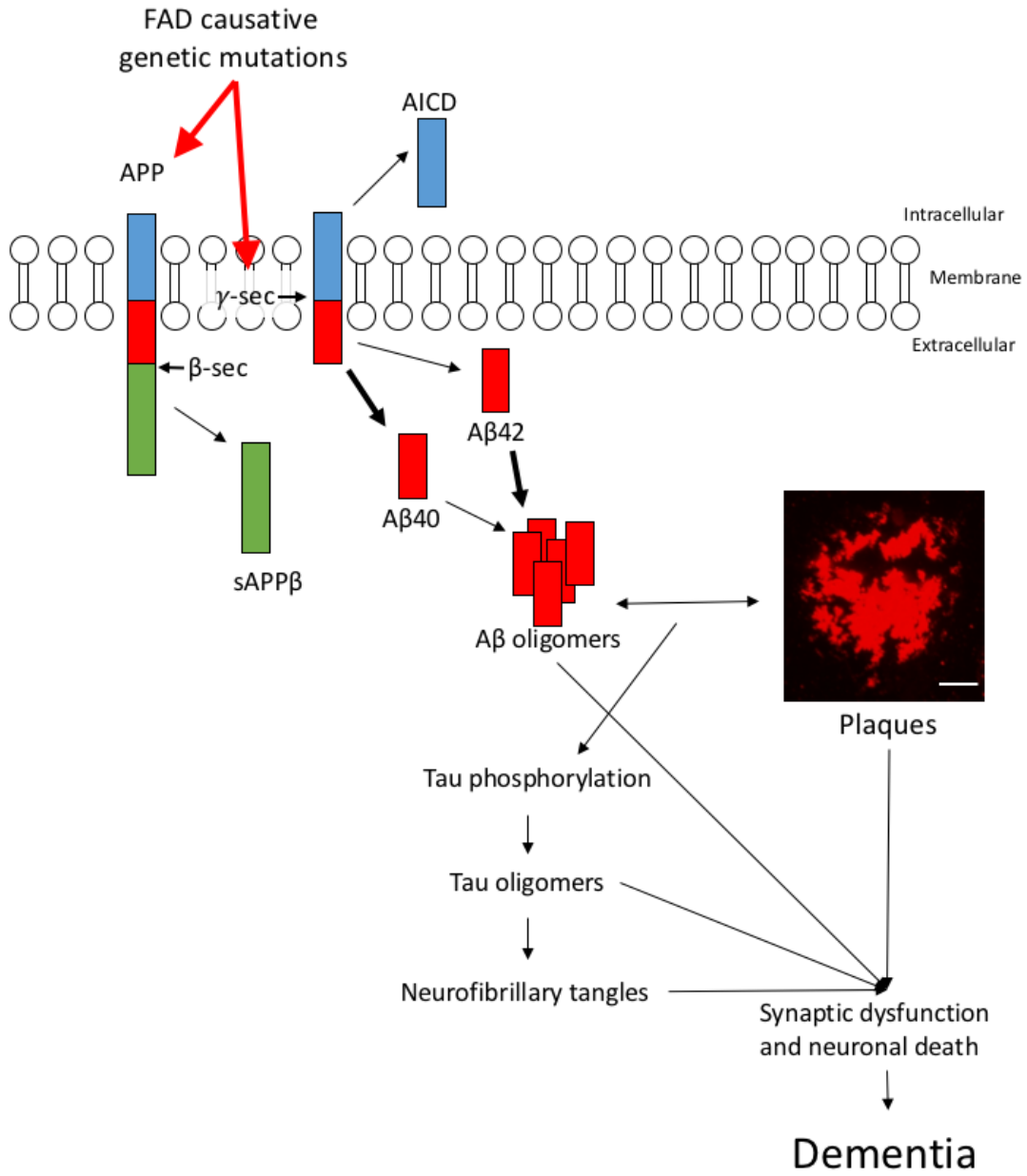

Figure 1.2: Amyloid processing and the amyloid cascade hypothesis. APP is cleaved by β-secretase and γ-secretase to form sAPPβ, Aβ, and an APP intracellular domain (AICD). In the healthy brain $A\beta_{40}$ is the most commonly produced form of Aβ but $A\beta_{42}$ is also produced. Aβ aggregates into oligomers with $A\beta_{42}$ more likely to aggregate than $A\beta_{40}$. The amyloid cascade hypothesis is that these oligomers form fibrils and then plaques which cause the other pathological hallmarks of disease including tau phosphorylation and aggregation, synaptic dysfunction and neuronal death. Scale bar 5μm.

Aβ related mutations almost all either increase the ratio of $A\beta_{42}$:$A\beta_{40}$ or the total amount of Aβ present in the brain but they are found in number of different genes and thus affect the production of Aβ in different ways. Many of the fAD mutations found in APP promote the generation of Aβ by favouring proteolysis by β or γ secretases however there are also mutations internal to the Aβ sequence which increase the propensity of Aβ to aggregate (Tanzi, 2012). Trisomy 21, also known as Down syndrome, causes an extra copy of the APP gene and individuals with Down syndrome get AD if they live past 50 years of age(Tyrrell *et al.*, 2001). Mutations in APP that protect against AD by reducing the level of β-secretase cleavage have been found and these also protect against normal cognitive aging proposing a link between Aβ and cognitive decline even in the absence of AD (Jonsson *et al.*, 2012). There are also mutations that have been found in the presenilin proteins 1 and 2 (PS1, PS2). The presenilin proteins act as the catalytic component of γ-secretase, and mutations in the presenilins increase the production of $A\beta_{42}$ (Bertram and Tanzi, 2008). As fAD recapitulates all of the neuropathological hallmarks of the more common sAD it is these mutations in APP, PS1, and PS2 that many of our Alzheimer's model organisms are based on.

However, in recent years the evidence for the amyloid cascade hypothesis has been questioned. Despite senile or neuritic plaques being one of the most characteristic hallmarks of Alzheimers Disease, the number of plaques correlates poorly with the speed and severity of cognitive decline (Giannakopoulos *et al.*, 2003). Indeed a growing cohort of individuals with a large number of plaque deposits post-mortem but no cognitive deficit in life are evidence against the amyloid cascade hypothesis (Perez-Nievas *et al.*, 2013). The failure of a number of high cost, high profile drug trials which targeted and reduced Aβ and Aβ plaque deposition in the brain have similarly called into question the validity of the amyloid cascade hypothesis (Small and Duff, 2008). These trials also call into question the usefulness of many of the current AD animal models in which these drugs worked very well. Proponents of the amyloid hypothesis will pertinently point out that it is possible that these therapeutics were administered too late in the course of the disease to have any therapeutic benefit or did not effectively engage their intended targets at the

concentrations administered, and clinical trials are currently underway to assess the validity of this statement (Karran *et al.*, 2011). It is also worth noting that, more recently it has been postulated that the main target of therapeutics should be the oligomeric forms of Aβ as these have been found to be the most toxic forms of the molecule, although there is still some debate as to which species of oligomer is most toxic(Mably *et al.*, 2015).

It is obvious however that AD is more complicated than the amyloid cascade hypothesis can effectively display. That despite over 20 years of Aβ directed research no effective therapeutics have been found is evidence that researchers are only beginning to understand certain elements of this heterogeneous and multifaceted disease. It is now essential that researchers begin to focus their attentions on alternative theories and targets while not undermining the clearly important role that Aβ plays in this disease.

1.1.2 The role of Tau in disease pathogenesis

In contrast to Aβ, the genetic evidence linking tau to AD is much less compelling as dementia causing mutations in tau cause FTD, although genetic risk factors for AD have been found in tau (Coppola *et al.*, 2012; Pastor *et al.*, 2015). However, NFTs made up of hyperphosphorylated and misfolded tau, correlate better with the cognitive decline seen in AD than Aβ plaques (Giannakopoulos *et al.*, 2003). NFTs are associated with neuron loss and there is strong evidence that some neurons with tangles in them die over the course of the disease, although tangle formation is clearly not required for neuron loss. Much like with Aβ, there is now a growing base of evidence that argues that it is the soluble oligomeric forms of tau that are toxic to the neurons and synapses rather than NFTs themselves (Kopeikina *et al.*, 2012). It is proposed by some that the phosphorylation and aggregation of tau is downstream of Aβ aggregation while others propose that tau aggregation and Aβ aggregation occur concurrently causing disease (Small and Duff, 2008). Indeed research using both mouse models and human imaging

studies indicate that Aβ and tau pathologies are not only linked but are dependent on one another (Pooler *et al.*, 2015; Sepulcre *et al.*, 2016).

Tau pathology and the deposition of NFTs follows a very defined path through the brain. In 1991 Braak and Braak described the extent of tangle deposition using six stages which define the extent and location of NFTs (Braak and Braak, 1991). The early stages describe a brain with some tangles found in the transentorhinal (stage I) and entorhinal cortex (EC) (stage II). Most individuals to reach 50 years of age will have some tangles in these two areas making most elderly people at least stage I. Stages III and IV see tangle deposition in limbic areas of the brain including the hippocampus as well as an increase in the deposition of tangles in the transentorhinal and entorhinal cortex. Often times individuals with a Braak stage III or IV will present with Mild Cognitive Impairment (MCI) or even mild AD in life. Stages V and VI are considered, neuropathologically, to be full AD when Aβ plaques are also present. They are characterized as an increase in tangles in all previously affected areas as well as tangle deposition in the neocortex (Braak and Braak, 1995). Braak staging correlates very well with an individuals' cognitive ability in life.

In the 1960s it was discovered that the NFTs discovered by Alzheimer in 1907 were made up of abnormal filaments termed paired helical filaments and straight filaments (Kidd, 1963). This was followed in 1986 by the discovery that these filaments were made up a heavily phosphorylated form of the microtubule associated protein tau (Grundke-Iqbal *et al.*, 1986). This discovery began a flurry of research into both the physiological and pathological roles of tau not only in AD, but in a wide range of neurodegenerative disorders including FTD, amyotrophic lateral sclerosis, and Pick's disease.

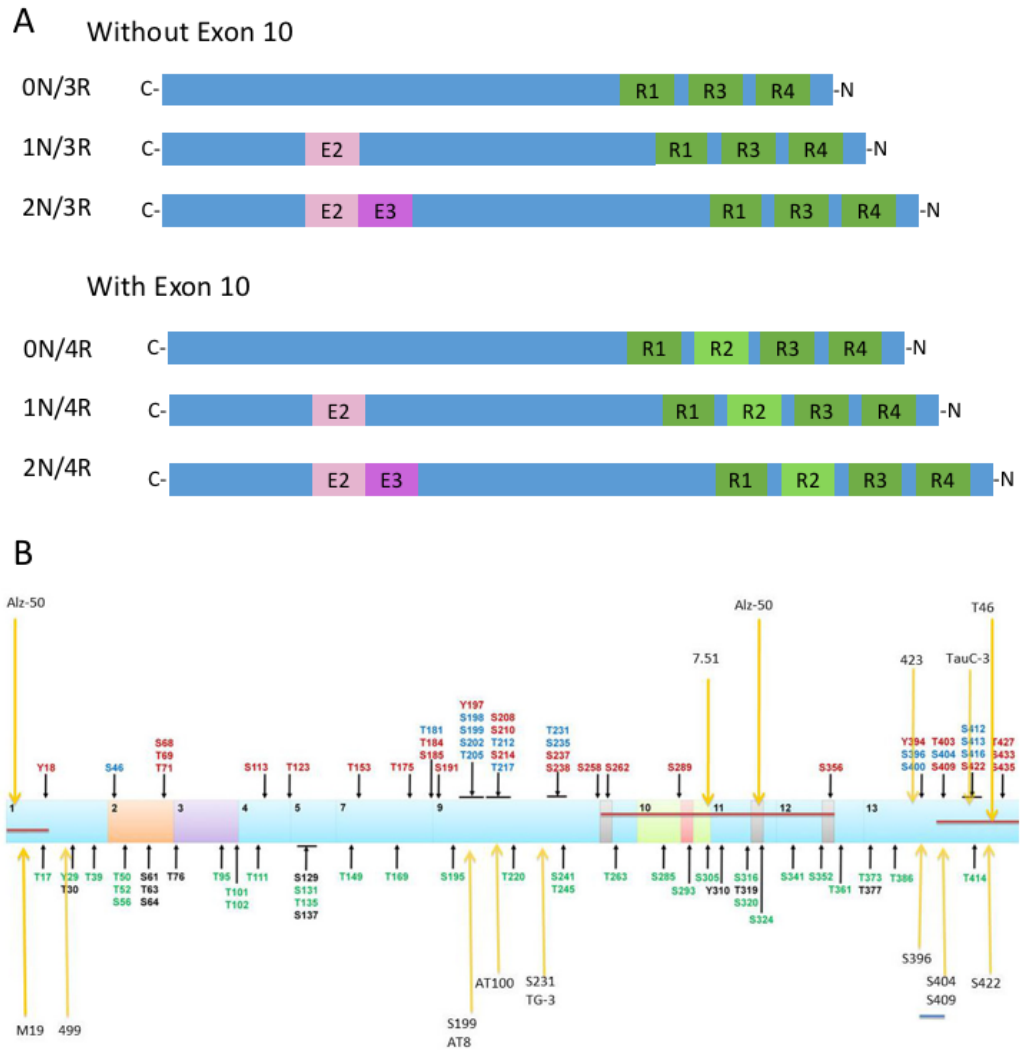

Figure 1.3: The isoforms and phosphorylation sites of tau. Tau has six isoforms in the human brain due to the inclusion or exclusion of exons 2, 3, and 10. Inclusion of exon 10 results in the inclusion of another microtubule binding motif (R2) (A). Tau can be phosphorylated at a number of sites some of which are found more commonly in the healthy brain (green) and others more commonly in AD (red). Residues found phosphorylated are colored in blue and putative sites of phosphorylation for which there is no experimental evidence are in black. Yellow arrows are the epitopes recognized by phosphorylation specific antibodies and residues are numbered according to 2N/4R tau (B). B is taken from (Luna-Munoz *et al.*, 2013) and is reproduced under CC BY 3.0 license.

Tau had been already been discovered to play an important role in microtubule assembly and function in the 1970s (Weingarten *et al.*, 1975). Investigations into the sequence and structure of Tau lead to the discovery of 6 isoforms of the protein which contained either 3 or 4 repeats (3R and 4R respectively) of a conserved microtubule

binding motif due to the exclusion or inclusion of exon 10 (Goedert *et al.*, 1989). 4R Tau includes another copy of this binding motif and thus it binds microtubules more tightly. In combination with 3R and 4R a tau molecule has 2, 1 or 0 N-terminal inserts generating the 6 different isoforms of tau (Ballatore *et al.*, 2007) (Figure 1.3A). Tau is most prominently expressed during foetal development when predominantly 3R tau is expressed however the adult brain expresses all six isoforms of tau with the ratio of 3R to 4R tau being roughly equal (Goedert and Jakes, 1990). Some of the tau mutations associated with dementia disrupt this ratio of 3R to 4R tau although others affect the phosphorylation or aggregation propensity of tau (Park *et al.*, 2016).

In the healthy brain Tau is expressed most abundantly in the axons of central nervous system where it helps to bind and stabilize the microtubules. Tau is not required for microtubule development or function and tau knockout mice develop normally with no neurodegeneration, although these mice do show slight muscle and balance weakness at advanced ages (Ke *et al.*, 2012). However, these mice also show an increased expression of other microtubule associated proteins indicating that several proteins play a role in microtubule development and stabilization and that these other microtubule associated proteins can compensate for the loss of tau. Tau has several other possible functions including cell signalling, neuron development, and apoptosis. There is also more recent evidence that tau plays a role in synaptic scaffolding (Ittner and Götz, 2011).

The role of tau in binding and stabilizing microtubules is dependent on the post-translational modifications that the proteins undergo. Tau is particularly prone to phosphorylation and the phosphorylation status of the molecule changes how likely it is to bind and stabilize microtubules (Jameson *et al.*, 1980; Lindwall and Cole, 1984). Tau is hyperphosphorylated in the AD brain with a two to threefold increase in the amount of phosphate bound to tau. The largest isoform of tau (4R/2N) has 85 potential phosphorylation sites over 40 of which are phosphorylated in AD (Figure 1.3B) (Iqbal *et al.*, 2016; Šimić *et al.*, 2016). The main sites of phosphorylation on tau are serine or threonine residues followed by a proline. Proline-directed protein kinases such as glycogen synthase kinase-3β (GSK-3β) are currently being looked at as possible

therapeutic targets for AD and other tau based diseases (Mazanetz and Fischer, 2007). Not only does this hyperphosphorylation cause tau to dissociate from microtubules, potentially interrupting axonal transport, but it also increases the pool of soluble tau free in the cytosol to misfold and aggregate into tangles (Ballatore *et al.*, 2007). This likely causes a toxic gain of function as soluble tau misfolds, mislocalizes, and aggregates in AD although currently, it is unknown which of these processes is toxic. Going forward research must assess the combinatorial effects of tau and Aβ as well as their individual impacts on the brain and it is important that therapeutics balance both the loss of tau function and the gain of tau toxicity.

Table 1.1: Summary of pathological mechanisms considered as mediators of degeneration in AD

Protein or process	Major effects
Amyloid beta (Carrillo-Mora *et al.*, 2014)	Initiates a cascade of neurotoxic events
	Synaptic dysfunction and impairment of LTP
	Increase in neuroinflammation
	Mitochondrial dysfunction
	Increase in tau phosphorylation
Tau (Beharry *et al.*, 2014; Pooler *et al.*, 2014)	Impaired axonal transport along microtubules
	Synaptic dysfunction
	Mitochondrial dysfunction
	Cell death
Neuroinflammation (Heneka *et al.*, 2015)	Reduced clearance and degradation of pathological proteins
	Reduced support of neurons and surrounding tissue
	Synapse and neuron death
Impairment of the neurovascular unit (Zlokovic, 2011)	Reduced oxygen and glucose to the brain
	Reduced ability to clear waste through the neurovascular unit
	Breakdown of the blood brain barrier

1.1.3 Glial cells, Inflammation and the immune system

Alzheimer also noted in 1907 that the glial cells of his patient appeared to differ from normal glia (Alzheimer *et al.*, 1907). Glia refers to non-neuronal cells and they perform a wide range of tasks in the brain including providing myelin, helping maintain

homeostasis, and functioning as the immune system in the brain. In recent years it has become apparent that these non-neuronal cells of the brain play an integral role in the progression of AD. In fact neuroinflammation, the process by which some of these glial cells become activated, has been suggested to have a causal role in the synaptic degeneration associated with AD (Heneka *et al.*, 2015).

One of the major glia cells types associated with AD are the microglia. Microglia make up between 5-12% of brain cells, depending on the region of the brain (Lawson *et al.*, 1990). They have long been considered to play the role of the immune system in the brain, particularly in phagocytosis of foreign material or cell debris; however microglia also support tissue maintenance by secreting neurotrophic factors (Heneka *et al.*, 2015). Microglia have also been shown to have an important role in synaptic pruning and phagocytosis of apoptotic neurons in the healthy brain particularly in the healthy developing brain (Stevens *et al.*, 2007; Tremblay *et al.*, 2011).

Microglia have been found to bind to Aβ oligomers and fibrils and engulf them by phagocytosis (Tarasoff-Conway *et al.*, 2015). Microglia use multiple cell-surface receptors to bind to Aβ and after binding, become activated; this is thought to begin the inflammatory process that occurs in AD. Activated microglia are particularly found around Aβ plaques however once Aβ is aggregated into plaques it is unable to enzymatically destroyed. This leads to aberrant activation of microglia and an increase in pro-inflammatory pathways which cause other microglia and glial cells to become activated (Malm *et al.*, 2015). This continuous activation of microglia in AD can be neurotoxic having negative effects both on neurons and synapses. In this way microglia are not only failing to clear the amyloid load but also producing neuroinflammatory molecules which themselves can be harmful to the surrounding tissue (Guillot-Sestier and Town, 2013).

Another major glial cell type that plays a role in AD pathogenesis are the astrocytes. Astrocytes play an important role in the homeostatic control of the brain particularly in regulating the ionic environment of the brain, structurally supporting synapses and neurons, providing metabolites and glucose to neurons, and maintaining

the blood brain barrier (Osborn *et al.*, 2016). Astrocytes also play a major role in clearing soluble Aβ which is mediated through Apolipoprotein E (ApoE) one of the major genetic risk factors for AD (discussed later) (Tai *et al.*, 2015). Activated astrocytes are also found around plaques where, along with microglia, they are though to cordon off plaques from the rest of the tissue. Astrocytes in AD are likely activated by the pro-inflammatory molecules produced by the microglia and once activated begin to produce pro-inflammatory molecules themselves which turns on a positive feedback loop that proves difficult to end (Steardo *et al.*, 2015). As with microglia it is likely that astrocytes contribute to the pathology of AD both through loss of normal homeostasis controlling functions as well as gain of toxicity production of neuroinflammatory molecules.

1.2 Synapses

There are approximately 10^{11} neurons in the human brain and these interact in exquisitely intricate and complex arrangements to make us the people we are; responsible for our thought, senses, movement, emotion, and memories. To allow the human brain and body to perform these many complex and incredibly varied tasks neurons need to be able to coordinate with other cells, most especially other neurons. This communication occurs at synapses, the specialized connections that allow neurons to exchange information in a way that is rapid, controlled, and highly plastic. The plasticity of synapses, their ability to grow stronger when frequently used or grow weaker when unnecessary was proposed over 100 years ago by the pioneer of modern neuroscience Ramon Y Cajal (Cajal, 1894). Even before physical evidence supporting the existence of synapses was available Ramon Y Cajal proposed that the connections between neurons and the strength of those connections could be the mechanism for memory formation, rather than an increase in the number of neurons. Over 50 years later Hebb built on this knowledge by suggesting that neurons which fired at the same time were more likely to become more strongly connected and in 1973 this phenomenon was first shown experimentally in the hippocampus of a rabbit and termed long term potentiation (LTP) (Hebb, 1949; Bliss and Lømo, 1973). Synaptic size,

strength and number are now known to increase due to increased stimulation. Furthermore synapses are weakened or lost due to inactivity thus allowing for, among other things, the making, keeping, and losing of memories (Collingridge *et al.*, 2010).

1.2.1 Synapses in the healthy brain

Synapses are the critical connection point between neurons. Most of the synapses in the human brain are chemical synapses meaning that a signal is passed from the presynaptic region of one neuron to the postsynaptic region of another through extracellular chemical messengers known as neurotransmitters, which are released into the synaptic cleft. (Figure 1.4). Spanning the synaptic cleft are cell adhesion proteins which hold opposing presynaptic and postsynaptic terminals in place ensuring efficient transfer of neurotransmitter (Südhof, 2008). The most well studied of these cell adhesion proteins are the neuroligins and neurexins and these proteins play a crucial role in synaptic function (Südhof, 2008). Indeed, genetic dysregulation or dysfunction of these proteins has been implicated in autism and schizophrenia (Jamain *et al.*, 2003; Pardo and Eberhart, 2007; Südhof, 2008).

Chemical synapses can be either inhibitory or excitatory and these inputs are summed within the postsynaptic cell which can have up to 10,000 different presynaptic inputs. The vast majority of excitatory synapses in the CNS use the neurotransmitter glutamate, while γ-aminobutyric acid (GABA) and glycine are the main neurotransmitters of inhibitory synapses in the CNS although there are other neurotransmitters used in the CNS including acetylcholine, dopamine and serotonin. However, the excitation or inhibition of the postsynaptic neuron is dependent not only on the neurotransmitter but also on the receptors it acts on. Neurotransmitter binding to excitatory postsynaptic receptors neurons make the post synaptic cell more likely to fire whereas neurotransmitter binding to inhibitory postsynaptic receptors hyperpolarize the membrane making a cell less likely to fire (Kandel *et al.*, 2012). As well as differences in neurotransmitters inhibitory and excitatory synapses tend to have different morphologies with excitatory synapses having rounder synaptic vesicles and

large electron dense regions at the action zone and post synaptic density (PSD) and inhibitory synapses having oval like vesicles with less dense active zones and PSDs (Klemann and Roubos, 2011). However, morphology does not correlate perfectly with synaptic function, and does not accurately reflect the huge diversity of synaptic receptors found at the presynaptic and postsynaptic membrane that are responsible for their widely varying functions.

Presynaptic Features

At chemical synapses, neurotransmitters are packaged into vesicles that are released from specialised swellings of the axon called the presynaptic bouton or terminal. Thus, many of the proteins in the presynaptic terminal are involved in the trafficking, packaging, release, and recycling of neurotransmitters. Many of the proteins that decorate synaptic vesicles aid in the function and control of vesicles in neurotransmitter release. For example: Synapsins, Vesicular glutamate transporter (VGLUT), and synaptophysin are all required for the functioning of glutamatergic synapses. Antibodies against these proteins are often used experimentally to indicate the presence of excitatory presynaptic terminals. Synapsin proteins are involved in binding a pool of synaptic vesicles to the actin cytoskeleton and making them available for release when required in a Ca^{2+} dependent manner (Cesca *et al.*, 2010). VGLUT transports glutamate from the cytoplasm into vesicles and these proteins in part regulate the amount of neurotransmitter present within each vesicle (Wilson *et al.*, 2005). Synaptophysin is not only involved in the transport of synaptic vesicle precursors down the axon through its interaction with axon transport proteins but it is also important in synaptic vesicle endocytosis and recycling (Okada *et al.*, 1995; Santos *et al.*, 2009). Inhibitory synapses are often marked with antibodies against vGAT which is responsible for packaging GABA and glycine into synaptic vesicles. GAD65, an enzyme responsible for generating GABA from glutamate is also occasionally used as a marker of inhibitory synapses. (Buddhala *et al.*, 2009).

Presynaptic Function

Synaptic vesicle release is by necessity a fast process and to enable this vesicles are held in readiness at the active zone by members of the Soluble NSF Attachment Protein Receptor (SNARE) protein complex (Han *et al.*, 2017). The SNARE protein complex is made up of synaptobrevin (also called VAMP-1/-2) which is bound to the vesicle membrane, and syntaxin and SNAP-25 which are bound to the plasma membrane (Trimble *et al.*, 1988; Oyler *et al.*, 1989; Bennett *et al.*, 1992). Synaptic vesicles and their cargo are released in a Ca^{2+} dependent manner which is often a result of a propagating action potential reaching the presynaptic terminal, although spontaneous release of vesicles does also occur (Südhof, 2012; Li and Kavalali, 2017). An action potential traveling down the axon causes voltage gated Ca^{2+} channels within the presynapse to open triggering fusing of the vesicle and plasma membranes and release of neurotransmitter into the synaptic cleft (Tokumaru *et al.*, 2001; Basu *et al.*, 2005; Pang *et al.*, 2006; Kümmel *et al.*, 2011; Han *et al.*, 2017). Ca^{2+} has a very localized area of action as free Ca^{2+} ions are rapidly buffered by a wide array of Ca^{2+} binding proteins including calbindin, calcineurin and calmodulin. Ca^{2+} is also removed by a Na^{+}/Ca^{2+} exchanger proteins, or pumped into the endoplasmic reticulum or mitochondria in an ATP dependent manner (Scott, 2007). As such voltage gated Ca^{2+} channels are tethered extremely close to SNARE protein complexes in a mechanism that requires neurexins and other scaffolding proteins (Augustine *et al.*, 2003; Kaeser *et al.*, 2011; Südhof, 2012).

The dominant Ca^{2+} response proteins controlling synaptic vesicle release are the synaptotagmin family, particularly synaptotagmin 1. Indeed deletion of this protein results in loss of fast calcium triggered exocytosis and an increase in asynchronous and spontaneous release (Südhof, 2013). Synaptotagmins are phospholipid binding proteins that bind to the SNARE protein complex and upon binding to Ca^{2+} trigger membrane fusion (Sudhof, 2012; Rizo and Xu, 2015). Complexin 1, from the complexin family of proteins, also regulates the exocytosis of vesicles in response to Ca^{2+} influx, likely through an interaction with synaptotagmin as complexin itself does not bind Ca^{2+}. Complexin knockout in a mouse leads to a loss of synchronous neurotransmitter

release similar to that seen of syntotagmin1 knock out, and also decreases the readily-releasable pool of synaptic vesicles indicating that complexin acts as both activator and a clamp of synaptic vesicles (Maximov *et al.*, 2009; Yang *et al.*, 2010). It is thought that complexin and synaptotagmin bind to SNARE complexes priming them for release but preventing membrane fusion until Ca^{2+} binds to synaptotagmin which releases a clamp held in place by complexin (Sudhof, 2012).

Endoyctosis at the synaptic memebrane is also an important process, in that it allows for the recycling of vesicle membranes (Saheki and De Camilli, 2012). There are four known mechanisms of endocytosis, which differ in their speeds, mechanisms, and usage. Clathrin-independent ultra fast endocytosis and kiss and run endocytosis both take less than a second while clathrin mediated endocytosis and activity-dependent bulk endocytosis both take longer (Li and Kavalali, 2017). The different methods of endocytosis used by the cell depend on the type of synapses, the stimulation strength and synaptic maturation and more than one method of endocytosis can be used by a cell (Wu *et al.*, 2007; Smith *et al.*, 2008). Of the four, clathrin mediated endocytosis is the best studied although less is known about endocytosis than exocytosis in general. Like exocytosis, many of the regulatory elements of endocytosis act through Ca^{2+}. Calcinuerin, for example, is a calcium dependent phosphatase that affects endocytosis by dephosphorylating dynamin which is responsible for pinching off new vesicles (Cousin and Robinson, 2001). The calpain family of proteases also regulate endocytosis in a calcium dependent manner both by interacting directly with endocytic machinery and also through GSK3β and calcineurin (Wang and Zhang, 2017). These regulatory proteins affect the different methods of endocytosis differently for example those regulatory elements that affect dynamin do not affect kiss-and-run endocytosis which is dynamin-independent.

Control and Support of Presynaptic Function

As well as the proteins directly involved in vesicle release a large number of proteins go into supporting vesicle release. The large scaffolding proteins piccolo and bassoon for example are important for the assembly of presynaptic active zone and

appear to be involved in targeting vesicles to the active zone (Hallermann *et al.*, 2010; Mukherjee *et al.*, 2010). RIM proteins and RIM binding proteins are also important scaffolding proteins and are involved in the tethering of Ca^{2+} channels to the active zone, ensuring that these channels cause vesicle release (Sudhof, 2012). RIM proteins also bind Munc13 which is crucial for vesicle priming by modifying syntaxin to allow it to form SNARE protein complexes (Stevens *et al.*, 2005; Gerber *et al.*, 2008). These protein interactions are in part response for the close proximity of SNARE protein complexes and Ca^{2+} channels ensuring efficient and specific vesicle release. Thus these proteins are key in regulating short term plasticity of synapses by changing the number of docked vesicles and voltage gated Ca^{2+} ion channels as well as the number of SNARE protein complexes decorating each vesicle which increases the speed and likelihood of exocytosis (Castillo *et al.*, 2002; Schoch *et al.*, 2002).

Neurotransmitters released from the presynapse mostly bind to receptors on the postsynapse however presynaptic terminals also have neurotransmitter binding proteins. These receptors are important for LTP and long term depression (LTD) and have a number of effects such as increasing or decreasing the amount of neurotransmitter released from the presynaptic terminal (Schlicker and Feuerstein, 2017). Receptors on the presynapse also bind to signalling molecules released from the postsynaptic terminal. For example, endocannabionoids released from the postsynapse in during LTD act on cannabinoid receptors at the presynaptic terminal to cause inhibition of voltage-gated Ca^{2+} channels. This effects both sort-term and long-term synaptic strength and acts at both excitatory and inhibitory synapses (Chevaleyre *et al.*, 2006; Branco and Staras, 2009). Calcium signalling within the presynapse also has a potent effect both on long-term and short- term plasticity. Calmodulin, for example, binds to Munc13 when activated by Ca^{2+} and increases the pool of readily releasable synaptic vesicles (Junge *et al.*, 2004). Indeed a large number of proteins at the synapse are phosphorylated not only by calcium binding proteins but also in response to other second messengers. The targets of these kinases include Ca^{2+} channels which increase Ca^{2+} influx leading to plasticity (de Jong and Verhage, 2009). A number of G-protein coupled receptors (GPCRs) are also found at the presynapse and are involved in

downstream second messenger cascades through a number of second messengers to cause changes in synaptic plasticity (de Jong and Verhage, 2009).

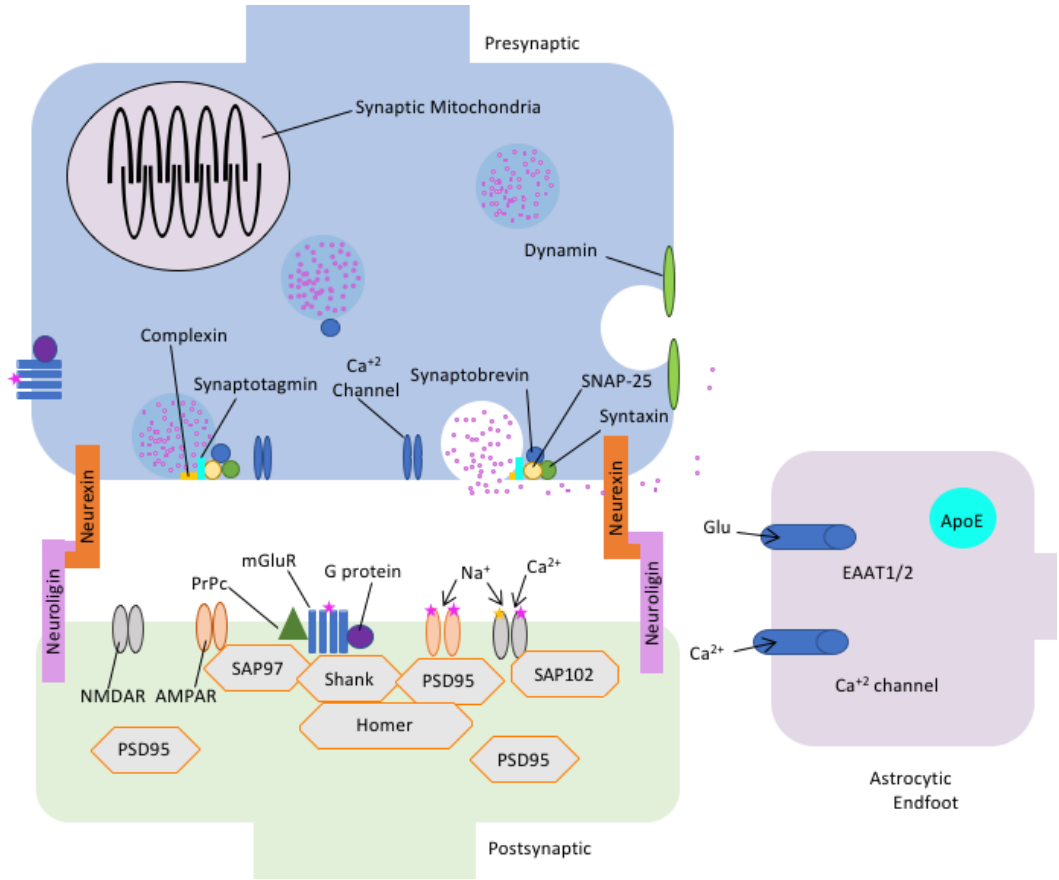

Figure 1.4: Basic schematic of an excitatory glutamatergic synapse. Diagram highlighting a select few of the proteins found in the synaptic cleft, presynaptic, postsynaptic, and astrocytic components of the synapse. Neurexin and neuroligin stabilize the synaptic cleft and hold the presynaptic active zone opposite the post synaptic density. Members of the SNARE protein complex (synaptobrevin, syntaxin and SNAP-25) cause the release of vesicles upon Ca^{2+} influx through Ca^{2+} channels due to synaptotagmin and complexin. Neurotransmitter binds to AMPAR and NMDAR to allow the influx of Na^{+} and Ca^{2+} into the postsynaptic terminal which is stabilized by multiple proteins. Activation of mGluRs causes down-stream signalling cascades through activation of g-proteins. Dynamin controls endocytosis of unbound neurotransmitter and astrocytic end feet also bind to and uptake neurotransmitter as well as excess Ca^{2+}.

Postsynaptic Features

The bulk of receptors for neurotransmitters are found on the postsynaptic density (PSD), which is opposite the active zone of the presynaptic terminal and allows

for efficient transfer of signals through the synaptic cleft. Some receptors on the PSD cause the direct influx of ions (ionotropic) while others work through downstream signalling cascades to cause changes in protein homeostasis (metabotropic). Excitatory neurotransmitters cause ion channels that have a depolarizing effect on neurons to open, making it more likely to propagate an action potential; while inhibitory neurotransmitters cause an influx of hyperpolarizing ions making an action potential less likely (Kandel *et al.*, 2012). The activation of a single receptor or even many receptors within a single postsynaptic density rarely cause an action potential, rather actions potentials in a postsynaptic cell are the sum of all the inputs to that cell, often from many hundreds of other neurons (Kandel *et al.*, 2012).

Function and Control of Glutamatergic Postsynapses

Glutamate binds to ionotropic receptors (iGluR) which are found primarily at excitatory postsynapses however the mechanism of action depends on the type of receptor it binds to. There are three main types of ionotropic glutamate receptors; α-amino-3-hydroxy-5-methyl-4-isoxazolepropionic acid receptor (AMPARs), kainate receptors and N-methyl-D-aspartate receptor (NMDARs) all of which are formed of four subunits. The different iGluRs have different mechanisms of action and the different subunits and thus the iGluR they make up are unique in their functional properties, making for a huge variety of glutamate receptors. The iGluR subtypes and assembled receptors can differ from one synapse to another and vary according to developmental stage, activity of the synapse, brain area, and disease (Smart and Paoletti, 2012). Although these three iGluRs all gate for ions that depolarize the membrane they perform very distinct functions at the synapse and in neuronal processes.

Of these three types of iGluRs the least is known about kainate receptors due in part to a lack of efficient and selective tools to study their function. Unlike AMPARs or NMDARs which are predominantly found on the PSD, kainate receptors are found both presynaptically and postsynaptically and serve a crucial role in the regulation of presynaptic LTP. Glutamate binding to kainate receptors on the presynaptic terminal causes an influx in Ca^{2+} increasing the chance of vesicle release. Kainate receptor

activation affects both glutamatergic and GABAergic presynapses and the result of this activation depends both on the subunits involved, the type of neuron, and the strength of receptor activation (Frerking *et al.*, 1998; Rodríguez-Moreno and Lerma, 1998; Rodríguez-Moreno and Sihra, 2011). Independent of their ionic function, kainate receptors also act through GPCRs, however this is likely through interactions with intermediaries or scaffolding proteins as kainate receptors do not have G-protein binding motifs (Rozas *et al.*, 2003; Contractor *et al.*, 2011).

Upon glutamate binding, AMPARs open rapidly and become permeable to both Na^+ and K^+ which depolarizes the postsynaptic terminal. In this way activation of AMPARs directly increases the likelihood of postsynaptic cell firing. Changes in the number of AMPAR at the PSD is one of the major ways in which the efficacy of synaptic transmission is altered (Chater and Goda, 2014). The number of AMPARs at a particular PSD correlates well with spine size and synaptic strength and changes in AMPAR number are regulated by a number of different proteins. Some of these proteins, such as TARPs and cornichons, are responsible for trafficking AMPAR from the ER to the synapse although local translation of AMPAR at the synapse has been shown to occur, and this causes an increase in the number of AMPARs available for insertion into the membrane (Tang and Schuman, 2002). Other proteins are involved in altering the number of AMPARs embedded in the membrane at the PSD. Many of these proteins are controlled by Ca^{2+} either directly or indirectly through Ca^{2+} binding proteins. In the adult brain, RNA editing of the GluA2 subunit causes almost all AMPAR to be Ca^{2+} impermeable, however some AMPAR lacking either GluA2 or this substitution are Ca^{2+} permeable and also allow for faster and large single channel conductance (Greger *et al.*, 2003). Ca^{2+}most often enters the PSD through NMDARs and as such these proteins are responsible for much of the control of LTP and LTD.

Unlike AMPARs and kainate receptors which require only glutamate for activation, NMDARs activation requires the binding of both glutamate and glycine as well as membrane depolarization. Membrane depolarization is crucial as it removes the Mg^{2+} normally blocking the channel, allowing cations, Na^+, K^+, and Ca^{2+} to flow through (Kandel *et al.*, 2012). The influx of Ca^{2+} through NMDARs is crucial for the regulation of

LTP and LTD with strong, quick Ca^{2+} influx causing LTP and low, sustained Ca^{2+} influx causing LTD. Low levels of Ca^{2+} engages high affinity Ca^{2+} molecules such as calcineurin. Activation of these molecules leads to downstream signalling events such as the dephosphorylation of GluA1, which results in the removal of AMPARs from the synaptic membrane and leads to LTD (Jurado *et al.*, 2010). Rapid increase in intracellular Ca^{2+} concentrations leads to activation of molecules such as CaMKII which leads to LTP (Sanhueza and Lisman, 2013). CaMKII is a protein kinase that when bound to Ca^{2+} phosphorylates target proteins such as GluA1. CaMKII can bind to the GluN2B subunit of NMDARs which causes it to be in close contact to the site of Ca^{2+} influx and this interaction has been shown to be important for LTP (Sanhueza and Lisman, 2013). Although the phosphorylation of GluA1 and other PSD proteins is important for LTP or LTD it is not crucial, indicating that other processes are also at play and NMDARs and CaMKII interact with each other and other signalling proteins to cause changes in synaptic strength (Sanhueza and Lisman, 2013).

Metabotropic receptors for glutamate (mGluRs) are found on both the pre- and postsynaptic membranes. These GPCRs are part of the C class of GPCRs. This class of GPCRs form obligatory dimers and have large venus flytrap and amino terminal domains which have been shown to bind allosteric modifiers and Ca^{2+} (Jiang *et al.*, 2010; Willard and Koochekpour, 2013; Hanlon and Andrew, 2015). These GPCRs affect synaptic strength and size through a number of second messengers including PLC, cAMP, and adenylyl cyclase (Mukherjee and Manahan-Vaughan, 2013). There are three groups of mGluRs and all mGluRs have been found both presynaptically and postsynaptically. Group 1 receptors are predominantly found postsynaptically and Groups 2 and 3 receptors are predominantly found presynaptically. Even within the same group these different mGluRs have very different functions. For example, although both group 1 mGluRs, mGlu1 is involved in the induction of persistent LTP while mGlu5 is mainly involved in the protein synthesis and maintenance of LTP as well as being incredibly important for LTD (Mukherjee and Manahan-Vaughan, 2013). mGlu1 functions by increasing the intracellular Ca^{2+} levels both through interactions with NMDARs and also through second messengers which release Ca^{2+} from intracellular stores. Group 2 and 3 mGluRs are critically required for LTD (Mukherjee

and Manahan-Vaughan, 2013). These receptors have been shown to inhibit Ca^{2+} channels to prevent transmitter release from both glutamatergic and GABAergic presynaptic terminals as well as other downstream effects of second messenger cascades.

Structural proteins of Glutamatergic Postsynapses

The PSD contains a large number of proteins that make up a scaffolding that hold receptors in place and disruptions to this scaffolding are detrimental to synaptic function (Bayés and Grant, 2009). A core component of the PSD is PSD95 which is closely related to PSD93, SAP102, and SAP97 all of which are present at the PSD although to a lesser degree than PSD95 (Gao *et al.*, 2013). These proteins are all responsible for binding to both AMPARs and NMDARs at the postsynaptic membrane. Although these proteins are structurally similar they have different affinities for specific molecules and neurotransmitter receptors and thus the scaffolding protein composition of the PSD is integral to its function. For example, SAP97 interacts directly with the AMPAR subunit GluR1, while PSD95 only interacts with AMPARs through transmembrane AMPAR regulatory proteins, for example stargazin, in a process that crucial for LTP (Opazo *et al.*, 2012). SAP102 preferentially interacts with NR2A-containing NMDARs while PSD95 preferentially interacts with NR2B containing NMDARs (Gao *et al.*, 2013). Other postsynaptic scaffolding proteins include the Shank family and the Homer family. Homer1 and Shank 3 are particularly important due to their interaction with mGluRs and knock down of either protein results in reduced mGlu5 dependent LTD and LTP (Gao *et al.*, 2013). Actin also plays a major role as a scaffolding protein at the PSD and a major role of Ca^{2+} activated CaMKII in LTP is in stabilizing new actin filaments. This promotes LTP by increasing the size and stability of the PSD (Gordon-Weeks and Fournier, 2014).

GABAergic Postsynapses

Scaffolding proteins, ionotropic and metabotropic receptors also play a major role at inhibitory synapses. The major scaffolding protein present in inhibitory synapses

is gephyrin and post-translational modifications of this protein, specifically phosphorylation, are crucial to strengthing and weakening of inhibitory synapses (Zacchi *et al.*, 2014). Gephyrin stabilizes $GABA_A$ receptors ($GABA_AR$) at the PSD which are fast acting ligand gated Cl- ion channels found at the inhibitory postsynapse (Kandel *et al.*, 2012). This causes the membrane potential to drop to -70mV from its normal -65mV increasing the amount of positive ion influx required to cause an action potential. $GABA_ARs$ are heteropentamers and there are many $GABA_AR$ subunits which all have slightly different effects similar to the iGluRs discussed earlier (Vithlani *et al.*, 2011). $GABA_B$ receptors ($GABA_BR$) are the main GABAergic receptors of the inhibitory synapse and these are coupled to G proteins which influence synaptic transmission through second messengers at both the presynapse and the postsynapse (Kandel *et al.*, 2012). These receptors also have different mechanisms of action depending on the subunits that make them up and the localization of the receptor. At the presynapse for example, $GABA_BR$ activation can cause the inhibition of Ca^{2+} influx causing less vesicle release. The activation of $GABA_BRs$ can also affect the actions of nearby NMDARs affecting the LTP and LTD of nearby excitatory synapses and of the cell overall (Gassmann and Bettler, 2012).

1.2.2 Synapses in the Alzheimer's brain

The primary symptom of AD is progressive memory loss and thus it is perhaps not surprising that synapses and indeed synaptic dysfunction and dysregulation are important in the disease. Of all the neuropathological hallmarks of AD synaptic loss correlates best with the cognitive impairment that is the phenotype of AD (DeKosky *et al.*, 1990, 1996). Plaques and tangles are often found in aged individuals without any cognitive symptoms, indicating that they in themselves are not sufficient to cause disease however the soluble oligomeric forms of Aβ and tau play a role in synaptic degeneration and the accompanying memory loss (Spires-Jones and Hyman, 2014).

Certainly, synaptic loss appears to correlate with the presence of oligomeric forms of Aβ. Koffie *et al.* found that in both the APP/PS1 model of AD and post mortem

human brain synaptic loss was greatest in the core and halo of dense core plaques, areas with high oligomeric Aβ levels. Synaptic density then returns to control levels greater than 30μm from the plaque where the number of synapses associating with Aβ is less (Koffie *et al.*, 2009, 2012). They also found that a subset of synapses near the plaques contain oligomeric Aβ and these synapses are on average smaller, potentially indicating synaptic shrinkage. Work by a number of labs has confirmed that oligomeric Aβ causes synaptic or neuronal loss (Walsh *et al.*, 2002; Lacor *et al.*, 2007; Shankar *et al.*, 2008; Tomiyama *et al.*, 2010; Klein, 2013). There are a number of mechanisms by which oligomeric Aβ is thought to mediate synaptic shrinkage and loss which have been studied by a variety of experimental procedures and it is likely that many if not all of these play a role in the human disease. It is important to note that many of these experiments both in vitro and in vivo involve overexpression or high concentrations of Aβ often much higher than is found physiologically or pathologically in the human brain, although there a notable exceptions (Shankar *et al.*, 2010).

Electrophysiological studies of rodent hippocampal slices have shown that both the application of exogenous Aβ as well as over production of Aβ by transgenic models impairs LTP and facilitates LTD (Walsh *et al.*, 2002). Aβ is proposed to affect LTP through dysregulation of various Ca^{2+} release processes within the cell which also affects some of the downstream regulatory proteins dependent on calcium that cause changes in membrane receptor availability. In vitro and in vivo studies have shown that Ca^{2+} dysregulation in both the pre- and the postsynapse precedes spine shrinkage and loss of synaptic connections (Shankar *et al.*, 2007; Kuchibhotla *et al.*, 2009; Wu *et al.*, 2010; Busche *et al.*, 2012; Chakroborty *et al.*, 2012). Evidence demonstrates that Aβ can aberrantly enhance the activity of NDMARs in favour of LTD induction. Soluble Aβ causes a slow influx of Ca^{2+} through GluN2B-containing NMDARs to cause downstream second messenger signals, including PP1 as well as calcineurin activation (Guntupalli *et al.*, 2016). This then leads to the endocytosis of AMPARs and LTD as well as activation of GSK3β which is one of the major tau kinases in AD (Hernandez *et al.*, 2013). GSK3β activation also enhances LTD by phosphorylating PICK1 which is fundamental for AMPAR reduction at the PSD (Peineau *et al.*, 2007). Aβ can also interact with NMDARs to cause their internalization by causing the dephosphorisation of the GluN2B subunit.

Although there is evidence that the major effect of Aβ on NMDARs is through their metabotropic actions this internalization of receptors will also prevent ion influx upon activation (Snyder *et al.*, 2005; Nabavi *et al.*, 2013).

Other synaptic binding partners of Aβ cause alterations in LTP and LTD. Aβ has been shown to interact with the cellular prion protein (PrPc) to cause aberrant activation of Fyn kinase. This kinase then goes on to phosphorylate mGluR5 protein increasing LTD and impairing LTP (Renner *et al.*, 2010; Hamilton *et al.*, 2014; Xia *et al.*, 2016). Aβ has also been shown to bind acetylcholine receptors specifically α7-nicotinic acetylcholine receptor (α7nAChR). Acetylcholine is used by multiple cell types in the CNS including short range interneurons and those forming long-range projections from the basal forebrain to the neocortex and hippocampus (Lombardo and Maskos, 2015). Although studies currently disagree as to how the interaction between α7nAChR causes disruptions in LTP and downstream neuron loss, the current drugs approved for use in AD are acetylcholinesterase inhibitors, although it is important to note that these drugs are symptomatic only (Lombardo and Maskos, 2015; Xia *et al.*, 2016). The effects of Aβ also appear to be dependent on an interaction with APP itself although the reasons for that have yet to be determined (Wang *et al.*, 2017). The size and species of Aβ at the synapse also affects the toxicity and influences synaptic impairment. It appears that small soluble species of Aβ are more neurotoxic than the larger conformers and fibrils (Yang *et al.*, 2017).

The mechanisms by which tau affects synapse loss are much less well established although mouse models show that knocking out tau prevents some of the detrimental effects of Aβ on cognition and seizure susceptibility (Roberson *et al.*, 2007). Mouse models of tauopathy indicate that tau pathology is sufficient to cause synapse and neuron loss although in contrast to Aβ, Ca^{2+} dysregulation is not involved (Kopeikina *et al.*, 2013). Pathogenic forms of tau are found to be localized to both the pre- and postsynaptic terminals and similar to Aβ evidence suggests that it is the oligomeric species of these proteins that have a direct effect on synaptic function (Rocher *et al.*, 2010; Crimins *et al.*, 2013). Studies in fly and rat neurons show that pathogenic tau disrupts presynaptic vesicle mobility thus lowering neurotransmission

(Zhou *et al.*, 2017). Studies in mice have shown that pathogenic species of tau affect the number and stability of specific postsynaptic spines indicating that tau acts at both the pre- and the postsynapse to cause synaptic dysregulation (Crimins *et al.*, 2013).

Given the role of tau as a microtubule transporter synapse dysfunction could result from an impairment of transport down the axon (Stoothoff *et al.*, 2009; Kanaan *et al.*, 2011; Kopeikina *et al.*, 2011). Indeed, tau overexpression in vitro leads to impairment of transport. This effect of tau could be due to an increase toxicity as some groups show that knocking out mouse tau does not affect cognition. However others have shown a small effect in cognition in older age groups including plasticity deficits (Roberson *et al.*, 2007; Ahmed *et al.*, 2014; Ma *et al.*, 2014). This loss of transport has been shown to affect, among other things, mitochondria that are needed for energy demanding synapses to function (Kopeikina *et al.*, 2011). Synapses are extremely dependent on mitochondria, not only for ATP production but also for their calcium buffering capabilities. Studies have shown that mitochondria trafficked to the synapse show a different proteomic signature from those which are found non-synaptically in neurons (Völgyi *et al.*, 2015). However synaptic mitochondria appear to be more susceptible to Ca^{2+} dysregulation and oxidative phosphorylation as well as Aβ accumulation in AD (Brown *et al.*, 2006; Du *et al.*, 2012). Mitochondria also play an important role in both apoptotic and non-apoptotic caspase activation which has been shown to be important in AD (Takuma *et al.*, 2004; Moreira *et al.*, 2010).

It is not just the presynapses and postsynapses that are affected in AD but also the end feet of astrocytes which make up “tripartite synapses”. Astrocytes have been shown to provide ATP to neurons, be important for calcium buffering, and to modulate LTP and LTD through the release of small signalling molecules (Vincent *et al.*, 2010). Astrocytes are also important in the uptake of glutamine and GABA from the synaptic cleft which contributes to the termination of signal (Chung *et al.*, 2015). Aβ causes dysregulation of calcium signalling in astrocytes impairing not only their ability to modulate LTP but also impairing control of the neurovascular unit (Kuchibhotla *et al.*, 2009; Peters *et al.*, 2009; Vincent *et al.*, 2010). This impairment of the neurovascular unit is no doubt exacerbated by the vascular pathology that often accompanies and is a

risk factor for AD and likely reduces the flow of oxygen to the brain further impairing the mitochondria (Dickstein *et al.*, 2010).

Microglia also play a role both in normal synaptic function and in AD. In the healthy brain microglia support neurons both by clearing extracellular debris and by releasing extracellular growth factors such as brain-derived neurotrophic factor (Ueno *et al.*, 2013; Southam *et al.*, 2016). In AD mouse models, microglia appear to be responsible for synapse loss in a Complement C1q, C3 dependent manner (Hong *et al.*, 2016; Shi *et al.*, 2017). Although this removal of synapses occurs normally in development, over-activation of this system in disease is detrimental to the synapses (Paolicelli *et al.*, 2011; Hong *et al.*, 2016; Shi *et al.*, 2017). Although microglia and astrocytes are clearly important in the disease pathogenesis, in vitro work shows that they are not a requirement for synaptic dysfunction and loss in the presence of pathogenic proteins.

Synapses also contribute to the spread of disease throughout the brain. Tau pathology in particular follows a very well-defined spreading pattern, which follows pathways of neurons which are synaptically connected. This finding led groups to look at whether synaptic connections were involved in the spread of pathological forms of tau. Mice that express pathological tau only in the EC show accumulation of pathological tau in the subiculum, the denate gyrus, and CA1 of the hippocampus, areas which are monosynaptically connected to the EC (de Calignon *et al.*, 2012; Harris *et al.*, 2012; Liu *et al.*, 2012). Similar mouse models show that Aβ increases the rate of spread of this tau pathology (Pooler *et al.*, 2015). Cell culture studies hint at the mechanism behind this as Aβ is known to increase local synaptic activity and increased neuronal activity stimulates tau release from neurons (Renner *et al.*, 2010; Pooler *et al.*, 2013). Synaptic spread of tau in the absence of cell death or synapse loss has been has also been shown in vivo indicating that presynaptic terminals do not have to degenerate for tau to spread through the brain (Pickett *et al.*, 2017).

Synaptic degeneration is undoubtedly important to AD pathogenesis and preventing this degeneration or increasing synaptogenesis could be a mechanism of

halting the cognitive decline that accompanies AD. The plasticity of synapses and their regenerative properties make them attractive targets for therapeutics however their complexity combined with the complexity of AD itself mean that we still have much to learn about how and why synaptic degeneration occurs in AD as well as how to prevent it.

1.3 ApoE and other risk factors for AD

Epidemiological studies indicate that many factors are associated with an increase the risk of developing LOAD including education, physical inactivity, diabetes, cardiovascular health, and genetics. Many of these factors particularly those related to cardiovascular health are important in midlife and predispose individuals to cognitive decline even in the absence of AD. Indeed, distinguishing between vascular dementia and AD clinically is sometimes difficult due to the overlapping and heterogeneous factors at play (Imtiaz *et al.*, 2014). High blood pressure and hypertension in midlife, in particular, are associated with an increased risk of AD. However physical activity can help mitigate this risk and a recent study has shown that physical activity can even reduce the progression of AD (Kivipelto *et al.*, 2001, 2013; Stephen *et al.*, 2017). Cardiovascular health affects the amount of oxygen that can be delivered to the brain and poor cardiovascular health causes an increase in small white matter hyper-intensities as well as thinning of the surface of the cortex. This increases not only the risk of AD but also the rate of cognitive decline in individuals without AD (Kivipelto *et al.*, 2001). Type II Diabetes Mellitus is associated with cognitive impairments as well as an increased risk of AD although the magnitude of the effect of diabetes is still debated (Jayaraman and Pike, 2014).

Genetic risk factors are also important in LOAD (Figure 1.4). Although not causative of disease like mutations in APP and PS1 and PS2, genome wide association studies have found many genes that increase the risk of AD (Figure 1.5). Many of these are involved in cholesterol metabolism, endocytosis and the regulation of the immune system. Clusterin (also called Apolipoprotein J) for example is involved in both

cholesterol metabolism and the regulation of the immune system and likely plays a role in Aβ processing as well (Li *et al.*, 2014). TREM2, another important risk factor in AD, is a potent mediator of microglial function in AD and highlights the importance of the glial cells in AD (Jonsson *et al.*, 2013). Gender is also an important risk factor for AD with women having a higher incidence of AD (Pike, 2017) (Figure 1.1C). The reasons behind this are still unclear but it is known that gender interacts with other important risk factors including Apolipoprotein E (Shi *et al.*, 2014).

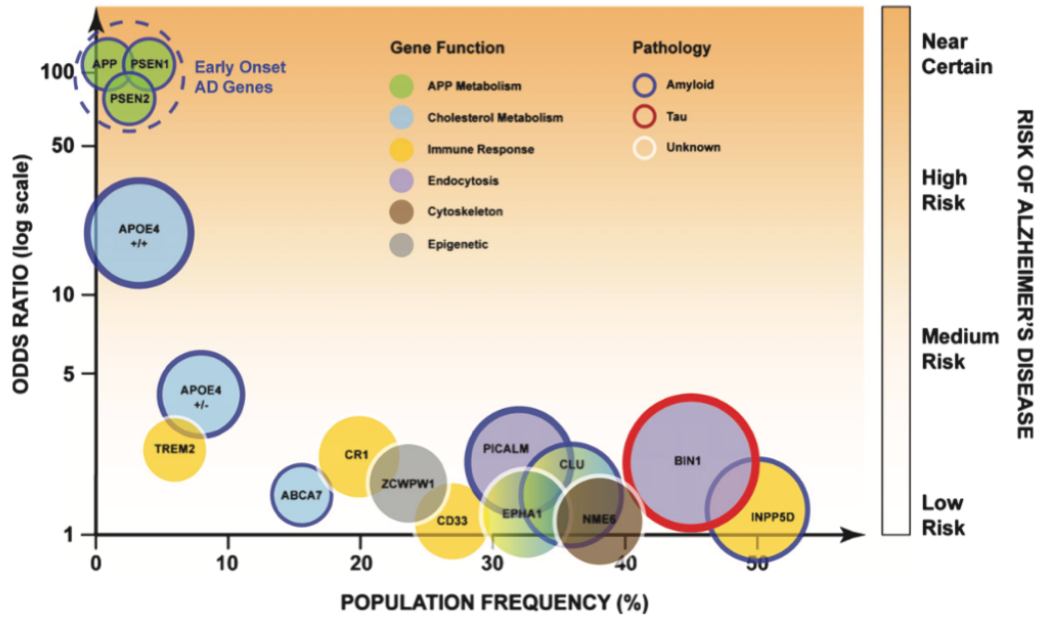

Figure 1.5: Genetic risk factors for AD. Genes in which mutations are causative for AD have the highest risk but affect relatively few people while other genes are much more prevalent but have less risk associated with them. High risk genes are not only associated with higher risk of developing AD but also earlier age of onset and increased severity of disease. The area of each circle indicates that genes' influence of AD within the population. Taken from (Robinson *et al.*, 2017) and is reproduced under CC BY-NC 4.0.

1.3.1 ApoE

The greatest genetic risk factor for LOAD is a polymorphism in the apolipoprotein ε (*APOE)* gene encoding for apolipoprotein ε (ApoE). The *APOE* ε4 allele has been shown to increase the risk of AD in a dose dependent manner when compared to the more common *APOE* ε3 allele where as the much rarer *APOE* ε2 allele has been shown to be

protective (Corder *et al.*, 1994). The possession of two copies of *APOE* ε4 has been shown to not only increase the chance of getting AD by 12 fold that of a person with two copies of *APOE* ε3, but also lower the average age of clinical onset to 68 years of age. One copy of *APOE* ε4 increases the chance of AD by 3 times and lowers the average age of onset to 76 years of age from an average age of onset of 84 for an individual with two copies of *APOE* ε3 (Corder *et al.*, 1993). Although mentioned in association with AD most frequently, ApoE has also been linked to Parkinsons Disease (Li *et al.*, 2004), FTD (Agosta *et al.*, 2009) and other neurological diseases (reviewed in Huynh *et al.* 2017) as well as linked to lower cognition in non-demented aged individuals (Deary *et al.*, 2004). The pathways by which ApoE impacts the development of AD have been widely studied both in vitro and in vivo however the exact mechanisms have yet to be uncovered. It is clear however that the effects of this important risk factor need to be studied further not only in AD but also in healthy ageing cohorts.

1.3.2 ApoE role in the healthy brain

ApoE is the most abundant apolipoprotein in the brain and the central nervous system (CNS) is the second largest site of ApoE synthesis after the liver (Holtzman *et al.*, 2012). Apolipoproteins bind lipids allowing them to be soluble in water and transporting them through the blood and body. In the brain ApoE is primarily synthesized by astrocytes and to a lesser extent other glial cells although neurons have been shown to produce ApoE under certain stressful conditions such as injury (Pitas *et al.*, 1987). Within the brain the function of ApoE includes the transport and delivery of the essential lipid membrane protein cholesterol as well as other lipids (Mahley, 1988; Mahley and Rall, 2000). As neurons do not make enough cholesterol for their needs this delivery of cholesterol by ApoE is important for neurons and has also been shown to have a function in synaptogenesis (Mauch *et al.*, 2001; Dietschy and Turley, 2004). Apoe knock out mice develop normally indicating that the presence of ApoE is not necessary for either development or survival and no overt cognitive defects have been seen in humans missing the *APOE* gene although individuals lacking ApoE do get

hypercholesterolemia and premature atherosclerosis (Anderson *et al.*, 1998; Holtzman *et al.*, 2012; Mak *et al.*, 2014). This is likely due to the presence of other apolipoproteins present in the brain such as ApoA1 and ApoJ also called Clusterin, which can replace some of the functions of ApoE. However the rate at which Apoe knock out mice clear and repair axonal injury is slower than that of wild type mice and Apoe knock out mice also show an age dependant loss of synapses, learning deficits, cholinergic dysfunction and tau hyperphosphorylation indicating that there are some roles which ApoE alone plays (Fagan *et al.*, 1998; Lane-Donovan *et al.*, 2016).

1.3.3 ApoE structure and state

The different *APOE* alleles are all fairly common in the population. The most common allele found in the population is the *APOE* ε3 allele which has a frequency of 79% while *APOE* ε4 and *APOE* ε2 have frequencies of 14% and 7% respectively (AlzGene, 2017). ApoE2 and ApoE4 differ from ApoE3 by a single amino acid substitution each, and thus differ from one another by two amino acids, although rarer polymorphisms within these 3 isoforms have been found (Nickerson, 2000). ApoE2 contains the amino acid cysteine at positions 112 and 158 while ApoE 3 has a cysteine at position 112 and an arginine at position 158 and ApoE 4 has an arginine at both position 112 and 158 (Holtzman *et al.*, 2012) (Figure 1.6A). The different ApoE isoforms also found in different concentrations in the cerebrospinal fluid fluid (CSF) with *APOE* ε2/2 individuals having the greatest amount of measurable ApoE in the CSF and *APOE* ε4/4 individuals the lowest (Riddell *et al.*, 2008). This is likely due to the structural differences between the isoforms with ApoE4 being the most unstable and thus the most likely to be degraded as there is no evidence that genotype affects ApoE production (Zhao *et al.*, 2017).

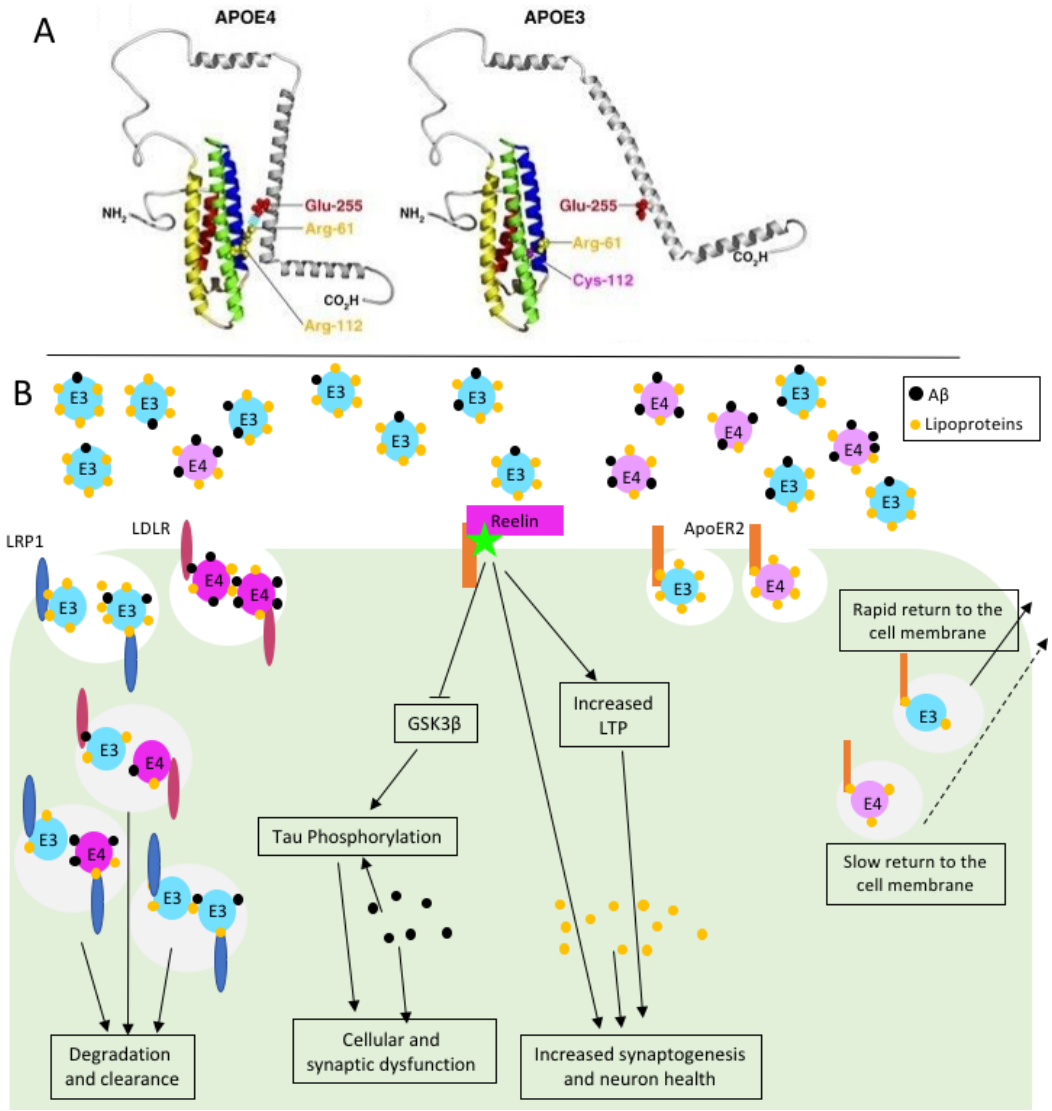

Figure 1.6: Basic schematic of the mechanisms of ApoE signalling through receptors. The structure of ApoE3 and ApoE4 showing the polymorphism at 112 that causes the C terminal domain to be in a more open conformation in ApoE3 and a more closed conformation in ApoE4 **(**A) taken from (Caesar and Gandy, 2012) and is reproduced under CC BY 2.0. ApoE3 and ApoE4 interact with a number of ApoE receptors at the cell surface which have number of downstream processes. ApoE3 and ApoE4 both bind LRP1 and LDLR which then target the apolipoprotein and any bound Aβ for degradation or clearance through the BBB. LRP1 preferentially interacts with ApoE3 and is more efficient at endocytosis and degradation of the ApoE-Aβ complexes than LDLR. ApoER2 binds both ApoE3 and ApoE4 causing endocytosis, however ApoER2 returns to the cell membrane much more slowly when bound to ApoE4 than ApoE3 which prevents its beneficial interactions with Reelin. (B)

The structure of ApoE is made up of a C-terminal region which is connected to a 4 helix bundle which makes up the N-terminal region by a flexible hinge. The presence

of Arg112 in ApoE4 allows for an interaction between Arg61 and Glu225 causing the C-terminal region to be close to the N-terminal region, in ApoE3 and ApoE2, Arg112 is Cys112 which does not allow for this Arg61-Glu225 interaction causing the C-terminal region to be more extended (Hatters *et al.*, 2005) (Figure 1.6A). This difference in structure affects the stability of the resulting ApoE molecule with ApoE4 more likely to form an unstable globular intermediate. Crucially the changes in structure change the propensity of ApoE isoforms to bind to the different types of lipids that ApoE transports around the brain and body (Zhong and Weisgraber, 2009). In particular, ApoE4 binds preferentially to lower density lipoproteins (LDL) while ApoE3 and ApoE2 bind higher density lipoproteins (HDL)(Weisgraber, 1990).

In comparison to the plasma where ApoE associates mainly with very low-density lipoprotein (VLDL) particles ApoE secreted in the brain is mainly found in HDL particles (Zhao *et al.*, 2017). Due to the role of the blood brain barrier, ApoE made in the CNS remains in the CNS and there is very little or no infiltration of ApoE from the periphery (Lane-Donovan *et al.*, 2016). ApoE in the CNS is mainly lipidated by ATP-binding cassette transporter A1 (ABCA1) although other proteins do play a role and the different ApoE isoforms have different levels of interaction with ABCA1 causing them to be differently lipidated (Wahrle *et al.*, 2004). The lipidation status of ApoE affects not only which lipids are transported by ApoE but also which receptors the molecule binds to.

1.3.4 ApoE Receptors

ApoE interacts with a large number of cell surface receptors allowing it to play a wide variety of roles from lipid transport to cell signalling through MAP kinase cascades (Holtzman *et al.*, 2012). Among the ApoE binding receptors are the low-density lipoprotein receptor family (LDLR), ApoE receptor 2 (ApoER2), very low-density lipoprotein receptors (VLDLRs), and lipoprotein receptor-related protein 1 (LRP1). These proteins all have short cytoplasmic C-terminal domains with a tetra-amino acid NPxY motif through which they interact with other proteins to cause downstream

effects inside the cell (Holtzman *et al.*, 2012). Although all ApoE receptors can bind any ApoE isoform, the affinity for an ApoE molecule will change depending on the isoform and the lipid moieties it is carrying. It could be argued that many of the differences between the ApoE isoforms are due to their different interactions with ApoE receptors.

Many of the ApoE receptors play an important role in receptor-mediated endocytosis of lipoprotein particles. These receptors are important for bringing in the cholesterol and lipids that allow for the maintenance of the lipid bilayer that is important to cell function and survival. LRP1 in particular is crucially important for cholesterol transport and although ApoE deficiency does not lead to cholesterol deficiency in the brain, LRP1 deficiency does (Liu *et al.*, 2007). This indicates that there are ApoE independent mechanisms of cholesterol transport in the brain. LDLR and LRP1 are also known to influence ApoE levels through endocytosis and then either subsequent lysosome degradation or recycling of ApoE through recycling vesicles (Figure 1.6B). Removal of either LDLR or LRP1 from a mouse model containing humanized ApoE increases the amount of ApoE in the brain (Fryer *et al.*, 2005; Liu *et al.*, 2007). The different specificities for these receptors that the isoforms of ApoE display may be the reason for the higher levels of abundance of ApoE2 in the brain as ApoE2 is known to bind poorly to both LDLR and LRP1 when compared with ApoE3 (Kowal *et al.*, 1990).

Some of the ApoE receptor proteins, namely ApoEr2 and VLDLR, are also known to bind Reelin, a cell signalling molecule with crucial roles in development (Sharaf *et al.*, 2013; Hirota *et al.*, 2015). Post development Reelin is known to have roles in LTP, LTD, and synapse development and morphology as well as being a neuroprotective agent (reviewed in Holtzman 2012). In later life it has been shown to naturally decrease in abundance. Although ApoE and Reelin do not bind the same site on these receptors, ApoE binding to ApoER2 causes it to be endocytosed and thus not available to bind Reelin (Chen *et al.*, 2010). While endocytosed ApoE3 is recycled quickly and efficiently, ApoE4 has been shown to remain trapped in endosomes with ApoER2 thus depleting the cell surface of ApoER2 and preventing it from interacting with Reelin as well as the

down stream neuroprotective effects of such an interaction (Chen *et al.*, 2010) (Figure 1.6B).

1.3.5 ApoE and the synapse

ApoE and the ApoE receptors play an important role at the synapse. ApoE, is the main transporter of cholesterol in the brain and cholesterol is important for synaptogenesis. Cell culture studies indicate that although neurons produce enough cholesterol to maintain their own survival, synaptogenesis on a large scale only occurs in the present of cholesterol produced by astrocytes and delivered by ApoE (Mauch *et al.*, 2001). Mouse studies have indicated that mice expressing humanized ApoE4 have reduced branching, shorter dendrites, less spines, and reduced synaptic transmission when compared with those expressing humanized ApoE3 (Wang *et al.*, 2005). Behavioural experiments show that ApoE4 mice particularly female ApoE4 mice are impaired at Morris water maze when compared with ApoE3 mice (Grootendorst *et al.*, 2005).

Many of the ApoE receptors also affect synapses through their interaction with Reelin. The binding of Reelin to ApoER2 and VLDLR causes a signalling cascade through NMDA receptors resulting in LTP (Chen, 2005). ApoE4 reduces the availability of these receptors to bind Reelin thus preventing this increase in LTP (Chen *et al.*, 2010). LRP1 also interacts with NMDAR promoting its endocytosis from the cell surface leading to LTD (Nakajima *et al.*, 2013). The interaction of ApoER2 or VLDLR with Reelin also causes a signalling cascade at the PSD that increases dendritic spine growth and mice that have increased Reelin expression have a greater spine density and complexity (Bosch *et al.*, 2016). This interaction also has effects on the presynapse causing an increase in Ca^{2+} which in turn causes a spontaneous release of vesicles (Bal *et al.*, 2013). It is unknown what role if any the different ApoE isoforms play in this interaction.

1.3.6 ApoE and Aβ

Much of the work looking at ApoE in AD investigates its relationship with Aβ. Early post mortem work found a positive correlation between *APOE* ε4 allele dose and Aβ plaque density in individuals with AD (Rebeck *et al.*, 1993). In vivo imaging in humans has shown that fibrillar Aβ can be detected in individuals with an *APOE* ε4 allele 20 years earlier than *APOE*3/3 individuals (Reiman *et al.*, 2004; Fleisher *et al.*, 2013). This build up of detectable Aβ in the brain occurs well before the onset of clinical symptoms and is often accompanied by a decrease in Aβ42 in the CSF (Sunderland *et al.*, 2004; Morris *et al.*, 2010). A wide range of studies indicate that ApoE4 affects the production, clearance, aggregation, and intra- and extracellular localization of Aβ but also that Aβ affects the localization and receptor binding properties of ApoE.

An increase in the amount of Aβ with an *APOE* ε4 genotype could be due in part to an increase in production of Aβ. The ApoE receptor LRP1 and the closely related LRP1B have been implicated in potential effects of ApoE on Aβ synthesis. The production of Aβ occurs when APP is endocyosed and brought into contact with β-secretase and thus an increase in APP endocytosis likely increases Aβ production. LRP1 causes an increase in the rate of APP endocytosis while LRP1B potentially causes a decrease in Aβ by preventing APP endocytosis (Ulery *et al.*, 2000; Cam *et al.*, 2004, 2005). A recent study has also indicated that ApoE can cause a signalling cascade through ERK1/2 which causes an increase in APP production (Huang *et al.*, 2017). This study found that ApoE4 up-regulates this signalling cascade more than ApoE3 and thus causes an increase in APP production. However, this study which took place in cell culture contradicts others which have found no such interaction instead implying that the increase of Aβ in APOE4 cases is due to changes in Aβ clearance (Castellano *et al.*, 2011). The authors of this paper themselves state that when neurons are grown in co-culture with astrocytes this phenomenon ceases to exist (Huang *et al.*, 2017). Nevertheless this implies that the effect of ApoE on APP production could play an important role in the onset and thus prevention of AD.

The effects of the different ApoE isoforms on clearance and degradation of Aβ from the brain has long been a subject of study. Apoe-KO mice have an increased rate of Aβ clearance from the brain compared with mice expressing murine ApoE (DeMattos *et al.*, 2004) and mice expressing humanized ApoE4 have slower levels of Aβ clearance than those expressing humanized ApoE3 thus highlighting the importance of ApoE in regulating Aβ levels (Castellano *et al.*, 2011). Although neurons cannot clear or degrade Aβ, astrocytes and microglia can (Cole and Ard, 2000; Wyss-Coray *et al.*, 2003; Mandrekar *et al.*, 2009). Astrocytes clear Aβ mainly through Blood Brain Barrier (BBB) but also through internal degradation. The internalization of Aβ by astrocytes is dependent on ApoE and is prevented in ApoE-KO astrocytes (Koistinaho *et al.*, 2004). The ApoE receptors LRP1 and LDLR both contribute to the internalization of Aβ-ApoE complexes although at different rates, with LRP1 being the quicker of the two (Figure 1.6B). However Aβ-ApoE4 complexes are preferentially cleared by LDLR which results in a slower rate of clearance of these molecules compared with Aβ-ApoE3 complexes which are cleared through the faster LRP1 (Deane *et al.*, 2008). However not all Aβ is cleared through the BBB. Microglia also phagocytose Aβ in an ApoE dependent fashion in a process that is dependent on ApoE isoform and both microglia and astrocytes produce proteases that mediate the degradation of Aβ peptides. ApoE3 is more effective at causing this release of Aβ proteases than ApoE4 (Jiang *et al.*, 2008; Mulder *et al.*, 2012). While most studies show that ApoE4 slows clearance and degradation of Aβ resulting in damage to the brain parenchyma, therapeutics targeting ApoE or ApoE receptors could end up being detrimental if they also increase the amount of Aβ internalized by neurons (Billings *et al.*, 2005).

Intriguingly although ApoE KO increases the rate of Aβ clearance into the CSF Apoe KO from fAD mice show increased Aβ deposition (DeMattos *et al.*, 2004) in some models of AD (Bales *et al.*, 1997). Knocking out the closely related ApoJ (also called Clusterin) increases Aβ deposition further (DeMattos *et al.*, 2004). This shows ApoE and Clusterin have profound effects on Aβ in terms of its aggregation into oligomers and plaques as well as the deposition of those plaques in the brain. In vitro experiments have shown that ApoE4 increases the extent of Aβ fibrillization compared with ApoE3

and amyloid imaging scans back up these studies with the finding that *APOE* ε2-positive individuals rarely develop fibrillar Aβ and *APOE* ε4 individuals often do (Morris *et al.*, 2010; Garai *et al.*, 2014). It has also been found in vitro that the lipidation state of ApoE affects the fibrillization of Aβ. This is backed up by in vivo work in mice where the ApoE lipidating protein ABCA1 is overexpressed in APP Tg mice resulting in a decrease in Aβ deposition (Wahrle *et al.*, 2008).

ApoE also has effects on the localization of Aβ deposition. For example, mice which express humanized ApoE4 have an increased amount of cerebral amyloid angiopathy compared with mice which express ApoE3 or mouse ApoE (Fryer *et al.*, 2005). ApoE4 individuals also contain more Aβ at the synapse (Koffie *et al.*, 2012). This increase in Aβ is accompanied by an increase in ApoE which may be the result of ApoE transporting Aβ to the synapse where it has a detrimental effect. Cell culture studies indicate that when Aβ is incubated with primary neurons in the presence of ApoE4 or ApoE3 that the cells incubated with Aβ and ApoE4 have more Aβ at the synapse (Koffie *et al.*, 2012).

1.3.7 ApoE and Tau

Although ApoE has a much stronger association with Aβ, ApoE also affects tau pathologies. Tiraboschi *et al.* showed in 2004 that in a large post mortem cohort of AD individuals, two copies of an ApoE4 allele correlate with an increase in Aβ plaques and NFTs in all brain areas except the hippocampus (Tiraboschi *et al.*, 2004). This study also showed that while a copy of the "protective" ApoE2 did reduce the number of Aβ plaques in individuals with AD there was no effect on the number of NFTs in this cohort (Tiraboschi *et al.*, 2004). This could indicate that while ApoE2 does have a beneficial role in regards to Aβ pathology only ApoE4 affects both Aβ and tau.

One reason for this could be that the main effect of ApoE on tau is likely through its interaction with its receptors, ApoER2, VLDLR and LRP1. LRP1 polymorphisms have been shown to interact with tau and increase the risk of AD in an

ApoE independent manner (Vázquez-Higuera *et al.*, 2009). As for ApoER2 and VLDR, ApoE2 and ApoE3 have very similar receptor binding properties with these receptors while ApoE4 is markedly different (Chen *et al.*, 2010). These receptors both bind to Reelin to control the activation of GSK-3β which phosphorylates tau at one of the major site of interest in AD (Hiesberger *et al.*, 1999; Beffert *et al.*, 2002; Ohkubo *et al.*, 2003). Disruption of this signalling pathway potentially by the sequestering of these receptors by ApoE4 leads to reduced phosphorylation of GSK3β and thus hyperphosphorylation of tau. As hyperphosphorylation of tau causes it to dissociate from microtubules, and increases its propensity to aggregate this is likely a mechanism by which ApoE4 affects tau pathology in AD (Rankin *et al.*, 2007). This could also help to explain the effect of ApoE4 in increasing the risk of FTD a disease in which Aβ plays less of a role (Fabre *et al.*, 2001).

1.4 Methods of studying synapses in Alzheimer's Disease

Studying the effects of AD on the synapse is clearly important to furthering our understanding of this disease. However, synapses are both very complex and very small which presents methodological challenges to investigating the effect of AD on these structures. Therefore, to further understand this disease requires the study of both human post mortem tissue and model systems with powerful techniques to help resolve the limitations of size and complexity.

1.4.1 Array Tomography

The discovery of green fluorescent protein and the resulting development of fluorescently tagged antibodies has dramatically increased our understanding of biological systems by allowing for the identification of more than two proteins in biological samples (Micheva and Smith, 2007). However fluorescent light microscopy has a number of limitations not least of which is that the axial resolution of the z

direction is about 800nm depending on the wavelength used (Pawley and Pawley, 2006). This means that for very small structures such as synapses co-localization of a protein marker with a synapse could indicate either that said protein is in the synapse or merely near the synapse. To overcome this problem Micheva and Smith developed the high resolution microscopy technique array tomography and in 2011 Kay *et al.* modified the technique for use in human tissue (Micheva and Smith, 2007; Kay *et al.*, 2013).

Array tomography requires that tissue be embedded in hard acrylic resin similar to that used for electron microscopy. This allows the tissue to be sectioned into 70nm thick ribbons of serial sections. These ribbons can be stained using standard fluorescently tagged antibodies and imaged using a fluorescent light microscope. Image processing then allows for a 3D visualization of the imaged tissue with a z axis resolution of 70nm. This allows for synaptic co-localization to be assessed with greater confidence than standard light microscopy. Array tomography has already been put to good use looking at the synapse in both AD and in healthy aging (Koffie *et al.*, 2009, 2012; Henstridge *et al.*, 2015; Pickett *et al.*, 2017).

1.4.2 Proteomics

Proteomics is defined as the investigation of the protein properties of a system on a large scale and in an unbiased manner. The technical capabilities of proteomic systems have advanced greatly in recent years to allow for not only the identification but also the quantification of proteins to a high degree of accuracy and sensitivity (Bantscheff *et al.*, 2012). Proteomic systems have been put to good use exploring the changing protein landscape of different diseases in an unbiased method. This has already led to the discovery of the role of certain proteins in important cellular activities and diseases, and will undoubtedly lead to many more.

The most common form of proteomics is shotgun proteomics where a sample full of a mix of proteins is digested by a protease, normally trypsin, which is then

separated by reverse-phase liquid chromatography (LC) and then analysed by mass spectrometers. The mass spectrometers can detect the mass to charge ratio, intensity, and sequence information for each peptide which are then searched in a database to identify the proteins present in the sample. For samples where a known amount of analyte is added prior to analysis (also called labelled proteomics) the protein quantification can be absolute but in cases of label free proteomics the quantification of proteins is relative to other proteins detected by the system. Although shotgun label free proteomics is very useful in the identification and quantification of proteins it inherently has poor reproducibility due in part to the many factors which can introduce variation between samples (Piehowski *et al.*, 2013). This necessitates the maintenance of techniques which look specifically at an individual protein such as ELISA or western blot. These techniques have high reproducibility and accuracy and are very popular to explore the role of a subset of proteins but require good quality antibodies against the target protein and are not suitable for studying many proteins at once.

1.4.3 Proteomic studies of AD

Proteomics studies of AD have been carried out on brain tissue, blood, and CSF from animal models and human post-mortem cases. The analysis of blood and CSF has be valuable to the discovery of biomarkers which are particularly important in AD as cognitive tests have low accuracy and dynamic range thus preventing investigation of subtle changes in cognitive function (Fiandaca *et al.*, 2014). Clinical trials for disease modifying treatments in AD have thus far failed and one explanation is that treatments are applied after the onset of clinical systems which may be too late in the disease course. Biomarkers which allow for the identification of preclinical AD and MCI would allow for trials to occur in these individuals allowing drug companies to test drugs which prevent the onset of AD.

Explorative proteomics in post-mortem human brain has shed light on the pathological protein changes that occur in disease and lead to neurodegeneration. However so far proteomic studies have failed to reach a consensus on the protein

changes that are linked with AD. This is no doubt due in part to technical problems particularly with 2D electrophoresis and inherent variability between individuals and cohorts but are also likely due to the variety of brain areas and sample processing used (Brinkmalm *et al.*, 2015). A list of proteomics studies undertaken in post-mortem human brain is presented in Table 1.1. However even with advances in proteomic techniques and careful sample processing of the same brain area different labs continue to report largely different protein sets (Andreev *et al.*, 2012; Musunuri *et al.*, 2013; Moya-Alvarado *et al.*, 2016). There are several possible reasons for this continued variability, the first being that the brain is a very complex tissue with many cell types that are differently affected by AD. The second is that AD is a very heterogeneous disease with many comorbidities and variability between individuals will play a big role in data sets. These limitations do not negate the usefulness of proteomics in AD but rather highlight the role of proteomics as a hypothesis generator placing proteomics studies at the front of further AD research.

One mechanism of reducing variability in proteomics studies is to remove the effect of genetic variability and post-mortem interval differences and for that animal or cell models are needed. These models can be very powerful in looking at the changes that occur in the progression of a disease or at the response of proteins to a single insult, such as Aβ, Tau hyperphosphorylation, or oxidative stress. However, it is important to highlight that to date no mouse model has fully recapitulated the disease and the failed clinical trials discussed earlier have been successful in mouse models and yet failed in humans. Moya-Alvarado *et al.* show a nicely comprehensive table of proteomic studies performed in mouse models of AD (Moya-Alvarado *et al.*, 2016).

Table 1.2: Previous proteomics studies of post mortem human AD brain.

Title	Year	Type of Proteomics	Brain area and subcellular fraction used	# Changes Detected	Major Conclusions
Proteomic analysis of the brain in Alzheimer's disease: molecular phenotype of a complex disease process (Schonberger *et al.*, 2001)	2001	2D electrophoresis followed by in gel trypsin digestion and then HPLC and sequence identification	Whole tissue homogenate from Hippocampus (Hp), temporal cortex (tCx), entorhinal cortex (EC), Cerebellum (Cb), cingulate gyrus (cGy) and sensorimotor cortex (sCx) from AD and matched controls	76 in Hp 62 in tCx 39 in EC 34 in Cb 125 in cGy 75 in sCx	Protein differences in AD are not specific to regions of severe degeneration. Proteins changed in AD were involved in synaptic neurotransmission, stress response, lipid transport, glycolysis, and known Diabetes pathways
Proteomic Profiling and Neurodegeneration in Alzheimer's Disease (Tsuji *et al.*, 2002)	2002	2D electrophoresis, followed by in gel digestion and LC-MS/MS	Whole tissue homogenate of temporal cortex from AD and controls	35	This seems to have been a proof of concept for the techniques used.
Proteomics Analysis of the Alzheimer's Disease Hippocampal Proteome (Sultana *et al.*, 2007)	2007	2D electrophoresis, followed by in gel digestion and MALDITOF mass spectrometry	AD and control inferior parietal lobule and hippocampus	18	Found changes in energy related enzymes, scaffolding proteins particularly HSP70, structural proteins, cell cycle, tau phosphorylation and Aβ production
An Increase in S-Glutathionylated Proteins in the Alzheimer's Disease Inferior Parietal Lobule, a Proteomics Approach (Newman *et al.*, 2007)	2007	redox proteomics: 2D electrophoresis	AD and control inferior parietal lobule and hippocampus	4	specific proteins have an increased S-glutathionylation in the AD brain which probably diminishes their activity

Analysis of microdissected neurons by 18O mass spectrometry reveals altered protein expression in Alzheimer's disease (Hashimoto *et al.*, 2012)	2012	AD samples were labelled with O18 while control samples were not. Samples were then trypsinized and LC-MS/MS was used	Microdissected neurons from the hippocampus of AD and control tissue	68	Many of the proteins found to be different were involved in glycolysis
Analysis of a membrane-enriched proteome from postmortem human brain tissue in Alzheimer's disease. (Donovan *et al.*, 2012)	2012	Trypsin digest followed by reverse phase LC-MS/MS	Membrane enriched sample from frontal cortex of AD v matched controls	13	Tau was the most significantly changed protein in AD cases
Label-Free Quantitative LC-MS Proteomics of Alzheimer's Disease and Normally Aged Human Brains (Andreev *et al.*, 2012)	2012	Accurate mass and time tag with a LTQ Orbitrap mass spec	Temporal lobe homogenate	197	Protein families shown to changed included signal transduction, regulation of protein phosphorylation, immune response, cytoskeleton organization, lipid metabolism, energy production, and cell death. Also highlighted are the proteins that differed from published literature
Proteomic Analysis of Postsynaptic Density in Alzheimer Disease (Zhou *et al.*, 2013)	2013	Label free LC-MS/MS	PSD enriched from cortex of AD, probable AD and control cases using a sucrose gradient	25	The family of proteins that regulate actin dynamics were changed. This was more of a pilot study to show that PSD could be used for proteomics and has not been followed up.
Brain site-specific proteome changes in aging-related dementia (Manavalan *et al.*, 2013)	2013	Proteins were digested in gel following 2D electrophoresis then iTRAQ tags were added and LC-MS/MS was used.	Whole tissue homogenate from the hippocampus (Hp), parietal cortex (pCx) and cerebellum (Cb) of AD and age matched control females	31 Total 22 in Hp 8 in pCx 16 in Cb	Different areas of the brain have different and overlapping proteins changes in AD. Tau was found to be different in AD in both the Hp and the Cb and Aβ was different in both the Hp and pCx.

Semiquantitative proteomic analysis of human hippocampal tissues from Alzheimer's disease and age-matched control brains (Begcevic *et al.*, 2013)	2013	Trypsin digestion followed by semiquantitative label-free LC-MS/MS	Whole tissue homogenate from AD and control hippocampus	204 detected only in AD and 600 in only control	Many of the proteins of the AD Hp proteome are involved in protein binding, catalytic activity and nucleotide binding. 40 of the AD specific and 106 of the control specific proteins are detected in CSF indicating they could be biomarkers
The synaptic proteome in Alzheimer's disease (Chang *et al.*, 2013)	2013	2D differential in-gel electrophoresis, then time of flight mass spec on dots of interest.	Synaptosomes of 2 affected areas- hippocampus and inferior temporal gyrus and 2 unaffected areas- occiptial cortex and motor cortex.	26	No significant difference between the unaffected areas in both AD and non AD cases therefore these were used to normalize expression in affected areas.
An investigation of the molecular mechanisms engaged before and after the development of Alzheimer disease neuropathology in Down syndrome: a proteomics approach (Cenini *et al.*, 2014)	2014	2D differential in-gel electrophoresis followed by in gel digestion and then mass spectrometry	Frontal cortex homogenate from AD, down syndrome (DS), DS with AD tissue (AD/DS) and both young (YC) and old controls (OC)	7 (DS v YC) 3 (AD/DS v OC) 3 (DS v AD/DS) 10 (YC v OC)	Redox protein changes are important in DS and AD. ApoE is found to be less abundant in young DS brains compared with young controls.
Quantification of the brain proteome in Alzheimer's disease using multiplexed mass spectrometry. (Musunuri *et al.*, 2014)	2014	Trypsin digestion followed by stable-isotope dimethyl labelling and then nanoLC-MS/MS	Whole tissue homogenate of temporal neocortex from AD and matched controls	69	Proteins increased in AD were involved in metabolic processes, oxidative stress and inflammation, proteins decreased in AD were involved in altered synaptic function and signal transduction

Differential expression of proteins in brain regions of Alzheimer's disease patients (Zahid *et al.*, 2014)	2014	2D electrophoresis, followed by in gel digestion and ESI-QTOF-MS/MS	Whole tissue homogenate of Hippocampus (Hp), substantia nigra (SN) and frontal cortex (fCx) from AD and control cases	48 total 13 in Hp 20 in SN 22 in fCx	Protein changes were differently regulated in the different brain areas. Differentially expressed proteins from AD Hp, fCx and SN are involved in metabolism, transport and the cytoskeleton.
Apolipoprotein E*4 (APOE*4) Genotype Is Associated with Altered Levels of Glutamate Signaling Proteins and Synaptic Coexpression Networks in the Prefrontal Cortex in Mild to Moderate Alzheimer Disease (Sweet *et al.*, 2016)	2016	Trypsin digestion followed by C13 labeling and LC-MS/MS	Synaptosomes from AD, FTD, and control humans as well as ApoE3 and ApoE4 mice were isolated using a sucrose gradient from the Dorsolateral prefrontal cortex (DLPC) and the Entorhinal cortex (EC)	1 in DLPC in AD 95 in DLPC in FTD 95 in EC in AD	The AD human samples clustered into two groups which were enriched for ApoE3 or ApoE4 genotypes. The main pathway that differed between the two groups were glutamate signaling indicating that ApoE4 could play a role in reducing glutamate signalling although this finding was not recapitulated in the ApoE4 mice.

1.4.4 Proteomic studies of synapses

Given the prominent role of synapses in the brain knowing their constituent elements is beneficial to understanding brain function both in health and disease. Proteomics of synapses biochemically isolated from brain tissue has been used to reveal over 2,000 proteins and has also been used in a number of diseases (Bayés and Grant, 2009). The first step in synaptic proteomics is biochemically isolating synapses from tissue and there are a number of different methods by which scientists do this which are aptly reviewed in table 1 of Dieterich and Kreutz 2016 (Dieterich and Kreutz, 2016). The majority of synaptic proteomic studies so far have taken place in isolated PSDs although others investigate the presynapse, spine head, and astrocytic end feet in different combinations depending on the isolation method used. These experiments have been instrumental in discovering the great richness of proteins in healthy synapse as well as changes that occur in the synapse in disease.

One of the biggest downsides of proteomics of the synapse is that synapses are diverse and dynamic and proteomics involves a snapshot picture of all the synapses in a sample. For identification purposes this is not a problem but in comparative studies, for example when studying the effect of a disease on the proteome, the proteins changes in one synapse could be offset by another. To begin to understand synaptic protein differences in greater depth scientists are now using new proteomics techniques to look at the post-translational modifications that these proteins can undergo in an attempt to understand the physiological role of these proteins in a static "snapshot" image (Trinidad *et al.*, 2012). This is of course still only an attempt at understanding the role of these proteins in different conditions and need to be followed up with studies of a few proteins of interest in systems that allow greater depth of understanding. As always investigation of a system balances depth and width of understanding although techniques are advancing remarkably quickly to the point where we might be able to investigate both in a single experiment.

1.5 Models of Alzheimer's Disease

1.5.1 Animal Models of Alzheimer's Disease

The discovery of mutations that caused Aβ plaques and tau tangles has lead to the production of several animal models which recapitulate to different degrees some aspects of AD. As AD is a heterogeneous disease with many features it is perhaps unsurprising that many animal models, 127 at time of writing, have been developed over the years to answer a variety of questions (Alzforum, 2017). It is important to point out, even though it has already been highlighted in this introduction, that none of these animal models fully recapitulate the disease. This however does not negate their usefulness in providing information about disease onset, progression and pathology. Indeed, the ability to test the effects and interactions of proteins, networks, and different cell types in a mammalian model which develops age-related pathology is invaluable.

Most of our mouse models focus on trying to recapitulate the disease pathology using clues from fAD. As many of these individuals have mutations in APP or PS1 which cause an increase in the production of $A\beta_{42}$, so to many of our mouse models contain mutated forms of these genes often under an exogenous promoter although knock in lines, are becoming more common (Hiroki, 2017). Mice which express these mutated fAD genes have a build up of Aβ pathology that looks remarkably similar to that seen in humans. There are a number of different AD causing mutations that have been found in both APP and PS1 and many of these have been introduced into animal models to create animals with different disease progressions and timelines (Lamb *et al.*, 1997; Oakley *et al.*, 2006; Alzforum, 2017).Most of the animals harboring fAD mutations have amyloid plaques, and behavioural deficits with some neuron and synapse loss. However while some tau pathology such as hyperphosphorylation and neuritic dystrophies is seen in fAD mouse models none of these mice get the characteristic tau tangles and gross neuron loss that occur in human cases of AD.

In an effort to recapitulate both the plaque and the tangle pathology of AD, mouse models which contained fAD mutations alongside tau mutations were developed (Oddo *et al.*, 2003). However the mutations in tau that cause the formation of tangles in mouse models are found not in AD individuals but individuals with FTD. These mouse models have helped answer some of the questions about the interactions of tau and Aβ in AD. For example the triple transgenic mouse line which over expresses mutated APP, PS1, and tau show Aβ pathology prior to the onset of tau pathology (Oddo *et al.*, 2003). However when APP/PS1 mice are crossed with mice which do not produce endogenous tau there is rescue not of the Aβ pathology but of the cognitive impairment that accompanies it (Roberson *et al.*, 2007). This suggests that while Aβ pathology precedes tau pathology, tau is necessary for the cognitive effect of Aβ on mice. The interactions of these two proteins in regulating the spread of pathogenic proteins has also been studied and here labs have shown than Aβ increases the speed of tau spread and toxicity (Pooler *et al.*, 2015). Although this would indicate that Aβ pathology precedes tau pathology which then causes disease, both tau pathology and Aβ pathology cause cognitive deficits in the absence of overt pathology of the other protein. The interactions between tau and Aβ are clearly complex and much is still unknown about how tau and Aβ interact to cause AD in humans.

1.5.2 Human Cell Culture Models of Alzheimer's Disease

Cell culture systems allow for the study of different protein interactions in an easily modifiable system. Cell culture systems also offer a unique opportunity to investigate the role of different cell types on the different aspects of AD. Much of the work looking at AD in cell culture systems thus far has been done using rodent primary cultures either from AD models or by adding exogenous Aβ or tau to cells from a control mouse. This work which has been performed by a number of labs over a number of years has been instrumental in highlighting the spread of pathogenic proteins from one cell to another, the effects of Aβ on neurons and the importance of astrocytes in AD pathology (Frost *et al.*, 2009; Garwood *et al.*, 2011; Kayed and Lasagna-Reeves, 2012). However the development of induced pluripotent stem cell

(iPSC) technology has presented scientists with the opportunity to move this work into human cells thus increasing the translational value of the system (Takahashi *et al.*, 2007). Yagi *et al.* created the first stem cells from familial AD patients in 2011 and since then many AD related lines have been created from patients harbouring a variety of mutations (Yagi *et al.*, 2011). Some of these fAD mutation harboring iPSC lines have been used to study the effect of APP processing and Aβ production finding that many of these fAD mutations increase the ratio of Aβ42:Aβ40 which leads to an increase in tau phosphorylation (Arber *et al.*, 2017). Recently Maloney and colleagues have used iPSC lines containing a mutation in APP to show that this mutation confers protection by reducing the efficiency of β-secretase cleavage of APP into Aβ (Maloney *et al.*, 2014). Other molecular phenotypes have been studied using iPSCs from fAD patients among them altered endosomal processing to oxidative stress and mitochondrial dysfunction and a list of these lines is reviewed in Arber *et al.* (Arber et al. 2017).

However iPSC culture still has major limitations, the biggest limitations of which are the lack of cellular diversity in the culture dish, the developmental phenotype of the cells, and the fact that cells are missing a major phenotype of the disease, protein aggregates. However advances are being made towards ameliorating some of these limitations. Firstly co-culture systems and organoid technology are becoming more popular. Co-culture systems allow for different cell types to be cultured together and have pointed to some of the very important effects that astrocytes play in neuron development in a dish (Kuijlaars *et al.*, 2016; Liao *et al.*, 2016). Simply adding astrocytes to the neuronal cell culture dish or even adding astrocyte conditioned media increases the speed at which neurons develop (Cordero-Llana *et al.*, 2011; Kuijlaars *et al.*, 2016). As well as allowing for a greater understanding of these non-neuronal cells in AD, increasing the speed of neuronal development is very useful in a disease that is primarily a disease of aging. Human iPSC neurons take longer to develop than mouse primary neurons and this is a disadvantage in AD research particularly in the study of tau which is developmentally regulated (Goedert *et al.*, 1989; Sposito *et al.*, 2015). Neurons derived from iPSCs show a phenotype similar to that of a neuron in the developing embryo when only 0N3R tau is produced. This prevents scientists from studying the effects of fAD mutations on longer forms of tau. Fortunately new

protocols are being developed to allow for faster differentiation of neurons both in the presence and absence of astrocytes (Qi *et al.*, 2017).

Most of the work done in cell culture has been done in 2D culture in a dish however 3D cultures have also been used to study AD. Although these culture systems are more difficult to set up and maintain and thus lack the high throughput nature of 2D systems they are very valuable to research. This is especially true of the 3D culture system set-up by Choi *et al.* where neural precursor cells expressing fAD mutations were differentiated to neurons within an artificial 3D support matrix. This showed for the first time plaques and tau filaments forming in a cell culture dish and also showed that pharmacological manipulation could prevent the further accumulation of tau (Choi *et al.*, 2014). This culture system also shows faster maturation of neurons when compared to conventional 2D although no model system to date has produced tau tangles in the absence of tau mutations, potentially due to how long tangles take to form. No model is perfect, however all have their place in answering specific questions about AD, and when used in combination both with other models and with post mortem tissue derived from patients and controls then we get ever closer to the answers that we so desperately need to help combat this life threatening and ever more present disease.

1.6 Summary and Aims

Synapse loss is the greatest correlate to the cognitive decline seen in AD and yet causes of synapse dysfunction in AD are still not well understood. Although it is clear that the major pathological proteins of AD, Aβ and tau, are important, it is unclear how these proteins interact with each other and other risk factors for AD to cause protein changes in the synapse leading to synaptic dysfunction. Using novel mouse and cellular models of AD combined with proteomics and high-resolution imaging of human post mortem tissue this thesis will investigate the synaptic protein changes in AD with a focus on the risk factor *APOE* ε4.

Aim 1: To characterize synaptic density in a new mouse model of AD using the high-resolution imaging technique Array Tomography. In this novel mouse line mutated APP and PS1 as well as wild type human tau are expressed. Investigating this model will contribute to knowledge about how tau and Aβ interact to cause AD like pathology and synaptic loss in a mouse.

Aim 2: To further understand the effects that AD has on the synaptic proteome as well as the effects of ApoE4 on those protein changes both in AD and healthy aged control using unbiased label free proteomics on synaptoneurosomes isolated from post mortem tissue. This will provide a greater understanding of the proteins that underlie synaptic dysfunction in AD and will allow for further investigation of the role of ApoE on these proteins changes.

Aim 3: To investigate the effect of *APOE* genotype on the synaptic localization of Clusterin, Aβ and ApoE using the high resolution imaging technique Array tomography. Clusterin was chosen from the results of aim2 to be followed up due to the genetic links with AD and due to its physiological similarities to ApoE.

Aim 4: To develop a novel cell culture model of Aβ derived synaptic puncta loss using Aβ derived from human brain extract and cortical neurons derived from human iPSCs. This will allow for an easily modifiable humanized system to further test the results of the proteomics screen without the need for fAD mutations or rodent primary culture.

2 Methods

All chemicals were purchased from Sigma-Aldrich (St. Louis, MO) unless otherwise specified.

2.1 Array Tomography

2.1.1 Embedding Tissue

Mouse

All animal experiments conformed to national and institutional guidelines including the Animals [Scientific Procedures Act] 1986 (UK), and the Council Directive 2010/63EU of the European Parliament and the Council of 22 September 2010 on the protection of animals used for scientific purposes, and had full IACUC and Home Office ethical approval.

APP/PS1 mice (stock #004462, Jackson Labs, Bar Harbor, Maine), which express APP^{swe} and $PS1^{\Delta exon9}$ under the control of the PrP promoter, were crossed with rTg21221 mice (Hoover *et al.*, 2010) which overexpress wild-type human tau (hTau) under the control of a recombinant tetracycline activator protein expressed under a forebrain-specific promoter. The F1 generation contained mice with both the APP/PS1 genotype and mice with the APP/PS1/hTau genotype and animals were genotyped by collaborators at Massachusetts General Hospital. Array blocks prepared as described in Micheva and Smith 2007 (Micheva and Smith, 2007) were made from the cortex of both these APP/PS1/hTau mice (n=5) and APP/PS1 (n=3) littermates. This was performed by collaborators Nikita Rudinskiy and Jonathan Hawkes at Massachusetts General Hospital.

Human

Use of human tissue for post-mortem studies has been reviewed and approved by the Edinburgh Brain Bank ethics committee and the ACCORD medical research ethics committee, AMREC (ACCORD is the Academic and Clinical Central Office for Research and Development, a joint office of the University of Edinburgh and NHS Lothian). The

Edinburgh Brain Bank is a Medical Research Council funded facility with research ethics committee (REC) approval (11/ES/0022).

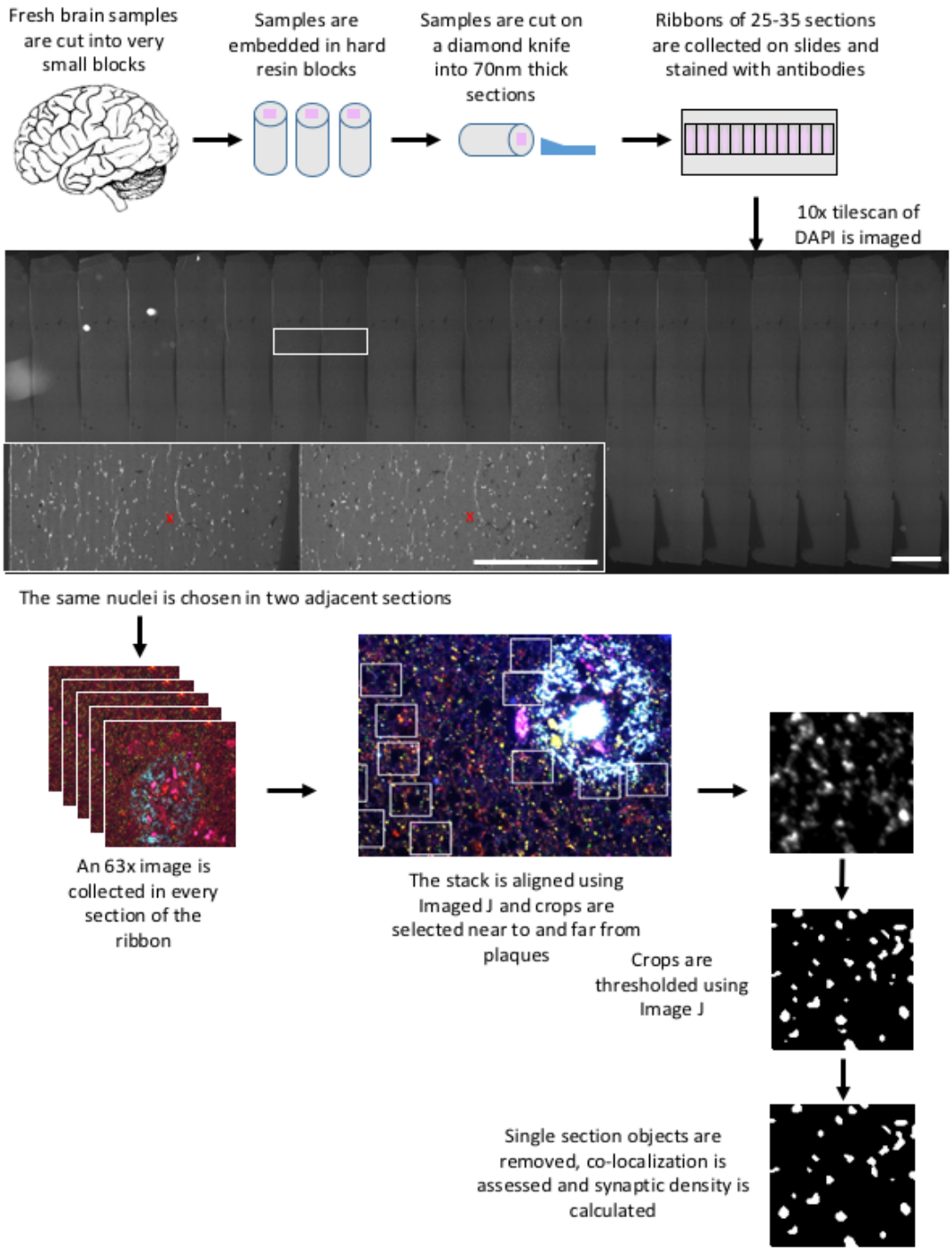

Figure 2.1: Array Tomography method. Small blocks of fresh tissue is fixed and then embedded into hard resin which is then sectioned into 70μm thick ribbons of serial sections. These are then stained with antibodies and imaged on a light microscope. Images are then aligned and processed using Image J which makes a crop binary and then Matlab which removes single slice objects and calculates co-localization and synaptic density. Scale bar of tile scan 200μm, scale bar of insert 50μm, crop boxes are 10μm by 10μm

Tissue from the BA41/42 area of the cortex was embedded as described in described in Kay *et al.* 2013 (Kay *et al.*, 2013). In brief fresh post-mortem samples were cut into small cortical blocks and fixed in 4% paraformaldehyde. Samples were then dehydrated in ascending concentrations of ethanol and then incubated with LR white resin over night. Cortical blocks were then embedded in LR white resin which was polymerized by baking at 56°C for 24 hours. Resin embedded blocks were then stored at room temperature until needed. Embedding was performed by Dr. Chris Henstridge and Professor Tara Spires-Jones.

2.1.2 Cutting Ribbons

Thickness No. 1 glass coverslips (VWR, Radnor, PA) were coated in a solution of 0.1% fish skin gelatin and 0.01% chromium potassium sulphate and allowed to dry. Cortical blocks from the mice and blocks containing BA41/42 from the humans were sectioned onto these cover slips using a Jumbo Histo Diamond Knife (Diatome, Hatfield, PA) and an EM UC7 ultracut microtome (Leica Microsystems, Cambridge, UK). Approximately 25-35 70nm thick serial sections were collected in a ribbon and mounted on the coverslip which was then allowed to dry on a heat block before being outlined using a hydrophobic pen. Ribbons were stored in a box and kept for up to 6 months at room temperature.

2.1.3 Staining and Imaging

Ribbons were first incubated with 50mM glycine in Tris buffered saline (TBS) for 5 minutes at room temperature. This was then removed and with no delay was replaced with array tomography block buffer (0.1% fish skin gelatin, 0.05% tween in TBS). Ribbons were incubated in block buffer for 45 minutes at room temperature before being replaced by primary antibody mix. Primary antibodies were diluted in array tomography block and ribbons were incubated in primary antibody solution at 4°C overnight. The solution was then removed and the ribbon was washed 5 times using TBS ensuring that there was always liquid covering the ribbon. Ribbons were then incubated with secondary antibodies diluted in array tomography block for 45 minutes

at room temperature in the dark. Secondary antibodies were removed and the ribbon was washed 5 times using TBS before being incubated with DAPI diluted 1:100 in array tomography block for 5 minutes at room temperature in the dark. The DAPI solution was removed and the ribbon was washed twice with TBS before being mounted on microscope slides (VWR international, Radnor, PA) using Immunomount (Thermo Fisher Scientific, Waltham, MA).

2.1.4 Image Acquisition

Images were obtained using a Zeiss axio Imager Z2 epifluorescent microscope, a Coolsnap digital camera and the AxioImager software with array tomography macros (Carl Zeiss Ltd., Cambridge, UK). First a tilescan of the DAPI channel for the entire ribbon was obtained at a 10x magnification. Then using the AxioImager software one nucleus was chosen and was indicated on two adjacent sections. For ribbons which contained plaques the nucleus selected was chosen such that the plaque was visible in the image stack, for ribbons were no plaque was present the selection was random. Once the nuclei were selected a 63x objective was used to obtain a single image in the same location in every slice of the ribbon. This process is graphically explained in Figure 2.1 and the linked video (http://dx.doi.org/10.7488/ds/297). Two image stacks were obtained per ribbon.

Ribbons were then stripped of antibodies using stripping buffer (0.2M NaOH, 0.02% SDS in dH_2O) for 15-20 minutes with gentle shaking. Ribbons were then washed once in 1x TBS for 10 minutes and once in dH_2O for 5 minutes with gentle shaking. Ribbons were then allowed to dry on a slide heater and stored for no more than 2 weeks before the array tomography procedure was repeated with day 2 primary antibodies.

2.1.5 Image processing

Image stacks were aligned using the DAPI channel with the Image J program (Fiji) and the mutistackreg macro (Thevenaz *et al.*, 1998). 10μm x 10μm crops were selected from image stacks within the neuropil avoiding cell bodies, blood vessels,

areas of high noise or background. Where a plaque was present crops were chosen near the plaque (<10μm from halo edge) and far from plaques (>45μm from halo edge). In stacks were there was no plaque, crops were chosen randomly throughout the stack. Custom image J macros were used to threshold the crops and are included in appendix 1 (chapter 3) and 3 (chapter 5). Custom MATLAB scripts were used to remove puncta that were only found in one slice. As synapses are greater than 70nm, it is assumed that puncta which only appear in one slice are background noise. MATLAB scripts (appendix 1 and 3) were also used to assess co-localization with proteins of interest, filter EAAT positive end feet from tripartite synapses and calculate synaptic density.

2.2 Biochemistry

2.2.1 Protein Assay

A Bicinchoninic acid (BCA) assay (Thermo Fisher Scientific, Waltham, MA) was used on all samples used in western blotting and proteomics to determine protein amount. Samples were run along side a Bovine Serum Albumen standard curve that consisted of samples at 2mg/ml, 1.5mg/ml, 1mg/ml, 0.75mg/ml, 0.5mg/ml, 0.25mg/ml and 0.125mg/ml. Samples were diluted 1:5, 1:10, or 1:25 with diH2O to be brought into the range of the standard curve. 25μl of standard or diluted sample was added to a single well of a 96 well plate in triplicate. Standards and samples were incubated with 200ul of a 1:50 Reagent B:Reagent A (Thermo Fisher Scientific, Waltham, MA) mixture at 35°C for 30 minutes and the optical density was measured at 570nm using a MRX micro plate reader (Dynex Technologies, Worthing, UK). The slope and y-intercept of the standard curve as well as the protein concentration of each sample were generated in excel.

2.2.2 Western blotting

Protein assay results were used to prepare samples with either 5, 10, or 15μg of protein. The appropriate volume of protein sample was added to 7μl of 2x laemmli (Sigma-Aldrich, St Louis, MO) and the total volume was brought up to 14μl with diH_2O. Proteins were then denatured at 70°C for 10 minutes on a hot block. Samples and a molecular weight marker (Li-Cor Biosciences, Lincoln, NE) were loaded onto NuPAGE 4-

12% Bis-Tris precast polyacrylamide 15 well gels (Invitrogen) using a 25µL Hamilton Syringe. The proteins were then separated by weight using sodium dodecyl sulfate polyacrylamide gel electrophoresis (SDS-PAGE) for 2 hours at 100V. The gels were run in an XCell SureLock™ Mini-Cells (Invitrogen, Carlsbad, CA) NuPAGE using morpholineethanesulfonic acid SDS running buffer (Invitrogen, Carlsbad, CA).

Proteins were electro-transferred onto nitrocellulose membrane (Bio-Rad, Watford, UK) at 30V for 1.5 hours using the XCell II™ Blot Module system (Invitrogen, Carlsbad, CA) in tris-glycine transfer buffer (25mM Tris, 192mM Glycine, 10% Methanol). Membranes were incubated in blocking buffer (10ml Odyssey blocking buffer (Li-Cor Biosciences, Lincoln, NE) diluted 1:1 with Phosphate Buffered Saline (PBS)(Sigma-Aldrich, St Louis, MO) for 1 hour to reduce background staining. Membranes were then incubated with primary antibodies diluted in blocking buffer with added 0.1% Tween-20 over night at room temperature while shaking.

Primary antibodies were removed and saved for reuse and membranes were washed 4 times for 10 minutes in PBS with 0.1% Tween-20. The appropriate 680 and 800 IR dye secondary antibodies (Li-Cor Biosciences, Lincoln, NE) were diluted 1:5000 in blocking buffer with 0.1% Tween-20 and incubated with the nitrocellulose membranes in the dark at room temperature for 1 hour while shaking gently. The membranes were then washed 4 times for 10 minutes in PBS with 0.1% Tween-20. The membranes were imaged using Odyssey infrared imaging system, and analysed using Odyssey software (Li-Cor Biosciences, Lincoln, NE).

2.2.3 *APOE* Genotyping

Extracting DNA

DNA was extracted from ~25mg of cerebellum for each case using the QIAamp DNA mini kit (Qiagen, Hilden, Germany) which was used as per the manufacturers instructions, thus all buffers, collection tubes, and the column were provided by Qiagen unless otherwise stated. To do this 25mg of tissue was cut up into small pieces and added to a 1.5ml microcentrifuge tube and 180µl of Buffer ATL was added to each

tube. 20μl of proteinase K was then added to the tube and the contents were then mixed by vortexing. The samples were then incubated at 56°C on a hot block placed on a shaker for 3 hours. 200μl of buffer AL was then added to the sample which was then vortexed and incubated at 70°C for 10 minutes. 200μl of ethanol was then added to the samples which was vortexed and then added to a QIAamp Mini spin column placed inside the provided 2ml collection tube. The samples were then centrifuged at 6,000G for 1 minute, the column was added to a clean 2ml collection tube and the old collection tube and the filtrate were discarded. 500μl of Buffer AW1 was then added to the column which was then centrifuged at 6,000G for 1 minute. Again the column was placed in a clean collection tube and the old collection tube and filtrate were discarded. 500μl of Buffer AW2 was then added to the column which was then centrifuged at 17,000G for 5 minutes. The column was then placed into a clean and labelled 1.5ml microcentrifuge tube and the collection tube and filtrate were discarded. 200μl of Buffer AE was then added to the column and incubated at room temperature for at least 1 minute. The column (and microcentrifuge tube) was then centrifuged at 6,000G for 1 minute and the column was discarded. The filtrate was considered the DNA sample and was stored at -20°C.

Polymerase Chain Reaction

Polymerase chain reaction (PCR) was performed on the extracted DNA. PCR was set up in 20μl per reaction which contained 1μM of primer and 10% DMSO. For this 10μl of 2x Master mix (Promega, Madison, WI) was combined with 1μl of primer stock (20μM forward primer, 20μM reverse primer), 2μl of DMSO (Sigma-Aldrich, St Louis, MO), 6μl ddH_2O and 1μl of isolated DNA. The forward primer was 5'taagcttggcacggctgtccaagg3' and the reverse primer 5'acagaattcgccccggcctggtacactgcc3' (Figure 2.2A). Pure *APOE* ε2, *APOE* ε3, and *APOE* ε4 DNA were also amplified by PCR to use at as reference and were treated in the same way as unknown samples throughout. The reactions were then heated to 94°C for 10 minutes before being cycled 32 times in a thermal cycler (Thermo Fisher Scientific, Waltham, MA). The cycle consisted of 30 seconds of denaturing at 94°C, 30 seconds of annealing at 56°C and then 1 minute of elongation at 72°C (Figure 2.2A).

A

Forward primer: 5'taagcttggcacggctgtccaagg3'
Reverse primer: 5'acagaattcgccccggcctggtacactgcc3'

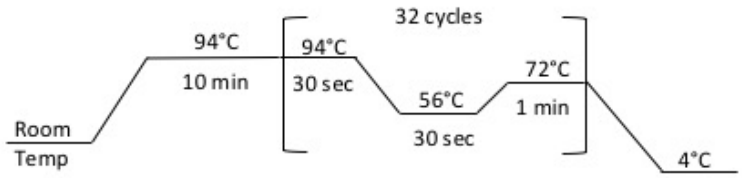

B

APOE 2: 38 bp, 16 bp, 91 bp, 18 bp, 81 bp

taagcttGGCACGGCTGTCCAAGGAGCTGCAGGCGGCGCAGGCCCGGCTGGGCGCGGACATGGAGGACGTGTGCGGCCGCCTGG
TGCAGTACCGCGGCGAGGTGCAGGCCATGCTCGGCCAGAGCACCGAGGAGCTGCGGGTGCGCCTCGCCTCCCACCTGCGCAAG
CTGCGTAAGCGGCTCCTCCGCGATGCCGATGACCTGCAGAAGTGCCTGGCAGTGTACCAGGCCGGGGCgaattctgt

APOE 3: 38 bp, 16 bp, 91 bp, 18 bp, 48 bp, 33 bp

taagcttGGCACGGCTGTCCAAGGAGCTGCAGGCGGCGCAGGCCCGGCTGGGCGCGGACATGGAGGACGTGTGCGGCCGCCTGG
TGCAGTACCGCGGCGAGGTGCAGGCCATGCTCGGCCAGAGCACCGAGGAGCTGCGGGTGCGCCTCGCCTCCCACCTGCGCAAG
CTGCGTAAGCGGCTCCTCCGCGATGCCGATGACCTGCAGAAGCGCCTGGCAGTGTACCAGGCCGGGGCgaattctgt

APOE 4: 38 bp, 16 bp, 19 bp, 72 bp, 18 bp, 48 bp, 33 bp

taagcttGGCACGGCTGTCCAAGGAGCTGCAGGCGGCGCAGGCCCGGCTGGGCGCGGACATGGAGGACGTGCGCGGCCGCCTGG
TGCAGTACCGCGGCGAGGTGCAGGCCATGCTCGGCCAGAGCACCGAGGAGCTGCGGGTGCGCCTCGCCTCCCACCTGCGCAAG
CTGCGTAAGCGGCTCCTCCGCGATGCCGATGACCTGCAGAAGCGCCTGGCAGTGTACCAGGCCGGGGCgaattctgt

C

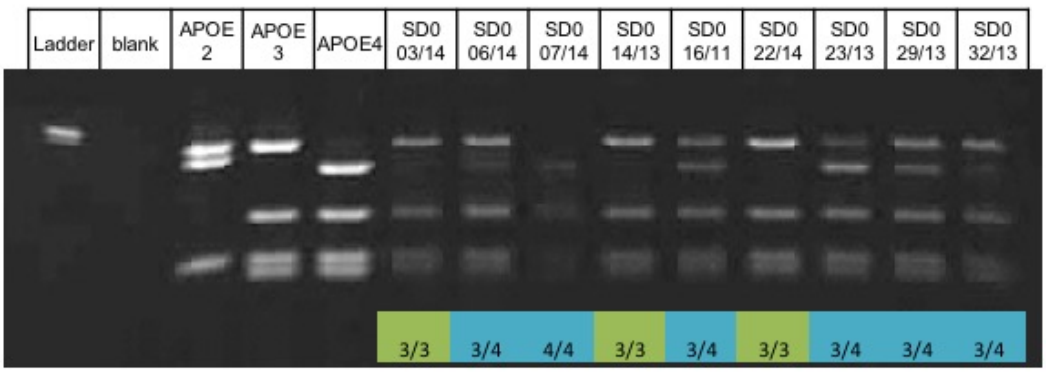

Figure 2.2: ApoE Genotyping method. The forward and reverse primers (A) are added to a PCR reaction tube along with DNA extracted from the cerebellum of human cases. PCR is run through the cycle depicted in A and the product is cut using the HhaI restriction endonuclease which cuts the PCR product at GCGC (in red) into different length segments depending on isoform (B). The resulting digestion is run on an electrophoresis gel (C) and analyzed.

Digestion

The product from PCR was then digested using the restriction endonuclease HhaI (New England Biolabs, Ipswich, MA). For this 0.5μl of enzyme, 2.5μl of 10x CutSmart buffer (New England Biolabs, Ipswich, MA) and 2μl of ddH_2O were added to each PCR reaction tube to give a total volume of 25μl. The final volume contains 50 mM Potassium Acetate, 20 mM Tris-acetate, 10 mM Magnesium Acetate, and 100 μg/ml BSA as a result of the CutSmart buffer and 10 units of HhaI. The mixture was then incubated overnight at 37°C. (Figure 2.2B)

Electrophoresis

After digestion incubation 5μl of 6x Blue Loading dye (Promega, Madison, WI) containing 0.4% orange G, 0.03% bromophenol blue, 0.03% xylene cyanol FF, 15% Ficoll® 400, 10mM Tris-HCl (pH 7.5) and 50mM EDTA (pH 8.0) was added to the the reaction tube. 14μl of this mixture was then loaded onto precast 15 well Novex TBE 20% gel (Thermo Fisher Scientific, Waltham, MA) using a 25μL Hamilton Syringe. The DNA were then separated by size using electrophoresis for 2 hours at 200V. The gels were run in an XCell SureLock™ Mini-Cell (Invitrogen, Carlsbad, CA) using Novex TBE running buffer (Thermo Fisher Scientific, Waltham, MA).

After electrophoresis, the gel was removed from the cassette and incubated in 15ml of 2μg/ml ethidium bromide (Sigma-Aldrich, St Louis, MO) diluted in 1x Novex TBE running buffer (Thermo Fisher Scientific, Waltham, MA) for 10 minutes. Alternatively, the gel was removed from the cassette and incubated in 15ml of 10x SYBR safe DNA Gel Stain (Thermo Fisher Scientific, Waltham, MA) diluted in 1x Novex TBE running buffer (Thermo Fisher Scientific, Waltham, MA). After incubation the gel was then visualized using UV light on a gene genius bio imaging system (Syngene, Cambridge, UK). The banding pattern of the resulting PCR and digestion indicated which *APOE* genotype an individual was (Figure 2.2 shows details) and pure *APOE* ε2, *APOE* ε3, and *APOE* ε4 DNA was used to confirm that the experiment worked.

2.2.4 Aβ ELISA

To assess the amount of Aβ in the human brain extract the Aβ42 (292-64501, Wako, Neuss, Germany) and Aβ40 (294-64701, Wako, Neuss, Germany) kits were used according to the manufacturers instructions. The protocol is the same for both the Aβ42 and Aβ40 kits and all reagents were provided by Wako unless otherwise stated. Solutions for a standard curve were made using the provided 100pmol/L Aβ40 and Aβ42 and the provided standard diluent. The standard curve contained 100, 50, 25, 10, 5, 2.5, and 1 (pmol/L) and all solutions were run in duplicate on the provided microplate. Brain extracts were diluted 1:20 using the provided standard diluent and were run in triplicate. 100µl of standard curve, brain extract or standard diluent (used as a blank) were added to each well of the provided microplate which was then covered using a plate seal and incubated overnight at 4°C with gentle shaking.

The plates were then washed 5 times using 200µl 1x wash solution before being incubated with 100µl of HRP-conjugated Antibody at 4°C for 2 hours with gentle shaking and a plate seal. The plate was washed again 5 times using 200µl 1x wash solution. 100µl of TMB solution was then added to the wells and the plate was incubated for 30 minutes in the dark at room temperature with a plate seal. 100µl of stop solution was then added to the well and the plate was then read at 450nm using a MRX micro plate reader (Dynex Technologies, Worthing, UK). The standard curve was then used to calculate the concentration of Aβ in the brain extract.

2.3 Biochemical isolation of synaptic fractions

2.3.1 Centrifugation method

This protocol is depicted in Figure 2.3A. About two hundred milligrams of fresh-frozen human brain tissue was homogenized in a glass dounce homogenizer with 1 mL ice-cold buffer C (0.32M Sucrose, 1mM EDTA and 5mM Tris-HCl pH 7.4). A 200-µL aliquot of the homogenate was saved. This was mixed with 200 µL water and 70 µL 10% SDS, and boiled to prepare the crude homogenate.

To prepare synaptosomes the remainder of the homogenate was centrifuged at 900G for 10 minutes. The supernatant was removed and saved and the pellet was resuspended in 300µl Buffer C and centrifuged at 900G for 10 minutes. The supernatant was removed and combined with the supernatant from the first centrifugation step. The pellet (P_1) was then snap frozen on dry ice.

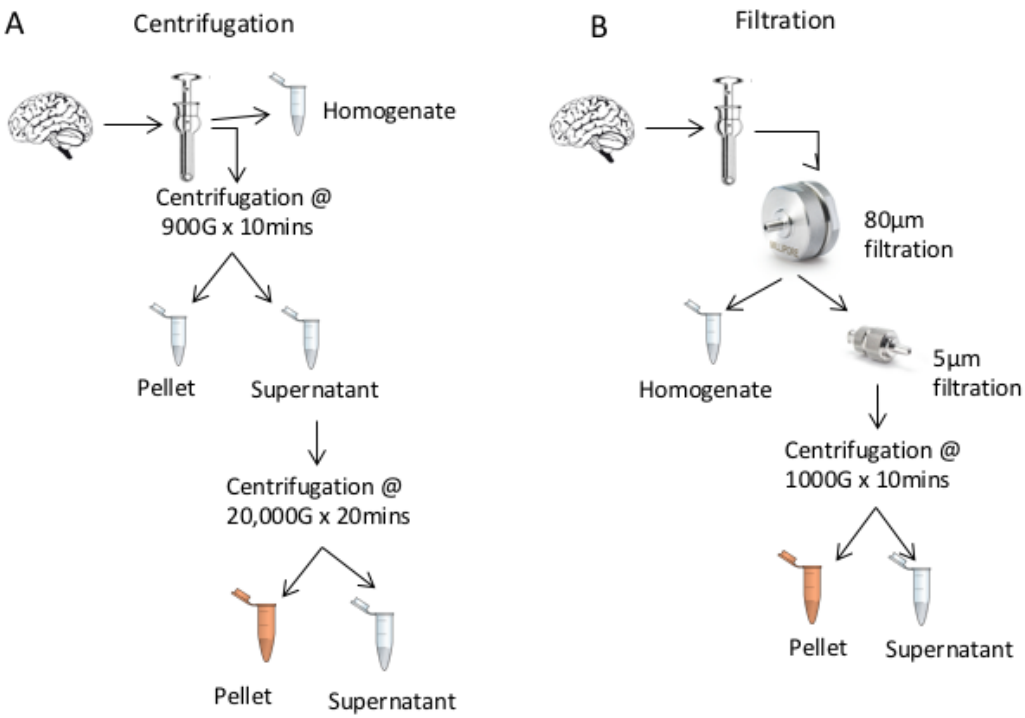

Figure 2.3: Two methods of isolating synaptic fractions. Synapses were isolated using serial centrifugation, first low speed centrifugation at 900G and then high speed centrifugation at 20,000G for 20 minutes (A). Synapses were also isolated using serial filtration (B) through first a 80µm filter and then a 5µm filter before low speed centrifugation at 1,000G.

The supernatant was divided into two fractions, one for western blotting and one for electron microscopy. Both fractions were centrifuged for 20 minutes at 20,000G to yield the synaptosome pellet. The supernatant was removed and snap frozen on dry ice. The synaptosome pellet for western blotting was resuspended in 400 µl of Buffer B (50 mmol/L Tris [pH 7.5], 1.5% SDS, and 2 mmol/L DTT) and boiled for 5 minutes. The pellet for electron microscopy was placed in 200µl of EM buffer (4% Paraformaldehyde, 2.5 % Gluteraldehyde in 0.1M Phosphate Buffer). After 48 hours in

EM buffer the EM pellet was transferred to 0.1M Phosphate buffer and kept at 4°C ready for EM embedding.

2.3.2 Filtration method

This protocol is depicted in Figure 2.3B. Synaptoneurosomes and crude homogenate were prepared according to Tai *et al.* (Tai *et al.*, 2012). About two hundred milligrams of fresh-frozen human brain tissue was homogenized in a glass dounce homogenizer with 1 mL ice-cold buffer A (25 mmol/L HEPES pH 7.5, 120 mmol/L NaCl, 5 mmol/L KCl, 1 mmol/L MgCl2, and 2 mmol/L CaCl2), supplemented with 2 mmol/L DTT, protease inhibitors (cOmplete mini, roche, Basel Switzerland), and phosphatase inhibitors (Millipore, Billerica, MA). The homogenate was passed through 2 layers of 80-µm nylon filters (Millipore, Billerica, MA), and a 200µL aliquot of the filtered homogenate was saved. The saved aliquot was mixed with 200 µL water and 70 µL 10% sodium dodecyl sulfate (SDS) and boiled to prepare the crude homogenate.

To prepare synaptoneurosomes, the remainder of the homogenate was passed through a 5-µm Durapor membrane filter (Millipore, Billerica, MA) to remove large organelles and nuclei. The Filtrate was centrifuged at 1,000G for 10 minutes. The supernatant containing cytoplasmic proteins was removed, and the pellet was resuspended in 200µl buffer A. If needed the resuspended pellet was divided into three microcentrifuge tubes, one for electron microscopy (EM), one for western blots, and one for proteomics and all were centrifuged again at 1,000G for 5 minutes. The supernatant was discarded and the synaptoneurosome pellets for western blot and proteomics were snap frozen on dry ice and then transferred to -80°C.

The pellet for electron microscopy was placed in 200µl of EM buffer (4% Paraformaldehyde, 2.5 % Gluteraldehyde in 0.1M Phosphate Buffer). After 48 hours in EM buffer the EM pellet was transferred to 0.1M Phosphate Buffer (PB) and kept at 4°C ready for EM embedding. The synaptoneurosome pellet for western blotting was resuspended in 400 µL of Buffer B (50 mmol/L Tris [pH 7.5], 1.5% SDS, and 2 mmol/L DTT) and boiled for 5 minutes. 10% SDS was added to the supernatant fraction to bring it up to 1.5% SDS and this was also boiled for 5 minutes to prepare for western blotting.

2.4 Electron Microscopy

2.4.1 Embedding the prep

Pellets to be embedded for EM were centrifuged at 10,000G for 2 minutes to compact the pellet further. Pellets were then washed twice in 0.1M PB for 10 minutes before being incubated for 30 minutes in 1% osmium tetroxide in 0.1M PB in the dark with gentle agitation. Pellets were then washed twice in 0.1M PB and three times in boiled dH_2O for 15 minutes each. Pellets were then dehydrated in 50% ethanol for 15 minutes before being exposed to uranyl acetate (1% in 70% ethanol) for 40 minutes in the dark with gentle agitation. Samples were then incubated for 15 minutes in each of an ascending concentration of ethanol (95%, 100%, 100%) before being incubated in propylene oxide for 15 minutes. Pellets were then incubated with Durcupan resin overnight at 4°C before being embedded in Durcupan resin which was polymerized by being baked at 60°C for 48 hours.

2.4.2 Transmission Electron Microscopy Imaging

EM blocks were cut into 70nm sections with a Leica Ultracut microtome (as described for array tomography) and mounted onto formvar/carbon coated EM grids. These were imaged on a JOEL TEM in the Philly Dake Electron microscopy Center at Massachusetts General Hospital (with thanks to Prof Marian DiFiglia for use of the microscope). TEM imaging was performed by Professor Tara Spires-Jones.

2.5 Proteomics

2.5.1 Extracting the proteins from the prep

Synaptoneurosome pellets were stored at -80°C until ready for extraction. 100µl of extraction buffer (100nM Tris-HCL pH7.6, 4% (w/v) SDS) with protease inhibitors (cOmplete mini, roche, Basel, Switzerland) was then added to each tube containing the prep. The prep was then mixed by pipetting up and down and was then spun at 20,000 G in a 5417R centrifuge (Eppendorf, Hamburg, Germany). The supernatant was then collected in a clean tube protein assayed and stored at -80°C.

2.5.2 LC-MS/MS

Peptides were generated desalted and run through nLC/MS-MS by the team at FingerPrints Proteomics in Dundee. The protocol used was as in Sarvestany 2014 (Sarvestany *et al.*, 2014).

2.5.3 Progenesis

Raw data from the LC/MS-MS was imported into Progenesis QI (Nonlinear Dynamics, Newcastle upon Tyne, UK). Data were aligned and peptides were filtered (power >0.7, $p<0.05$). Data sets were exported from Progenesis for subsequent identification of peptides sequences (94,569 peptides) using Mascot Search Engine (Matrix Science, Boston, MA). Mascot -generated data was imported into Progenesis for protein expression comparison. Quantification of protein expression was only done on proteins identified by two or more unique peptides. Using these requirements 1,043 proteins were detected across all samples. Proteins were considered significantly different in abundance if $p<0.05$ and fold change was >1.2. p values were calculated by Progensis using one-way ANOVA and fold change was calculated in excel. Progenesis was run by the Whishart group at the Roslin Institute and Mascot was run by the team at FingerPrints Proteomics in Dundee.

2.5.4 IPA

In-silico pathway analysis was performed using Ingenuity Pathway Analysis (IPA) (Qiagen, Hilden, Germany) software with the help of the Wishart group at the Roslin Institute. All proteins which met significance cut offs ($p < 0.05$, fold changes > 1.2) for each observation (control v AD, control APOE3 v control APOE4, AD APOE3 v AD APOE4) were uploaded into IPA. Analysis was set so that all experimentally observed direct and indirect relationships from all data sources were assessed. These relationships were allowed to have been observed in all species and cell lines. Network analysis was caped at 35 molecules per network with up to 10 networks per observation.

2.5.5 DAVID

Database for Annotation, Visualization and Integrated Discovery (DAVID) was used to assess enrichment of GO terms and functionally related gene groups (Huang *et al.*, 2009). All proteins which met significance cut offs ($p < 0.05$, fold changes > 1.2) for each observation (control v AD, control APOE3 v control APOE4, AD APOE3 v AD APOE4) were uploaded into DAVID as were all proteins detected. DAVID was also used to convert the assession codes into official gene symbols for use in IPA analysis. DAVID analysis was performed on the given gene list with the *Homo sapiens* background and functional annotation clustering was used.

2.6 Extracting Aβ from human brain

This protocol is depicted in Figure 2.4.

2.6.1 aCSF extraction of Aβ

Artificial cerebrospinal fluid (aCSF) (124mM NaCl, 2.8mM KCl, 1.25mM NaH_2PO_4, 25.9mM $NaHCO_3$) was made fresh on day 1 of the protocol, filtered through a 0.2μm filter, and kept at 4°C until needed. Protease inhibitors (cOmplete mini, roche, Basel, Switzerland) were added fresh to 10ml of aCSF and which was then kept on ice. 0.2g of brain was defrosted and homogenized in 1ml of aCSF with protease inhibitors using 50 strokes of a dounce homogenizer. Homogenates were kept on ice until all brain samples were processed and were then loaded into 600μl ultracentrifuge tubes (41121703, Beckman Coulter, High Wycombe, UK). Samples were spun at 200,000G for 110 minutes at 4°C using a TLA 120.1 rotor (Beckman Coulter, High Wycombe, UK) and an optima max-xp ultracentrifuge (Beckman Coulter, High Wycombe, UK). The supernatant was then removed and all AD or control cases were pooled (Shankar *et al.*, 2010).

2.6.2 Dialysis

To remove any potentially active compound from the human homogenate dialysis was used with 2kDa pore size. A 2000 molecular weight cut off dialysis cassette

(87719, Thermo Fisher Scientific, Waltham, MA) was prepared by soaking it in aCSF for 2 minutes. The cassette was then opened and 15ml of of aCSF was added using a 10ml pipette to ensure the buffer does not leak. The aCSF was then discarded and the Aβ extract was added and the lid secured. The cassette was placed in a 1L bucket of aCSF overnight at 4°C with gentle stirring. The aCSF in the bucket was then replaced and after 24 hours was replaced for a second time. 24 hours later the cassette was removed from the bucket and aliquoted or used for Immunodepletion.

Table 2.1: Aβ extraction case information

	Case Number	Diagnosis	Sex	ApoE Genotype	MRC BBN
AD Pool 1	52/12	AD	M	3/4	9505
	28/13	AD	F	3/4	15259
	19/14	AD	M	4/4	20995
	18/13	AD	F	3/4	15810
Control Pool 1	14/13	NDC	F	3/3	14395
	46/13	NDC	M	3/3	18407
	35/14	NDC	F	3/4	22629
Control ApoE3 Pool	34/15	NDC	M	3/3	26308
	10/15	NDC	F	3/3	24780
	38/13	NDC	M	3/3	18391
Control ApoE4 Pool	46/13	NDC	M	3/4	18407
	11/15	NDC	M	3/4	24781
	54/13	NDC	F	4/4	19687
AD ApoE3 Pool	02/14	AD	F	3/3	19994
	45/13	AD	F	3/3	19600
	35/13	AD	F	3/3	18798
AD ApoE4 Pool	46/14	AD	F	4/4	24360
	38/14	AD	F	3/4	23394
	21/13	AD	F	3/4	15811
	28/13	AD	F	3/4	15259
AD Pool 2	988	AD	F	4/4	-
	1028	AD	F	3/3	-
	970	AD	F	3/4	-
AD Pool 3	1003	AD	F	3/3	-
	1636	AD	M	3/3	-
	1329	AD	F	3/4	-

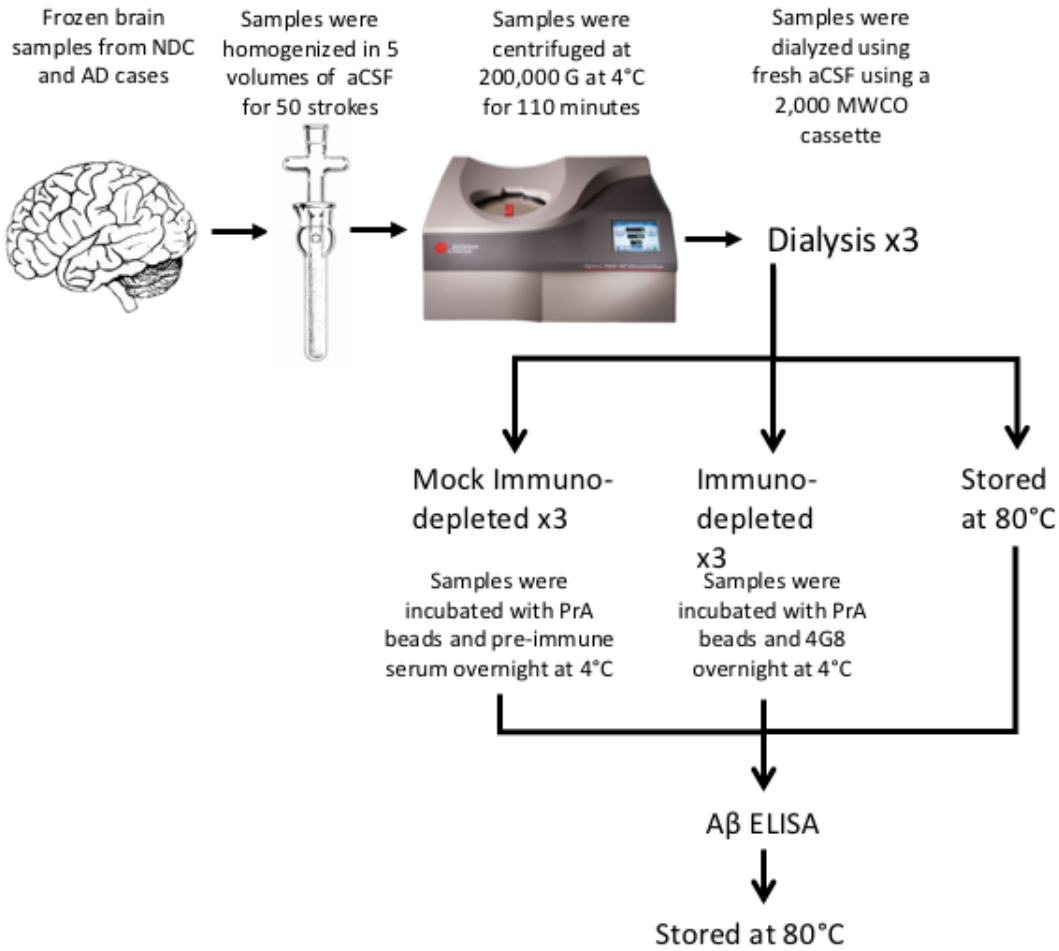

Figure 2.4: Schematic showing isolation of Aβ from human tissue. 0.2g of human cortex was homogenized in 1ml of aCSF in a dounce homogenizer. This was then centrifuged at 200,000G for 110 minutes at 4C. Samples were then dialyzed to remove small molecules. Some of the extract was then immuno-depleted or mock immuno-depleted of Aβ and ELISA was used to determine Aβ amount.

2.6.3 Immunodepletion of Aβ

To ensure that Aβ is the toxic element in AD brain homogenate, some brain homogenate was immunodepleted of Aβ using 4G8 an antibody against Aβ. To ensure that the immunodepletion protocol did not effect the toxicity of the homogenate a different aliquot of homogenate was depleted using pre-immune mouse serum.

Protein A (PrA) beads (Thermo Fisher Scientific, Waltham, MA) were washed 3 times in aCSF by resuspending in double the amount of aCSF, centrifuging at 6,000 rpm for 5 minutes and then removing the supernatant. 0.8ml aliquots of Aβ extract were placed in pro-lo bind tubes (Sigma-Aldrich, St Louis, MO) and marked either for

immunodepletion (ID) or mock immunodepletion (MID). For ID aliquots 40μl of washed PrA beads were added to the aliquot along with 8μl of mouse anti-Aβ (4G8, BioLegend, San Diego, CA). For MID, PrA beads and 8μl of pre-immune mouse serum (Sigma-Aldrich, St Louis, MO) were added to the extract. All tubes were then incubated for 24 hours at 4°C with constant mixing. Tubes were then centrifuged at 6,000 rpm for 5 minutes. The supernatant was then removed and placed in a new tube along with 30μl fresh PrA beads and either 4G8 or sera as appropriate. Tubes were then incubated for 24 hours at 4°C with constant mixing. This occurred for three round of immunodepletion at which point the supernatant was incubated with 50μl of PrA beads only for 4 hours at 4°C with constant mixing. After a final centrifugation at 6,000 rpm for 5 minutes, the supernatant was removed and aliquots were pooled as ID or MID samples and realiquoted. One aliquot was used for Aβ ELISA and the others were stored at -80°C until added to cell culture.

2.7 Cell culture

2.7.1 NPC culture

All reagents for growing and maintaining cells were purchased from Life Technologies (Carlsbad,CA) unless otherwise stated. Neuronal precursor cells (NPC) were derived from induced pluripotent stem cells (iPSC) made from a control individual by Dr. Karen Burr in the Chandran lab as previously described (Bilican *et al.*, 2014). NPCs were maintained at high density in NPC media (DMEM/F12, 1% PSF, 1% Glutamax, 1% N2, 0.1% B27, and 10 ng/mL FGF2 (PeproTech, London, UK)) and were passaged 1:2 once a week using Acutase (Sigma-Aldrich, St Louis, MO). Cells were maintained in a 6 well plate coated with 1:100 Reduced-growth factor Matrigel (BD Biosciences, Oxford, UK) and were kept at 37°C with 3% O_2, 5% CO_2 and high humidity (Panasonic Biomedical, Loughborough, UK).

2.7.2 Coating Coverslips

To coat the coverslips, 1 round 13mm thickness No. 0 glass coverslip (VWR, Radnor, PA) was placed into the well of a 24 well plate and incubated with 1:100 poly-

ornithine (Sigma-Aldrich, St Louis, MO) in water for embryo transfer overnight at room temperature. The poly-orninthine was then removed and the coverslips washed three times in water for embryo transfer (Sigma-Aldrich, St Louis, MO) before being allowed to dry completely. The coverslips and plates were then placed under a UV light inside a laminar flow hood for 25 minutes. The coverslips were the incubated with a coating solution (0.01mg/ml Laminin (Sigma-Aldrich, St Louis, MO), 0.02mg/ml Fibronectin (Sigma-Aldrich, St Louis, MO), 1:10 matrigel (BD Biosciences, Oxford, UK) in DMEM/F12) overnight at 4°C. This coating was then removed immediately prior to cell plate down. Cells were maintained at 37°C with 3% O_2, 5% CO_2 and high humidity (Panasonic Biomedical, Loughborough, UK).

2.7.3 Cortical Neuron Culture

To generate cortical neurons NPCs were lifted using Actuase and then plated down in 0.5ml default media (DMEM/F12, 1% P/S, 0.5% Glutamax, 0.5% N2, 0.2% B27, 2 μg/mL Heparin (Sigma-Aldrich, St Louis, MO)) onto coated coverslips at a density of 100,000 cells per well of a 24 well plate. On day 4 the existing media was topped up with 0.5ml of default media. After this cells were fed using a half media change twice a week. Default media was supplemented with 10μM Forskloin (Tocris Biosciences, Bristol, UK) for weeks 2 and 3 and with 5 ng/mL BDNF (R&D Biosystems, Minneapolis, MN) and 5 ng/mL GDNF (R&D Biosystems, Minneapolis, MN) until cells were fixed.

2.7.4 Addition of siRNA

To knock down the expression of Clusterin siRNA (sc-43688, Santa Cruz Biotechnology, Dallas, TX) was used and control siRNA-A (sc-370007, Santa Cruz Biotechnology, Dallas, TX) was used as control. For each well, 3μl of siRNA was mixed with 34μl of transfection media (sc-36868, Santa Cruz Biotechnology, Dallas, TX). Separately, 2.5μl of transfection reagent (sc-29528, Santa Cruz Biotechnology, Dallas, TX) was mixed with 34.5 μl of transfection media. The siRNA mixture was then added to the transfection reagent mixture and mixed by pipetting. The solution was then incubated for 30 minutes at room temperature in the dark.

7.5 week old neurons were removed from the incubator and the media was aspirated off. They were then washed twice with transfection media. 300μl of transfection media was added to the siRNA mix and it was then applied to the cells. The neurons were returned to the incubator for 7 hours before 200μl of BDNF/GDNF media was added. The cells were then left for 48 hours and then the media was replaced with fresh BDNF/GDNF media or human derived Aβ in BDNF/GDNF media for 48 hours before fixing or lysing for western blot. Cells for western blot were scraped from the plate surface in sterile PBS and then pelleted at 6,000G for 2 minutes. The supernatant was removed and the cells were lysed in Buffer B (50 mmol/L Tris [pH 7.5], 1.5% SDS, and 2 mmol/L DTT).

2.7.5 Addition of human derived Aβ

7.5-8.5 week old neurons were removed from the incubator and the current media was removed. The media was then replaced with brain extract, immunodepleted brain extract or the same volume of aCSF and the total volume in the well was topped up to 500μl with BDNF/GDNF media. Cells were then incubated at 37°C with 3% O_2, 5% CO_2 and high humidity for 48 hours before the media was removed and the cells were fixed in 4% PFA for 20 minutes.

2.7.6 Staining and imaging

Fixed cells were washed 3 times with PBS and then permeabilized with 0.5% triton in PBS for 20 minutes at room temperature. Cells were then washed three times for 5 mintues with PBS. Cells were then blocked for 2 hours at room temperature with gentle shaking in 5% normal goat serum and 5% normal donkey serum in PBS. Cells were then incubated with primary antibodies which were diluted in 1% normal goat serum in PBS at 4°C over night with gentle shaking. Primary antibodies and dilutions used were 1:1000 guinea pig anti-MAP2 (188 004 synaptic systems, Goettingen, Germany), 1:500 mouse anti-synaptophysin (Ab 8049, abcam, Cambridge, U.K.) and 1:1000 rabbit anti-PSD95 (D27E11, Cell Signaling, Leiden, The Netherlands).

Cells were then washed 3 times with PBS before being incubated with secondary antibodies diluted in 1% normal goat serum in PBS for 2 hours at room temperature in the dark with gentle shaking. Secondaries used were goat anti-rabbit cy5 (97077, abcam, Cambridge, UK), goat anti-mouse cy3 (97035, abcam, Cambridge, UK), and goat anti guinea pig 488 (706-545-148, Jackson ImmunoResearch, West Grove, PA) and all were used at a 1:700 dilution. After incubation with secondary antibodies cells were washed 3 times in PBS and then incubated with DAPI diluted 1:10,000 in PBS for 10 minutes at room temperature in the dark with gentle shaking. Cells were then washed 3 times with PBS and cover slips were removed from the culture plate and mounted using Immunomount (Thermo Fisher Scientific, Waltham, MA) onto microscope slides.

Cells were imaged using a Leica DM6 CS upright microscope with a TCS SP8 confocal platform. 5-10 z-stacks per coverslip were obtained at 63x using a 250μm step. The coverslip was randomly sampled excluding areas where cells had detached from the coverslip.

2.7.7 iPSC neuron Image processing

Images were converted to tiffs and each channel stack was flattened to a single image using the maximum intensity of each pixel using custom image J macros (appendix 4). Background subtraction was then performed in image J using a 30 pixel rolling ball and then images were processed using custom cell profiler pipelines (Carpenter *et al.*, 2006; Nieland *et al.*, 2014)(appendix 4). CellProfiler was used to select MAP2 positive dendrites but exclude cell bodies. The pipeline then when on to find synaptic puncta which co-localized with MAP2 using a local maxima and primary characteristic selection of the synaptic channels. The output of this was an excel spreadsheet where the number of synaptic puncta per dendrite and the length of the dendrite were outputs. Excel was then used to calculate the number of synaptic puncta per μm of dendrite and a mean of all dendrites over 5μm from each coverslip was generated for each well.

Different plate downs had slightly different cell densities and thus slightly different synaptic puncta densities. To compare between plate downs a percent of control value was calculated. To calculate this value a mean of all control wells (aCSF) was generated. All wells were then compared with this mean value. For plates that had siRNA added the mean value was generated from the control well (aCSF) with control siRNA added.

3 Investigating the effect of wild type human tau on synapse loss using array tomography in a novel mouse model of Alzheimer's Disease

3.1 Background and Aims

The vast majority of AD cases have no known genetic cause, however the discovery that mutations in the proteins responsible for Aβ production, namely APP, PS1, and PS2, are responsible for rare genetic AD gave rise to the Aβ cascade hypothesis. This hypothesis posits that Aβ is responsible for the initiation of disease and that all other pathologies including the glial, neuronal, and tau related neuropathological hallmarks follow on from Aβ deposition (Hardy and Higgins, 1992). The Aβ hypothesis is well supported by genetic evidence as sporadic cases of AD have the same neuropathological hallmarks as familial forms of the disease and it is this hypothesis that many of our animal models of AD are based on, with mutated human APP, PS1, or both knocked into various mouse lines. However, these mouse models do not recapitulate all of the pathological features of AD especially the NFTs associated with tau or the gross neuron loss seen in AD. Mutations in tau that cause NFTs in mice are causative of FTD in humans rather than AD and yet NFTs correlate better with the cognitive decline seen in AD cases (Hutton, 2000; Ingelsson *et al.*, 2004). However neither tau nor Aβ pathology correlate as well with cognitive decline as synaptic loss although mouse lines expressing either fAD mutations or tau mutations both show synapse loss (Koffie *et al.*, 2009; Lasagna-Reeves *et al.*, 2011). These two pathologies when co-expressed in a mouse model affect each other but the molecular pathways linking Aβ and wild type tau to synapse degeneration require further elucidation (Oddo *et al.*, 2003; Pooler *et al.*, 2015).

This chapter investigates the interactions between wild type human tau and Aβ by using a novel mouse model to analyse the effects of human tau on Aβ induced pathologies and most particularly within the context of this thesis, the synaptic toxicity.

There is strong evidence that tau is necessary for Aβ mediated synapse loss and memory deficits and reducing tau in an fAD mouse model protects against synaptic pathology and cognitive impairment(Roberson *et al.*, 2007). Equally there is evidence that Aβ pathology affects tau distribution and pathology in both humans and mice (Pooler et al., 2015; Sepulcre et al., 2016). This novel model was used to assess the impact of wild type human tau on Aβ pathology and the effect of Aβ on non-mutant tau.

This chapter is made up of a published paper (Jackson *et al.*, 2016) and my contribution involved the data collection and analysis of synapses by array tomography (Figures 5 and 6). I also contributed to Figure 3 by increasing the n for the neurite curvature experiments and performed the western blots for Figure 4. All other data was collected by the co-authors particularly, Dr. Nikita Rudinskiy, Mr. Shaun Croft, Ms. JeeSoo Monica Kim, and Ms. Veselina Petrova and analysed by me. The manuscript was written by me with input from co-authors most particularly Prof. Tara Spires-Jones.

EJN European Journal of Neuroscience

FENS Federation of European Neuroscience Societies

European Journal of Neuroscience, Vol. 44, pp. 3056–3066, 2016 doi:10.1111/ejn.13442

MOLECULAR AND SYNAPTIC MECHANISMS

Human tau increases amyloid β plaque size but not amyloid β-mediated synapse loss in a novel mouse model of Alzheimer's disease

Rosemary J. Jackson,[1] Nikita Rudinskiy,[2] Abigail G. Herrmann,[1] Shaun Croft,[1] JeeSoo Monica Kim,[1] Veselina Petrova,[1] Juan Jose Ramos-Rodriguez,[3] Rose Pitstick,[4] Susanne Wegmann,[2] Monica Garcia-Alloza,[3] George A. Carlson,[4] Bradley T. Hyman[2] and Tara L. Spires-Jones[1]

[1]Centre for Cognitive and Neural Systems and Centre for Dementia Prevention, The University of Edinburgh, 1 George Square, Edinburgh, EH8 9JZ, UK

[2]Massachusetts General Hospital and Harvard Medical School, Charlestown, MA, USA

[3]University of Cadiz, Cadiz, Spain

[4]McLaughlin Research Institute, Great Falls, MT, USA

Keywords: Alzheimer, amyloid beta, plaque, synapse, tau

Edited by Giovanna Mallucci

Received 11 July 2016, revised 21 September 2016, accepted 13 October 2016

Abstract

Alzheimer's disease is characterized by the presence of aggregates of amyloid beta (Aβ) in senile plaques and tau in neurofibrillary tangles, as well as marked neuron and synapse loss. Of these pathological changes, synapse loss correlates most strongly with cognitive decline. Synapse loss occurs prominently around plaques due to accumulations of oligomeric Aβ. Recent evidence suggests that tau may also play a role in synapse loss but the interactions of Aβ and tau in synapse loss remain to be determined. In this study, we generated a novel transgenic mouse line, the APP/PS1/rTg21221 line, by crossing APP/PS1 mice, which develop Aβ-plaques and synapse loss, with rTg21221 mice, which overexpress wild-type human tau. When compared to the APP/PS1 mice without human tau, the cross-sectional area of ThioS+ dense core plaques was increased by ~50%. Along with increased plaque size, we observed an increase in plaque-associated dystrophic neurites containing misfolded tau, but there was no exacerbation of neurite curvature or local neuron loss around plaques. Array tomography analysis similarly revealed no worsening of synapse loss around plaques, and no change in the accumulation of Aβ at synapses. Together, these results indicate that adding human wild-type tau exacerbates plaque pathology and neurite deformation but does not exacerbate plaque-associated synapse loss.

Introduction

Alzheimer's disease (AD) is a progressive neurodegenerative disease that is the most common cause of dementia in the elderly. It is characterized neuropathologically by the aggregation of amyloid beta (Aβ) into senile plaques and tau into neurofibrillary tangles (NFTs), as well as by pronounced synapse loss, neuron loss and gliosis (Duyckaerts *et al.*, 2009).

The amyloid cascade hypothesis of disease pathogenesis posits that AD is initiated by the accumulation of Aβ, which then leads to glial-, neuronal- and tau-related neuropathological hallmarks (Hardy & Higgins, 1992). This hypothesis is strongly supported by the genetics of familial early onset AD, which is caused by mutations in the proteins that are essential for the generation of Aβ: amyloid precursor protein (APP), presenilin-1 (PS1) and presenilin-2 (PS2; Tanzi, 2012). The accumulation of Aβ plaques correlates less well with cognitive decline in AD than NFTs (Ingelsson *et al.*, 2004), although mutations in the tau gene, *Mapt,* cause fronto-temporal dementia (FTD) but not AD (Hutton, 2000). However, neither plaques nor tangles correlate as well with cognitive decline as synapse loss, emphasizing the important role of synapse toxicity for pathogenesis and disease progression in AD (Spires-Jones & Hyman, 2014).

Animal models and human studies have shown that soluble oligomers of both Aβ- and FTD-associated mutant tau contribute to synapse loss (Walsh *et al.*, 2002; Shankar *et al.*, 2008; Koffie *et al.*, 2009, 2012; Kopeikina *et al.*, 2011; Lasagna-Reeves *et al.*, 2011; Bilousova *et al.*, 2016). When expressed in the same animal model, these small pathological molecules can affect the distribution and pathology of each other (Oddo *et al.*, 2003; Pooler *et al.*, 2015). Modulation of one of the pathologies often affects the other in these models, strongly indicating that these processes are interconnected

Correspondence: Tara L. Spires-Jones, as above.
E-mail: tara.spires-jones@ed.ac.uk

(Oddo *et al.*, 2006; Castillo-Carranza *et al.*, 2015) but the molecular pathways linking Aβ, tau, and synapse degeneration remain largely unknown.

There is strong evidence that tau is necessary for Aβ-mediated synaptic pathology in animal models of plaque deposition. Genetically reducing endogenous tau is protective against synaptic phenotypes including LTP deficits, seizures, and axonal transport deficits (Roberson *et al.*, 2007, 2011; Shipton *et al.*, 2011; Vossel *et al.*, 2015). However, there are alternative hypotheses stipulating that tau and Aβ pathologies start independently but then act synergistically to cause synapse loss and cognitive decline (Small & Duff, 2008).

In this study, we examine Aβ-plaque load and synapse loss in the presence of human tau. We generate a mouse model (APP/PS1/rTg21221) of early AD, in which mutant human APP, PS1, and wild-type human tau are co-expressed. This novel mouse line allows analysis of interactions of human tau and Aβ in a mammalian brain with age-related pathology (which cannot be fully recapitulated *in vitro*). APP/PS1 mice expressing both mutant APP and PS1 (but no human tau) show plaque deposition at 4–6 months of age (Jankowsky *et al.*, 2004). Cognitive impairments, synapse loss around plaques (Koffie *et al.*, 2009) and disruption of Ca2+ regulation in dendritic spines are well-established phenotypes of this line (Wu *et al.*, 2010). In contrast, rTg21221 mice that overexpress wild-type human tau (hTau) show only slight behavioral phenotypes and tau hyperphosphorylation, no tau aggregation into NFTs, and no synapse loss (Hoover *et al.*, 2010). By crossing these two lines, we tested the synergy between Aβ and tau, how tau contributes to Aβ-related pathology, and how Aβ effects non-mutant tau.

We hypothesized that increasing the amount of tau in a mouse model of AD would worsen synapse loss. However, surprisingly, we found that while over-expressing wild-type human tau increases Aβ-plaque size and dystrophic neurite number, it does not exacerbate Aβ-mediated synapse loss, neuron loss or gliosis.

Materials and methods

Generation of App/PS1/rTg21221 mice

B6.C3 APP/PS1 mice (stock #004462, Jackson Laboratories Bar Harbor, ME), which express APP^{swe} and $PS1^{\Delta exon9}$ (Jankowsky *et al.*, 2004), were crossed with B6.129-Tg(CK-tTA) mice that express the tet transactivator, CK-tTA, under the control of the calcium calmodulin kinase 2 alpha (CamK2α) promoter. Offspring positive for both the APP/PS1 and CK-tTA transgene were then crossed to transgene homozygous Tg(tetO-$HuTau_{wt}$) 21221 mice (Hoover *et al.*, 2010). Expression of human wild-type human 4-repeat tau in rTg21221 mice is under the control of a dox-off tetracycline transactivator responsive promoter. Mice positive for the APP/PS1, CK-tTA and rTg21221 transgenes (APP/PS1/rTg21221) overexpress APP^{swe} and $PS1^{\Delta exon9}$ as well as wild-type human tau in the forebrain.

Mice used were 8–10 months old and of mixed sex. Animals were group housed, and had *ad libitum* access to food and water. Animals were killed with CO_2 and brains collected. Brain hemispheres were fixed for 48 h in 4% paraformaldehyde (PFA) in PBS, cryoprotected in 15% glycerol in PBS, then frozen in dry ice and sectioned into 50 μm thick coronal sections using a freezing microtome (Leica 2010R). From the other hemisphere, small samples of somatosensory cortex ($1 \times 1 \times 5$ mm^3) were dissected freshly from each brain for array tomography, and the remainder brain tissue was flash-frozen at −80 °C for biochemical analyses. The number of animals used in each experiment can be found in the figure legend for that experiment. All animal experiments conformed to national and institutional guidelines including the Animals [Scientific Procedures Act] 1986 (UK), and the Council Directive 2010/63EU of the European Parliament and the Council of 22 September 2010 on the protection of animals used for scientific purposes, and had full IACUC and Home Office ethical approval.

Synaptoneurosome preparation

Synaptoneurosomes and crude homogenate were prepared as described previously (Tai *et al.*, 2012). In brief, < 100 mg of frozen murine frontal cortex was homogenized in 700 μL of ice-cold buffer A (25 mmol/L HEPES pH 7.5, 120 mmol/L NaCl, 5 mmol/L KCl, 1 mmol/L MgCl2 and 2 mmol/L CaCl2), supplemented with 2 mmol/L di-thiothreitol, protease inhibitors (Roche complete mini) and phosphatase inhibitors. The homogenate was passed through two layers of 80-μm nylon filters (Millipore, Watford, UK), and a 200 μL aliquot of the filtered homogenate was saved. The saved aliquot was mixed with 200 μL water and 70 μL 10% SDS, to prepare the crude homogenate.

To prepare synaptoneurosomes, the remainder of the homogenate was passed through a 5-μm Durapor membrane filter (Millipore) to remove large organelles and nuclei and centrifuged at 1000 ***g*** for 5 min. The non-synaptic supernatant containing cytoplasmic proteins was removed, and the pellet was washed once with buffer A and centrifuged again, yielding the synaptoneurosome pellet. The synaptoneurosome pellet was suspended in 400 μL of Buffer B (50 mmol/L Tris [pH 7.5], 1.5% SDS, and 2 mmol/L DTT) and boiled for 5 min. Protein concentrations were determined using a BSA assay (Thermo Fisher, Renfrew, UK).

Western blotting

Five microgram of protein from either isolated synaptoneurosomes or crude homogenate was loaded onto NuPAGE 4–12% Bis-Tris precast polyacrylamide 15 well gels (Invitrogen, Paisley, UK) along with molecular weight marker (Li-Cor, Cambridge, UK). Proteins were electro-transferred to nitrocellulose membrane (Bio-Rad, Hemel Hempstead, UK). Membranes probed with the following primary antibodies: Aβ(82E1,IBL,1 : 100), Tau13 (MMS-520R-500, Covance, 1 : 2000), β-actin (ab8226, Abcam, 1 : 2000), Synaptophysin (AB8049, Abcam, 1 : 10 000), α-tubulin (ab4074, Abcam, 1 : 1000), GFAP (0334, DakoCytomation, 1 : 500), GAPDH (ab8245, Abcam, 1 : 2000). Proteins were visualized on an ODYSSEY infrared system using the appropriate 680 and 800 IR dye secondary antibodies (1 : 50 000, LI-COR Biosciences) and were analyzed using ODYSSEY software (LI-COR Biosciences).

ELISA

Aβ42 concentration was quantified, in isolated synaptoneurosomes, using a colorimetric Aβ42 ELISA kit (Wako, Japan) as previously described with minor modifications (Ramos-Rodriguez *et al.*, 2016). Briefly, 5 μL of synaptoneurosomes were diluted in 50 μL of lysis buffer with inhibitor cocktail (Thermo Scientific Pierce, Spain). Samples were loaded and standard curves were completed with human Aβ42 provided in the kit. Absorbance was measured spectrophotometrically at 450 nm (MQX200R2, Biotekinstruments, Burlington VT, USA) and data were expressed as pMol Aβ42/mg synaptoneurosome protein.

Immunohistochemical analyses of plaque load, neuron loss, gliosis and neurite damage

To quantify plaque-associated neuron loss, a series of every 10th coronal section through the brain hemisphere was stained with 0.05% Thioflavin-S (ThioS) in 50% ethanol for 8 min to label dense-core plaques and NFTs and washed in 80% ethanol for 30 s. Sections were then permeabilized for 10 min in 0.1% Triton X-100 in TBS, washed twice for 5 min in TBS, then incubated in NeuroTrace red fluorescent Nissl stain (1 : 500; Molecular Probes, Inc.) for 1 h at room temperature to label neurons. Sections were mounted onto superfrost plus slides using Immuno-Mount mounting media and a cover slip was placed on top. Another series of sections were stained with primary antibody against glial-fibrillary acidic protein (GFAP; 1 : 1000, Dako Cytomation 0334) to stain for reactive astrocytes and the Alexa Fluor conjugated secondary antibody donkey anti-rabbit 647 (1 : 200; Life Technologies, Carlsbad, CA).

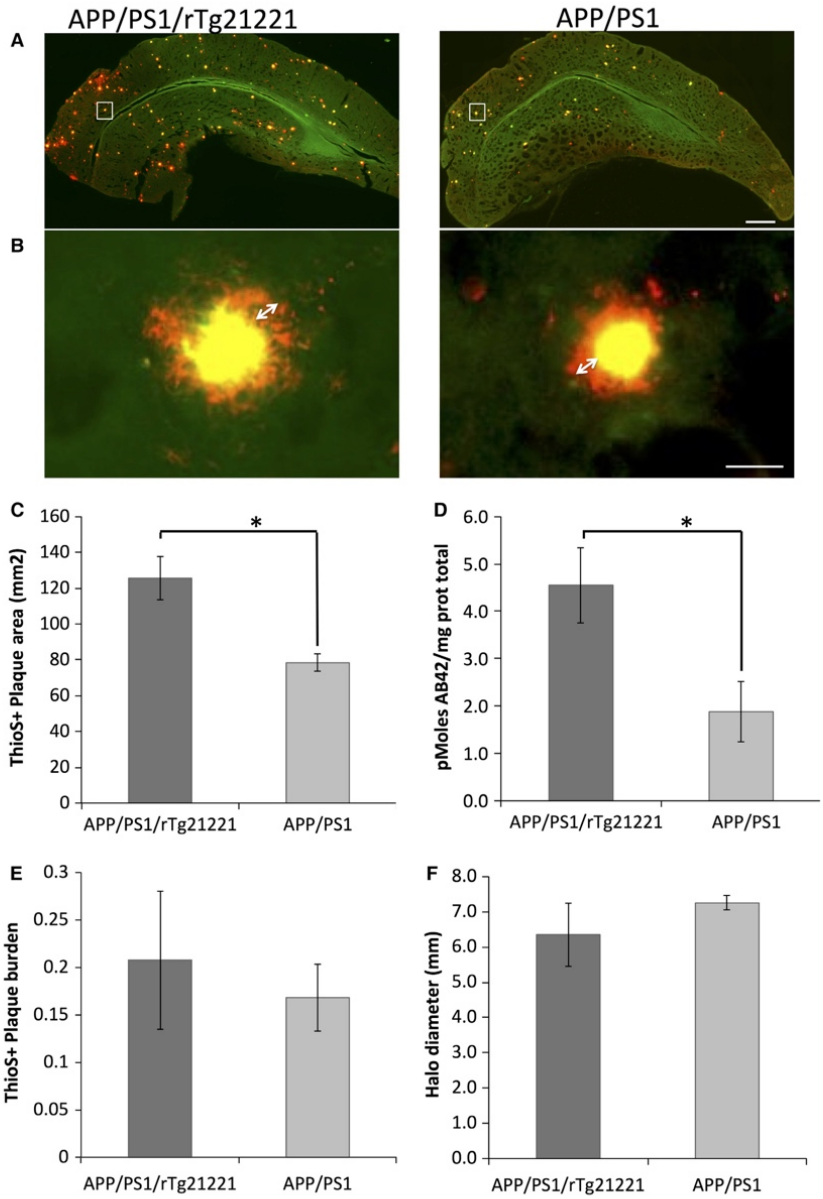

FIG. 1. Overexpression of human tau increases the cross-sectional area of ThioS-positive plaques but not the overall plaque burden. Representative images of dense Aβ-plaques (ThioS, yellow) and total Aβ (AW7, red) in brain sections were used to measure plaque characteristics (A). Higher resolution images demonstrate the halo of soluble Aβ (white arrows) surrounding dense plaques in APP/PS1/rTg21221 mice and APP/PS1 mice (B). The mean cross-sectional area of individual ThioS-positive plaques increased in APP/PS1/rTg21221 compared to APP/PS1 mice (**t*-test, df = 6, $P = 0.03$) (C). ELISA on crude brain homogenates showed a significant increase (**t*-test df = 8.673, $P = 0.023$) in the amount of Aβ42 in APP/PS1/rTg21221 mice (D). The percentage area of cortex occupied by plaques (plaque burden) was unchanged (E) as was the thickness of the soluble Aβ halo around dense plaques (F). APP/PS1/rTg21221 $n = 5$, APP/PS1n = 3, scale bars represent 500 μm in (A) and 20 μm in (B). [Colour figure can be viewed at wileyonlinelibrary.com].

Sections were counterstained with ThioS and mounted onto slides as described above.

Low-resolution tile scan images of every other section in the series (coronal sections 1 mm apart) were taken at 5× magnification with an epifluorescence microscope (Zeiss Axio Imager Z2; Carl Zeiss, Ltd., Cambridge, UK). Cortical thickness was measured at three equi-distant points on each section. The cortex was outlined and 6–10 plaques in each section were randomly chosen and imaged at 63× magnification (1.4 NA plan apochromat objective) using the AXIOVISION REL. 4.8.2 software to take a z-stack through each section at every 3 µm thickness. Neuronal numbers in the vicinity of dense-core plaques (in a 30 × 30 × 50 µm volume) and far from plaques (at least 100 µm in a 30 × 30 × 50 µm volume in the same cortical layer) were obtained by stereological sampling using STEROINVESTIGATOR software. Plaque burden (the percentage of cortex occupied by plaques) and individual plaque area were measured in IMAGE J. For astrocyte counts, the same sampling scheme was used on GFAP stained sections to choose plaques on low-resolution images and take high-resolution images of 6–10 plaques per section on every 20th section. GFAP-positive astrocytes around dense-core plaques were counted in a 30-µm radius circle from the edge of the plaque.

To label dystrophic neurites and axons, Alz50 (kind gift of Peter Davies) and Smi312 (ab24574, Abcam) were used at concentrations of 1 : 1000 and 1 : 5000, respectively. Alz50-positive neurites within the area of the ThioS-positive plaques were counted. Neurite curvature was calculated by measuring the length of each axon segment and dividing it by the end-to-end distance of the segment. Neurite distance from a plaque was calculated by taking an average of the distance to the plaque from each end and the middle of the axon segment measured. Axons were only measured if they could be followed up for more than 20 µm and in total, 339 axons from eight mice were measured and an average was taken for each mouse.

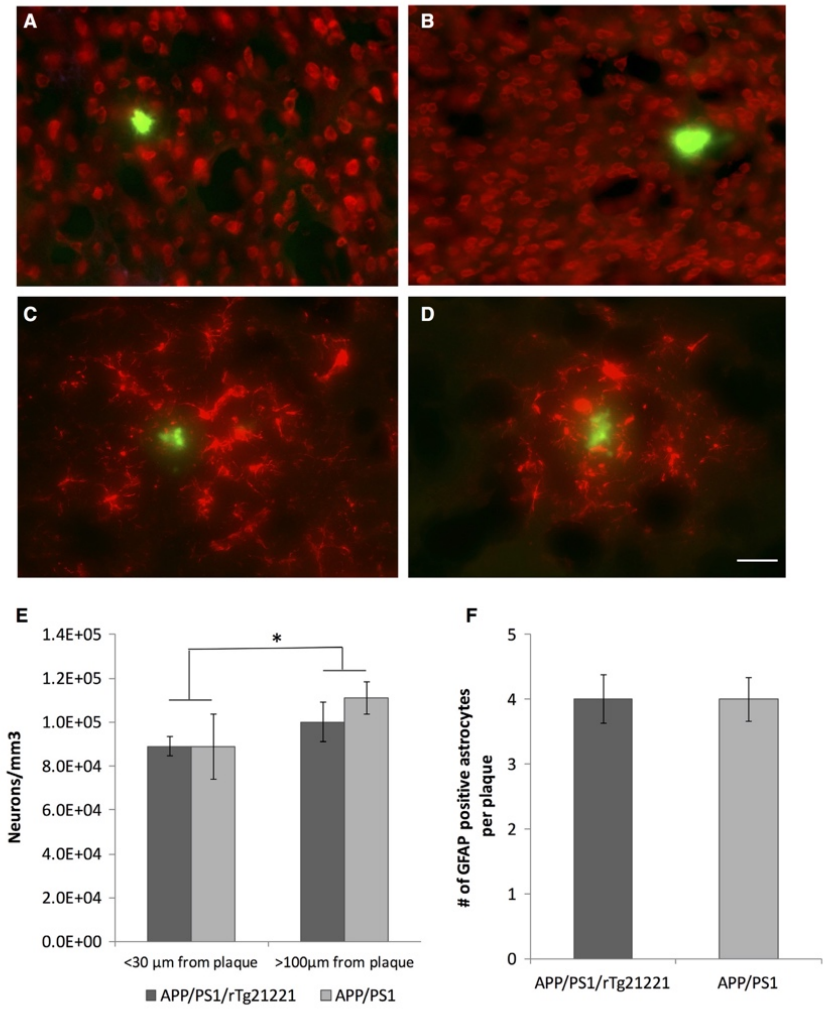

FIG. 2. Overexpressing human tau does not affect plaque-associated neuron loss and astrogliosis in APP/PS1 mice. Representative images of neurons (red, *Neurotrace* stained; A,B) and GFAP-positive astroglia (red; C,D) and ThioS-positive plaques (green) in APP/PS1 (A,C) and APP/PS1/rTg21221 (B,D) mice. Neurons were counted in a 30 × 30 µm box for areas near (< 30 µm) and far (> 100 µm) from plaques and as expected there was a decrease in neuronal density in the immediate vicinity of plaques (*two-way ANOVA $F_{1,12} = 6.852$, $p = 0.022$). No difference was seen between genotypes (E). GFAP-positive astrocytes counted in a radius of 30 µm around ThioS-positive plaques showed no difference either (F). APP/PS1/rTg21221 $n = 5$, APP/PS1n = 3, scale bar is 30 µm. [Colour figure can be viewed at wileyonlinelibrary.com].

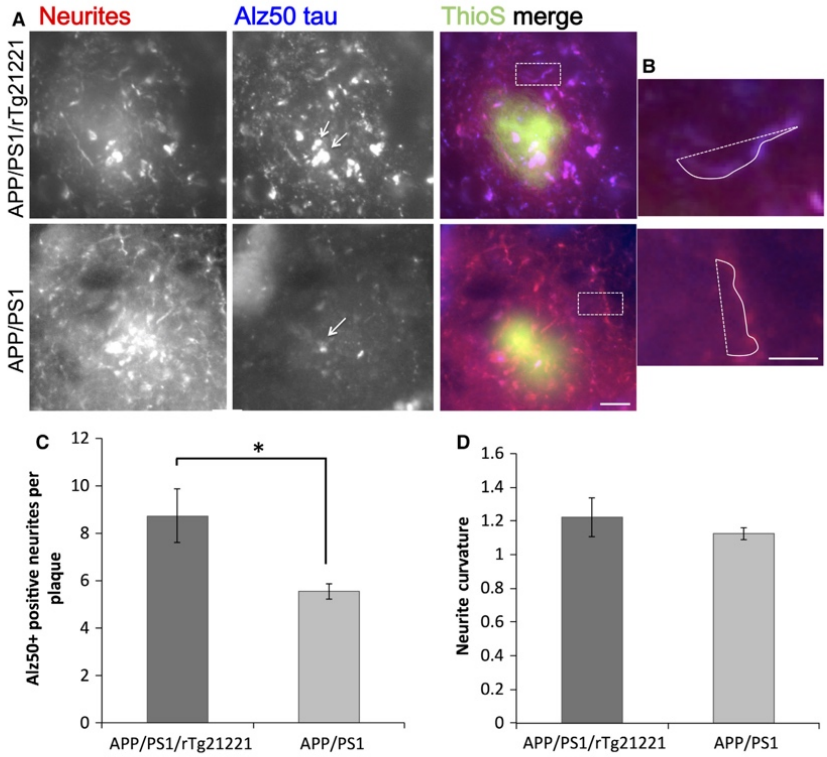

FIG. 3. Overexpression of human tau exacerbates plaque-associated dystrophic neurites but does not affect neurite curvature. Staining of cortical sections neurites (smi312, red), misfolded tau (Alz50, blue), and plaques (ThioS, green) shows the accumulation of tau-positive dystrophic neurites and the abnormal curvature of neurites near plaques in both APP/PS1 and APP/PS1/rTg21221 mice (A). Neurite curvature was measured by dividing the length (solid line) by the end-to-end distance (dotted line) of each neurite segment (B). Quantification reveals an increase in Alz50-positive dystrophic neurites around plaques in APP/PS1/rTg21221 mice (C) (*t-test df = 0.047, P = 0.047), whereas the neurite curvature does not change in presence of human tau (D). APP/PS1/rTg21221 n = 5, APP/PS1 n = 3, scale bars are 10 μm (A) and 3 μm (B). [Colour figure can be viewed at wileyonlinelibrary.com].

Array tomography

Brain tissue from somatosensory cortex was prepared for array tomography as described previously (Micheva & Smith, 2007; Kay *et al.*, 2013). In brief, tissue from five APP/PS1/rTg21221 and six APP/PS1 mice was embedded in acrylic resin and cut into ribbons of 70 nm sections that were collected on gelatin-coated glass coverslips. The ribbons were then stained with antibodies and imaged along the ribbon. The ribbons were then stripped (0.2 M NaOH, 0.02%SDS in dH_2O) and reprobed with a second set of antibodies and images were taken in the same location as those on day 1. Primary antibodies on day 1 were 1C22 [1 : 50, kind gift of Dominic Walsh (Yang *et al.*, 2015)], rabbit anti-synapsin-1 (1 : 100, AB1543P, Millipore) and goat anti-PSD95 (1 : 50, ab12093, Abcam). Primary antibodies used on day 2 were AW7 (1 : 1000, kind gift of Dominic Walsh), mouse anti-Tau13 (1 : 50, MMS-520R-500, Covance) and goat anti-PSD95 (1 : 50, ab12093, Abcam). 1C22 recognizes conformer specific oligomeric Aβ and was raised in a mouse and AW7 recognizes total Aβ and was raised in a rabbit. Secondary antibodies were purchased from Invitrogen and were used at 1 : 50. Alexa Fluor conjugated secondary antibodies used on day 1 were donkey anti-mouse 488 (A21202), donkey anti-rabbit 594 (A21207) and donkey anti-goat 647 (A21447). Secondary antibodies used on day 2 were donkey anti-mouse 488 (A21202), donkey anti-rabbit 647 (A31573) and donkey anti-goat 594 (A11058).

Images from each section in the ribbon were complied to create a 3D stack and aligned using IMAGEJ multistackreg macros (Thevenaz *et al.*, 1998). Regions of interest (10 × 10 μm) were selected near plaques (< 20 μm) and far from plaques (> 40 μm). Images were thresholded in IMAGEJ/FIJI (Schindelin *et al.*, 2012) and custom MATLAB macros were used to remove single slice punctate, count synaptic punctuate and assess co-localization with 1C22 (all custom analysis macros will be freely available along with data spreadsheets supporting this manuscript at http://dx.doi.org/10.7488/ds/1507).

Statistics

In these experiments, we compare APP/PS1 mice to APP/PS1/rTg21221 mice with the experimental unit being a single animal. Numbers of animals in each experiment are shown in figure legends. For each parameter, a mean or median (depending on normality) was calculated for each animal, and then the group mean or median was calculated. The null hypothesis was no difference between APP/PS1 and APP/PS1/rTg21221 mice for each measured parameter. Statistical analysis on the data obtained was performed using SPSS software (version 21 IBM Armonk, New York, USA). Each data set was individually tested for normal distribution using the Shapiro–Wilk normality test. When data were normally distributed such as the astrocytes quantification around plaques, ANOVA or Students T-test was used to test for difference between the means for

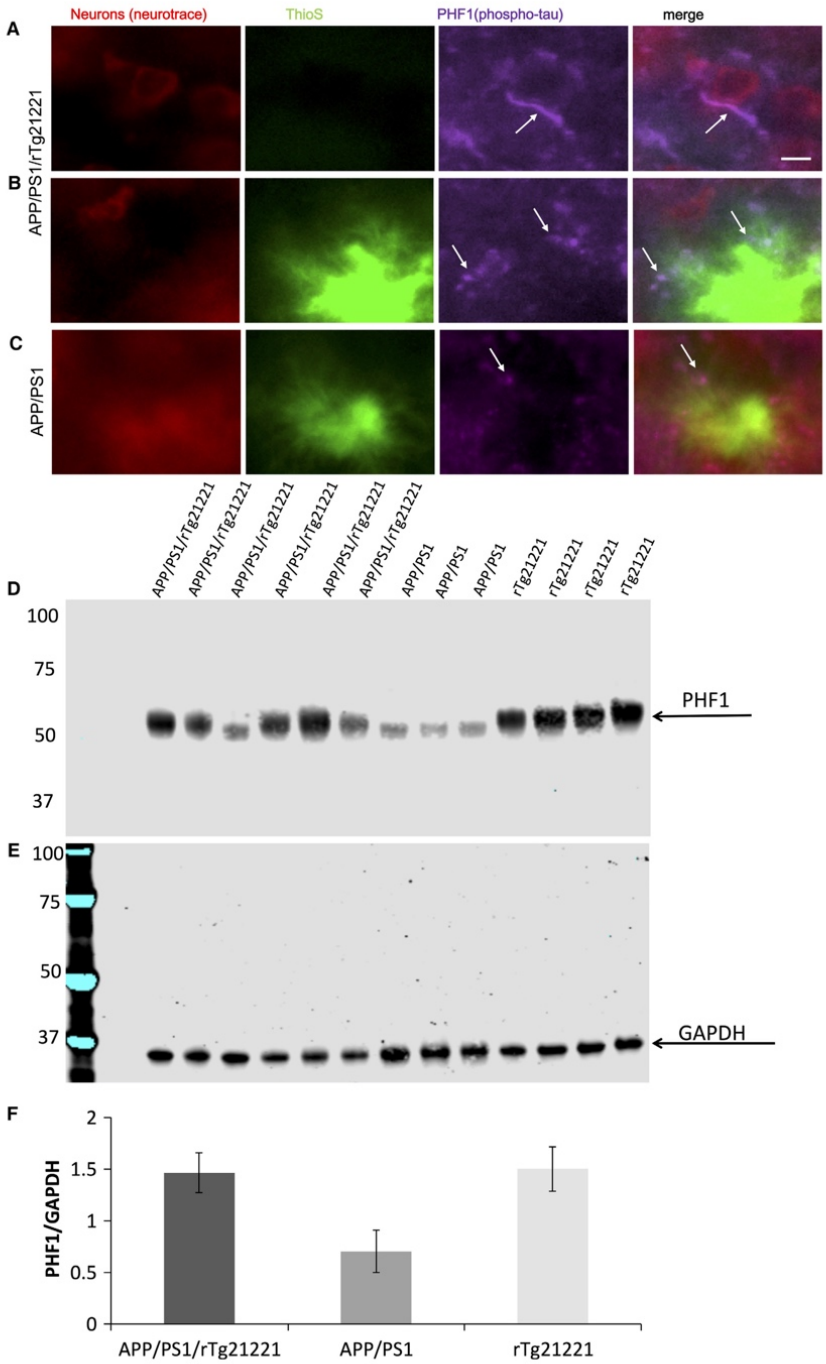

FIG. 4. Overexpression of human tau does not cause tangle formation or increase tau hyperphosphorylation. PHF1 positive tau accumulates in neuropil threads in APP/PS1/rTg21221 mice (A) and in dystrophic neurites in both APP/PS1/rTg21221 (B) and APP/PS1 mice (C). A western blot of crude homogenate from the cortex of a mouse (5 μg protein) was probed for PHF1 (D) and GAPDH (E) as a loading control. The PHF1 bands between 55–65 kDa were quantified and the overexpression of human tau did not change the overall levels of PHF1 (F). APP/PS1/rTg21221 $n = 6$, APP/PS1n = 3, rTg21221 $n = 4$ Scale bar 5 μm. [Colour figure can be viewed at wileyonlinelibrary.com].

each individual animal data across the experimental conditions. Tukey's *post hoc* multiple comparisons test was also applied. When data were not normally distributed, such as the neuronal and microglial counts as well as the quantification of the western blot data, a non-parametric Kruskal–Wallis test was used to test for significant difference between the medians for each individual animal across the experimental groups. All statistics were carried out at 95% confidence intervals, therefore a significant threshold of $P < 0.05$ was used in all analyses; the number of mice used in each experiment can be found in the figure legends.

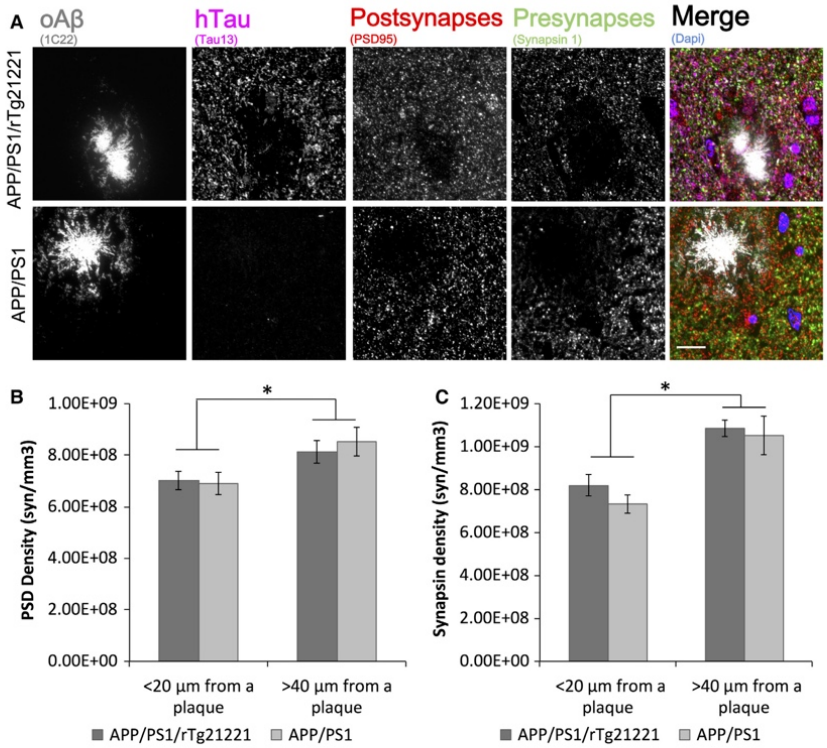

FIG. 5. Overexpression of human tau does not increase synapse loss in APP/PS1 mice. To investigate synapse loss, array tomography ribbons from APP/PS1 (n = 6) and APP/PS1/rTg21221 mice (n = 5) were stained for oligomeric Aβ (oAβ; 1C22), human tau (Tau13), post-synapses (PSD95), and pre-synapses (synapsin-1) (A). There was synapse loss in both genotypes within 20 µm of plaques (*PSD data effect of plaque distance $F_{1,21}$ = 8.4, P = 0.01; synapsin data *$F_{1.21}$ = 16.6, P = 0.001). There is no exacerbation of synapse loss with expression of human tau of either post-synaptic terminals (B) or pre-synaptic terminals (C) (two-way ANOVA effect of genotype $F < 0.5$, $P > 0.05$). Scale bar is 10 µm. [Colour figure can be viewed at wileyonlinelibrary.com].

Results

Effects of hTau overexpression on pathology in APP/PS1 mice

Raw analysed data from this manuscript and custom analysis macros used in analysis are available at http://dx.doi.org/10.7488/ds/1507. APP/PS1 mice begin to develop amyloid plaques at around 4–6 months of age (Garcia-Alloza *et al.*, 2006b). To determine whether hTau overexpression affects plaque deposition in these 8–10-month-old animals, Thioflavin-S (ThioS) was used to stain dense plaques, and AW7 was used to immunolabel all Aβ depositions. Cortical ThioS-positive plaque burden was unchanged with hTau overexpression (0.21 ± 0.16% in APP/PS1/rTg21221 mice; 0.17 ± 0.06% in APP/PS1 mice without hTau), as was the burden of total Aβ−plaques immunostained with AW7 (0.55 ± 0.42% in APP/PS1/rTg21221 mice; 0.39 ± 0.05% in APP/PS1 mice, Fig. 1E). The variability in plaque burden in the mice overexpressing human tau was very high, and we did observe a significant increase (df = 6, P = 0.03, t-test) in the size (the average cross-sectional area of plaques) of ThioS-positive plaques in APP/PS1/rTg21221 (Fig. 1C). There was no difference in AW7-positive plaque size or the diameter of the halo of Aβ around dense plaques. Consistent with larger dense plaques detected with histology, we observed an increase in Aβ42 levels in brain homogenates by ELISA in APP/PS1/rTg21221 (Fig. 1D; 4.6 pmol Aβ42/mg protein) compared to APP/PS1 mice (2.1 pmol Aβ42/mg protein, df = 8.673 P = 0.023 Kruskal–Wallis test).

Neuronal loss is one of the key neuropathological hallmarks of Alzheimer's disease. In plaque-bearing mice, there is generally not much overt neuronal loss without overexpressing FTD mutant tau. Subtle plaque-associated neuron loss has been reported for APP/PS1 mice (Rupp *et al.*, 2011). We assessed the impact of human tau overexpression on plaque-associated neuronal loss. As described previously, we observed subtle neuronal loss near plaques (two-way ANOVA $F_{1,12}$ = 6.852, P = 0.022 for regions near plaques vs. far from plaques). We did not see any exacerbation of plaque-associated neuronal loss in APP/PS1/rTg21221 mice (two-way ANOVA, $P > 0.05$ for genotype and genotype × plaque distance interaction, Fig. 2).

Plaque deposition is associated with local gliosis and degenerative changes in neurites including dystrophic swellings that accumulate pathological forms of tau (McLellan *et al.*, 2003; Spires *et al.*, 2005). To examine whether human tau overexpression affects gliosis, activated astrocytes (GFAP-positive) within 30 µm of a plaque were counted in APP/PS1/rTg21221 and APP/PS1 mice (Fig. 2). No change in the number of activated astrocytes per plaque was detected (Student T-Test $P > 0.05$), and quantitative western blot of cortical homogenates confirmed no global change in the amount of GFAP (Fig. S1).

Staining of brain sections with ThioS, PHF1 and Alz50 did not show neurofibrillary tangles for either genotype (Fig. 1 for ThioS, Fig. 3 for Alz50 and Fig. 4 for PHF1;). However, Alz50-positive and PHF1-positive tau accumulations were observed in dystrophic neurites around plaques (Figs 3 and 4). To examine the toxic effect

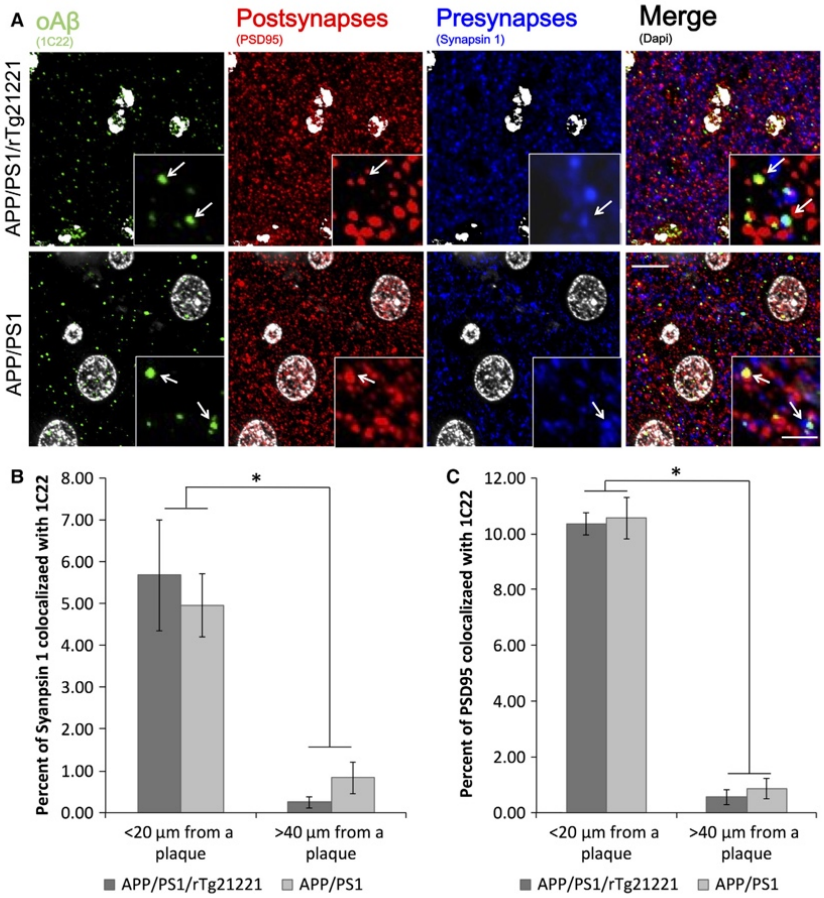

FIG. 6. Overexpression of human tau does not affect the localization of Aβ at synapses. Analysis of the co-localization of Aβ labeled with 1C22 and PSD95 or synapsin-1 (A) show that Aβ presence at pre-synapses (B) or post-synapses (C) does not change when human tau is overexpressed in APP/PS1/rTg21221 mice (two-way ANOVA effect of genotype $F < 0.3$, $P > 0.05$). In both pre and post synapses, there is a significantly higher percentage of synapses containing Aβ near plaques vs. far from plaques (PSD data effect of plaque distance $*F_{1,21} = 363.6$, $P = 2.19 \times 10^{-13}$; synapsin data $*F_{1,21} = 13.3$, $P = 0.002$). APP/PS1/rTg21221 $n = 5$, APP/PS1 $n = 6$, scale bar is 10 µm, scale bar for insert is 2 µm. [Colour figure can be viewed at wileyonlinelibrary.com].

of Aβ and hTau on neurites around plaques, brain sections were co-immunostained for misfolded tau (Alz50) and neurofilaments (smi312), and dystrophic Alz50-positive neurite swellings (diameter > 2.5 µm) associated plaques were counted (Fig. 3A). With overexpression of human tau, there was a significant increase in dystrophies per plaque (df = 6, $P = 0.036$ Student's T-Test, Fig. 3C). Curvature of smi312-positive neurites, which is known to increase around Aβ-plaques (Garcia-Alloza *et al.*, 2006a), was not significantly altered in APP/PS1/rTg21221 compared to APP/PS1 mice ($P > 0.05$ Mann–Whitney U test, Fig. 3D). PHF1 staining also showed an absence of tangles but the presence of dystrophic neurites and neuropil threads in APP/PS1/rTg21221 mice. APP/PS1 mice without human tau also demonstrated plaque-associated PHF1-positive neuritic dystrophies but qualitatively less neuropil threads far from plaques (Fig. 4). Western blot analysis indicated that there is a trend toward change (ANOVA $F_{2,12} = 3.614$, $P = 0.066$) in the amount of phosphorylated tau in APP/PS1/rTG21221 compared with APP/PS1 alone or when compared with rTG21221 mice with no APP/PS1 (Fig. 4).

Together, these histologic data indicate an increase in amyloid deposition and exacerbation of neuritic dystrophies around plaques with the overexpression of human tau in APP/PS1 mice; in the absence of neurofibrillary tangle pathology.

No effect of hTau overexpression on Aβ-mediated synaptic loss

To determine if the overexpression of wild-type human tau increased Aβ-induced synaptic loss, array tomography was used to quantify synapse density in the neocortex. Tissue ribbons were stained for oligomeric Aβ using the conformer-specific 1C22 antibody. A total of 126 210 synapses in APP/PS1 ($n = 6$ animals) and 139 412 synapses in APP/PS1/rTg21221 mice ($n = 5$ animals) were analyzed. No change in synapse density was seen for either the pre-synaptic marker synapsin-1 or the post-synaptic marker PSD95 (Fig. 5). However, both APP/PS1 and APP/PS1/rTg21221 mice showed a significant decrease in the densities of pre- and post-synapses near plaques (< 20 µm from plaque border) compared to distant from plaques (> 40 µm from plaque border), similar to what has been reported previously (Koffie *et al.*, 2009). Western blot analysis of the pre-synaptic marker synaptophysin in crude cortical homogenates also suggested no change in synaptic

protein levels between APP/PS1 and APP/PS1/rTg21221 mice (Fig. S2).

As there is evidence that the accumulation of Aβ at synapses contributes to synaptic shrinkage and loss (Koffie *et al.*, 2009), we next assessed the co-localization of synaptic markers with the oligomeric Aβ antibody 1C22 (Fig. 6). While both genotypes had significantly more Aβ at synapse near plaques than far from plaques, the overexpression of human tau did not increase the amount of Aβ found co-localized with the synapse. This finding was confirmed biochemically by assaying synaptoneurosome preparations using a human Aβ ELISA (Fig. S3A), and by western blot analysis of the same preparations using Aβ antibody (82E1; Fig. S3B and C); both assays showed no difference between mice APP/PS1 and APP/PS1/rTg21221 mice. Furthermore, the presence of Aβ in APP/PS1/rTg21221 mice did not increase the amount of human tau found in synaptoneurosomes compared to rTg21221 mice (Fig. S3D and E).

Discussion

From genetic data, it is clear that changes in APP processing, leading to increased Aβ42 levels, initiate the disease process in familial AD (fAD), and likely also in sporadic AD (Hardy & Selkoe, 2002). It is also clear that pathological changes in tau correlate better than plaque deposition with neuronal death observed in AD (Gomez-Isla *et al.*, 1997). However, the connection between Aβ and tau pathologies remains enigmatic and it is still unknown how changes in amyloid processing can cause neurotoxicity related to tau.

The synergistic effects of Aβ and tau in the deposition of the classic pathological lesions – plaques and neurofibrillary tangles – have been modeled in mice expressing fAD mutant APP and FTD mutant tau, such as the 3×Tg line (Oddo *et al.*, 2003), which develops both pathologies. In these mice, amyloid deposition precedes tau deposition, and the removal of Aβ by immunotherapy also reduces early tau pathology (phospho-tau) but tangles remain unchanged (Oddo *et al.*, 2004). However, immunotherapies directed against tau do not affect Aβ, indicating a role for Aβ upstream of tau pathology (Walls *et al.*, 2014). Recently, we generated mouse model that expresses brain-wide human mutant APP and human mutant P301L tau only in the entorhinal cortex by crossing APP/PS1 mice with rTgTauEC mice (Pooler *et al.*, 2015). In these mice, the presence of human Aβ accelerates tau propagation through the brain and increases plaque size and plaque-associated dystrophic neurites. Together, these studies support the idea of an interaction between plaques and tangles, at least in the presence of disease-associated mutations in both Aβ and tau. In contrast, at the relatively young age we examined in our focus on synapse loss, we did not observe neurofibrillary tangles in APP/PS1 mice overexpressing wild-type human tau (APP/PS1/rTg21221), however, we found larger plaques and exacerbated dystrophic neurites, similar to our previous observations in APP/PS1xrTgTauEC mice (Pooler *et al.*, 2015). A recent study found that mice with high levels of human Aβ oligomers do develop neurofibrillary tangle pathology at much older ages (18 months) when crossed with wild-type human tau expressing mice (Umeda *et al.*, 2014). This is likely due to the different ages examined (as here we focus on earlier synaptic changes) but could also be due to the different forms of APP and tau expressed in the two lines.

Synapse loss is the strongest pathological correlate of dementia (DeKosky & Scheff, 1990; Terry *et al.*, 1991), and is thought to be the key pathogenic process driving AD symptoms (Spires-Jones & Hyman, 2014). Synaptic degeneration downstream of oligomeric Aβ has been very well established not only in animal models of the disease (Walsh *et al.*, 2002), but also in several studies of human brains (Koffie *et al.*, 2012; Perez-Nievas *et al.*, 2013; Bilousova *et al.*, 2016). Animal models of FTD expressing mutant human tau also exhibit synaptic loss and dysfunction, along with pronounced neurodegeneration (Rocher *et al.*, 2010; Crimins *et al.*, 2013; Menkes-Caspi *et al.*, 2015). From these data, it became clear that pathological changes in both can independently drive synapse loss, but it is unclear whether Aβ and tau act on the same pathway to synapse degeneration.

When plaque-bearing mice are crossed onto a mouse tau knock-out strain (*Mapt*$^{0/0}$), the Aβ-induced synaptic phenotypes – including seizures and LTP deficits – become ameliorated. The removal of tau was also found to be protective against memory loss associated with Aβ expression in mice, likely due to protection against synapse loss (Roberson *et al.*, 2007, 2011; Shipton *et al.*, 2011). These findings provided evidence for the synergistic action of Aβ and tau toward synapse dysfunction. Here, we directly tested whether overexpression of wild-type human tau exacerbates synaptic loss associated with Aβ-plaques. Surprisingly, the increased level of non-mutant tau in APP/PS1/rTg21221 mice did not worsen the synapse pathology related to Aβ. Together with the *Mapt*$^{0/0}$ data, this indicates that the endogenous mouse tau is sufficient to cause the negative effects associated with Aβ, and that there is a ceiling effect of the requirement of tau for Aβ-mediated synapse toxicity. Indeed, it has been shown that the knock-out of endogenous mouse tau reduces the neurotoxicity of overexpressed human mutant P301L tau (Wegmann *et al.*, 2015). However, given that in human brain-derived synaptosomes, a recent study observed that phospho-tau is increased in Aβ-positive synaptosomes in early AD (Bilousova *et al.*, 2016), it is possible that at the time point studied here, synapse loss had already reached its maximum level and thus it was too late to see the potentially early effects of human tau expression. Together, these data indicate that endogenous tau may play an important role in the neurotoxicity of tau and Aβ in mouse models and that this role may be at earlier stages of the disease. As the data do not refute the possibility that tau and Aβ are on different pathways to synapse loss, a mouse model that expressed wild-type human tau in the absence of mouse tau studied at multiple time points would be beneficial to studying the possible interaction between these two important molecules in the context of human AD and synapse loss.

Author contributions

Performed experiments – RJJ, NR, AGH, SC, JSK, VP, JJRR, RP, SW, MG-A. Experimental design and analysis – RJJ, NR, GAC, BTH, TS-J. Wrote and commented on manuscript – RJJ, SW, GAC, MG-A, BTH, TS-J.

Conflict of interests

All authors declare no competing interests.

Supporting Information

Additional supporting information can be found in the online version of this article:

Fig. S1. Overexpression of human tau does not affect reactive astrocyte protein levels. A western blot of crude homogenate from the cortex of a mouse (5 μg protein) was probed for GFAP (A) and GAPDH (B) as a loading control. The GFAP band at 55 kDa was

quantified and the overexpression of human tau did not change the overall levels of GFAP (C). APP/PS1/rTg21221 $n = 5$, APP/PS1n = 3.

Fig. S2. Overexpression of human tau does affect synapse protein levels. Western blot of crude homogenates from mouse cortices (5 μg protein) probed for (A) synaptophysin and (B) α-tubulin as a loading control. The overexpression of human tau in APP/PS1 mice did not change the levels of synaptophysin (C). APP/PS1/rTg21221 $n = 5$, APP/PS1 $n = 4$, rTg21221 $n = 5$.

Fig. S3. Overexpression of human tau does not affect protein levels at the synapse. ELISA of synaptoneurosomes showed no difference in Aβ42 levels between APP/PS1 and APP/PS1/rTg21221 (A) Western blot of synaptoneurosomes (5 μg protein) was probed for (B) Aβ (82E1) and (C) human tau (tau13) with β-actin as loading control. The overexpression of human tau did not change the amount of Aβ found in synaptoneurosome when comparing APP/PS1/rTg21221 with APP/PS1 mice (D). Furthermore, Aβ did not affect the amount of human tau found in the synaptoneurosome when comparing APP/PS1/rTg21221 with rTg21221 mice (E). APP/PS1/rTg21221 $n = 5$, APP/PS1 $n = 3$, rTg21221 $n = 4$.

Acknowledgements

We thank Dominic Walsh and Peter Davies for providing antibodies. Funding was provided by Alzheimer's Research UK, the Scottish Government, the Alzheimer's Society, a University of Edinburgh Wellcome Trust ISSF, and an anonymous foundation.

Abbreviations

AD Alzheimer's disease; Aβ amyloid beta; PSD post-synaptic density.

References

Bilousova, T., Miller, C.A., Poon, W.W., Vinters, H.V., Corrada, M., Kawas, C., Hayden, E.Y., Teplow, D.B. *et al.* (2016) Synaptic amyloid-β oligomers precede p-Tau and differentiate high pathology control cases. *Am. J. Pathol.*, **186**, 185–198.

Castillo-Carranza, D.L., Guerrero-Munoz, M.J., Sengupta, U., Hernandez, C., Barrett, A.D., Dineley, K. & Kayed, R. (2015) Tau immunotherapy modulates both pathological tau and upstream amyloid pathology in an Alzheimer's disease mouse model. *J. Neurosci.*, **35**, 4857–4868.

Crimins, J.L., Pooler, A., Polydoro, M., Luebke, J.I. & Spires-Jones, T.L. (2013) The intersection of amyloid beta and tau in glutamatergic synaptic dysfunction and collapse in Alzheimer's disease. *Ageing Res. Rev.*, **12**, 757–763.

DeKosky, S.T. & Scheff, S.W. (1990) Synapse loss in frontal cortex biopsies in Alzheimer's disease: correlation with cognitive severity. *Ann. Neurol.*, **27**, 457–464.

Duyckaerts, C., Delatour, B. & Potier, M.C. (2009) Classification and basic pathology of Alzheimer disease. *Acta Neuropathol.*, **118**, 5–36.

Garcia-Alloza, M., Dodwell, S.A., Meyer-Luehmann, M., Hyman, B.T. & Bacskai, B.J. (2006a) Plaque-derived oxidative stress mediates distorted neurite trajectories in the Alzheimer mouse model. *J. Neuropath. Exp. Neur.*, **65**, 1082–1089.

Garcia-Alloza, M., Robbins, E.M., Zhang-Nunes, S.X., Purcell, S.M., Betensky, R.A., Raju, S., Prada, C., Greenberg, S.M. *et al.* (2006b) Characterization of amyloid deposition in the APPswe/PS1dE9 mouse model of Alzheimer disease. *Neurobiol. Dis.*, **24**, 516–524.

Gomez-Isla, T., Hollister, R., West, H., Mui, S., Growdon, J.H., Petersen, R.C., Parisi, J.E. & Hyman, B.T. (1997) Neuronal loss correlates with but exceeds neurofibrillary tangles in Alzheimer's disease. *Ann. Neurol.*, **41**, 17–24.

Hardy, J.A. & Higgins, G.A. (1992) Alzheimer's disease: the amyloid cascade hypothesis. *Science*, **256**, 184–185.

Hardy, J. & Selkoe, D.J. (2002) The amyloid hypothesis of Alzheimer's disease: progress and problems on the road to therapeutics. *Science*, **297**, 353–356.

Hoover, B.R., Reed, M.N., Su, J., Penrod, R.D., Kotilinek, L.A., Grant, M.K., Pitstick, R., Carlson, G.A. *et al.* (2010) Tau mislocalization to dendritic spines mediates synaptic dysfunction independently of neurodegeneration. *Neuron*, **68**, 1067–1081.

Hutton, M. (2000) Molecular genetics of chromosome 17 tauopathies. *Ann. NY. Acad. Sci.*, **920**, 63–73.

Ingelsson, M., Fukumoto, H., Newell, K.L., Growdon, J.H., Hedley-Whyte, E.T., Frosch, M.P., Albert, M.S., Hyman, B.T. *et al.* (2004) Early Abeta accumulation and progressive synaptic loss, gliosis, and tangle formation in AD brain. *Neurology*, **62**, 925–931.

Jankowsky, J.L., Fadale, D.J., Anderson, J., Xu, G.M., Gonzales, V., Jenkins, N.A., Copeland, N.G., Lee, M.K. *et al.* (2004) Mutant presenilins specifically elevate the levels of the 42 residue beta-amyloid peptide *in vivo*: evidence for augmentation of a 42-specific gamma secretase. *Hum. Mol. Genet.*, **13**, 159–170.

Kay, K.R., Smith, C., Wright, A.K., Serrano-Pozo, A., Pooler, A.M., Koffie, R., Bastin, M.E., Bak, T.H. *et al.* (2013) Studying synapses in human brain with array tomography and electron microscopy. *Nat. Protoc.*, **8**, 1366–1380.

Koffie, R.M., Meyer-Luehmann, M., Hashimoto, T., Adams, K.W., Mielke, M.L., Garcia-Alloza, M., Micheva, K.D., Smith, S.J. *et al.* (2009) Oligomeric amyloid beta associates with postsynaptic densities and correlates with excitatory synapse loss near senile plaques. *Proc. Natl. Acad. Sci. USA*, **106**, 4012–4017.

Koffie, R.M., Hashimoto, T., Tai, H.C., Kay, K.R., Serrano-Pozo, A., Joyner, D., Hou, S., Kopeikina, K.J. *et al.* (2012) Apolipoprotein E4 effects in Alzheimer's disease are mediated by synaptotoxic oligomeric amyloid-beta. *Brain*, **135**, 2155–2168.

Kopeikina, K.J., Carlson, G.A., Pitstick, R., Ludvigson, A.E., Peters, A., Luebke, J.I., Koffie, R.M., Frosch, M.P. *et al.* (2011) Tau accumulation causes mitochondrial distribution deficits in neurons in a mouse model of tauopathy and in human Alzheimer's disease brain. *Am. J. Pathol.*, **179**, 2071–2082.

Lasagna-Reeves, C.A., Castillo-Carranza, D.L., Sengupta, U., Clos, A.L., Jackson, G.R. & Kayed, R. (2011) Tau oligomers impair memory and induce synaptic and mitochondrial dysfunction in wild-type mice. *Mol. Neurodegener.*, **6**, 39.

McLellan, M.E., Kajdasz, S.T., Hyman, B.T. & Bacskai, B.J. (2003) *In vivo* imaging of reactive oxygen species specifically associated with thioflavine S-positive amyloid plaques by multiphoton microscopy. *J. Neurosci.*, **23**, 2212–2217.

Menkes-Caspi, N., Yamin, H.G., Kellner, V., Spires-Jones, T.L., Cohen, D. & Stern, E.A. (2015) Pathological tau disrupts ongoing network activity. *Neuron*, **85**, 959–966.

Micheva, K.D. & Smith, S.J. (2007) Array tomography: a new tool for imaging the molecular architecture and ultrastructure of neural circuits. *Neuron*, **55**, 25–36.

Oddo, S., Caccamo, A., Shepherd, J.D., Murphy, M.P., Golde, T.E., Kayed, R., Metherate, R., Mattson, M.P. *et al.* (2003) Triple-transgenic model of Alzheimer's disease with plaques and tangles: intracellular Abeta and synaptic dysfunction. *Neuron*, **39**, 409–421.

Oddo, S., Billings, L., Kesslak, J.P., Cribbs, D.H. & LaFerla, F.M. (2004) Abeta immunotherapy leads to clearance of early, but not late, hyperphosphorylated tau aggregates via the proteasome. *Neuron*, **43**, 321–332.

Oddo, S., Vasilevko, V., Caccamo, A., Kitazawa, M., Cribbs, D.H. & LaFerla, F.M. (2006) Reduction of soluble Abeta and tau, but not soluble Abeta alone, ameliorates cognitive decline in transgenic mice with plaques and tangles. *J. Biol. Chem.*, **281**, 39413–39423.

Perez-Nievas, B.G., Stein, T.D., Tai, H.C., Dols-Icardo, O., Scotton, T.C., Barroeta-Espar, I., Fernandez-Carballo, L., de Munain, E.L. *et al.* (2013) Dissecting phenotypic traits linked to human resilience to Alzheimer's pathology. *Brain*, **136**, 2510–2526.

Pooler, A.M., Polydoro, M., Maury, E.A., Nicholls, S.B., Reddy, S.M., Wegmann, S., William, C., Saqran, L. *et al.* (2015) Amyloid accelerates tau propagation and toxicity in a model of early Alzheimer's disease. *Acta. Neuropathol. Commun.*, **3**, 14.

Ramos-Rodriguez, J.J., Infante-Garcia, C., Galindo-Gonzalez, L., Garcia-Molina, Y., Lechuga-Sancho, A. & Garcia-Alloza, M. (2016) Increased spontaneous central bleeding and cognition impairment in APP/PS1 mice with poorly controlled diabetes mellitus. *Mol. Neurobiol.*, **53**, 2685–2697.

Roberson, E.D., Scearce-Levie, K., Palop, J.J., Yan, F., Cheng, I.H., Wu, T., Gerstein, H., Yu, G.Q. *et al.* (2007) Reducing endogenous tau ameliorates

amyloid beta-induced deficits in an Alzheimer's disease mouse model. *Science*, **316**, 750–754.

Roberson, E.D., Halabisky, B., Yoo, J.W., Yao, J., Chin, J., Yan, F., Wu, T., Hamto, P. *et al.* (2011) Amyloid-beta/Fyn-induced synaptic, network, and cognitive impairments depend on tau levels in multiple mouse models of Alzheimer's disease. *J. Neurosci.*, **31**, 700–711.

Rocher, A.B., Crimins, J.L., Amatrudo, J.M., Kinson, M.S., Todd-Brown, M.A., Lewis, J. & Luebke, J.I. (2010) Structural and functional changes in tau mutant mice neurons are not linked to the presence of NFTs. *Exp. Neurol.*, **223**, 385–393.

Rupp, N.J., Wegenast-Braun, B.M., Radde, R., Calhoun, M.E. & Jucker, M. (2011) Early onset amyloid lesions lead to severe neuritic abnormalities and local, but not global neuron loss in APPPS1 transgenic mice. *Neurobiol. Aging*, **32**, 2324 e2321–2326.

Schindelin, J., Arganda-Carreras, I., Frise, E., Kaynig, V., Longair, M., Pietzsch, T., Preibisch, S., Rueden, C. *et al.* (2012) Fiji: an open-source platform for biological-image analysis. *Nat. Methods*, **9**, 676–682.

Shankar, G.M., Li, S., Mehta, T.H., Garcia-Munoz, A., Shepardson, N.E., Smith, I., Brett, F.M., Farrell, M.A. *et al.* (2008) Amyloid-beta protein dimers isolated directly from Alzheimer's brains impair synaptic plasticity and memory. *Nat. Med.*, **14**, 837–842.

Shipton, O.A., Leitz, J.R., Dworzak, J., Acton, C.E., Tunbridge, E.M., Denk, F., Dawson, H.N., Vitek, M.P. *et al.* (2011) Tau protein is required for amyloid {beta}-induced impairment of hippocampal long-term potentiation. *J. Neurosci.*, **31**, 1688–1692.

Small, S.A. & Duff, K. (2008) Linking Abeta and tau in late-onset Alzheimer's disease: a dual pathway hypothesis. *Neuron*, **60**, 534–542.

Spires, T.L., Meyer-Luehmann, M., Stern, E.A., McLean, P.J., Skoch, J., Nguyen, P.T., Bacskai, B.J. & Hyman, B.T. (2005) Dendritic spine abnormalities in amyloid precursor protein transgenic mice demonstrated by gene transfer and intravital multiphoton microscopy. *J. Neurosci.*, **25**, 7278–7287.

Spires-Jones, T.L. & Hyman, B.T. (2014) The intersection of amyloid beta and tau at synapses in Alzheimer's disease. *Neuron*, **82**, 756–771.

Tai, H.C., Serrano-Pozo, A., Hashimoto, T., Frosch, M.P., Spires-Jones, T.L. & Hyman, B.T. (2012) The synaptic accumulation of hyperphosphorylated tau oligomers in Alzheimer disease is associated with dysfunction of the ubiquitin-proteasome system. *Am. J. Pathol.*, **181**, 1426–1435.

Tanzi, R.E. (2012) The genetics of Alzheimer disease. *Cold Spring Harb. Perspect Med.*, **2**, a006296. doi: 10.1101/cshperspect.a006296. [Epub ahead of print].

Terry, R.D., Masliah, E., Salmon, D.P., Butters, N., DeTeresa, R., Hill, R., Hansen, L.A. & Katzman, R. (1991) Physical basis of cognitive alterations in Alzheimer's disease: synapse loss is the major correlate of cognitive impairment. *Ann. Neurol.*, **30**, 572–580.

Thevenaz, P., Ruttimann, U.E. & Unser, M. (1998) A pyramid approach to subpixel registration based on intensity. *IEEE T. Image Process.*, **7**, 27–41.

Umeda, T., Maekawa, S., Kimura, T., Takashima, A., Tomiyama, T. & Mori, H. (2014) Neurofibrillary tangle formation by introducing wild-type human tau into APP transgenic mice. *Acta Neuropathol.*, **127**, 685–698.

Vossel, K.A., Xu, J.C., Fomenko, V., Miyamoto, T., Suberbielle, E., Knox, J.A., Ho, K., Kim, D.H. *et al.* (2015) Tau reduction prevents Aβ-induced axonal transport deficits by blocking activation of GSK3β. *J. Cell Biol.*, **209**, 419–433.

Walls, K.C., Ager, R.R., Vasilevko, V., Cheng, D., Medeiros, R. & LaFerla, F.M. (2014) p-Tau immunotherapy reduces soluble and insoluble tau in aged 3xTg-AD mice. *Neurosci. Lett.*, **575**, 96–100.

Walsh, D.M., Klyubin, I., Fadeeva, J.V., Cullen, W.K., Anwyl, R., Wolfe, M.S., Rowan, M.J. & Selkoe, D.J. (2002) Naturally secreted oligomers of amyloid beta protein potently inhibit hippocampal long-term potentiation *in vivo*. *Nature*, **416**, 535–539.

Wegmann, S., Maury, E.A., Kirk, M.J., Saqran, L., Roe, A., DeVos, S.L., Nicholls, S., Fan, Z. *et al.* (2015) Removing endogenous tau does not prevent tau propagation yet reduces its neurotoxicity. *EMBO J.*, **34**, 3028–3041.

Wu, H.Y., Hudry, E., Hashimoto, T., Kuchibhotla, K., Rozkalne, A., Fan, Z., Spires-Jones, T., Xie, H. *et al.* (2010) Amyloid beta induces the morphological neurodegenerative triad of spine loss, dendritic simplification, and neuritic dystrophies through calcineurin activation. *J. Neurosci.*, **30**, 2636–2649.

Yang, T., O'Malley, T.T., Kanmert, D., Jerecic, J., Zieske, L.R., Zetterberg, H., Hyman, B.T., Walsh, D.M. *et al.* (2015) A highly sensitive novel immunoassay specifically detects low levels of soluble Abeta oligomers in human cerebrospinal fluid. *Alzheimers Res. Ther.*, **7**, 14.

Conclusion

In this study we saw an increase in the cross sectional area of ThioS+ plaques and the number of Alz50+ positive neurites when human tau is over expressed. We did not detect a change in the size of the Aβ oligomer halo, neurite curvature, neuron loss, or synapse loss in APP/PS1/rTg21221 mice compared with APP/PS1 mice. As discussed in the paper tau is known to be necessary for much of the Aβ pathology found in AD models and thus is it surprising that an increase in tau would not have an effect (Roberson *et al.*, 2007, 2011; Shipton *et al.*, 2011). This lack of exacerbation could be due in part to a ceiling effect of mouse tau where by the amount of tau found endogenously in the mouse is sufficient to cause neuron and synapse loss. It is possible that while tau is necessary for Aβ mediated synapse loss an increase in tau does not affect the number of Aβ oligomers present at the synapse, potentially because any extra oligomers made are sequestered into dense core and reasonably inert plaques, hence the increase in ThioS+ plaque size. The lack of tangles or increased tau hyperphosphorylation seen in this model indicates that even in the presence of human tau the effect of Aβ on tau in a mouse is different from that seen in a human (Bilousova *et al.*, 2016). To further understand synapse loss in AD more information on the synaptic changes that occur in human disease is needed.

4 Investigating the proteomics of synapses in Alzheimer's Disease with a focus on the role of ApoE4

4.1 Background and Aims

Of the main pathological features of AD, synapse loss is the greatest correlate of the clinical cognitive decline that is the phenotype of the disease (Terry *et al.*, 1991; Koffie *et al.*, 2011). It is this loss of synapses that is thought to underlie most of the memory deficits that occur in AD. Much effort has gone into looking at the protein changes that accompany AD in the brain in general but thus far study of the synapse has been limited in comparison. Investigating the protein changes that underlie the synaptic degeneration caused by AD is crucial to our understanding of the pathological pathways that are initiated by this disease. Chapter 3 showed that while tau and Aβ are both important for synapse loss in mouse models a greater understanding of the effect of AD on synaptic dysfunction and degradation is needed. Chapter 3 also highlighted that while mouse models are powerful tools to study disease, integrating studies in models with those in post-mortem human cases will allow for a better understanding of the mechanisms of AD.

The greatest genetic risk factor for sporadic AD is *APOE.* Inheritance of a single copy of the *APOE ε4* allele will increase the risk of AD by 3 times the risk of an individual with two copies of the *APOE ε3* allele as well as decreasing the age of onset and increasing the speed of cognitive decline(Roses, 1996; Lim *et al.*, 2014). Two copies of the *APOE ε4* allele will increase the risk of AD by 12-15 times that of an individual with two copies of *APOE ε3* (Roses, 1996). As well as being a risk factor for dementia, studies indicate that inheritance of the *APOE ε4* allele has an effect on the cognitive function of non demented older adults but no effect on cognitive function in children or in mid-life (Schiepers *et al.*, 2012). The effects of *APOE* genotype on the synaptic proteome of both control and AD individuals therefore also merits investigation as proteomic

changes could indicate areas of dysfunction that could widely increase our knowledge of the disease and could potentially be therapeutic targets.

The aims of the experiments presented in this chapter are:

-Prepare highly enriched synaptoneurosomes from end stage human brain tissue from AD and non-demented control (NDC) individuals with known *APOE* Genotypes and send them for unbiased LC-MS proteomics

-Use bioinformatics techniques to investigate the protein changes that occur in the synapse in AD and the effect that an *APOE ε4* genotype has on synaptic protein changes both in a NDC condition and in an AD condition

- Validate some of the protein hits using fluorescent western blotting

Figure 4.1 graphically represents this plan

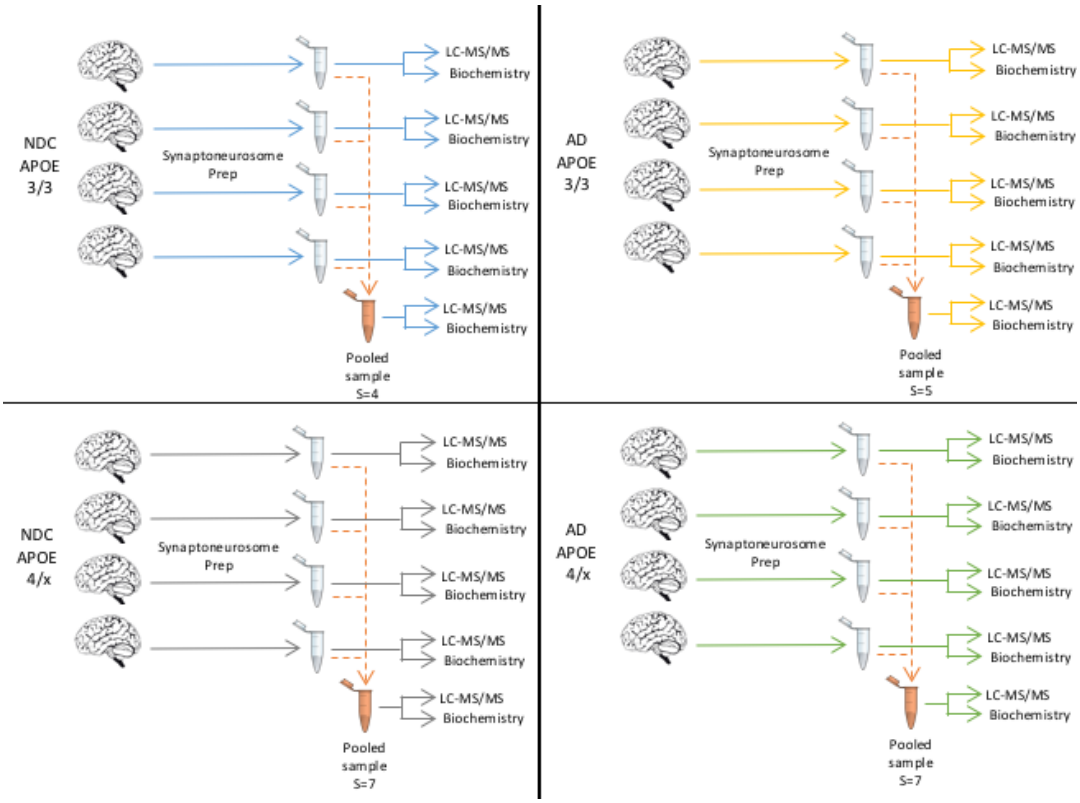

Figure 4.1: LC-MS Proteomic study design. Synaptoneurosome samples were prepared from the superior temporal gyrus from the brains of NDC and AD cases. Genotyping was used to spilt the conditions by genotype and 4 samples from each genotype and condition were sent for LC-MS/MS. A pooled sample was also run for all four experimental groups. S indicates the number of samples that were used to make the pooled sample.

4.2 Methods

Western blotting was carried out on samples sent for proteomics using the protocol as described in 2.2.2. The primary antibodies used are listed in Table 4.1. Cases used for western blotting are indicated by a star in Table 4.2.

Table 4.1: Antibodies using in western blotting in Chapter 4

Target	Host	Dilution	Catalogue number
PSD95	Rabbit	1:1000	D27E11
Synapsin	Rabbit	1:10000	AB1543
Beta-actin	Mouse	1:1000	ab8226
Histone H3	Rabbit	1:1000	ab1791
Synaptophysin	Mouse	1:5000	ab8049
NMDAR2B	Mouse	1:500	610416
GAPDH	Mouse	1:1000	ab8245
GAPDH	Rabbit	1:1000	ab9485
Flotillin 1	Rabbit	1:1000	A303-422A
LRP1	Rabbit	1:1000	Bs-2677R
Clusterin	Rabbit	1:1000	Sc-8354
Complement C4	Rabbit	1:250	ab181241

4.3 Results

4.3.1 Assessing two methods of preparing synaptoneurosomes

Synaptoneurosome prepared by both the filtration and the centrifugation methods resulted in synaptically enriched preperations which contained PSD and Synapsin1 (Figure 4.2A). The nuclear marker histone H3 was not present in either prep indicating the exclusion of nuclear material. Although both preps show enrichment of synaptic proteins by western blot, analysis by EM shows that the filtration method had better preservation of synapses (Figure 4.2B). This is potentially as the filtration method is quicker which reduces enzymatic degradation of the synaptic proteins. EM also showed that the filtration method resulted in higher preservation of both the pre and the postsynaptic densities as opposed to the centrifugation method which showed greater presynaptic isolation (Figure 4.2B). This was expected, as the centrifugation method is a synaptosome preparation which are known to be preferentially

presynaptic. As both presynaptic and postsynaptic protein changes are of interest in Alzheimer's disease the synaptonuerosomes were prepared using the filtration method were from all cases used in proteomics (Table 4.2).

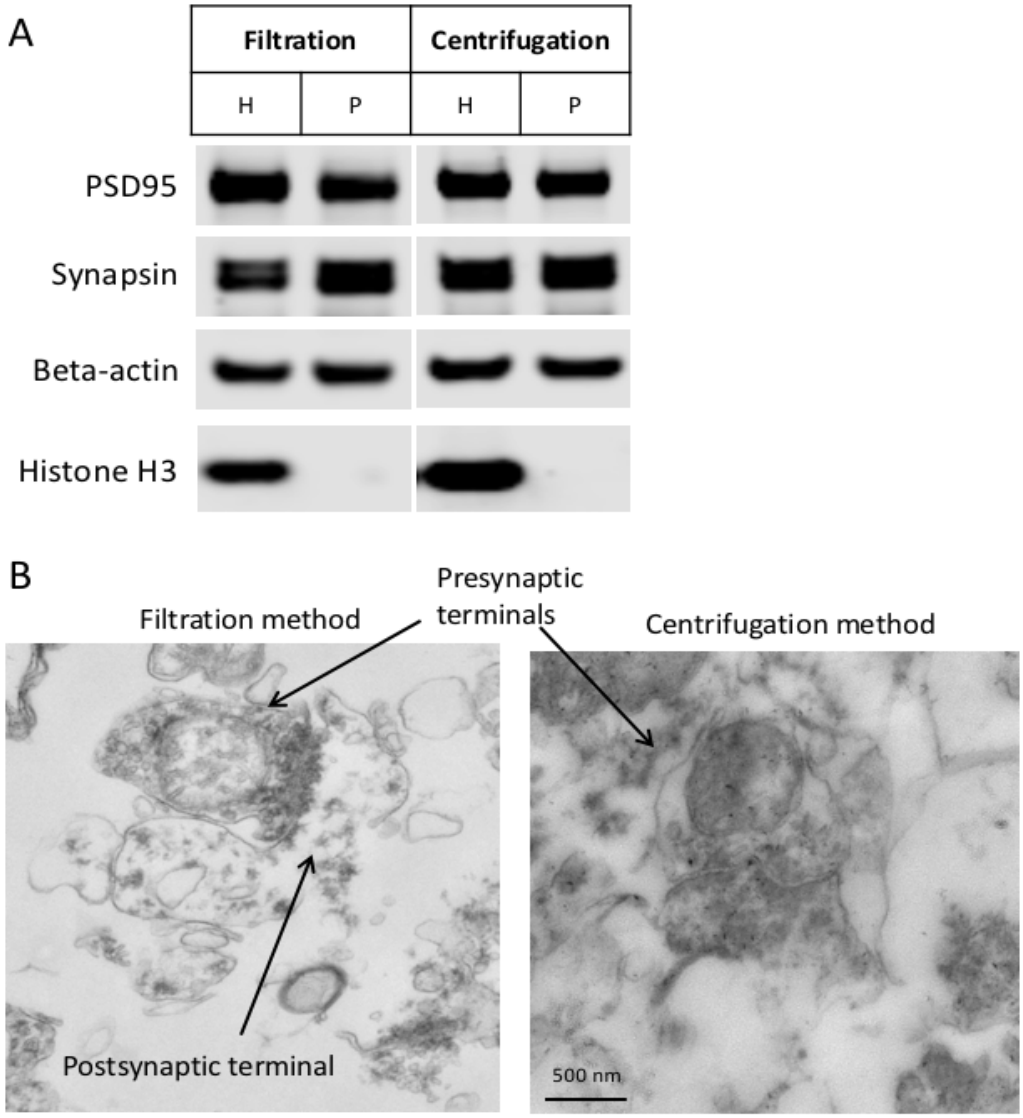

Figure 4.2: A comparison of two methods of isolating the synaptic fraction. A) The purity of the synaptic fraction (pellet, P) was compared to the crude homogenate (H) using western blotting and EM. Both methods show exclusion of nuclear material (histone) from the pellet and enrichment of the pre-synaptic proteins (synapsin) and post-synaptic proteins (PSD95). Beta-actin was using as a loading control. B) EM images of the synaptoneurosome preps from both protocols (performed by Tara Spires-Jones). EM shows that the filtration method shows greater isolation of intact synaptoneurosomes with the postsynaptic density attached. Filtration also provided a purer prep. Elements of interest are marked with arrows. Scale bar is 500nm.

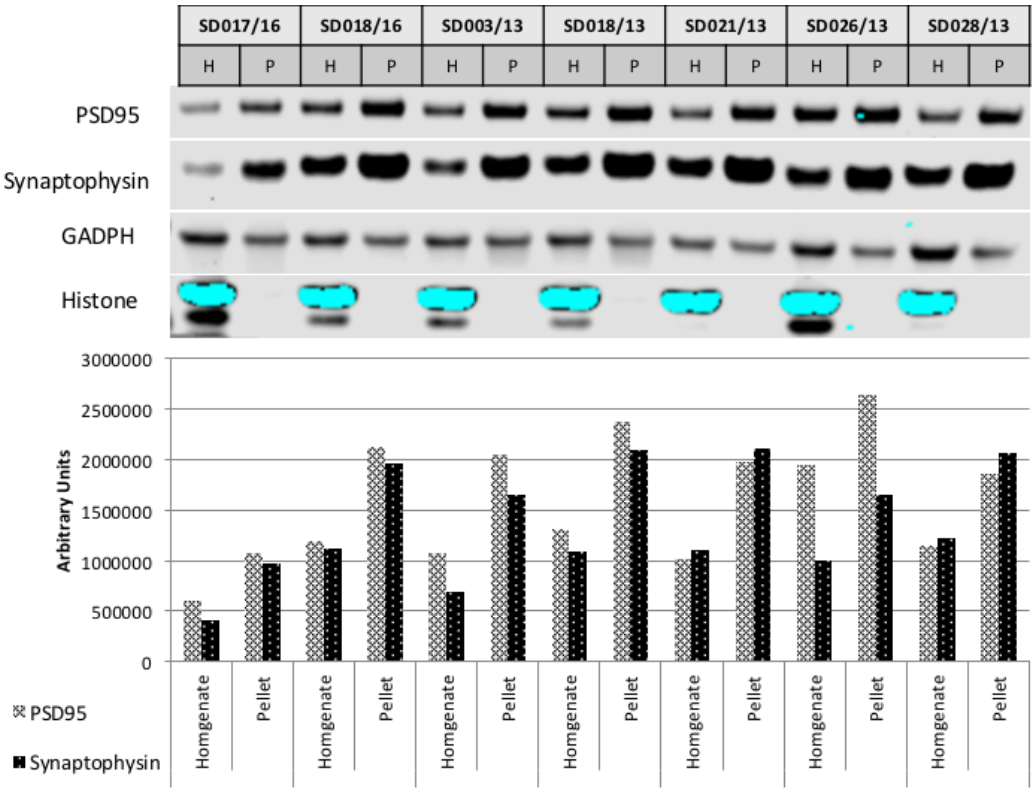

Figure 4.3: A representative enrichment blot and graphical representation of the enrichment of synaptic proteins. (A) 5µg of protein from the synaptoneurosome prep (P) from each sample was compared to 5µg crude homogenate (H) protein from that sample by western blot. Blots were probed for PSD95, synaptophysin, histone and GAPDH which was used as a loading control. (B) A graphical representation of PSD95 and Synaptophysin normalized to GAPDH. In every sample but SD023/13 there is more PSD95 and Synaptophysin present in the synaptoneurosome prep (P) than there is in the crude homogenate (H). The level of the synaptic proteins varies between the preps, however the enrichment of both synaptic proteins appears to be similar between preps.

4.3.2 Ensuring optimum protein integrity for LC-MS

Protein degradation was assessed using the "HUSPIR" ratio or degradation index (Bayés *et al.*, 2014). To find this value, synaptoneurosmes run on western blot were probed using an antibody against NMDAR2B which recognizes two bands, the full length protein at 170 kDa and a degradation product at 150kDa (Figure 4.4). This degradation product only occurs post-mortem as it is not found in autopsy tissue thus comparing these two bands is a good indication of post mortem synaptic protein degradation. The degradation index was found to significantly correlate to the RNA

integrity number (p=0.009, R^2=0.215, linear regression analysis) and lower but still significant correlation with brain pH (p=0.023, R^2=0.184, linear regression analysis) but not at all with Post Mortem Interval (Figure 4.5). This increased confidence that this marker was a good indicator of degradation.

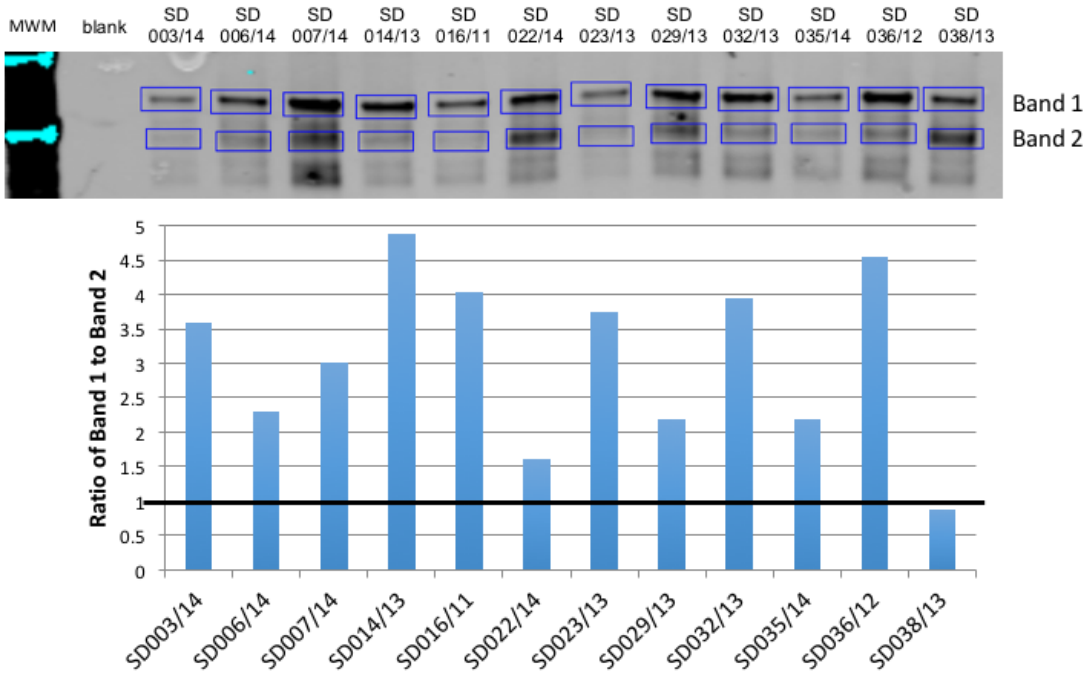

Figure 4.4: A sample degradation blot and graphical representation of the HUSPIR ratio. (A) Each synaptoneurosome prep was probed for NMDAR2B. Boxes indicate what was taken to be band 1 at ~170kDa and band 2 at ~150kDa. (B) A graphical representation of the Band 1/Band 2 ratio from this blot indicating the spread of ratios and thus the varied extent of degradation. Sample SD038/13 was considered to be below the cut off value of 1 and was therefore not included in proteomics.

Protein degradation was assessed using the degradation index, 7 out of 35 samples had a Band 1:Band 2 ratio of less than 1 (Table 4.2). Figure 4.4 shows a representative western blot where all but the sample SD038/13 show a good ratio of Band 1:Band 2. The ratio of Band 1 to Band 2 varied considerably between samples and in some cases Band 2 was barely visible in comparison with Band 1 indicating very good preservation of the synaptic proteins (Figure 4.4). Where the Band 1:Band 2 ratio was less than 1 the sample was not used for proteomics and where there were more than 4 samples of a given genotype and condition, samples with the highest Band 1:Band 2 ratio were sent as indicated by Table 4.3.

Table 4.2: Human cases from the Edinburgh sudden brain bank prepared for proteomics.

	Condition	Case No	MRC BBN	Gender	Age	PMI	pH	RIN	Degradation index
	NDC	SD042/14	24219	Male	63	76	5.9	3.5	0.187
	AD	SD050/12	9503	Male	61	38		4.1	0.459
	AD	SD039/13	19602	Male	86	21	6	4.1	0.607
	AD	SD015/13	15813	Male	92	25	6.3	4.5	0.608
	AD	SD052/12	9505	Male	81	34		3.5	0.740
	AD	SD032/14	22626	Female	81	60	6.5	3.4	0.858
	NDC	SD038/13	18391	Male	58	49	5.9	4.9	0.874
	AD	SD019/14	20995	Male	60	86	5.9	4.2	1.043
*	AD	SD003/13	10591	Male	86	76		5.8	1.400
*	AD	SD026/13	15258	Male	65	80	6.1	3.9	1.410
	NDC	SD022/14	22612	Male	61	70	6.1	4.6	1.617
	AD	SD038/14	23394	Female	88	59	6.3	5.2	1.712
	AD	SD018/13	15810	Female	73	96	6.2	4.3	1.870
*	AD	SD028/13	15259	Female	87	28	6.1	3.2	2.030
*	AD	SD056/14	24527	Male	81	74	6.1	6.3	2.047
*	AD	SD055/14	24526	Male	79	65	6.05	5.7	2.176
	NDC	SD035/14	22629	Female	59	53	6.3	5.6	2.191
	NDC	SD029/13	15809	Male	58	90	5.9	5.1	2.194
	NDC	SD006/14	20593	Male	60	52	6	5.6	2.302
	NDC	SD046/13	18407	Male	62	41	6.1	4.5	2.335
*	AD	SD062/13	19595	Male	87	58	6.5	4.5	2.466
*	NDC	SD007/14	20120	Male	53	97	6.4	4.9	3.007
*	AD	SD002/14	19994	Female	87	89	5.9	5	3.375
*	NDC	SD003/14	20122	Male	59	74	6.1	6.1	3.591
	NDC	SD023/13	15221	Male	53	114	6.1	5.4	3.753
*	NDC	SD032/13	16425	Male	61	99	6.2	5.8	3.944
*	NDC	SD016/11	2555	Male	74	66	6.3	5	4.041
	NDC	SD036/12	4174	Male	75	78	6.43	5.1	4.554
*	NDC	SD014/13	14395	Female	74	41	6.3	5.6	4.881
*	AD	SD021/13	15811	Female	81	41	6.3	3.8	5.104
*	NDC	SD051/14	24340	Male	53	53	6.5	5.6	5.305

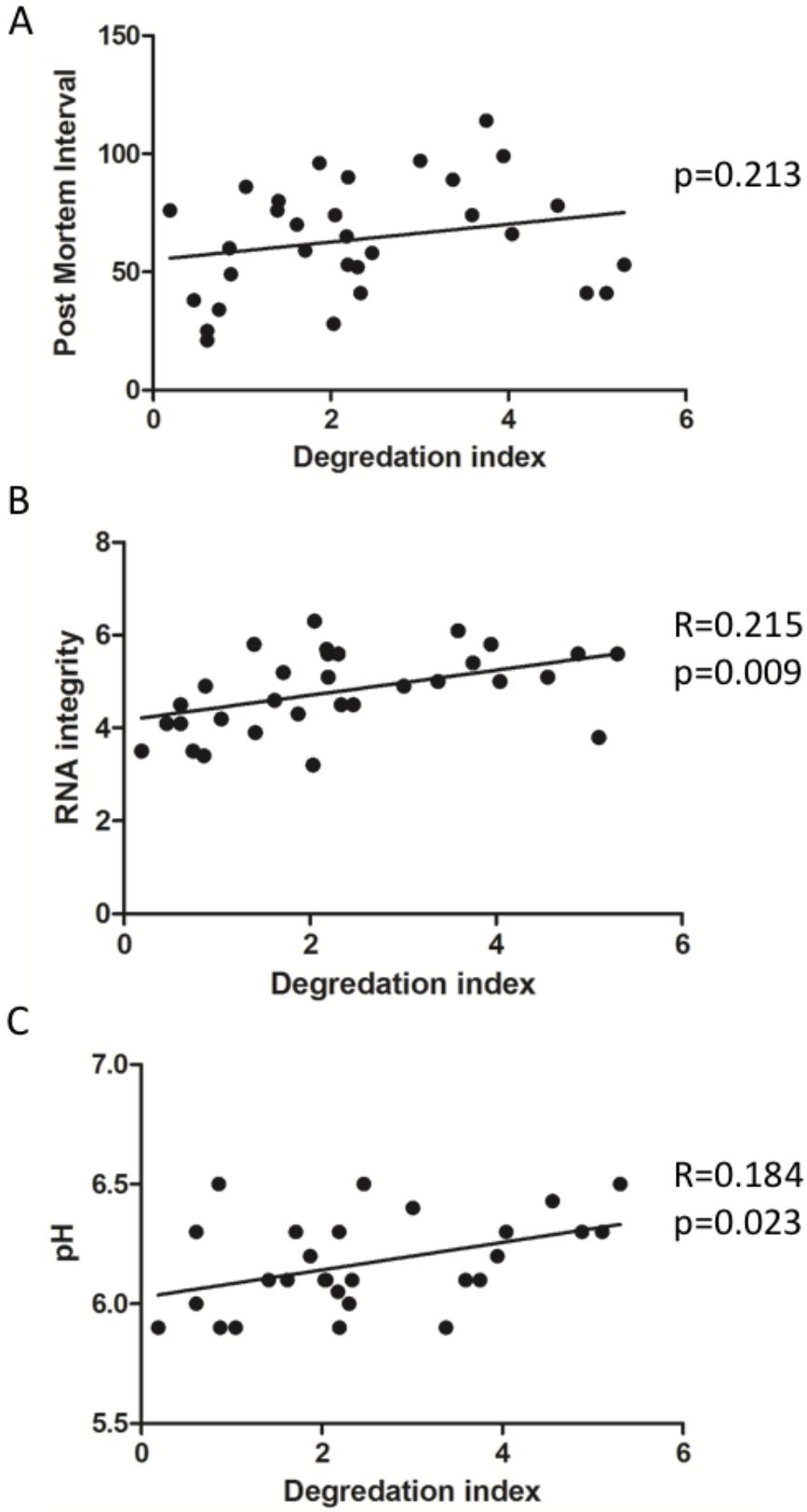

Figure 4.5: A Comparison of different methods of assessing protein integrity in post mortem tissue. (A) Linear regression analysis comparing the Degradation index and Post Mortem Interval (A), RNA integrity (B), and pH of the Brain (C).

Table 4.3: Individual and pooled samples that were sent for Proteomics

	Non-Demented Controls		AD	
	3/3	4/x	3/3	4/x
Samples sent for Individual Analysis as well as included in the pooled sample for that group	SD051/14	SD016/11	SD029/14	SD021/13
	SD014/13	SD032/13	SD062/13	SD055/14
	SD003/14	SD007/14	SD056/14	SD028/13
	SD022/14	SD023/13	SD026/13	SD018/13
Samples included only in the pooled sample for that group		SD035/14	SD02/14	SD003/13
		SD006/14		SD019/14
		SD029/13		SD038/14
Number of total samples in that group	4	7	5	7
Average age of group	61.75	59.71	84.4	79.42
% Female of group	25%	14.3%	60%	57.14%

4.3.3 Overview of the Proteomics Data

A total of 1043 proteins were identified by two or more unique peptides across all samples (Appendix 2). To ensure that synaptic enrichment had occurred as expected the total protein list was put into DAVID, a bioinformatic tool that allows for functional and biological annotation of large lists of genes (Huang *et al.*, 2008, 2009). DAVID is particularly powerful at identifying enriched gene ontology (GO) terms and biological themes, which it clusters to reduce redundancy. The synapse cluster was heavily enriched with an enrichment score of 11.48, as was the mitochondria cluster with an enrichment score of 40.88. As EM indicates that many of the mitochondria in the sample are synaptic mitochondria this is of particular interest as it could allow us to find disruptions in energy production in AD that are specific to the synapse and thus could indicate why the synapse is vulnerable in AD.

Comparison of AD synapses with NDC synapses showed that 173 proteins had significantly different levels of abundance ($p<0.05$, fold change >1.2), with 92 proteins found more abundantly in AD and 81 found to be less abundant (Table 4.4). Minimal

protein changes (41 proteins) were found when comparing APOE4 NDC with APOE3 NDC (Table 4.5). However, when comparing APOE4 AD cases with APOE3 AD cases 121 proteins were found to be significantly different in abundance with 40 found in less abundance in APOE4 cases and 81 found to be more abundant. (Table 4.6)

Table 4.4: Proteins found to be significantly different between AD and non-demented controls

Gene name	Protein name	Fold Change	p-value
PIP	prolactin-induced protein	8.95	0.00022
SBSN	suprabasin	6.82	0.00352
H1F0	H1 histone family, member 0	5.97	0.00004
AZGP1	alpha-2-glycoprotein 1, zinc-binding	4.97	0.00488
IGH	immunoglobulin heavy locus	3.54	0.00156
FLG2	filaggrin family member 2	3.51	0.00234
CALML5	calmodulin-like 5	3.31	0.00278
HSPB1	heat shock 27kDa protein 1	2.68	0.00000
C4A/C4B	complement component 4B (Chido blood group)	2.57	0.00003
APP	amyloid beta (A4) precursor protein	2.37	0.00004
IGKC	immunoglobulin kappa constant	2.36	0.00733
dkk3	dickkopf WNT signaling pathway inhibitor 3	2.32	0.00001
ADGRG1	adhesion G protein-coupled receptor G1	2.28	0.00474
RABGAP1	RAB GTPase activating protein 1	2.23	0.01140
FABP7	fatty acid binding protein 7, brain	2.13	0.01610
RAB27B	RAB27B, member RAS oncogene family	2.04	0.01690
IGLC2	immunoglobulin lambda constant 2 (Kern-Oz- marker)	2.03	0.00565
PAFAH1B3	platelet-activating factor acetylhydrolase 1b, catalytic subunit 3 (29kDa)	1.82	0.00011
ANXA2	annexin A2	1.77	0.00639
ALDH1L1	aldehyde dehydrogenase 1 family, member L1	1.67	0.00004
ATP5J	ATP synthase, H+ transporting, mitochondrial Fo complex, subunit F6	1.66	0.00369
MACROD1	MACRO domain containing 1	1.66	0.00124
ILF2	interleukin enhancer binding factor 2	1.65	0.00096
CLU	clusterin	1.63	0.00001
CA1	carbonic anhydrase I	1.62	0.04618
FLOT2	flotillin 2	1.59	0.00009
VAT1L	vesicle amine transport 1-like	1.58	0.00608
NPTX1	neuronal pentraxin I	1.57	0.00275

CASP14	caspase 14, apoptosis-related cysteine peptidase	1.56	0.03790
NANS	N-acetylneuraminic acid synthase	1.55	0.00007
PEA15	phosphoprotein enriched in astrocytes 15	1.54	0.00816
PHPT1	phosphohistidine phosphatase 1	1.53	0.01768
PLSCR4	phospholipid scramblase 4	1.50	0.00003
CPE	carboxypeptidase E	1.50	0.00472
LGI4	leucine-rich repeat LGI family, member 4	1.49	0.00149
PCSK1N	proprotein convertase subtilisin/kexin type 1 inhibitor	1.49	0.00294
ANXA1	annexin A1	1.45	0.00580
FLOT1	flotillin 1	1.45	0.00116
DCLK2	doublecortin-like kinase 2	1.45	0.00239
SLC32A1	solute carrier family 32 (GABA vesicular transporter), member 1	1.43	0.02741
CAPG	capping protein (actin filament), gelsolin-like	1.42	0.01288
S100A1	S100 calcium binding protein A1	1.41	0.04823
NCDN	neurochondrin	1.41	0.00071
CTTN	cortactin	1.40	0.02895
CTSD	cathepsin D	1.40	0.00058
PDE1B	phosphodiesterase 1B, calmodulin-dependent	1.40	0.00860
EIF5	eukaryotic translation initiation factor 5	1.40	0.00272
MLC1	megalencephalic leukoencephalopathy with subcortical cysts 1	1.38	0.03260
UBA1	ubiquitin-like modifier activating enzyme 1	1.38	0.01367
SLC1A3	solute carrier family 1 (glial high affinity glutamate transporter), member 3	1.37	0.00591
OLA1	Obg-like ATPase 1	1.37	0.02076
SNTA1	syntrophin, alpha 1	1.37	0.04158
PDPK1	3-phosphoinositide dependent protein kinase 1	1.35	0.01878
HLA-A	major histocompatibility complex, class I, A	1.34	0.02596
PHYHIP	phytanoyl-CoA 2-hydroxylase interacting protein	1.34	0.00075
RAPGEF2	Rap guanine nucleotide exchange factor (GEF) 2	1.34	0.04835
SELENBP1	selenium binding protein 1	1.33	0.00091
PLCD1	phospholipase C, delta 1	1.32	0.02837

AK1	adenylate kinase 1	1.30	0.00134
NAGK	N-acetylglucosamine kinase	1.30	0.00220
PSMB4	proteasome (prosome, macropain) subunit, beta type, 4	1.29	0.02370
PDXK	pyridoxal (pyridoxine, vitamin B6) kinase	1.29	0.00070
OTUB1	OTU deubiquitinase, ubiquitin aldehyde binding 1	1.29	0.02064
GGA3	golgi-associated, gamma adaptin ear containing, ARF binding protein 3	1.29	0.01195
NDRG4	NDRG family member 4	1.29	0.02482
GPX1	glutathione peroxidase 1	1.28	0.04337
ATP8A1	ATPase, aminophospholipid transporter (APLT), class I, type 8A, member 1	1.28	0.03207
RANBP1	RAN binding protein 1	1.28	0.03080
PBXIP1	pre-B-cell leukemia homeobox interacting protein 1	1.27	0.01359
FHL1	four and a half LIM domains 1	1.26	0.00815
PYGB	phosphorylase, glycogen; brain	1.26	0.00335
NDUFS6	NADH dehydrogenase (ubiquinone) Fe-S protein 6, 13kDa (NADH-coenzyme Q reductase)	1.26	0.01220
L1CAM	L1 cell adhesion molecule	1.26	0.04968
SIRT3	sirtuin 3	1.25	0.04316
WDR1	WD repeat domain 1	1.25	0.02335
KPNB1	karyopherin (importin) beta 1	1.25	0.00024
PRKAA2	protein kinase, AMP-activated, alpha 2 catalytic subunit	1.25	0.01254
MTHFD1	methylenetetrahydrofolate dehydrogenase (NADP+ dependent) 1	1.24	0.01311
PSAP	prosaposin	1.24	0.00110
ADD3	adducin 3 (gamma)	1.24	0.00443
ITGAV	integrin, alpha V	1.24	0.01427
PRDX5	peroxiredoxin 5	1.23	0.00256
PLEC	plectin	1.23	0.00345
FARSB	phenylalanyl-tRNA synthetase, beta subunit	1.23	0.00360
UCHL1	ubiquitin carboxyl-terminal esterase L1 (ubiquitin thiolesterase)	1.23	0.04856
LRP1	low density lipoprotein receptor-related protein 1	1.23	0.01797
FAM213A	family with sequence similarity 213, member A	1.22	0.03002
FASN	fatty acid synthase	1.21	0.04989

HNRNPK	heterogeneous nuclear ribonucleoprotein K	1.21	0.00247
PSD3	pleckstrin and Sec7 domain containing 3	1.21	0.01928
PGM1	phosphoglucomutase 1	1.21	0.02478
MTX3	metaxin 3	1.20	0.01317
Sept7	septin 7	-1.21	0.02548
MCCC2	methylcrotonoyl-CoA carboxylase 2 (beta)	-1.21	0.04101
TAGLN3	transgelin 3	-1.23	0.02569
PALM	paralemmin	-1.23	0.01377
IARS2	isoleucyl-tRNA synthetase 2, mitochondrial	-1.23	0.02219
CHMP4B	charged multivesicular body protein 4B	-1.24	0.01550
GSS	glutathione synthetase	-1.24	0.01008
NDUFS8	NADH dehydrogenase (ubiquinone) Fe-S protein 8, 23kDa (NADH-coenzyme Q reductase)	-1.25	0.02927
STX7	syntaxin 7	-1.25	0.01180
SNAP25	synaptosomal-associated protein, 25kDa	-1.25	0.00298
SEPT2	septin 2	-1.26	0.02808
NDUFB7	NADH dehydrogenase (ubiquinone) 1 beta subcomplex, 7, 18kDa	-1.26	0.03881
RAC1	ras-related C3 botulinum toxin substrate 1 (rho family, small GTP binding protein Rac1)	-1.27	0.04528
RUFY3	RUN and FYVE domain containing 3	-1.28	0.01262
CHCHD6	coiled-coil-helix-coiled-coil-helix domain containing 6	-1.28	0.01852
PDHX	pyruvate dehydrogenase complex, component X	-1.29	0.02459
GNG12	guanine nucleotide binding protein (G protein), gamma 12	-1.29	0.04449
LRPPRC	leucine-rich pentatricopeptide repeat containing	-1.30	0.00016
SLC25A22	solute carrier family 25 (mitochondrial carrier: glutamate), member 22	-1.30	0.00014
ADRM1	adhesion regulating molecule 1	-1.31	0.00024
MAP6	microtubule-associated protein 6	-1.31	0.01023
FSCN1	fascin actin-bundling protein 1	-1.31	0.03173
MARCKS	myristoylated alanine-rich protein kinase C substrate	-1.31	0.00884
FIS1	fission 1 (mitochondrial outer membrane) homolog (S. cerevisiae)	-1.32	0.00383
ACADSB	acyl-CoA dehydrogenase, short/branched chain	-1.33	0.04815
CYCS	cytochrome c, somatic	-1.33	0.00507

HADHB	hydroxyacyl-CoA dehydrogenase/3-ketoacyl-CoA thiolase/enoyl-CoA hydratase, beta subunit	-1.33	0.03733
DYNLRB1	dynein, light chain, roadblock-type 1	-1.33	0.03712
LASP1	LIM and SH3 protein 1	-1.34	0.04769
CDC42	cell division cycle 42	-1.35	0.04132
SYNPO	synaptopodin	-1.36	0.00293
FAM49B	family with sequence similarity 49, member B	-1.36	0.01172
GPM6B	glycoprotein M6B	-1.36	0.02208
QDPR	quinoid dihydropteridine reductase	-1.36	0.02972
IDH1	isocitrate dehydrogenase 1 (NADP+), soluble	-1.38	0.04546
CCBL2	cysteine conjugate-beta lyase 2	-1.38	0.04868
NDUFA7	NADH dehydrogenase (ubiquinone) 1 alpha subcomplex, 7, 14.5kDa	-1.41	0.01143
ADSS	adenylosuccinate synthase	-1.43	0.04470
ATP5L	ATP synthase, H+ transporting, mitochondrial Fo complex, subunit G	-1.44	0.00657
RPL11	ribosomal protein L11	-1.46	0.02048
TPP2	tripeptidyl peptidase II	-1.47	0.01334
DPYSL5	dihydropyrimidinase-like 5	-1.48	0.02756
IVD	isovaleryl-CoA dehydrogenase	-1.49	0.00398
DYNC1LI2	dynein, cytoplasmic 1, light intermediate chain 2	-1.50	0.00056
PLCL1	phospholipase C-like 1	-1.51	0.04570
RPL8	ribosomal protein L8	-1.52	0.00834
OMG	oligodendrocyte myelin glycoprotein	-1.53	0.04964
TXNDC5	thioredoxin domain containing 5 (endoplasmic reticulum)	-1.57	0.02718
DYNC1I2	dynein, cytoplasmic 1, intermediate chain 2	-1.60	0.00269
MARCKSL1	MARCKS-like 1	-1.61	0.01702
MYO1D	myosin ID	-1.61	0.02957
GNG7	guanine nucleotide binding protein (G protein), gamma 7	-1.65	0.00659
JAM2	junctional adhesion molecule 2	-1.67	0.00000
MAP4	microtubule-associated protein 4	-1.73	0.00158
GLTP	glycolipid transfer protein	-1.74	0.02757
FMNL2	formin-like 2	-1.76	0.01918

GPD1	glycerol-3-phosphate dehydrogenase 1 (soluble)	-1.77	0.04129
SEPT10	septin 10	-1.79	0.02979
MYADM	myeloid-associated differentiation marker	-1.81	0.04790
CADM4	cell adhesion molecule 4	-1.87	0.01451
ADAM10	ADAM metallopeptidase domain 10	-1.94	0.02719
SLC12A2	solute carrier family 12 (sodium/potassium/chloride transporter), member 2	-1.96	0.01194
OPALIN	oligodendrocytic myelin paranodal and inner loop protein	-1.97	0.00886
ENPP6	ectonucleotide pyrophosphatase/phosphodiesterase 6	-1.98	0.04195
CDC42EP1	CDC42 effector protein (Rho GTPase binding) 1	-2.00	0.01730
CNP	2',3'-cyclic nucleotide 3' phosphodiesterase	-2.01	0.03573
PITRM1	pitrilysin metallopeptidase 1	-2.06	0.02288
SLC44A1	solute carrier family 44 (choline transporter), member 1	-2.06	0.04131
MOG	myelin oligodendrocyte glycoprotein	-2.10	0.02783
ERMN	ermin, ERM-like protein	-2.19	0.00477
JAM3	junctional adhesion molecule 3	-2.21	0.01504
INF2	inverted formin, FH2 and WH2 domain containing	-2.21	0.01183
GLIPR2	GLI pathogenesis-related 2	-2.28	0.01709
SIRT2	sirtuin 2	-2.35	0.01492
RHOG	ras homolog family member G	-2.39	0.00969
CA14	carbonic anhydrase XIV	-2.52	0.01413
CLDN11	claudin 11	-2.52	0.01552
PMP2	peripheral myelin protein 2	-2.52	0.02069
MAG	myelin associated glycoprotein	-2.54	0.01206
MVP	major vault protein	-2.61	0.00537
PLA2G16	phospholipase A2, group XVI	-3.41	0.02816

Table 4.5: Proteins found to be significantly different between APOE3 NDC and APOE4 NDC

Gene Name	Protein Name	Fold Change	p-value
C4A/C4B	complement component 4B	2.00	0.00003
PITRM1	pitrilysin metallopeptidase 1	1.85	0.02288
CASP14	caspase 14, apoptosis-related cysteine peptidase	1.76	0.03790
PMP2	peripheral myelin protein 2	1.41	0.02069
HLA-A	major histocompatibility complex, class I, A	1.40	0.02596
STOM	stomatin	1.39	0.01512
PSAP	prosaposin	1.38	0.00110
FLOT2	flotillin 2	1.37	0.00009
GPM6B	glycoprotein M6B	1.35	0.02208
CPE	carboxypeptidase E	1.35	0.00472
RPL8	ribosomal protein L8	1.32	0.00834
GPD2	glycerol-3-phosphate dehydrogenase 2 (mitochondrial)	1.31	0.02658
CYB5R1	cytochrome b5 reductase 1	1.28	0.00392
DKK3	dickkopf WNT signaling pathway inhibitor 3	1.27	0.00001
APOE	apolipoprotein E	1.26	0.02077
APP	amyloid beta (A4) precursor protein	1.24	0.00004
LGI4	leucine-rich repeat LGI family, member 4	1.23	0.00149
IGH	immunoglobulin heavy locus	1.23	0.00156
ERP29	endoplasmic reticulum protein 29	1.22	0.02294
ENPP6	ectonucleotide pyrophosphatase/phosphodiesterase 6	1.21	0.04195
MYO1D	myosin ID	-1.20	0.02957
CA1	carbonic anhydrase I	-1.20	0.04618
PLCL1	phospholipase C-like 1	-1.21	0.04570
ARPC4-TTLL3	ARPC4-TTLL3 readthrough	-1.21	0.04241
MCCC2	methylcrotonoyl-CoA carboxylase 2 (beta)	-1.22	0.04101
AKR1A1	aldo-keto reductase family 1, member A1 (aldehyde reductase)	-1.22	0.00204
ATIC	5-aminoimidazole-4-carboxamide ribonucleotide formyltransferase/IMP cyclohydrolase	-1.24	0.01882
CA14	carbonic anhydrase XIV	-1.25	0.01413

LASP1	LIM and SH3 protein 1	-1.28	0.04769
SBSN	suprabasin	-1.30	0.00352
IPO7	importin 7	-1.31	0.01294
TPP2	tripeptidyl peptidase II	-1.31	0.01334
ILF2	interleukin enhancer binding factor 2	-1.36	0.00096
GGA3	golgi-associated, gamma adaptin ear containing, ARF binding protein 3	-1.38	0.01195
PYGM	phosphorylase, glycogen, muscle	-1.40	0.04450
GLTP	glycolipid transfer protein	-1.40	0.02757
AZGP1	alpha-2-glycoprotein 1, zinc-binding	-1.40	0.00488
PHPT1	phosphohistidine phosphatase 1	-1.52	0.01768
H1F0	H1 histone family, member 0	-1.59	0.00004
ITGB1	integrin, beta 1 (fibronectin receptor, beta polypeptide, antigen CD29 includes MDF2, MSK12)	-1.76	0.01027
FLG2	filaggrin family member 2	-2.49	0.01958

Table 4.6: Proteins found to be significantly different between AD APOE3 and AD APOE4 cases

Gene Name	Protein name	Fold change	p-value
PIP	prolactin-induced protein	3.77	0.0002
PMP2	peripheral myelin protein 2	3.34	0.0207
AZGP1	alpha-2-glycoprotein 1, zinc-binding	3.14	0.0049
ITGB1	integrin, beta 1 (fibronectin receptor, beta polypeptide, antigen CD29 includes MDF2, MSK12)	2.91	0.0103
SEPT10	septin 10	2.36	0.0298
HLA-A	major histocompatibility complex, class I, A	2.23	0.0260
H1F0	H1 histone family, member 0	2.20	0.0000
CALML5	calmodulin-like 5	2.10	0.0028
RABGAP1	RAB GTPase activating protein 1	2.05	0.0114
ENPP6	ectonucleotide pyrophosphatase/phosphodiesterase 6	1.98	0.0419
GLTP	glycolipid transfer protein	1.94	0.0276
PYGM	phosphorylase, glycogen, muscle	1.88	0.0445
CLDN11	claudin 11	1.88	0.0155
IVD	isovaleryl-CoA dehydrogenase	1.80	0.0040
CA14	carbonic anhydrase XIV	1.71	0.0141
DYNC1I2	dynein, cytoplasmic 1, intermediate chain 2	1.70	0.0027
PAFAH1B3	platelet-activating factor acetylhydrolase 1b, catalytic subunit 3 (29kDa)	1.70	0.0001
GPD1	glycerol-3-phosphate dehydrogenase 1 (soluble)	1.69	0.0413
MYO1D	myosin ID	1.66	0.0296
JAM3	junctional adhesion molecule 3	1.66	0.0150
PLA2G16	phospholipase A2, group XVI	1.66	0.0282
PLSCR4	phospholipid scramblase 4	1.64	0.0000
SIRT2	sirtuin 2	1.64	0.0149
MOG	myelin oligodendrocyte glycoprotein	1.63	0.0278
OPALIN	oligodendrocytic myelin paranodal and inner loop protein	1.63	0.0089
FLG2	filaggrin family member 2	1.62	0.0023
RHOG	ras homolog family member G	1.59	0.0097
ADSS	adenylosuccinate synthase	1.58	0.0447

PBXIP1	pre-B-cell leukemia homeobox interacting protein 1	1.58	0.0136
SCRN1	secernin 1	1.56	0.0092
GLIPR2	GLI pathogenesis-related 2	1.56	0.0171
AKR1A1	aldo-keto reductase family 1, member A1 (aldehyde reductase)	1.56	0.0020
IDH1	isocitrate dehydrogenase 1 (NADP+), soluble	1.55	0.0455
QDPR	quinoid dihydropteridine reductase	1.54	0.0297
SEPT2	septin 2	1.54	0.0281
C4A	complement component 4B (Chido blood group)	1.54	0.0000
MAG	myelin associated glycoprotein	1.53	0.0121
GNG12	guanine nucleotide binding protein (G protein), gamma 12	1.53	0.0445
CNP	2',3'-cyclic nucleotide 3' phosphodiesterase	1.52	0.0357
ADAM10	ADAM metallopeptidase domain 10	1.49	0.0272
MARCKSL1	MARCKS-like 1	1.48	0.0170
INF2	inverted formin, FH2 and WH2 domain containing	1.42	0.0118
ERMN	ermin, ERM-like protein	1.42	0.0048
NAGK	N-acetylglucosamine kinase	1.41	0.0022
ANXA1	annexin A1	1.41	0.0058
SBSN	suprabasin	1.41	0.0035
ADGRG1	adhesion G protein-coupled receptor G1	1.41	0.0047
MTX3	metaxin 3	1.41	0.0132
FKBP4	FK506 binding protein 4, 59kDa	1.38	0.0467
S100A1	S100 calcium binding protein A1	1.37	0.0482
CRKL	v-crk avian sarcoma virus CT10 oncogene homolog-like	1.36	0.0158
TXNDC5	thioredoxin domain containing 5 (endoplasmic reticulum)	1.35	0.0272
PLCL1	phospholipase C-like 1	1.35	0.0457
GNG7	guanine nucleotide binding protein (G protein), gamma 7	1.35	0.0066
MARCKS	myristoylated alanine-rich protein kinase C substrate	1.35	0.0088
JAM2	junctional adhesion molecule 2	1.34	0.0000
AKR1C3	aldo-keto reductase family 1, member C3	1.33	0.0115
PGM1	phosphoglucomutase 1	1.33	0.0248

MVP	major vault protein	1.32	0.0054
SLC44A1	solute carrier family 44 (choline transporter), member 1	1.31	0.0413
LASP1	LIM and SH3 protein 1	1.31	0.0477
CASP14	caspase 14, apoptosis-related cysteine peptidase	1.29	0.0379
PLCD1	phospholipase C, delta 1	1.28	0.0284
HSPB1	heat shock 27kDa protein 1	1.27	0.0000
APOE	apolipoprotein E	1.27	0.0208
PRKACB	protein kinase, cAMP-dependent, catalytic, beta	1.27	0.0026
SELENBP1	selenium binding protein 1	1.26	0.0009
CLU	clusterin	1.26	0.0000
RABGGTA	Rab geranylgeranyltransferase, alpha subunit	1.25	0.0197
FMNL2	formin-like 2	1.25	0.0192
RPL8	ribosomal protein L8	1.25	0.0083
CTTN	cortactin	1.25	0.0290
ASRGL1	asparaginase like 1	1.24	0.0480
AKR1B1	aldo-keto reductase family 1, member B1 (aldose reductase)	1.23	0.0220
CADM4	cell adhesion molecule 4	1.23	0.0145
APP	amyloid beta (A4) precursor protein	1.22	0.0000
PHPT1	phosphohistidine phosphatase 1	1.21	0.0177
ALDH1L1	aldehyde dehydrogenase 1 family, member L1	1.21	0.0000
SLC12A2	solute carrier family 12 (sodium/potassium/chloride transporter), member 2	1.20	0.0119
PSMA5	proteasome (prosome, macropain) subunit, alpha type, 5	1.20	0.0043
CAPNS1	calpain, small subunit 1	1.20	0.0090
HINT2	histidine triad nucleotide binding protein 2	-1.20	0.0240
ABI1	abl-interactor 1	-1.20	0.0102
HINT1	histidine triad nucleotide binding protein 1	-1.22	0.0187
CYCS	cytochrome c, somatic	-1.22	0.0051
NIPSNAP1	nipsnap homolog 1 (C. elegans)	-1.23	0.0489
NPTX1	neuronal pentraxin I	-1.23	0.0028
PRDX5	peroxiredoxin 5	-1.24	0.0026

NCKAP1	NCK-associated protein 1	-1.24	0.0341
TSFM	Ts translation elongation factor, mitochondrial	-1.25	0.0305
PALM	paralemmin	-1.25	0.0138
ADRM1	adhesion regulating molecule 1	-1.26	0.0002
DMTN	dematin actin binding protein	-1.26	0.0090
ERP29	endoplasmic reticulum protein 29	-1.27	0.0229
CAMK4	calcium/calmodulin-dependent protein kinase IV	-1.27	0.0317
MDH2	malate dehydrogenase 2, NAD (mitochondrial)	-1.27	0.0131
PACSIN1	protein kinase C and casein kinase substrate in neurons 1	-1.27	0.0314
NDUFS7	NADH dehydrogenase (ubiquinone) Fe-S protein 7, 20kDa (NADH-coenzyme Q reductase)	-1.28	0.0436
SOD2	superoxide dismutase 2, mitochondrial	-1.29	0.0084
HAGH	hydroxyacylglutathione hydrolase	-1.30	0.0210
ESYT2	extended synaptotagmin-like protein 2	-1.32	0.0059
MAP6	microtubule-associated protein 6	-1.32	0.0102
MRPS36	mitochondrial ribosomal protein S36	-1.32	0.0010
SV2B	synaptic vesicle glycoprotein 2B	-1.32	0.0462
ARPC1A	actin related protein 2/3 complex, subunit 1A, 41kDa	-1.33	0.0461
NDUFS4	NADH dehydrogenase (ubiquinone) Fe-S protein 4, 18kDa (NADH-coenzyme Q reductase)	-1.33	0.0293
SYNPO	synaptopodin	-1.34	0.0029
NGEF	neuronal guanine nucleotide exchange factor	-1.34	0.0383
ATP5H	ATP synthase, H+ transporting, mitochondrial Fo complex, subunit d	-1.35	0.0360
FAM213A	family with sequence similarity 213, member A	-1.36	0.0300
FLOT2	flotillin 2	-1.38	0.0001
RAB27B	RAB27B, member RAS oncogene family	-1.39	0.0169
FARSB	phenylalanyl-tRNA synthetase, beta subunit	-1.39	0.0036
TAGLN3	transgelin 3	-1.39	0.0257
FARSA	phenylalanyl-tRNA synthetase, alpha subunit	-1.39	0.0246
IGKC	immunoglobulin kappa constant	-1.41	0.0073
PITRM1	pitrilysin metallopeptidase 1	-1.41	0.0229
HAPLN1	hyaluronan and proteoglycan link protein 1	-1.46	0.0160

NDUFS6	NADH dehydrogenase (ubiquinone) Fe-S protein 6, 13kDa (NADH-coenzyme Q reductase)	-1.47	0.0122
CYB5R1	cytochrome b5 reductase 1	-1.55	0.0039
ATP5J	ATP synthase, H+ transporting, mitochondrial Fo complex, subunit F6	-2.41	0.0037

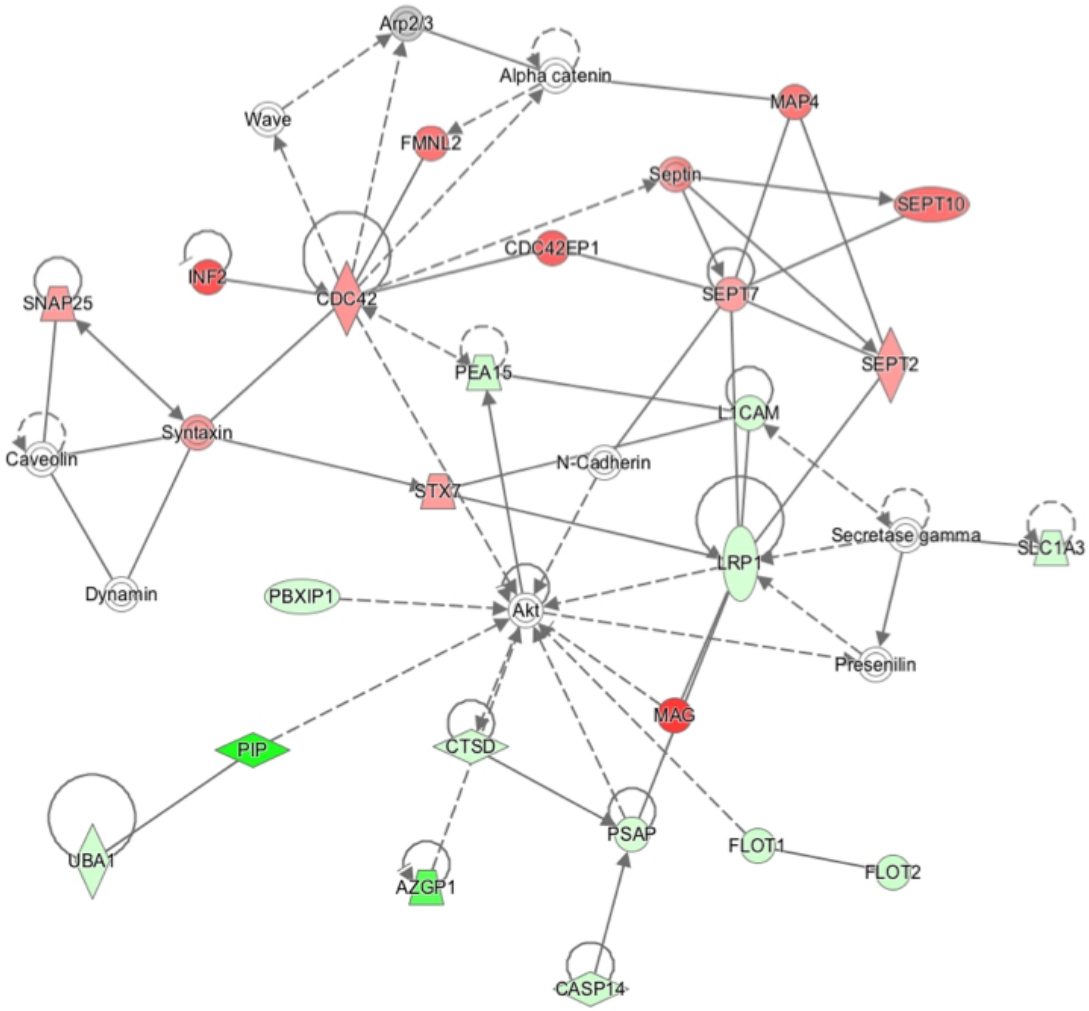

Figure 4.6: Changes in Cell Morphology Network in Alzheimer's Disease synapse. The highest scoring Ingenuity pathway analysis network found when comparing proteins changing in AD with NDC. Many proteins in this network are involved in the regulation of cell morphology, endocytosis and exocytosis and maintenance of the lipid bilayer. Colored nodes indicate proteins found to be significantly change in the proteomics data set. Red nodes indicate that a protein's expression has gone down in AD and green nodes indicate the expression has gone up. The intensity of the color indicates the size of the fold change where more intense coloring indicates a greater fold change. Uncolored nodes are inserted by IPA to increase the coherence of the network as are nodes which contain a circle inside a circle such as Septin. Solid lines indicate a direct relationship and dotted lines an indirect relationship.

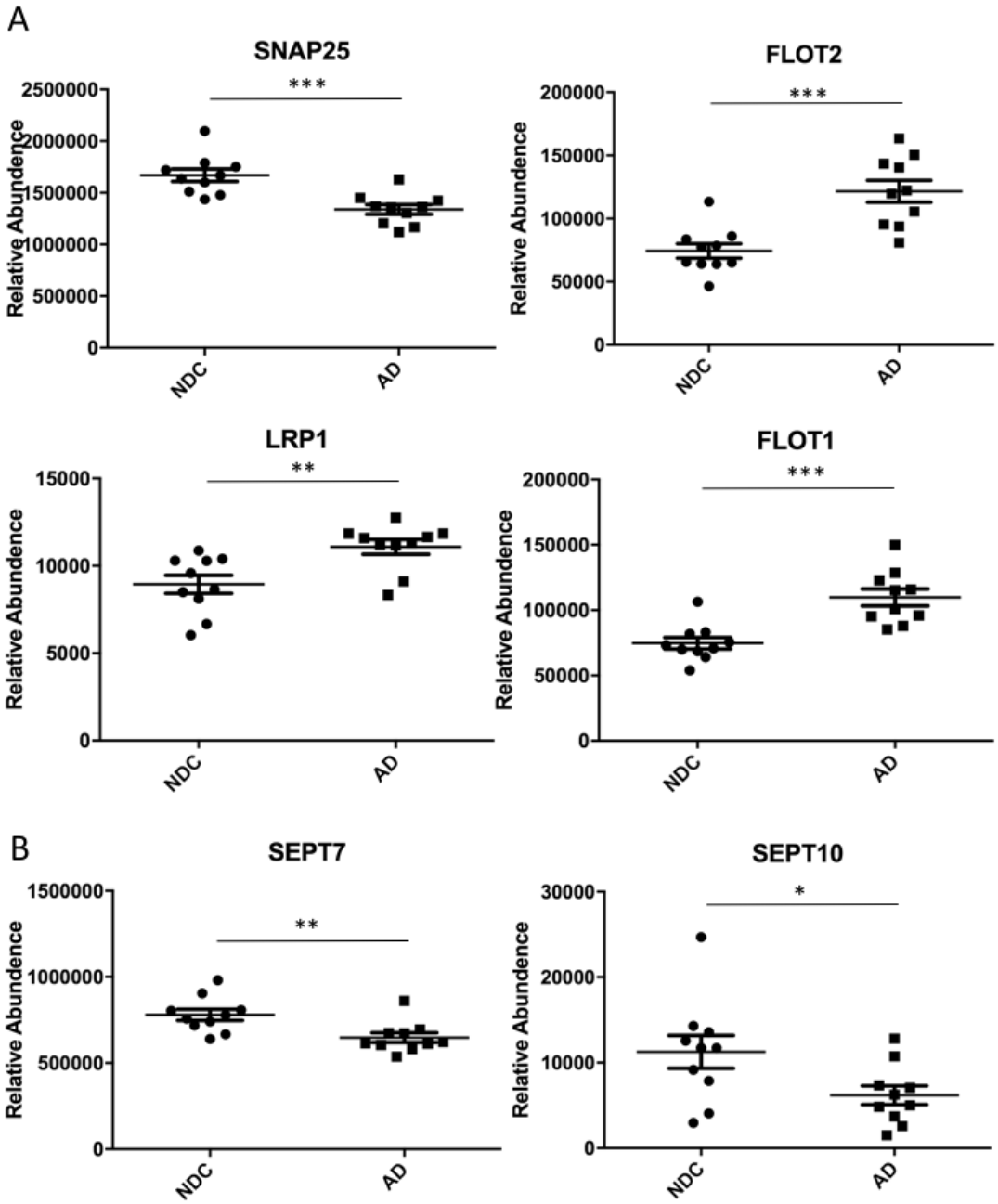

Figure 4.7: Changes in Cell Morphology, Maintenance of the Lipid Bilayer and Endosome Trafficking in Alzheimer's Disease synapse. Key proteins in Endosome Trafficking (SNAP25, FLOT2, FLOT1 and LRP1)(A) are changed in AD. Several Septin proteins, key proteins in maintenance of the actin cytoskeleton are down regulated in AD (B). Each point represents an individual sample (*** $p<0.001$, ** $p<0.01$, * $p<0.05$, T-test)

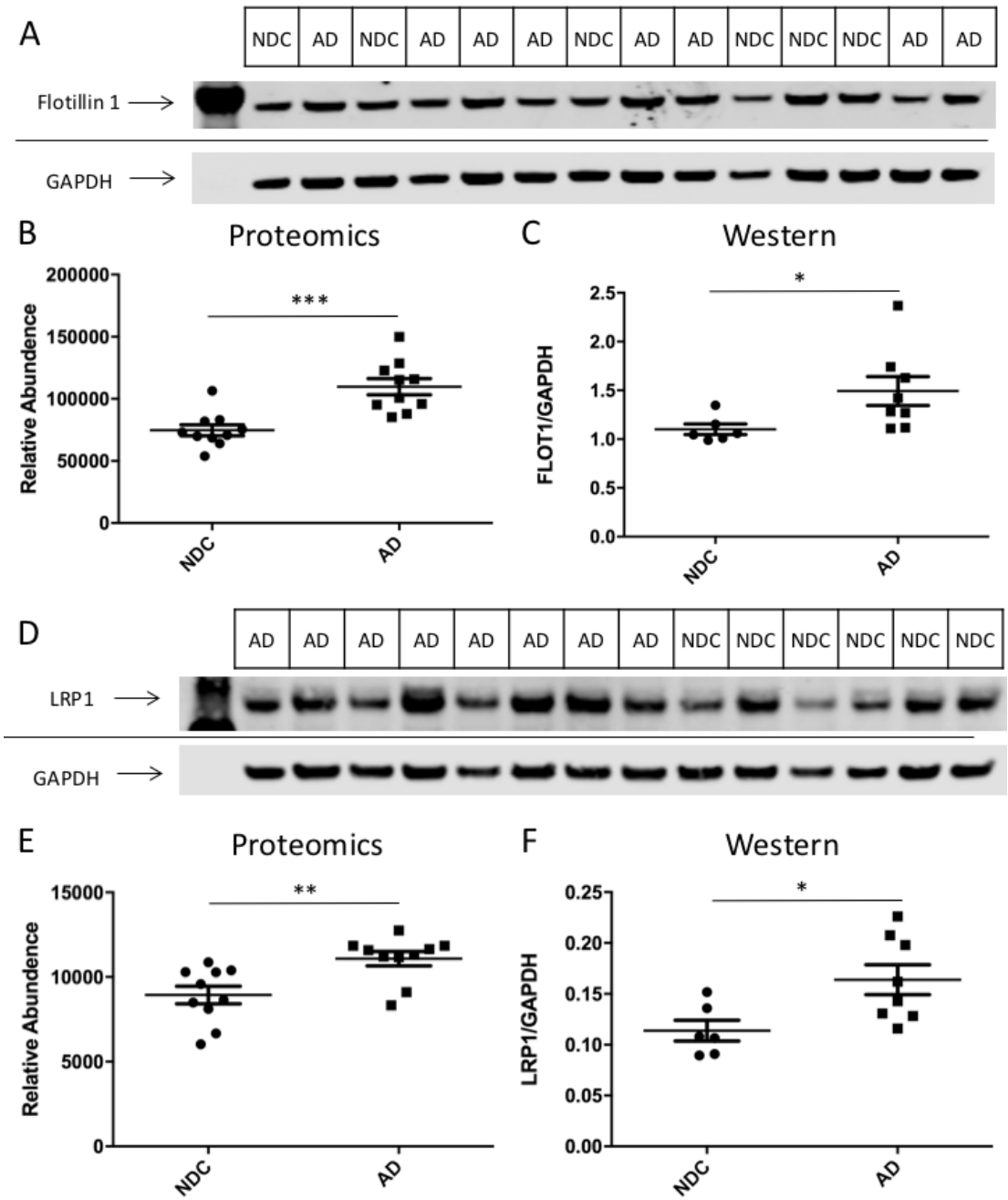

Figure 4.8: Western Blot confirmation of selected proteins involved in the regulation of the lipid bilayer. (A) A Western Blot of some of the synaptoneurosome preps sent for proteomics probed for FLOT1 and GAPDH. FLOT1 is up regulated by western blot (C) confirming the results of the proteomics data (B) by another technique. (D)) A Western Blot of synaptoneurosome preps probed for LRP1 and GAPDH. LRP1 is up regulated by western blot also confirming the results of the proteomics data. (*** $p<0.001$, ** $p<0.01$, * $p<0.05$, T-test)

4.3.4 Key protein clusters significantly changed in Alzheimer's Disease compared to non-demented controls

Ingenuity Pathway Analysis (IPA) allows functional protein-protein interactions to be defined and to be grouped into networks using computer algorithms with manual curation of protein-protein interactions. As IPA networks are generated from currently existing and published datasets the strength of predicted interactions is very high however it is skewed towards highly studied areas of science such as cancer. IPA created 10 proteins networks from the proteins that were significantly changed in AD compared to NDCs. The highest IPA network, with a network score of 46, highlighted proteins involved in cell morphology, endocytosis and exocytosis and regulation of the lipid bilayer as being significantly altered in AD synapses (Figure 4.6). Analysis using DAVID annotation clustering showed that 10 of the proteins significantly altered in AD are involved specifically in endocytosis and vesicle trafficking including Flotillin 1 and 2 (FLOT1 and FLOT2), LDL receptor related protein 1 (LRP1) and synaptosome associated protein 25 (SNAP25) (Figure 4.7). DAVID also showed that 21 proteins involved in cell morphology were significantly different in AD. These proteins again included the Flotillins as well as Septin proteins 2, 7 and 10 (SEPT2, SEPT7, SEPT10). Western blot analysis of Flotillin 1 and LRP1 confirmed the results of the proteomics using a different method (Figure 4.8).

Changes in proteins related to energy production and small molecule biochemistry were also highlighted by both IPA and DAVID analysis of the proteins significantly different in AD (Figure 4.9). 32 of the proteins significantly changed in the AD synapse classify under the GO term Mitochondria although only some of them cluster into this network. These proteins include many parts of complex 1 the first stage in the energy production process (Figure 4.10A). All of the mitochondrial proteins found to be altered in this proteomics data set are chromosomally encoded although no proteins encoded by the mitochondrial genome were detected by the LC-MS/MS. Of particular interest is pitrilysin metallopeptidase 1 (PITRM1) which is found to be less

abundant in the AD synapses and is responsible for degrading Aβ inside the mitochondria and APP which is found to be increased in AD (Figure 4.10B).

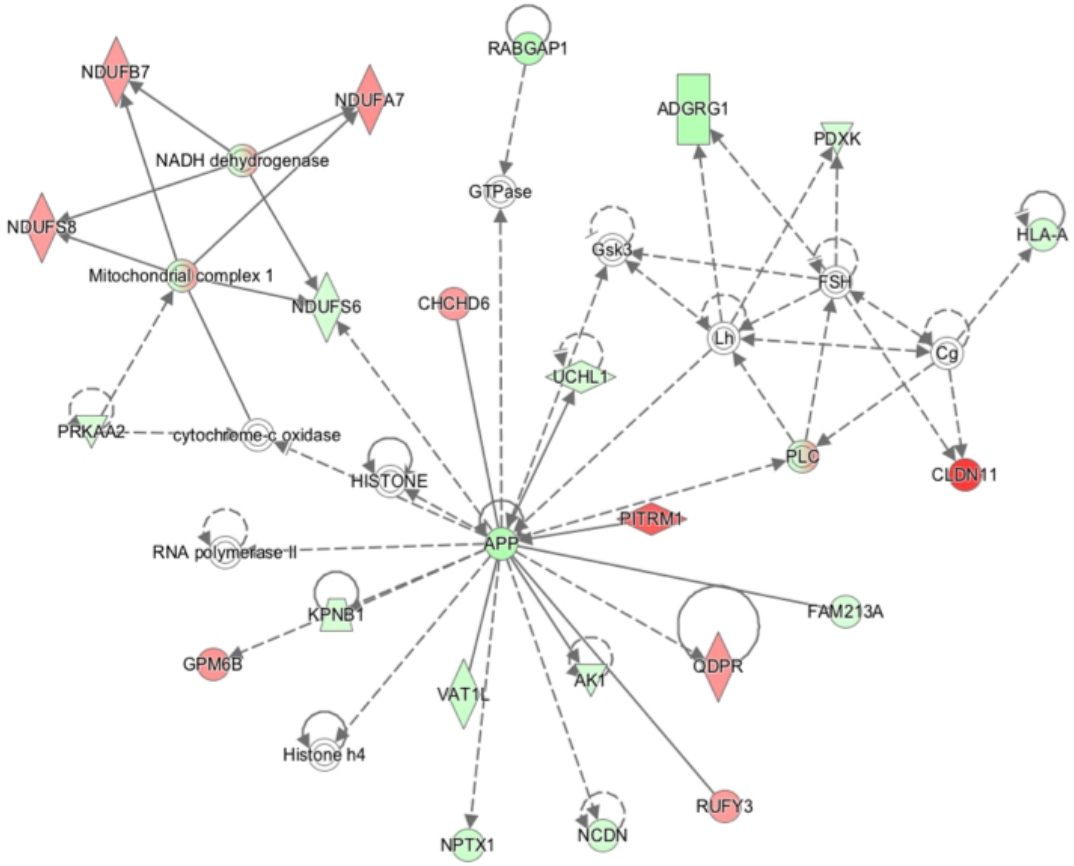

Figure 4.9: Changes in Energy Production and Small Molecule Biochemistry Network in Alzheimer's Disease synapse. (A) A high scoring Ingenuity pathway analysis network found when comparing proteins changing the AD synapse and the NDC synapse. Many proteins in this network are involved in energy production or are APP interactors. Colored nodes indicate proteins found to be significantly change in the proteomics data set. Red nodes indicate that a protein's expression has gone down in AD and green nodes indicate the expression has gone up. The intensity of the color indicates the size of the fold change where more intense coloring indicates a greater fold change. Uncolored nodes are inserted by IPA to increase the coherence of the networks are nodes which contain a circle inside a circle such as Mitochondrial complex 1. Solid lines indicate a direct relationship and dotted lines an indirect relationship.

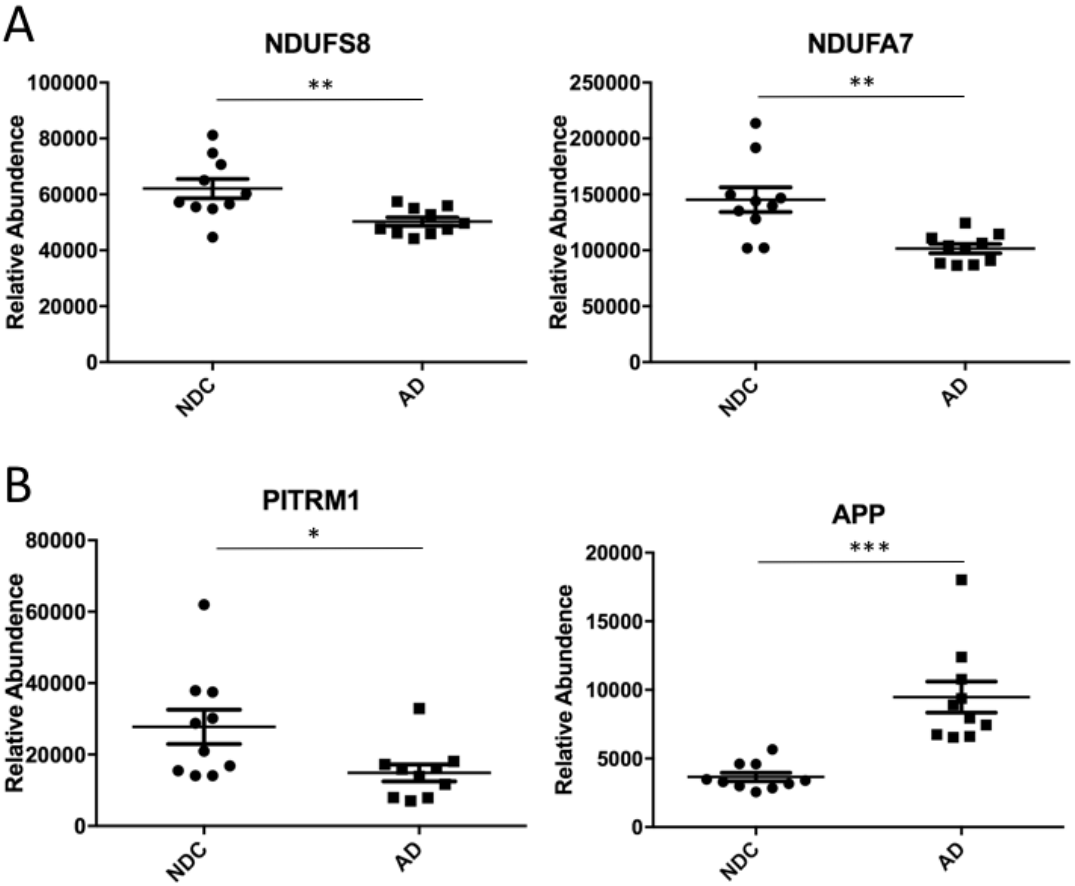

Figure 4.10: Mitochondiral proteins are altered in the AD synapse. (A) Mitochondrial Proteins NDUFS8 and NDUFA7 are both significantly down regulated in the AD synapse. Each point represents an individual sample (B) PITRM1 a molecule involved in degrading Aβ in the mitochondria is decreased in AD while APP is increased in the AD synapse. Each point represents an individual sample. (*** p<0.001, **p<0.01, *p<0.05, T-test).

Many proteins involved in cellular maintenance and homeostasis are increased in AD when compared to NDCs as indicated by Figure 4.11 although 7 are found to be less abundant. These protein changes could be a response to the large amount of dead and dying cells and synapses that are found in AD however closer inspection reveals that some of these proteins are involved in regulation of the immune system (9 proteins) and more specifically activation of the complement cascade (4 proteins). Western blot analysis of Clusterin and Complement C4 confirmed the results of proteomics by an independent technique (Figure 4.12).

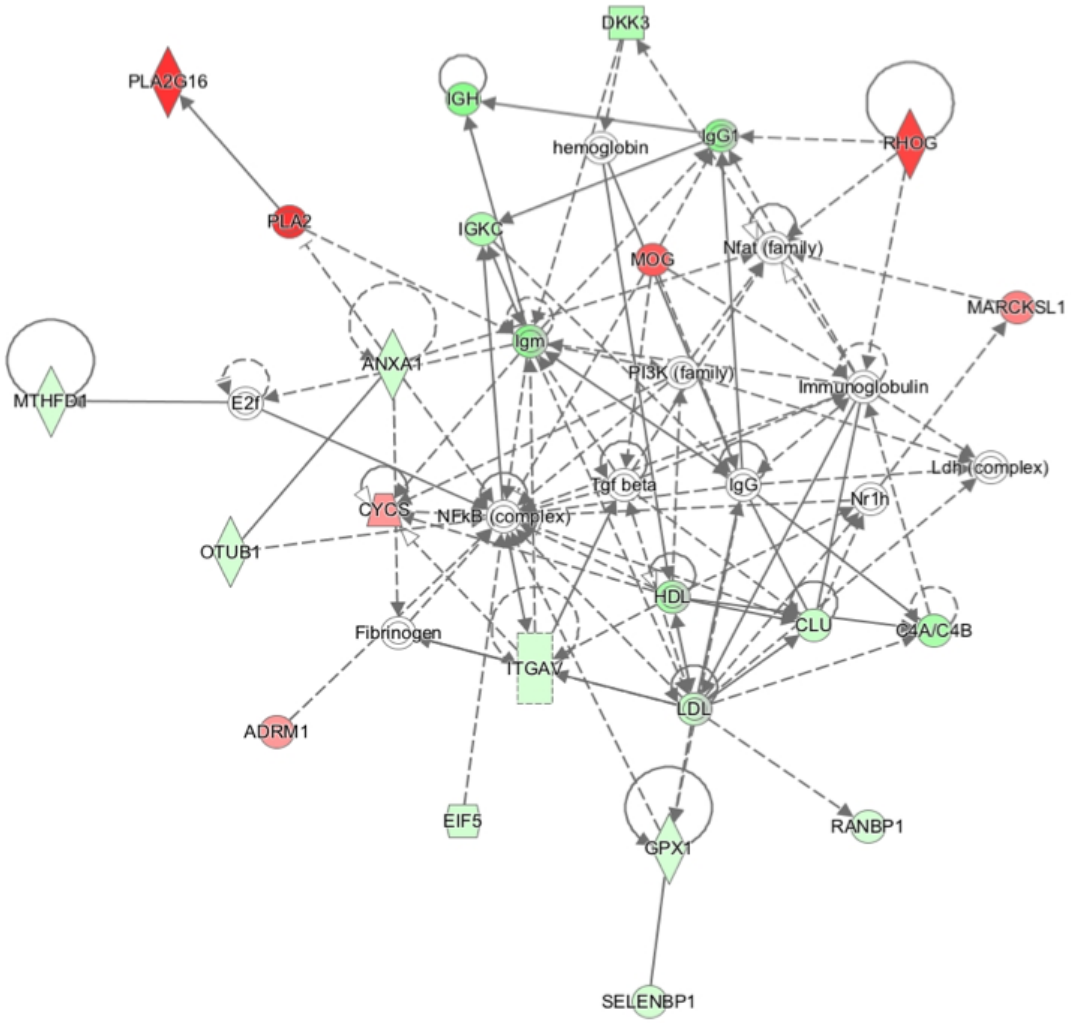

Figure 4.11: Changes in Cellular Maintenance Network in Alzheimer's Disease synapse. (A) A high scoring Ingenuity pathway analysis network found when comparing proteins changing the AD synapse and the NDC synapse. Many proteins in this network are involved in maintaining cellular function after a cell is compromised. Colored nodes indicate proteins found to be significantly change in the proteomics data set. Red nodes indicate that a protein's expression has gone down in AD and green nodes indicate the expression has gone up. The intensity of the color indicates the size of the fold change where more intense coloring indicates a greater fold change. Uncolored nodes are inserted by IPA to increase the coherence of the networks are nodes which contain a circle inside a circle such as IgG1. Solid lines indicate a direct relationship and dotted lines an indirect relationship.

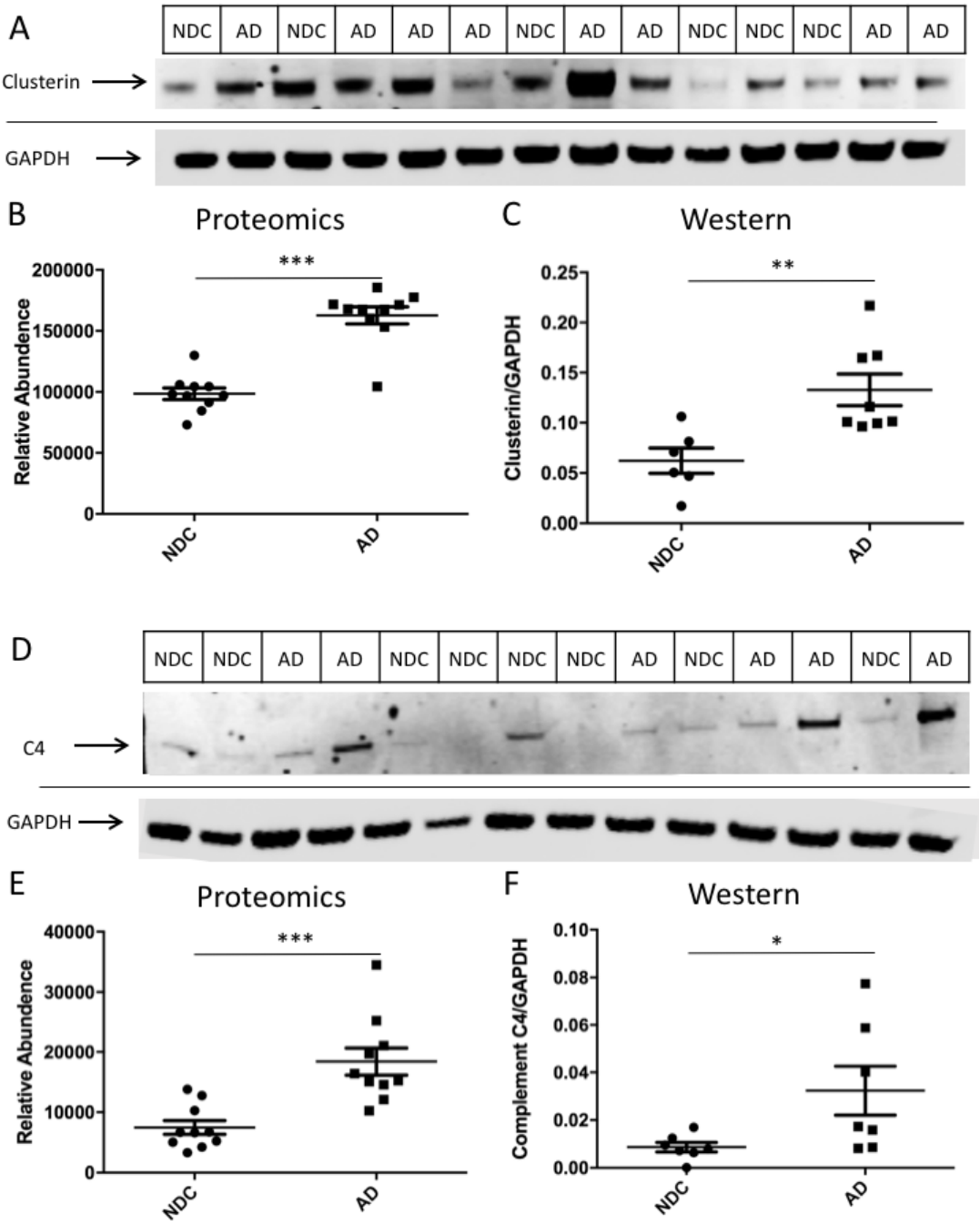

Figure 4.12: Western Blot confirmation of Complement C4 and Clusterin upregulation in AD. (A) A Western Blot of synaptoneurosome preps probed for Clusterin and GAPDH. Clusterin is up regulated by western blot when comparing AD to NDC cases confirming the results of the proteomics data (B) by another technique. (D) A Western Blot of synaptoneurosome preps probed for Complement C4 and GAPDH. Complement C4 is up regulated by western blot when comparing AD to NDC cases confirming the results of the proteomics data (B) by another technique. (*** $p<0.001$, ** $p<0.01$, * $p<0.05$, T-test)

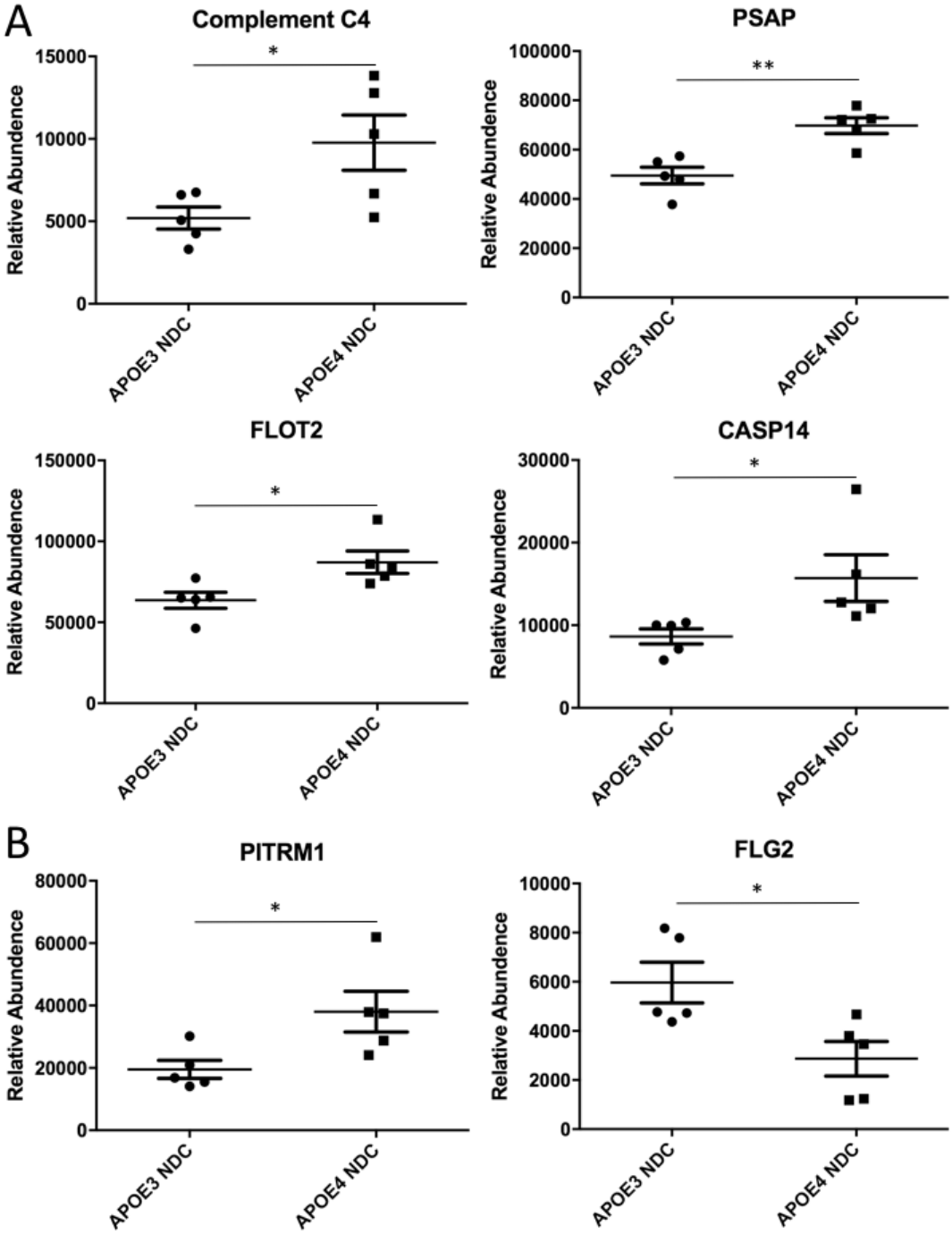

Figure 4.13: Significant changes in the NDC APOE4 proteome when compared to the NDC APOE3 proteome. (A) Many of the differences between the NDC proteomes are changed in the same direction when comparing the AD proteome with controls. Complement C4, PSAP, FLOT2 and CASP14 are all increased in NDC APOE4 cases compared with NDC APOE3 cases and also increased when comparing AD to NDC.(B) Some proteins such as PITRM1 and FLG2 however are regulated in the opposite direction. Each point represents an individual sample (**p<0.01, *p<0.05, T-test).

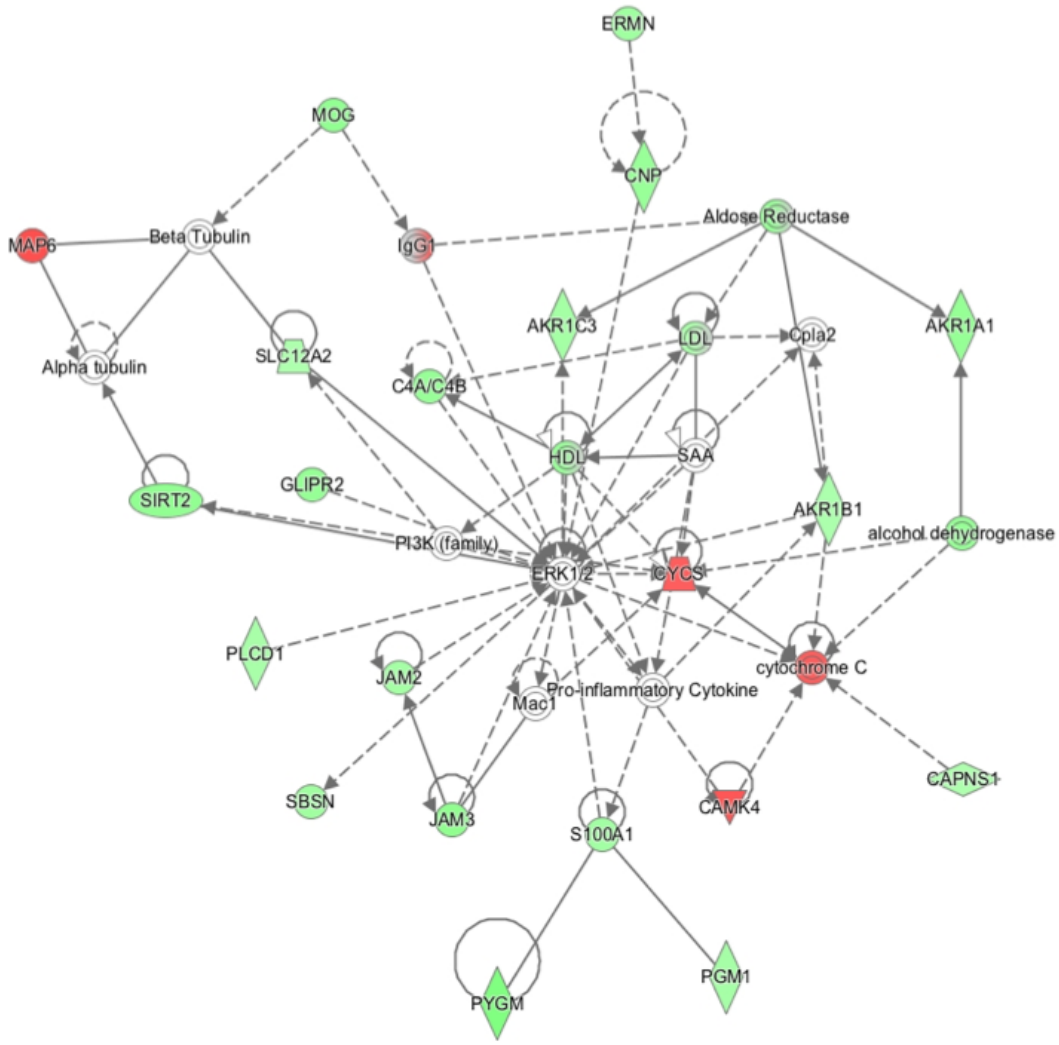

Figure 4.14: Changes in Cell Morphology Network in the AD APOE4 synapse compared to the AD APOE3 synapse. The highest scoring Ingenuity pathway analysis network found when comparing proteins in the AD APOE4 and the AD APOE3 synapse. Many proteins in this network are involved in regulation of cell morphology, endo- and exocytosis and regulation of the immune system. Colored nodes indicate proteins found to be significantly change in the proteomics data set. Red nodes indicate that a protein's expression has gone down in APOE4 AD and green nodes indicate the expression has gone up when compared to APOE3 AD. The intensity of the color indicates the size of the fold change where more intense coloring indicates a greater fold change. Uncolored nodes are inserted by IPA to increase the coherence of the networkas are nodes which contain a circle inside a circle such as IgG1. Solid lines indicate a direct relationship and dotted lines an indirect relationship.

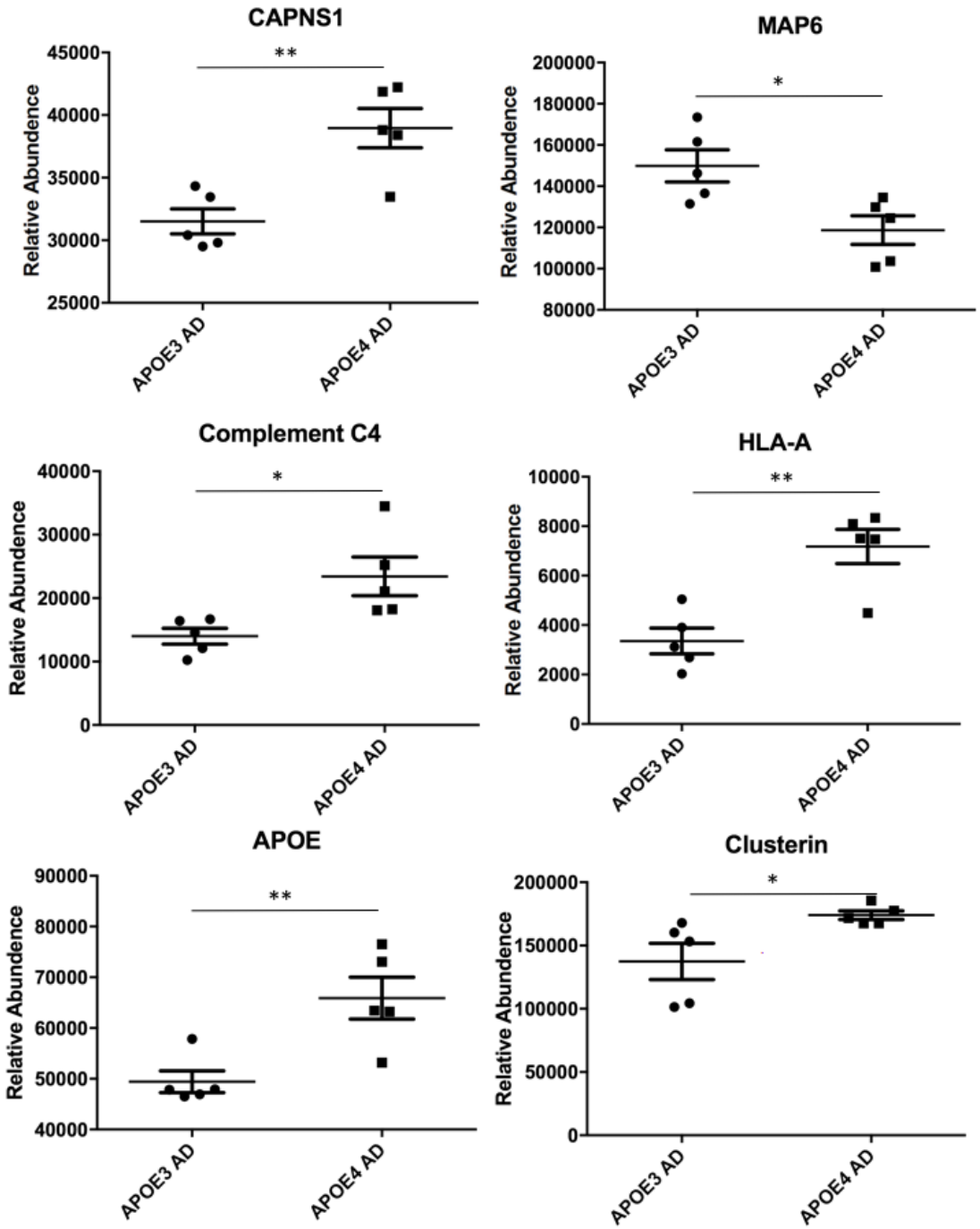

Figure 4.15: Significant changes in the AD APOE4 proteome when compared to the AD APOE3 proteome. Some of the proteins changed in the AD APOE4 synapse are also changed in the same direction in AD (Complement C4, MAP6, APOE, Clusterin) however some are not changed in AD when compared with controls (CAPNS1). (**p<0.01, *p<0.05, T-test)

4.3.5 Key proteins which are significantly changed in APOE4 controls compared to APOE3 controls

Only 41 proteins were found to be significantly different in the APOE4 NDC synapses compared to the APOE3 NDC synapses. Such small datasets should be viewed with caution as with a total discovery rate of 1043 and a significance cut off of $p<0.05$ one would expect 50 proteins to be altered by chance alone. However, after careful examination of this data set it transpired that many of the proteins are found in pathways that are already known to interact with ApoE such as Reelin signalling or are known to be deregulated in AD such as endocytosis (Figure 4.13).

4.3.6 Key proteins which are significantly changed in APOE4 Alzheimer's Disease synapses compared to APOE3 Alzheimer's Disease synapses

The comparison of AD APOE4 synapses with AD APOE3 synapses found that 121 proteins significantly differed in their abundance ($p<0.05$, fold change >1.2). The highest scoring IPA network from this analysis highlights proteins that are involved in the regulation of cell morphology, endocytosis and regulation of the immune system (Figure 4.14). Many of the proteins found to be different in the AD APOE4 synapse when compared to the AD APOE3 synapse such as Clusterin (CLU) and Apolipoprotein E (APOE) itself are also found to be changed in the AD synapse compared with NDC however some such as major CAPNS1 are found to be changed only when splitting the AD cases based on genotype and not when comparing AD with NDC (Figure 4.15).

Of the 120 proteins found to be different in the AD APOE4 synapse when compared to the AD APOE3 synapse 31% (38 proteins) are not found in the dataset comparing AD to NDC. Of the remaining 83 proteins, only 34 of them are found to be changed in the same direction as they are when comparing AD with NDC, the remaining 49 are found to be changed in the opposite direction. DAVID analysis shows that over

half of those proteins that are different in their directional change from AD appear to be mainly involved in the plasma membrane (28 proteins). Those proteins that are similar in their directional change to AD compared to NPC appear to be mainly involved in metal binding (26%, 9 proteins) and regulation of the immune system (23%, 8 proteins).

4.4 Discussion

This study examined the difference in proteome of synapses isolated from AD and NDC post-mortem tissue with known *APOE* genotypes using highly sensitive label-free quantitative LC-MS/MS. The use of a synaptoneurosome preparation meant that the study was able to look at both the presynaptic and postsynaptic changes while still remaining focused on the synapse and not allowing the protein changes that occur in the cell body, axon, astrocytes or microglia to affect the findings. This is important as it takes into account that changes in synapse are likely different to those changes in the cell body due not only to the long distance between these two cellular locations but also due to the break down in protein trafficking and transport that are known to accompany AD (Encalada and Goldstein, 2014). Using the highly sensitive system, label free quantitative LC-MS/MS, and limiting the samples used to samples with high protein integrity (Figure 4.4) gave confidence in the results and allowed for the detection of 1043 distinct proteins detectable by two or more unique peptides.

Changes in the Cell-Cell interactions and the lipid bilayer in AD

AD causes changes in many proteins related to the regulation of cell morphology, endocytosis, exocytosis and maintenance of the lipid bilayer (Figure 4.6). Endocytosis and exocytosis are necessary for synaptic function as they control the release and uptake of neurotransmitters into the synaptic cleft thus allowing signals to propagate from neuron to neuron. As several of the genes found by genome-wide association studies are known to be involved in endosomal mechanisms (Karch and Goate, 2015) and as endosomal changes are one of the first reported AD pathologies (Peric and Annaert, 2015), it is probable that endosome dysfunction plays a role in the

disease process. In this dataset changes in proteins such as Flotillin 1 and 2 (FLOT1 and FLOT2), LDL receptor related protein 1 (LRP1) and synaptosome associated protein 25 (SNAP25) indicate that endosomal and vesicle trafficking may be impaired or altered at the synapse leading to a decrease in the amount of neurotransmitter release or reuptake. As APP is cleaved to Aβ in the endosome changes in endosomal processes will also have an effect on the rate of Aβ production. Notably, Flotillin 2 not only regulates endocytosis but has also been shown to facilitate the endocytosis of APP. Down regulation of Flotillin 2 in primary neurons impairs the endocytosis of APP and thus reduces the production of Aβ (Schneider *et al.*, 2008). Western blot analysis of FLOT1 and LRP1 confirmed the results of the proteomics dataset by an independent technique thus furthering confidence in the findings.

Also crucial to the release of vesicles and synaptic communication is the lipid bilayer. Proteins such as LDL receptor related protein 1 (LRP1), Prosaposin (PSAP), Phospholipase C (PLCL1), and Phospholipase A2 group XVI (PLA2G16) are all involved in changing and regulating the composition of lipids within the lipid bilayer. Not only could disruption of the lipid bilayer also contribute to and or facilitate a disruption in endosome release but the composition of the lipid bilayer particularly the number, composition, and size of lipid rafts of cholesterol has been shown to play an important part in the pathogenesis of AD (Fabelo *et al.*, 2014). LRP1 in particular has been shown to have an important role in the pathogenesis of AD both in its role as an ApoE interactor protein but also through its interactions with cellular prion protein (PrPc) which allow for the internalization of Aβ into endosomes (Rushworth *et al.*, 2013).

Changes in cell to cell adhesion and particularly cadherin binding involved in cell-cell adhesion was the most significant cluster found on DAVID analysis with a high enrichment score of 9.14. This group of proteins includes Annexin A1 (ANXA1), Annexin A2 (ANXA2) and the Septins 2 (SEPT2), 7 (SEPT7) and 10 (SEPT10). The mis-regulation of this group of proteins indicates a loss of synaptic health as cell to cell adhesion is particularly important in maintaining the function and integrity of the synapse and the synaptic cleft (Leshchyns'ka and Sytnyk, 2016). Some of these protein changes, such at the septins which are downregulated in AD, are likely a result of the break down in

synaptic membranes and connections that occurs in AD. However others, such as Integrin alpha V (ITGAV) and L1 cell adhesion molecule (L1CAM) are potentially involved more directly in synaptic toxicity as they are known to bind Aβ (Wright *et al.*, 2007; Djogo *et al.*, 2013). In vitro analysis in primary neurons shows a role of ITGAV in increasing Aβ deposition and neurotoxicity (Wang *et al.*, 2008; Han *et al.*, 2013) and its increased presence at the AD synapse may be having just that effect.

Changes in energy production and mitochondria in AD

Synapses require large amounts of energy to not only maintain the ion gradients that enable normal function of neurons but also to mobilize, release and recycle vesicles. In many cases synapses are located far away from the cell bodies and thus mitochondria localized to the synapse are a key part of this structure. Mitochondria also help buffer Ca^{2+} which plays a key role in aiding Ca^{2+} dependent processes within the synapse such as the regulation of plasticity (Ly and Verstreken, 2006). Neurons use specialized transport systems to move mitochondria from the cell body to the synapse along the axon and mitochondria can be moved throughout the cell to respond to changes in energy demands (Cai and Tammineni, 2017). This mitochondrial transport is affected in AD as the microtubules which make up the main traffic highways of the cell begin to break down (Sheng and Cai, 2012). This prevents new and healthy mitochondria from reaching the synapse and replacing the old and often highly stressed mitochondria. However only one third of axonal mitochondria are motile and many mitochondria are targeted to the synapse and remain there. Once located at the synapse mitochondria undergo marked changes in protein signature (Stauch *et al.*, 2014). They are also longer lived and thus exposed to more oxidation in ageing (Du *et al.*, 2012). Dysfunction of mitochondria is thought to occur early in AD and multiple lines of evidence point towards mitochondrial dysfunction being important in disease progression and cognitive impairment. The degree of cognitive impairment in AD correlates with the amount of Aβ found in the mitochondria (Dragicevic *et al.*, 2010). Some of these lines of evidence including the reduction of glucose metabolism in AD patient brains indicates that mitochondrial dysfunction may

be worse in APOE4 individuals with AD although this could be due to ApoEs effects on Aβ rather than the effects of ApoE on the mitochondria itself (Cai and Tammineni, 2017).

The synaptoneurosome prep used here included synaptic mitochondria and thus several of the proteins altered in AD compared with NDC were mitochondrial. Complex I was represented by several proteins as was Complex IV (Figure 4.10 and Figure 4.11). Complex IV in particular has been implicated in the Aβ mediated effects of AD (Du *et al.*, 2010) while Tau appears to be responsible for defects in Complex I (Eckert *et al.*, 2014). Interestingly none of the protein changes were from proteins encoded for by the mitochondrial genome although several are known to be changed in synaptic mitochondria compared with non synaptic mitochondria (Stauch *et al.*, 2014) and mitochondrial DNA is known to be altered in synaptic mitochondria in AD (Lin *et al.*, 2002).

Also found in mitochondria is the protein pitrilysin metallopeptidase 1 (PITRM1) also called PreP (Figure 4.10). PITRM1 is a degradation enzyme localized to the mitochondria which binds to zinc and degrades small peptides in the range of 10-65 residues. Its degradation substrates include Aβ and decreases in PITRM1 activity have been found in AD brains as well as in AD mouse models (Alikhani *et al.*, 2011). This suggests that decreased activity as well as a decreased abundance of PITRM1 may be responsible for some of the mitochondrial dysfunction that occurs in AD. Of particular interest is the finding that PITRM1 is increased in NDC APOE4 cases when compared with NDC APOE3 cases (Figure 4.13). This early change in PITRM1 could indicate several possibilities. The first of which is that although these NDC were all cognitively normal at the time of death the APOE4 NDC group could contain individuals that are in the pre-clinical stage of AD and thus have higher intracellular Aβ. AD has a long pre-clinical stage where Aβ concentrations increase but no noticeable cognitive decline occurs. This early up regulation of PITRM1 could be a reaction to an increase in mitochondrial Aβ and in later stages of disease when mitochondrial numbers are reduced PITRM1 concentrations go down. It is also possible that a decrease in the amount of PITRM1 in later stages of disease could lead to mitochondrial death as they are unable to degrade

Aβ. Increasing PITRM1 could then potentially protect against mitochondrial death and thus help preserve synaptic integrity for longer. This merits further investigation as maintaining the function of mitochondria would be very beneficial in helping maintain the function of the synapses that depend on them.

Changes in the immune system in AD

Neuroinflammation, particularly due to the innate immune system, has recently been found to play a role, not only in AD, but also in many other neurodegenerative diseases. Neuroinflammation, which is controlled mainly by microglia and astrocytes, was previously thought to be due to the protein aggregation and neuronal death that are caused by neurodegenerative diseases, however in more recent years a role for neuroinflammation in disease initiation and progression has been suggested.

The role of neuroinflammation and the innate immune system in contributing to the disease pathogenesis rather than being a product of disease has been further solidified by recent genome wide association studies (GWAS) (Harold *et al.*, 2009). Many of the disease relevant SNPs found to be significant in AD were found in proteins relating to neuroinflammation and the innate immune system. One of these, Clusterin (CLU), also called Apolipoprotein J, was found to be altered in this proteomics data set. Clusterin has many roles in the brain including the regulation of inflammation (Zhang *et al.*, 2005a), inhibiting apoptosis (Zhang *et al.*, 2005b), and facilitating lipid transport (Nuutinen *et al.*, 2009). Crucially Clusterin has been shown to bind to Aβ preventing aggregation (Matsubara *et al.*, 1995) and promoting degradation and clearance (Bell *et al.*, 2006). Previous datasets have shown that increased Clusterin plasma levels correlate with increased progression from MCI to AD as well as speed of cognitive decline (Jongbloed *et al.*, 2015). Clusterin amount has been shown to correlate with the amount of Aβ in the AD human brain (Miners *et al.*, 2017) and Clusterin is increased in the entorhinal cortex of elderly people concomitantly with Aβ before the onset of dementia implying a possible early role in disease (Desikan *et al.*, 2014). This is the first

evidence that Clusterin is increased in the AD synapse and its structural and function similarities to ApoE indicate that it may play a role in Aβ trafficking to the synapse.

Microglia, the resident immune cells of the brain, have a role in synaptic pruning in development using the complement system of the innate immune system (Stevens *et al.*, 2007). Recently this process has also been implicated in synaptic effects in schizophrenia as genetic changes in the major histocompatibility complex locus cause changes in protein levels of human leukocyte antigen (HLA) as well as complement component 4 (C4) (Sekar *et al.*, 2016). This dataset shows that both complement C4 and HLA-1 are altered in the AD synapse and this data fits nicely with recent papers showing that other components of the complement cascade, namely C1q and C3, are up-regulated in the AD synapse which could indicate an aberrant activation of the innate immune system causing incorrect microglial synaptic pruning (Hong *et al.*, 2016; Shi *et al.*, 2017).

Annexin A1 (ANXA1) was discussed earlier in the context of cell to cell adhesion but ANXA1 also plays a role in targeting cells for phagocytosis by microglia. Under normal, non inflammatory, conditions ANXA1 is involved in removing apoptotic neurons while preventing inflammation. However, under inflammatory conditions, such as AD, this mechanism is overwhelmed and is likely part of the feed forward loop of neuroinflammation that has been seen in AD (McArthur *et al.*, 2010). The finding that ANXA1 is increased in the AD synapse points to it having a similar effect to the complement system in that it is targeting synapses for phagocytosis by microglia.

The effect of APOE genotype on the control proteome

Most of the information pertaining to the role of ApoE in cognitive decline focuses on its interaction with Aβ or occasionally tau however long term studies of cognition have shown that although *APOE* genotype has no effect on cognitive ability in early or middle life, presence of an *APOE ε4* allele does affect the rate of cognitive decline in an elderly population without AD (Schiepers *et al.*, 2012). This might be due

to preclinical AD and thus these individuals are experiencing the beginnings of AD associated cognitive decline. Alternatively, ApoE4 itself may have a impact on cognitive decline, which then makes the brain more susceptible to AD. Either way the effects of ApoE on the synaptic proteome in the absence of AD diagnosis or pathology is an interesting way of looking at this all important risk factor for disease.

Although very few proteins were significantly different between APOE3 NDC and APOE4 NDC the few that were, were very interesting especially when taken in context with the AD v NDC changes described above. For example, the increase seen in FLOT2 could be some of the reason for an increase in the amount of Aβ production in APOE4 cases. Schneider *et al.* have shown that FLOT2 causes an increase in the amount of APP clustering in a cholesterol dependent manner. This increase in clustering causes an increase in APP endocytosis which in turn cause an increase in Aβ production (Schneider *et al.*, 2008). As ApoE has important roles as a cholesterol transporter and the different ApoE isoforms transport cholesterol to different amounts (Dorey *et al.*, 2014). This difference in cholesterol amount could be part of this effect on *APOE* genotype on FLOT2 and moderating the effect of FLOT2 with APP could provide an important preventative therapeutic.

Also increased in the NDC APOE4 v NDC APOE3 synapse is the complement component C4 of the innate immune system. This is further increased in AD and increased again when an individual has an *APOE ε4* genotype and AD. The role of the complement system at the synapse in older aged people has yet to be elucidated but it is likely that it is responsible for synaptic pruning (Hong *et al.*, 2016). The increase in C4 in APOE4 NDC cases could be an indicator of early neuroinflammation that is thought to accompany preclinical AD. It is also possible that C4 could be causing non Aβ related synaptic loss causing a decrease in the amount of synapse and thus a decrease in cognitive ability and by extension cognitive reserve. This would then increase the chance of AD susceptibility because less synapses would need to be affected by AD before dementia onset. Further research is required to understand the interactions between ApoE and the innate immune system with particular regard paid to the effect on the synapse.

As discussed earlier an increase in PITRM in NDC APOE4 cases compared with NDC APOE3 could be result of an increase in Aβ in synaptic mitochondria. It is known that an *APOE ε4* genotype increases the amount of Aβ at the synapse both by reducing the clearance of Aβ and by targeting Aβ to the synapse (Koffie *et al.*, 2012). It follows then that an increase in the amount of PITRM could be a response the increase in the amount of Aβ. As PITRM is known to degrade Aβ it could be that an inability to produce PITRM could be what causes synaptic mitochondria to become susceptible to Aβ and thus once PITRM stops degrading the Aβ mitochondrial deficits start which then lead to synaptic loss and disease.

The effect of ApoE on the AD proteome

Calpain activity is known to be increased in the AD brain due to the increased Ca^{2+} that is known to occur in AD. Once activated calpain is known to interact with tau causing some of the tau pathology seen in AD (Ferreira and Bigio, 2011). In this dataset we see no change in the amount of any calpain subunits when AD is compared with NDC but when AD APOE4 cases are compared with AD APOE3 cases there is a modest increase in the amount of calpain small subunit 1 (CAPNS1). Mouse models expressing familial AD mutations as well as the different ApoE isoforms indicate that ApoE4 mice have increased calpain 1 and 2 and that this increases the amount of tau phosphorylation in a GSK3β independent manner (Zhou *et al.*, 2016). Also of note is that calpain goes on to activate PICALM which is another genetic risk factor for AD (Harold *et al.*, 2009). PICALM is known to play a role in endocytosis which, as discussed above has important roles in the production of Aβ, and PICALM also appears to play a role in abnormal tau hyperphosphorylation, compounding on the role that increased calpain plays (Ando *et al.*, 2013).

Also increased in AD APOE4 cases compared to AD APOE3 cases is Clusterin. As discussed previously Clusterin, also called apolipoprotein J, is an important risk factor for AD (Harold *et al.*, 2009). It is the second most abundantly expressed apolipoprotein

in the brain and has crucial roles in trafficking and clearance of Aβ similar to the role played by ApoE (Nuutinen *et al.*, 2009). Indeed there are many parallels between Clusterin and ApoE that make an interaction between them interesting not least of which is that their role in AD has been reported to be both protective and detrimental (Nuutinen *et al.*, 2009; Desikan *et al.*, 2014; Killick *et al.*, 2014). This study in particular highlights the potential role of both ApoE and Clusterin in the AD synapse. The role of ApoE and in particular the different ApoE isoforms in targeting Aβ to synapses has been investigated (Koffie *et al.*, 2012) and while less is known about Clusterin than ApoE, cell experiments indicate that knocking out Clusterin leads to protection from Aβ associated apoptosis (Killick *et al.*, 2014). However it remains to be seen if an increase in Clusterin correlates with an increase in Aβ at the synapse and indeed if that increase is protective due to the chaperone and anti-apoptotic qualities of Clusterin (Koch-Brandt and Morgans, 1996) or toxic due to an increased targeting of Aβ to the synapse.

5 Investigating the effect of an ApoE4 genotype on the synaptic co-localization of ApoE, Clusterin, and Aβ in Alzheimer's Disease using array tomography

5.1 Background and Aims

Chapter 4 investigated the changes in the proteome of synapses isolated from AD cases compared with those isolated from NDC and the effect that the different isoforms of ApoE had on those changes using quantitative label-free LC-MS/MS. A major finding from that data set was an increase in Clusterin in the AD synapse compared with NDC synapses and also Clusterin was increased in AD APOE4 synapses compared with AD APOE3 synapses. Clusterin, also called ApoJ, is the second most abundantly expressed apolipoprotein in the CNS and a genetic risk factor for AD (Harold *et al.*, 2009). There is evidence that ApoE and Clusterin perform similar roles in the CNS in terms of cholesterol and lipid transport and Clusterin and ApoE may have similar effects on and interactions with Aβ (Li *et al.*, 2014). In 2004 DeMattos *et al.* showed in the PDAPP model of AD that knock out of either ApoE or Clusterin did not change the percent Aβ load but knocking out both ApoE and Clusterin caused a significant increase in the amount of Aβ plaques (DeMattos *et al.*, 2004). This indicates that Clusterin and ApoE play similar and complementary roles in AD and the interaction between these proteins is an interesting path for further study.

The aims of the experiments presented in this chapter are:

- Investigate the effect of Alzheimer's disease and ApoE4 on the density of presynapse, postsynapse, and astrocytic end feet using array tomography of post mortem tissue from NDC and AD cases
- Examine the effect of Alzheimer's disease and ApoE4 on the co-localization of Clusterin, ApoE, and Aβ with synaptic elements using array tomography

5.2 Methods

5.2.1 Western blotting

Western blotting was performed as described in 2.2.2 and used the antibodies described in Table 5.1. The cases used are in Table 5.2.

Table 5.1: Antibodies used in western blotting in Chapter 5

Target	Host	Concentration	Catalogue number
Clusterin	Rabbit	1:500	sc-8354
GAPDH	Mouse	1:2,000	ab8245

Table 5.2: Cases used for western blotting in Chapter 5

Condition	Case number	Gender	Age	APOE genotype	MRC BBN
NDC	01/16	M	79	APOE 3/3	28406
NDC	17/16	F	79	APOE 3/3	28793
NDC	24/15	M	78	APOE 3/3	26495
NDC	51/15	M	79	APOE 3/3	19597
AD	14/15	F	85	APOE 3/4	25739
AD	40/15	M	78	APOE 3/4	26718
AD	48/15	M	76	APOE 3/4	26732
AD	49/14	M	80	APOE 3/4	24322
AD	55/14	M	79	APOE 3/4	24526
AD	02/14	F	87	APOE 3/3	19994
AD	56/14	M	81	APOE 3/3	24527
AD	10/16	M	85	APOE 3/3	28771
AD	29/14	F	87	APOE 3/3	22223
AD	05/16	F	62	APOE 3/3	28410

5.2.2 Array Tomography

The array tomography method, described in 2.1 was used on tissue embedded from the BA41/42 area of the cortex from 5 NDC cases, 6 AD *APOE* ε3/3 (APOE3) cases, and 5 AD *APOE* ε3/4 (APOE4) cases described further in Table 5.3. The staining protocol used is described in Table 5.4 and ribbons were stained for 6 markers, synaptophysin for presynapses, PSD95 for postsynapses and EAAT1 for astrocytic processes and end feet as well as Clusterin, ApoE, and 1C22 (gift of Dominic Walsh) which detects oligomers of Aβ (Mably *et al.*, 2015). Two different tissue blocks were imaged per case and at least two stacks were obtained from different each block to result in a total 4 image stacks per case. These stacks were aligned using Image J (Schindelin *et al.*, 2012) and 10µm x 10µm crops were chosen near (<10µm from plaque edge) and far (>45µm

from plaque edge) from plaques in images that contained a plaque and throughout the image for stacks that did not contain a plaque.

Table 5.3: Case information for the cases used in array tomography

Cases	Genotype	Diagnosis	Age	Gender	MRC BBN
01/16	APOE3/3	NDC	79	M	28406
24/15	APOE3/3	NDC	78	M	26495
17/16	APOE3/3	NDC	79	F	28793
63/13	APOE3/3	NDC	77	F	19686
51/15	APOE3/3	NDC	79	M	19597
1424	APOE3/3	AD Braak VI	89	M	-
1456	APOE3/3	AD Braak VI	81	M	-
05/16	APOE3/3	AD Braak VI	62	F	28410
10/16	APOE3/3	AD Braak VI	85	M	28771
56/14	APOE3/3	AD Braak V	81	M	24527
52/16	APOE3/3	AD Braak VI	78	F	29541
14/15	APOE3/4	AD Braak VI	85	F	25739
40/15	APOE3/4	AD Braak VI	78	M	26718
55/14	APOE3/4	AD Braak VI	79	M	24526
64/13	APOE3/4	AD Braak VI	57	M	19690
48/15	APOE3/4	AD Braak VI	76	M	26732

A total of 1141 crops were thresholded using custom Image J (Schindelin *et al.*, 2012) macros and then processed using a custom matlab script (all macros and scripts can be found in appendix C). Matlab was used to remove objects only found in single section as previously described. The astrocytic component of a tripartite synapses (ACTS) were defined in matlab as EAAT1 positive puncta that were within 0.5µm of either a presynapse or a postsynaptic terminal which allowed for a distinction from astrocytic processes which were EAAT1 positive. Synaptic puncta were defined as co-localized with ApoE, Clusterin, or Aβ if more than 50% of the puncta volume was occupied by the protein of interest.

Statistics were calculated using graph pad prism (version 7.0c). Normality was tested with the Shapiro-Wilk normality test. Two-way ANOVA was used to analyse density of all three synaptic markers with condition (NDC, AD ApoE3, AD ApoE4) as the column factor and proximity to plaque as the row factor followed by Bonferroni's

multiple comparisons post-hoc tests between all factors. Co-localization data was analysed with Kruskal-Wallis tests followed by post-hoc Mann-Whitney U tests.

Table 5.4: Antibodies used in staining human array tomography samples

Day	Primary Antibody Target	Primary Host	Concentration (mg/ml)	Primary Catalogue number	Secondary Antibody	Secondary Catalogue number
1	1C22	Mouse	0.02	-	Donkey anti-mouse 594	A21203
1	EAAT1	Rabbit	0.02	ab416 abcam	Donkey anti-rabbit 488	A21206
1	ApoE	Goat	0.02	ab7620 abcam	Donkey anti- goat 647	A21447
2	Clusterin	Goat	0.004	sc-6420 Santa Cruz Biotechnology	Donkey anti-Goat 594	A11058
2	Synaptophysin	Mouse	0.02	ab8049 abcam	Donkey anti-mouse 647	A31571
2	PSD95	Guinea Pig	0.02	124 014 synaptic systems	Donkey anti-guinea pig 488	706-545-148

5.3 Results

5.3.1 Clusterin is increased in the AD APOE4 synapse but not in Crude homogenate

Western blot analysis of a crude homogenate of post-mortem brain (Figure 5.1A) shows an increase in the amount of Clusterin in AD compared with NDC, with no effect of *APOE* genotype on this increase ($F(2,11)=6.454$, $p=0.0140$, between NDC and

AD APOE3 p=0.0492, between NDC and AD APOE4 p=0.0134)(Figure 5.1.C). This is consistent with previous studies, however a recent study indicated that Clusterin is increased in AD due in part to its interaction with Aβ plaques (Miners *et al.*, 2017). As Aβ plaques are more prevalent in individuals with an *APOE ε4* genotype one might expect a slight increase in the amount of Clusterin in AD APOE4 cases compared with AD APOE3 cases (Rebeck *et al.*, 1993). However it appears that in crude homogenate of post mortem cases that is not the case, potentially because any effect of *APOE ε4* on Clusterin is diluted with the rest of the cellular milieu. However, western blot analysis of synaptoneurosomes ($F(2,11)=20.83$, $p=0.0002$)(Figure 5.1B) shows an increase in Clusterin in AD cases (NDC and AD APOE3 p=0.0387, NDC and AD APOE4 p=0.0001) and a further increase in the APOE4 cases compared with APOE3 (p=0.0081) consistent with the proteomics results from chapter 4 (Figure 5.1D). This indicates that an *APOE ε4* genotype increases the amount of Clusterin at the synapse but not overall in the brain.

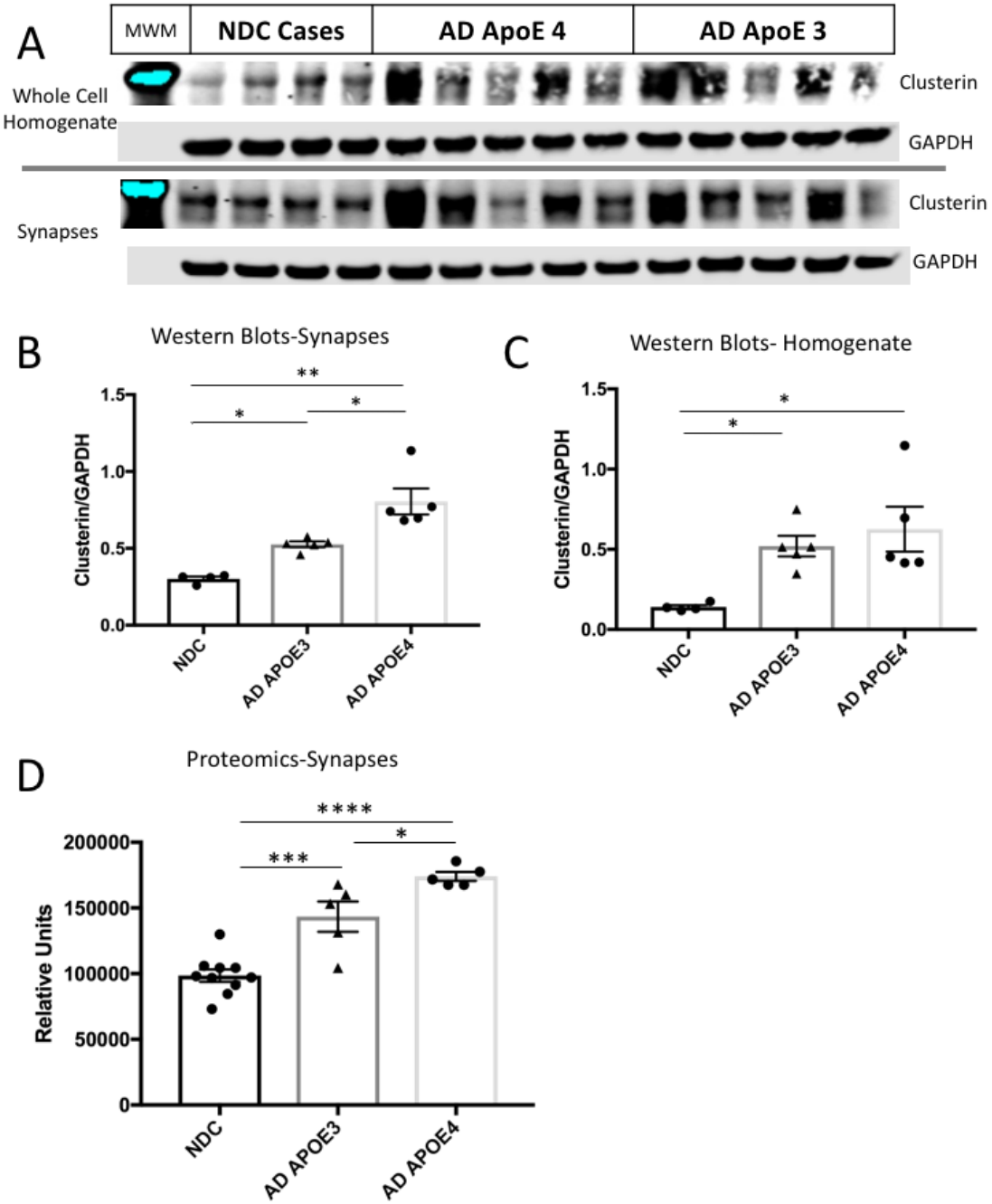

Figure 5.1: ApoE genotype affects the amount of Clusterin in the AD synapse but not in crude homogenates. Western blot (A) analysis shows that AD causes a significant increase in the amount of Clusterin in both the synapse and crude homogenate. ApoE genotype has a significant effect on the amount of Clusterin only in the synaptoneurosome (B) of AD cases but not in crude homogenate (C). This matches the results found in proteomics (D). (**** P<0.0001 , *** p<0.001, ** p<0.01, * p<0.05, T-test)

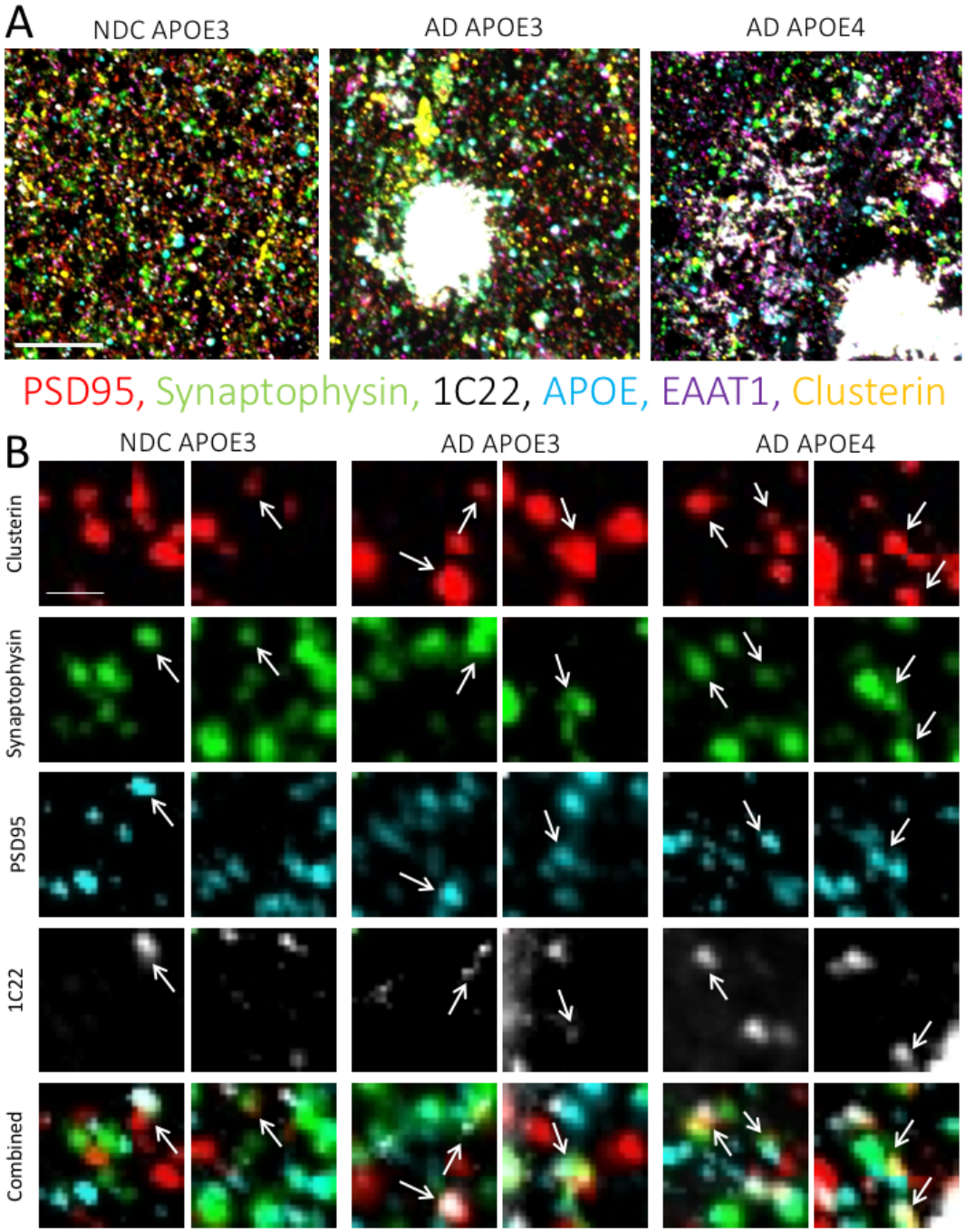

Figure 5.2: Representative images of array tomography. Array tomography ribbons from NDC APOE3, AD APOE3 and AD APOE4 individuals were stained for postsynapses (PSD95), presynapses (synaptophysin), oAβ (1C22), astrocytic endfeet (EAAT1), ApoE, and Clusterin. Image stacks (A) were cropped and analyzed. Images shown here are a Z-stack projection of 4 slices. Arrows indicate synapses with co-localizing proteins. Error bars are 5μm (A) and 2μm(B).

5.3.2 *APOE* ε4 is associated with exacerbated synaptic loss in AD

Previous studies using array tomography have shown that synapse loss occurs most prominently around Aβ plaques with synaptic density dropping to less than 50% of NDC levels inside the plaque halo made of Aβ species. This drop in synapse density gradually returns to NDC levels at a distances of >45μm from the plaque (Koffie *et al.*, 2012). To study the effect of *APOE* genotype on Aβ mediated changes in synaptic density, array tomography was used to study post-mortem tissue from NDC APOE3, AD APOE3, and AD APOE4 cases. Crops were taken from image stacks and divided into two groups, those which were near plaques (<10μm from plaque edge) and those far from plaques (>45μm from plaque edge) (Figure 5.2). Synaptophysin was used as a marker of presynapses, and PSD95 as a marker of postsynapses, and EAAT1 was used as a marker of astrocytic end feet. Consistent with previous studies there is a significant drop in presynaptic density near plaques when compared with far from plaques (Two-way ANOVA Row factor, $F(1,25)=16.80$, $p=0.0004$) for both AD APOE3 ($p=0.0248$) cases and AD APOE4 cases ($p=0.0190$) (Koffie *et al.*, 2012). AD APOE4 cases have a significantly (Two-way ANOVA Column factor, $F(1,25)=35.13$, $p<0.0001$) lower presynaptic density far from plaques when compared with the density of AD APOE3 ($p=0.0056$) cases and NDC ($p=0.0085$) meaning that APOE4 cases also have significantly lower presynaptic density near plaques compared with the presynaptic density near plaques in AD APOE3 cases ($p=0.0046$) (Figure 5.3A).

Analysis of postsynaptic puncta shows a significant (Two-way ANOVA Row factor, $F(1,25)=6.463$, $p=0.0176$, Column Factor $F(2,25)=4.62$, $p=0.0196$) decrease in the density of AD APOE4 cases near plaques compared with NDC ($p=0.0155$) and AD APOE4 cases far from plaques ($p=0.0416$) (Figure 5.3B). The densities of postsynaptic puncta are more variable than presynapses so in contrast to previous data (Koffie *et al.*, 2012) there is no difference between near and far from plaques in the AD APOE3 cases although with more cases it is probably that this differences would become significant. Indeed post hoc power analysis indicates that n=8 would be sufficient to detect significance at the $p<0.05$ level with a power of 0.8.

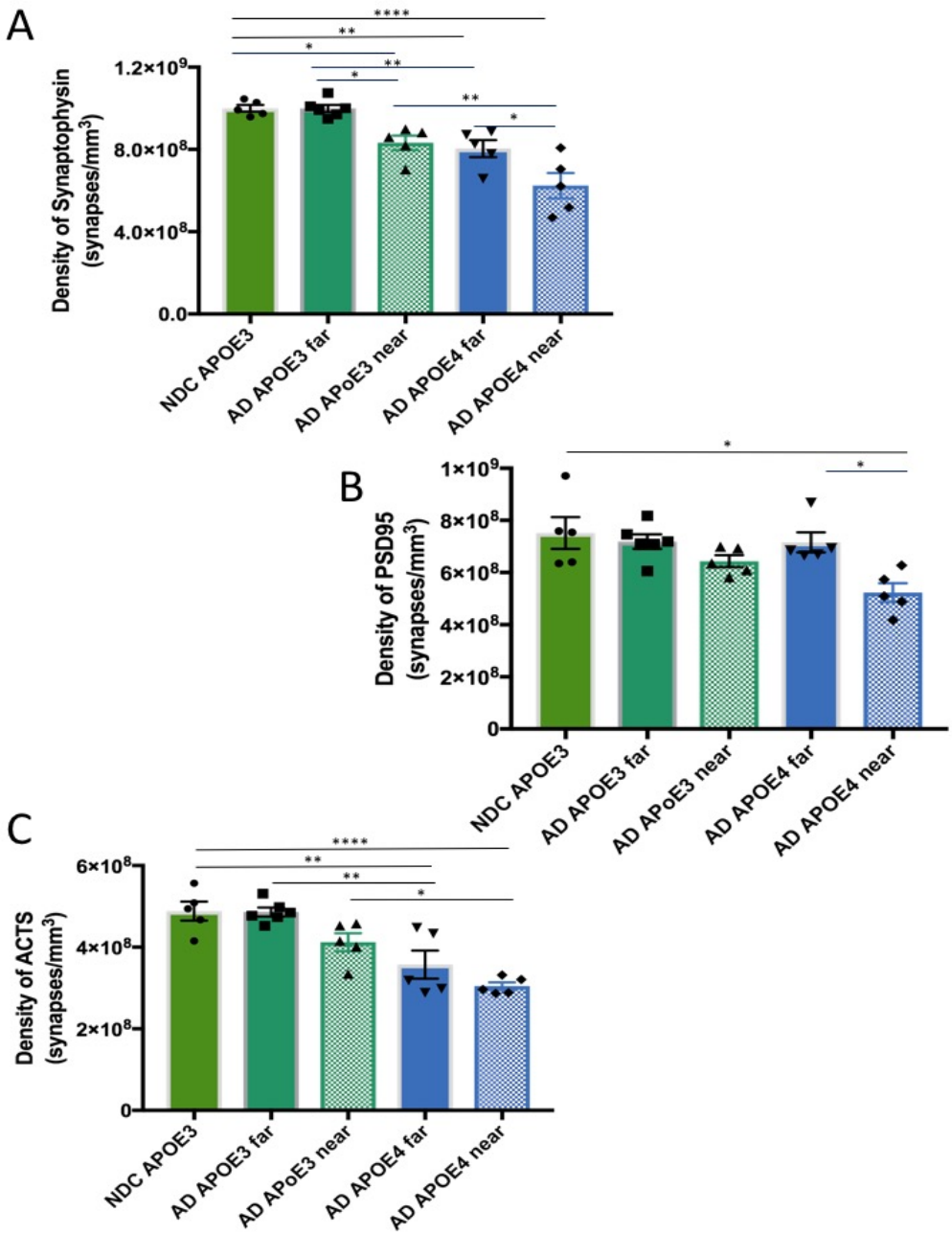

Figure 5.3: Density of Synaptic punctate by Array Tomography. (A) There is a significant decrease in the presynaptic density near plaques (<10um) compared with far from plaques (>45um) for both *APOE* genotypes. APOE4 cases have a significantly lower presynaptic density far from plaques when compared with controls and AD APOE3 cases. AD APOE4 cases also have a lower density near plaques when compared with AD APOE3 cases near plaques. (B) There is a significant decrease in the Postsynaptic density of AD APOE4 cases near plaques compared with AD APOE3 cases far from plaques and NDCs. (C) There is a significant difference in the number of ACTS when comparing NDCs and AD APOE3 cases with AD APOE4 cases however there is no difference in either genotype when comparing between near and far from plaques. (**** $p<0.0001$, *** $p<0.001$, ** $p<0.01$, * $p<0.05$, Two-way Anova with Bonferroni's multiple comparisons post-hoc test).

EAAT1 is found in astrocytic end feet near synapses but also in astrocytic processes and astrocytic end feet around blood vessels therefore the astrocytic component of tripartite synapses (ACTS) are defined as EAAT1 positive puncta that are within 0.5µm of either a presynaptic or a postsynaptic terminal. This is likely a lower estimate ACTS as tripartite synapses in the Z-direction are less likely to be taken into account in shorter ribbons. The distance from a plaque does not change the density of ACTS for either genotype but AD cases with an *APOE* ε4 genotype have a significantly lower (Two-way ANOVA Row factor, $F(1,25)=5.655$, $p=0.0254$, Column Factor $F(2,25)=27.8$, $p<0.0001$) end foot density both near to ($p=0.0302$) and far from ($p=0.0032$) plaques when compared with AD APOE3 or NDC cases ($p=0.0043$) (Figure 5.3C).

5.3.3 *APOE* ε4 genotype is associated with an increase in synaptic Aβ

Previous literature suggested that the amount of Aβ at the synapse is significantly increased in presynapse and postsynapses near plaques compared with those far from plaques (Koffie *et al.*, 2012). 1C22, an antibody which preferentially binds to oligomeric and aggregated species of Aβ, was used to assess the co-localization of Aβ with presynapse, postsynapse and ACTS (Mably *et al.*, 2015). Synapses near plaques were significantly more likely to co-localise with Aβ for both presynaptic ($\chi^2(4) =20.51$, $p=0.0004$) and postsynaptic ($\chi^2(4) =19.3$, $p=0.0007$) compartments as predicted (Figure 5.4). Koffie *et al.* also showed that AD APOE4 cases had a greater co-localization with Aβ (Koffie *et al.*, 2012), a finding which was replicated in this data set for presynapses ($p=0.0079$) and postsynapses ($p=0.0079$). Analysis of Aβ co-localizing with ACTS also shows an increase in the amount of Aβ at ACTS near plaques compared with far from plaques ($\chi^2(4) =18.82$, $p=0.0009$) but there is no difference between genotypes (Figure 5.4).

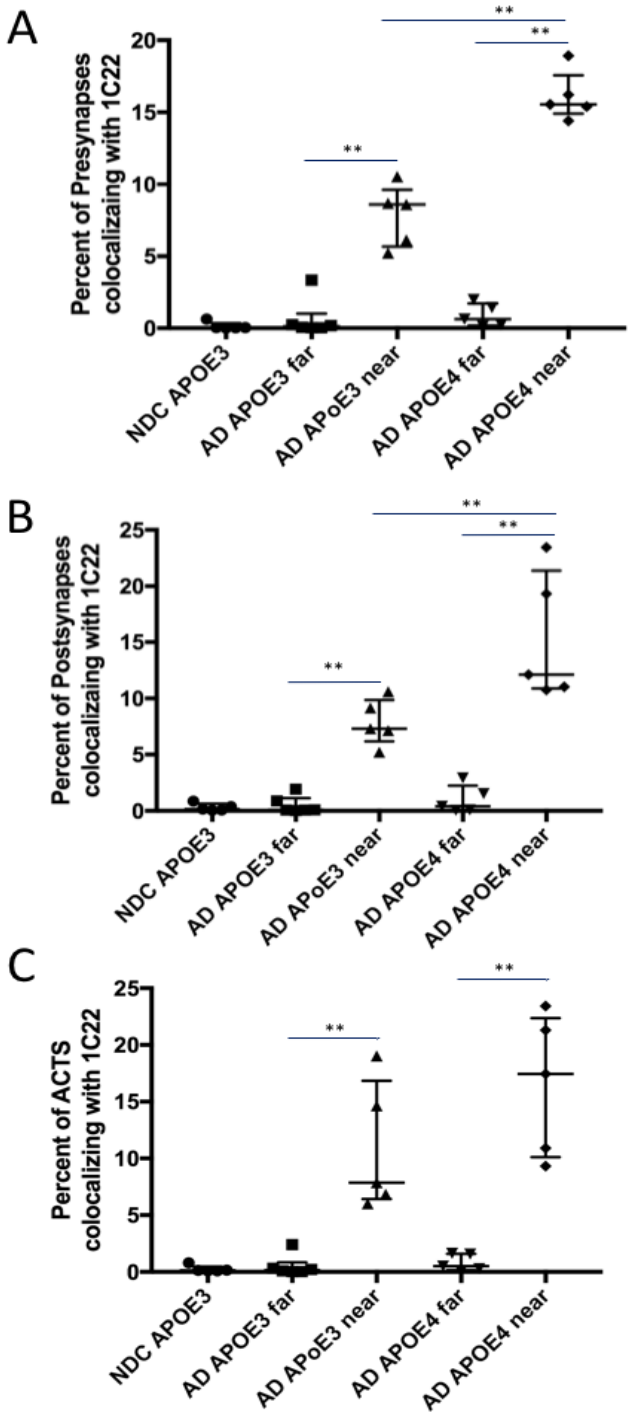

Figure 5.4: Percent of synaptic puncta co-localizing with Aβ. There is a significant increase in the percent of of Aβ (1C22) positive synapses near plaques compared with far from plaques for all three synaptic parts. There is a further significant increase in the percent of Aβ positive synapses in AD APOE4 cases compared with AD APOE3 cases for both presynapses (A) and postsynapses (B) although there is no difference between genotypes for ACTS (C). (** $p<0.01$ Kruskal-Wallis test with between groups Mann-Whitney U tests).

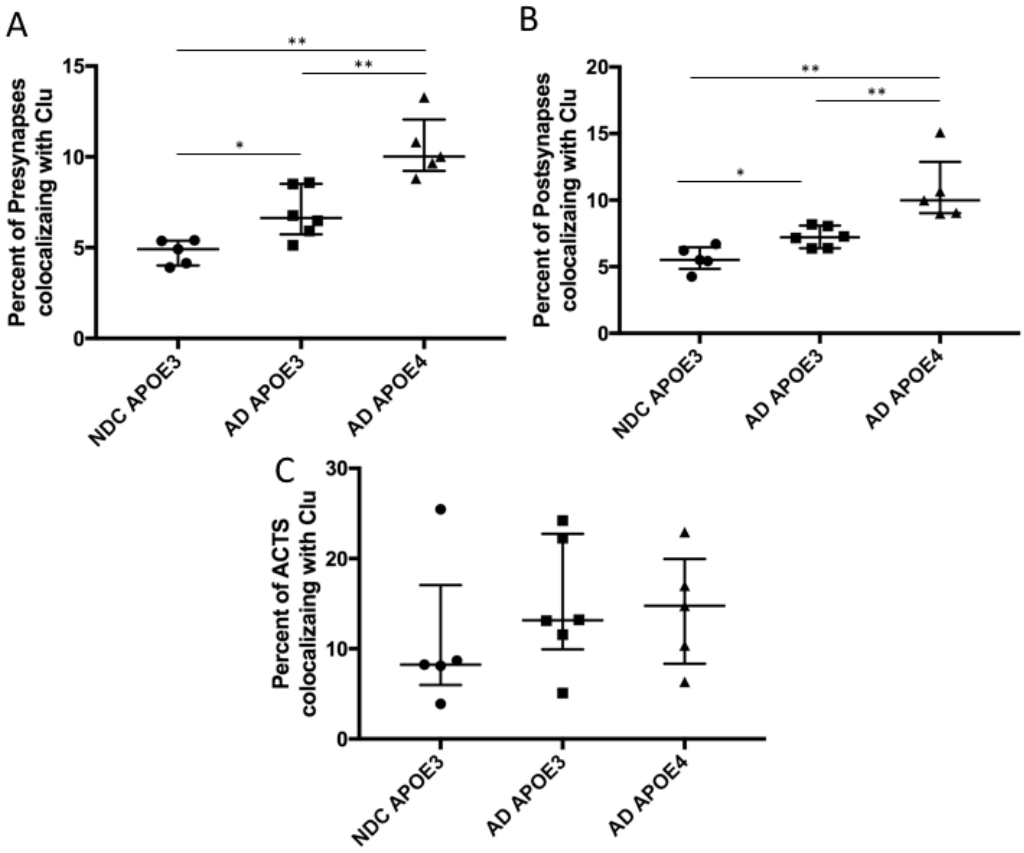

Figure 5.5: Percent of Synaptic puncta co-localizing with Clusterin. Analysis by array tomography shows a significant increase in the amount of Clusterin co-localizing with both presynapses (A) and postsynapses (B) in AD cases compared with NDC and a significant increase when comparing AD APOE4 cases with AD APOE3 cases. There is no difference in the amount of Clusterin co-localizing with ACTS (C). (**p<0.01, *p<0.05, Kruskal-Wallis test with between groups Mann-Whitney U tests)

5.3.4 ApoE4 is associated with an increased co-localization of Clusterin with presynapse and postsynapse in AD

Array tomography was used to investigate whether the increase in Clusterin seen in the synaptoneurosome using proteomics and western blot was due to an increase in Clusterin in the presynaptic compartment, the postsynaptic compartment, and or the ACTS. Analysis of array tomography shows that there is no difference in the percent of synapses with Clusterin when synapses near plaques are compared with synapses far from plaques therefore all synapses for each case were averaged together. This shows that there is an increase in the percent of presynapses ($\chi^2(2) = 12.44$, $p<0.0001$) and postsynapses ($\chi^2(2) = 12.44$, $p<0.0001$) co-localising with Clusterin in AD

cases compared with NDC for both APOE3 cases (presynapses p=0.0173, postsynapses p=0. 0173) and APOE4 cases (presynapses p=0.0013, postsynapses p=0.0013) and a further increase when AD APOE4 cases were compared with AD APOE3 cases (presyanpases p=0.0043, postsynapses p=0.0043) (Figure 5.5). However, there is no difference in the amount of ACTS co-localizing with Clusterin between any of the conditions (Figure 5.5).

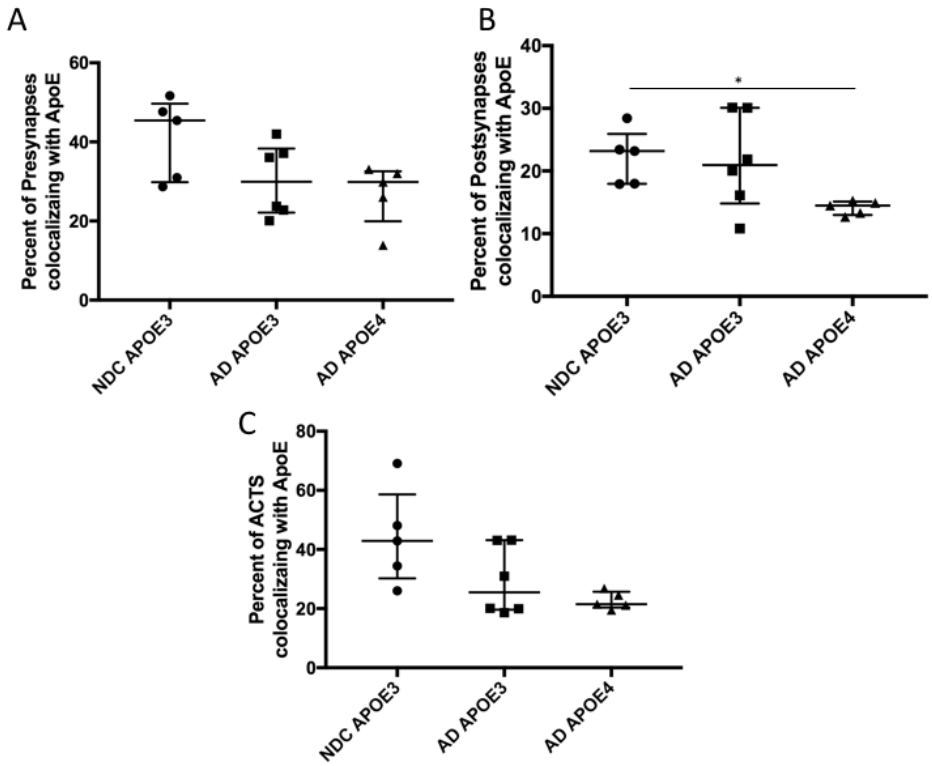

Figure 5.6: Percent of Synaptic puncta Co-localizing with ApoE. Array tomography shows a significant increase in the percent of postsynapses colocalizing with ApoE (B) in AD APOE4 cases compared with NDCs. There is no difference between groups in ApoE co-localizatiation with presynapses (A) or ACTS (C). (*p<0.05, Kruskal-Wallis test with between groups Mann-Whitney U tests).

In contrast to Clusterin, the amount of synapses co-localizing with ApoE goes down in AD APOE4 postsynapses compared with NDC synapses ($\chi^2(2) = 6.671$, p=0.0266, post-hoc p=0.0079). This is accompanied by a trend towards a decrease in the amount of presynapses ($\chi^2(2) = 4.663$, p=0.0932) and ACTS ($\chi^2(2) = 5.228$, p=0.0667) co-localizing with ApoE. With more cases it is likely that this trend would become significant as

Koffie *et al.* showed a decrease in ApoE with an APOE4 genotype using a different set of cases (Koffie *et al.*, 2012).

5.3.5 ApoE4 is associated with an increase in the amount of Aβ and apolipoproteins at the presynapse and postsynapse in AD

There is previous evidence indicating that ApoE is in part responsible for targeting Aβ to the synapse causing synaptic shrinkage and loss. It has also been shown that AD APOE4 cases are more likely to have Aβ at the synapse than AD APOE3 cases (Figure 5.4). One of the benefits of array tomography is the ability to strip antibodies and re-probe the same tissue ribbon with different antibodies thus allowing the analysis of the co-localization of several protein markers to the same synapse. We therefore looked at the co-localization of ApoE and Aβ together at the synapse to see if AD APOE4 cases were more likely to have synapses positive for both markers. As less than 1% of synapses far from plaques contain Aβ, this analysis focuses on crops taken near plaques only. There is an increase in the percent of synaptic puncta co-localizing with both Aβ and ApoE in APOE4 cases compared with APOE3 cases for both presynapses ($p=0.0317$, Figure 5.7A) and postsynapses ($p=0.0159$, Figure 5.8A). This appears to be due to an increase in synapses with ApoE containing Aβ in the APOE4 cases compared with the APOE3 cases (presynapses $p=0.0317$, postsynapses $p=0.0159$) (Figure 5.7B, Figure 5.8B). There is no difference in the percent of ACTS co-localizing with both ApoE and Aβ when comparing the two genotypes (Figure 5.9).

To see if this is also true of Clusterin we analysed synapses which co-localize for both Clusterin and Aβ. We found that there is an increase in the amount of presynapses ($p=0.0317$, Figure 5.10A) and postsynapses ($p=0.0159$, Figure 5.11A) that co-localize with both Clusterin and Aβ when APOE4 cases are compared with APOE3 cases. However, synapses which contain Clusterin are no more likely to contain Aβ in APOE4 cases than in APOE3 cases (Figure 5.10B, Figure 5.11B). As with ApoE and Aβ there are no difference between genotypes in the amount of Clusterin and Aβ at the ACTS (Figure 5.12).

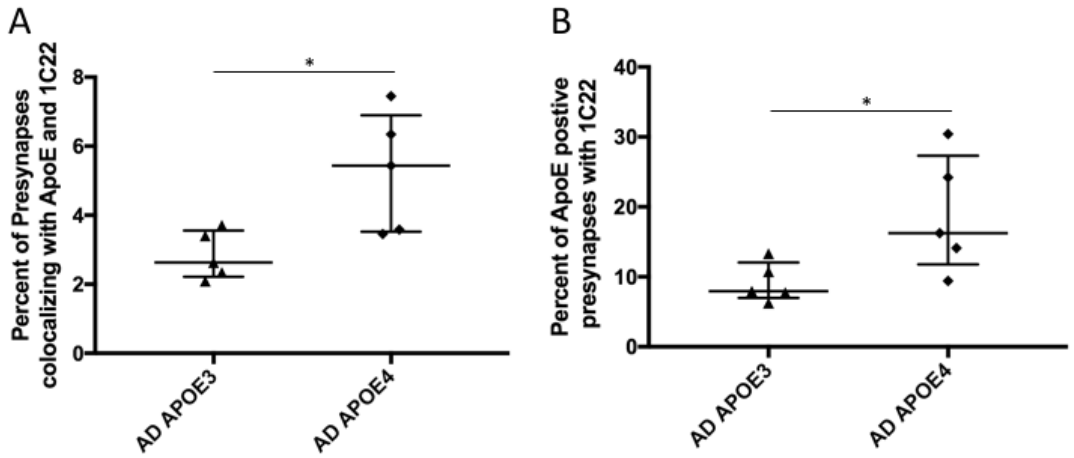

Figure 5.7: Co-localization of ApoE and 1C22 with presynapses. There is a significant increase in the amount of ApoE and 1C22 found together at the synapse (A) in APOE4 cases compared with APOE3 cases. Synapses which contain ApoE are more likely to also contain 1C22 in APOE4 cases compared with APOE3 (B). (* $p<0.05$, Mann-Whitney U tests).

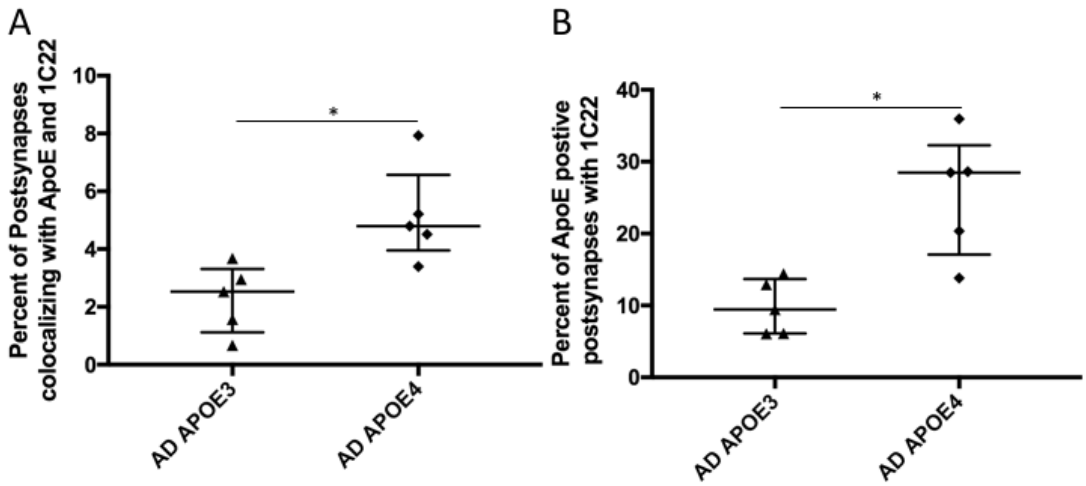

Figure 5.8: Co-localization of ApoE and 1C22 with postsynapses. There is a significant increase in the amount of ApoE and 1C22 found together at the synapse (A) in APOE4 cases compared with APOE3 cases. Synapses which contain ApoE are more likely to also contain 1C22 in APOE4 cases compared with APOE3 (B). (* $p<0.05$, Mann-Whitney U tests).

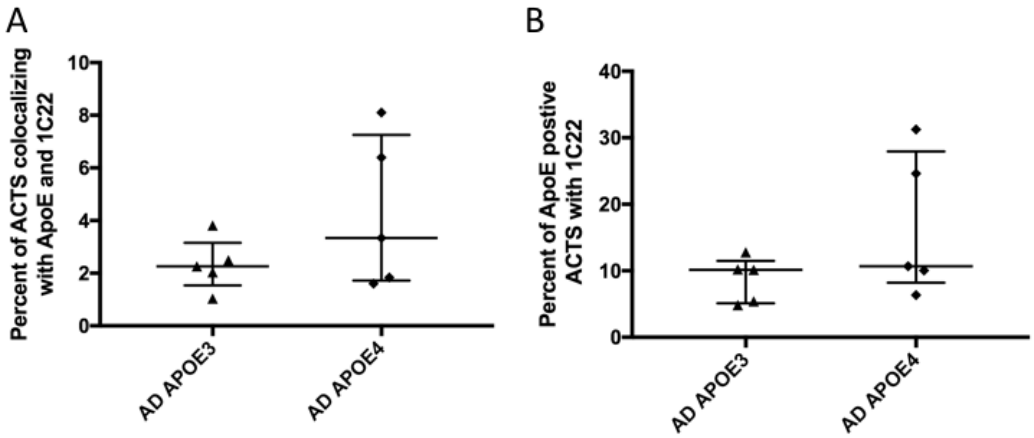

Figure 5.9: Co-localization of ApoE and 1C22 ACTS. ApoE genotype does not change the amount of ApoE and 1C22 co-localizing in ACTS (A) nor the amount of 1C22 found in synapses which contain ApoE (B).

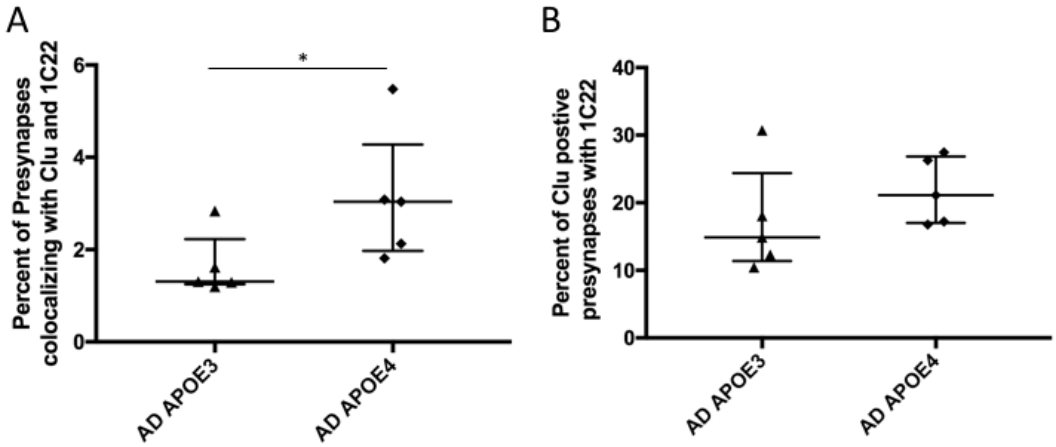

Figure 5.10: Co-localization of Clusterin and 1C22 with presynapses. There is a significant increase in the amount of Clusterin and 1C22 found together at the synapse (A) in APOE4 cases compared with APOE3 cases. Synapses which contain Clusterin are no more likely to also contain 1C22 in APOE4 cases compared with APOE3 (B). (* $p<0.05$, Mann-Whitney U tests)

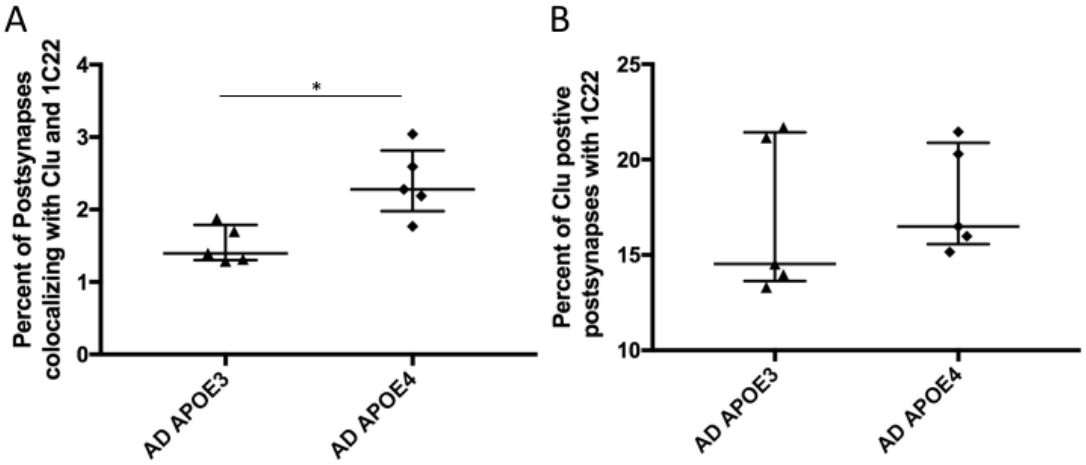

Figure 5.11: Co-localization of Clusterin and 1C22 with postsynapses. There is a significant increase in the amount of Clusterin and 1C22 found together at the synapse (A) in APOE4 cases compared with APOE3 cases. Synapses which contain Clusterin are no more likely to also contain 1C22 in APOE4 cases compared with APOE3 (B). (* $p<0.05$, Mann-Whitney U tests)

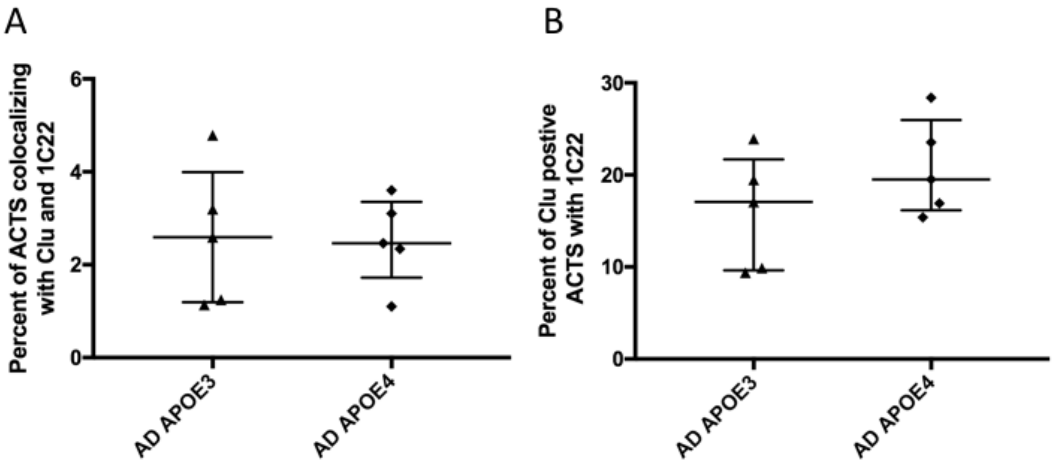

Figure 5.12: Co-localization of Clusterin and 1C22 with ACTS. ApoE genotype does not change the amount of Clusterin and 1C22 co-localizing in ACTS (A) nor the amount of 1C22 found in synapses which contain Clusterin (B).

5.4 Discussion

Chapter 4 showed an increase in the amount of Clusterin at the synapse in AD compared with NDC and a further increase in the synapse of AD APOE4 cases when compared with AD APOE3 cases (Figure5.1D). This finding was confirmed by western blot of synaptoneurosomes isolated from cases different to those sent for proteomics (Figure 5.1B). However, the effect of genotype on increased Clusterin was not found in whole cell homogenate although AD did cause a significant increase in Clusterin protein

levels (Lidström *et al.*, 1998)(Figure 5.1C). Given that transport of molecules is dysregulated in AD, this study highlights a need to look at specific subcellular compartments when investigating post-mortem tissue. Especially as changes at the synapse specifically are likely to have an impact in AD. Investigating the location and co-localization of proteins of interest in AD with synaptic elements will provide valuable information as to the role that these molecules play in disease pathogenesis. This is especially true of Clusterin as intracellular Clusterin has been shown to have apoptotic effects but extracellular Clusterin has been shown to be protective (Yu and Tan, 2012).

The effect of ApoE4 on synaptic density in AD

To further investigate the effects of ApoE4 in AD, array tomography was used on post-mortem tissue from NDC APOE3, AD APOE3, and AD APOE4 cases. Array tomography allows for the quantification and characterization of hundreds of thousands of synapses and assesses the co-localization of multiple protein markers to a single synapse (Micheva and Smith, 2007; Kay *et al.*, 2013). Looking in AD tissue, Koffie *et al.* showed in 2012 that synaptic density is decreased near plaques and that this density returns to NDC levels greater than 40μm from the plaque (Koffie *et al.*, 2012). This finding was replicated by this dataset examining different cases, which showed that crops near plaques have a significantly lower synaptic density compared with crops taken far from plaques, or crops taken from the NDC cases (Figure 5.3). This decrease in synaptic density near plaques is likely due in part to an increase in toxic Aβ species found near plaques (Figure 5.4). APOE4 cases were found to have a higher amount of Aβ at the presynapse and the postsynapse as well as a lower synaptic density near plaques when AD APOE4 and AD APOE3 cases were compared. As Aβ has been shown to be toxic to the synapse an increase in the amount of synapses containing Aβ could help to explain this difference between genotypes (Walsh *et al.*, 2002; Lacor *et al.*, 2007; Shankar *et al.*, 2008; Tomiyama *et al.*, 2010; Klein, 2013). However, this does not explain the decrease in synaptic density seen far from plaques in the AD APOE4 cases. There are a number of explanations as to why this could be and it is likely due to a number of factors. One explanation is that APOE4 cases often have a more aggressive

disease with a higher plaque load, more tau pathology, and higher neuron loss particularly in the temporal cortex (Tiraboschi *et al.*, 2004; Pievani *et al.*, 2011; Farfel *et al.*, 2016). This increase in neuron death likely causes the synaptic loss far from plaques as the projections from those neurons are lost. It is also possible that independent of AD, ApoE4 causes a global reduction in synapses even in healthy NDC. If this is the case then the density far from plaques in AD APOE4 cases is the density of APOE4 NDC. There are number of studies which indicate that this might be the case. In a study of a healthy aging cohort, Deary *et al.* showed that *APOE* ε4 carriers have reduced cognitive performance even in the absence of AD which could be due to a loss of synapses or neurons with age (Deary *et al.*, 2004). Studies using MRI have showed an effect of ApoE4 on cortical thinning in healthy adults and BOLD imaging also showed an effect of ApoE4 in an older cohort of healthy adults but not a younger one (Espeseth *et al.*, 2008; Machulda *et al.*, 2011). Mouse studies have also shown that ApoE4 knock in mice have reduced branching and less spines than ApoE3 knock in mice (Wang *et al.*, 2005). All this indicates that ApoE4 has an effect on the brain in healthy aging that might cause a reduction in synapse number however in order to confirm this hypothesis array tomography should be performed on APOE4 NDC and unfortunately not enough of these cases have been embedded for array tomography to adequately power a study.

The effect of ApoE4 on the density of astrocytic end feet

Astrocytic end feet are found at tripartite synapses and perform a myriad of important functions for synaptic development and maintenance. Among these roles are the provision of proteins and nutrients needed for the synapse to function as well as clearing away excess neurotransmitter from the synaptic cleft (Bernardinelli *et al.*, 2014; Chung *et al.*, 2015). This dataset found that although there is no significant loss of ACTS near plaques compared with far from plaques, APOE4 cases do have a significantly lower density of ACTS (Figure 5.3C). This is likely detrimental to the synapses in APOE4 cases as they will have lost the protective effects of those ACTS. However this dataset does not show if the loss of ACTS precedes the loss of synaptic terminals or ACTS loss follows the loss of presynapses and postsynapses. However this

finding does raise some important questions about the role of astrocytes at the synapse in AD. For example a major role of the astrocyte at the synapse is in regulation of glutamate and dysregulation of glutamate transports has been shown to cause excitotoxic neuronal death (Hazell *et al.*, 2010). Excitotoxicity is a prominent feature of AD with seizures a risk for many AD individuals and mouse models of AD. This indicates that loss of ACTS could be one of the ways in which ApoE4 affects AD (Horváth *et al.*, 2016). Astrocytes are also known to degrade Aβ and although array tomography shows that genotype does not affect the number of astrocytic processes that bind Aβ (Figure 5.4C). Loss of processes near the synapse could be responsible in part for the increased levels of Aβ in the synapse of APOE4 cases (Matsunaga *et al.*, 2003; Pihlaja *et al.*, 2011).

Synaptic Clusterin levels are increased in AD and in APOE4 cases

Array tomography shows an increase in the number of both presynapses and postsynapses co-localizing with Clusterin in AD cases and a further increase in the AD APOE4 cases compared with with APOE3 cases. As the second most abundantly expressed apolipoprotein in the brain Clusterin performs many of the same roles as ApoE including the transport of cholesterol and other necessary lipids to the neuron (Dong *et al.*, 2017). An *APOE* ε4 genotype has been shown to have an effect on the amount of ApoE in the brain due in part to the increased speed with which ApoE4 is degraded (Riddell *et al.*, 2008). Here array tomography has shown that there are less synapses with ApoE in APOE4 cases and it is possible, that the increase in Clusterin in the APOE4 cases is due to compensation for less ApoE. Indeed, when Apoe is knocked out of a mouse line there is an increase in the amount of Clusterin mRNA indicating that Clusterin can and does compensate for the loss of ApoE (Stone *et al.*, 1998). However, an increase in Clusterin at the synapse could also be due to a number of other reasons including neuron stress. It is known that stress, and specifically Aβ induced stress, results in an increase in intracellular Clusterin and a decrease in extracellular Clusterin (Killick *et al.*, 2014). A stress response could help explain the increase in the amount of Clusterin in AD. Adding to this hypothesis is a study showing that Clusterin is upregulated in the CSF of AD individuals and that higher CSF Clusterin

was associated with an increase in EC atrophy (Desikan *et al.*, 2014). Although this increase in CSF could be a response to neuron degradation rather than a contributing factor it does seed the question as to the role of Clusterin in Aβ mediated synapse loss.

ApoE and Clusterin are associated with Aβ at the AD synapse

Both Clusterin and ApoE are known to interact with plaques and bind to Aβ species in the brain, so to assess the interactions of these proteins with Aβ at the synapse we analysed the number of synapses that co-localize with both ApoE and Aβ as well as both Clusterin and Aβ. AD APOE4 cases have an increased number of presynapses and postsynapses which co-localize with both ApoE and Aβ and both Clusterin and Aβ (Figures 5.7A, 5.8A, 5.10A, 5.11A). However, the effect of *APOE* ε4 on these protein combinations is different. Analysis of the number of ApoE positive synapses containing Aβ shows that in APOE4 cases synapses which contain ApoE are more likely to also contain Aβ (Figure 5.7B, 5.8B). This indicates that ApoE4 is more likely to bind Aβ and deliver it to the synapse a finding confirmed by the experiments performed by Koffie *et al.* (Koffie *et al.*, 2012). In contrast synapses which contain Clusterin are no more likely to also contain Aβ in the APOE4 cases although APOE4 cases are more likely to contain both Clusterin and Aβ at the synapse (Figure 5.10, 5.11). This indicates that an *APOE* ε4 genotype does not change the likelihood of Clusterin binding Aβ in the way that it affects in the interaction of ApoE with Aβ. Figures 5.13-5.15 graphically show the extent of co-localization of each pathogenic protein marker with different synaptic puncta using Euler diagrams which make this difference clearer.

However, the question still remains as to whether this increase in Clusterin and Aβ in APOE4 cases is caused by an increase in Clusterin or an increase in Aβ. Clusterin is known to bind Aβ in the extracellular space and prevent fibrillization (Cascella *et al.*, 2013). This could indicate that the increase in Aβ and Clusterin at the synapse is due to and internalization of Clusterin bound to Aβ. However other studies have shown that intracellular Clusterin is increased following Aβ application indicating that up-regulation of intracellular Clusterin is a response to Aβ accumulation in the synapse (Killick *et al.*,

2014). Of course it is possible that both occur in the cell and that cellular stress caused by Aβ at the synapse causes internalization of Clusterin bound to Aβ causing a positive feedback loop. Another question raised by this dataset is whether an increase in Clusterin has a protective or a detrimental effect on the synapse. As mentioned before Clusterin has been shown to bind to Aβ, prevent fibrillization of Aβ and prevents the loss of LTP and memory when injected into a rat which points towards Clusterin having a protective role in AD (Cascella et al. 2013). On the other hand, knockout of Clusterin in rat primary neurons prevented Aβ induced neuronal death which indicates that Clusterin has detrimental roles in the neuron (Killick *et al.*, 2014). It is entirely likely that Clusterin has multiple roles in the brain and that these jobs depend in part upon subcellular localization of the protein. To fully understand the implications of this study, further investigation of the role of this important risk factor on the synaptic changes associated with Aβ and AD is required.

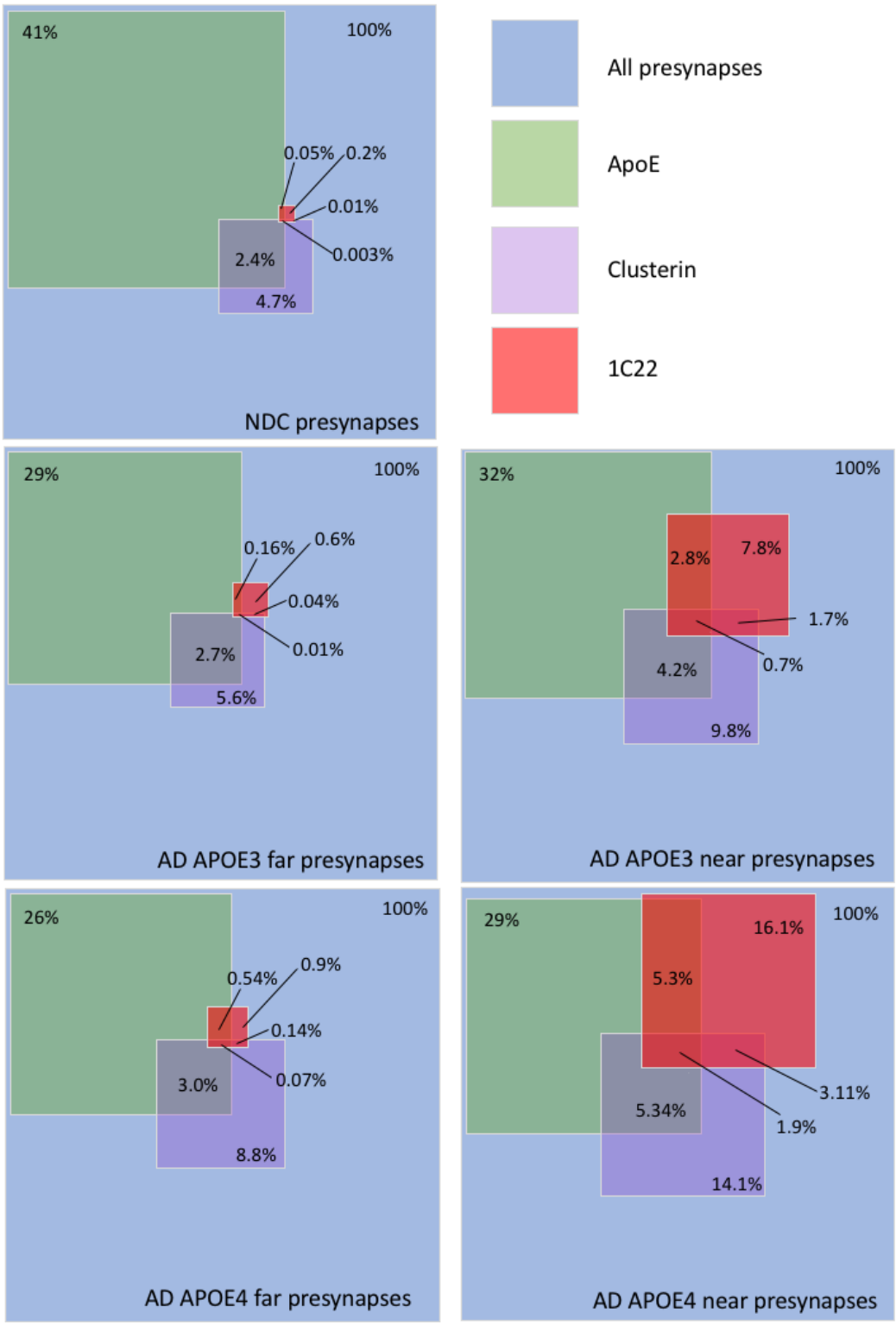

Figure 5.13: Euler diagram of Presynaptic Co-localization with ApoE, Clusterin, and 1C22. Blue boxes represent 100% of the presynapses for that condition and area of overlap with other colored boxes (green for ApoE, purple for Clusterin, and red for Aβ stained using 1C22) represent the percent of presynapses that co-localize with that or those markers. Numbers represent the percent of total presynapses co-localizing with that marker, for example 41% of presynapses in a control condition colocalize with ApoE.

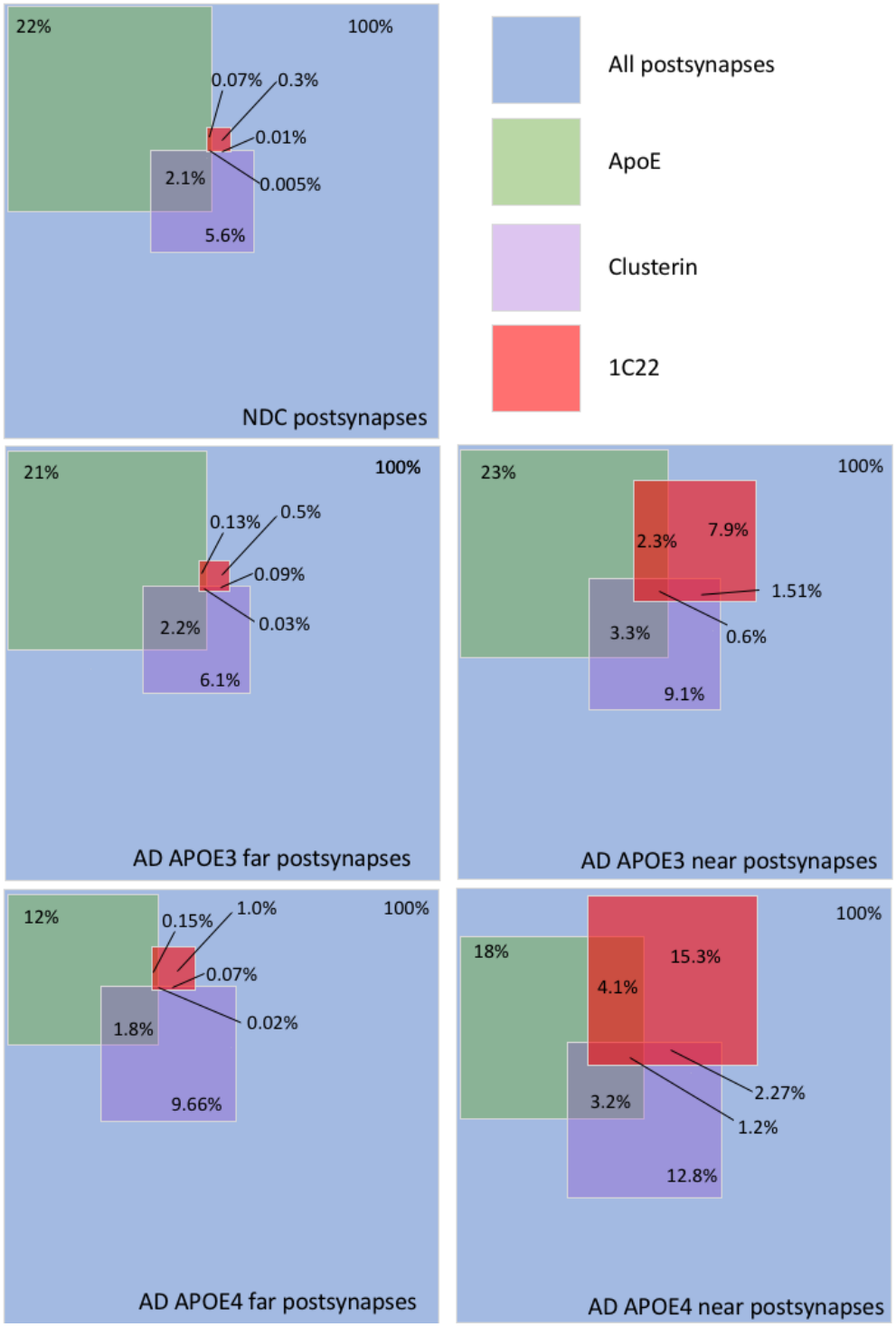

Figure 5.14: Euler diagram of Postsynaptic Co-localization with ApoE, Clusterin, and 1C22. Blue boxes represent 100% of the postsynapses for that condition and area of overlap with other colored boxes (green for ApoE, purple for Clusterin, and red for Aβ stained using 1C22) represent the percent of postsynapses that co-localize with that or those markers. Numbers represent the percent of total postsynapses co-localizing with that marker, for example 22% of postsynapses in a control condition colocalize with ApoE.

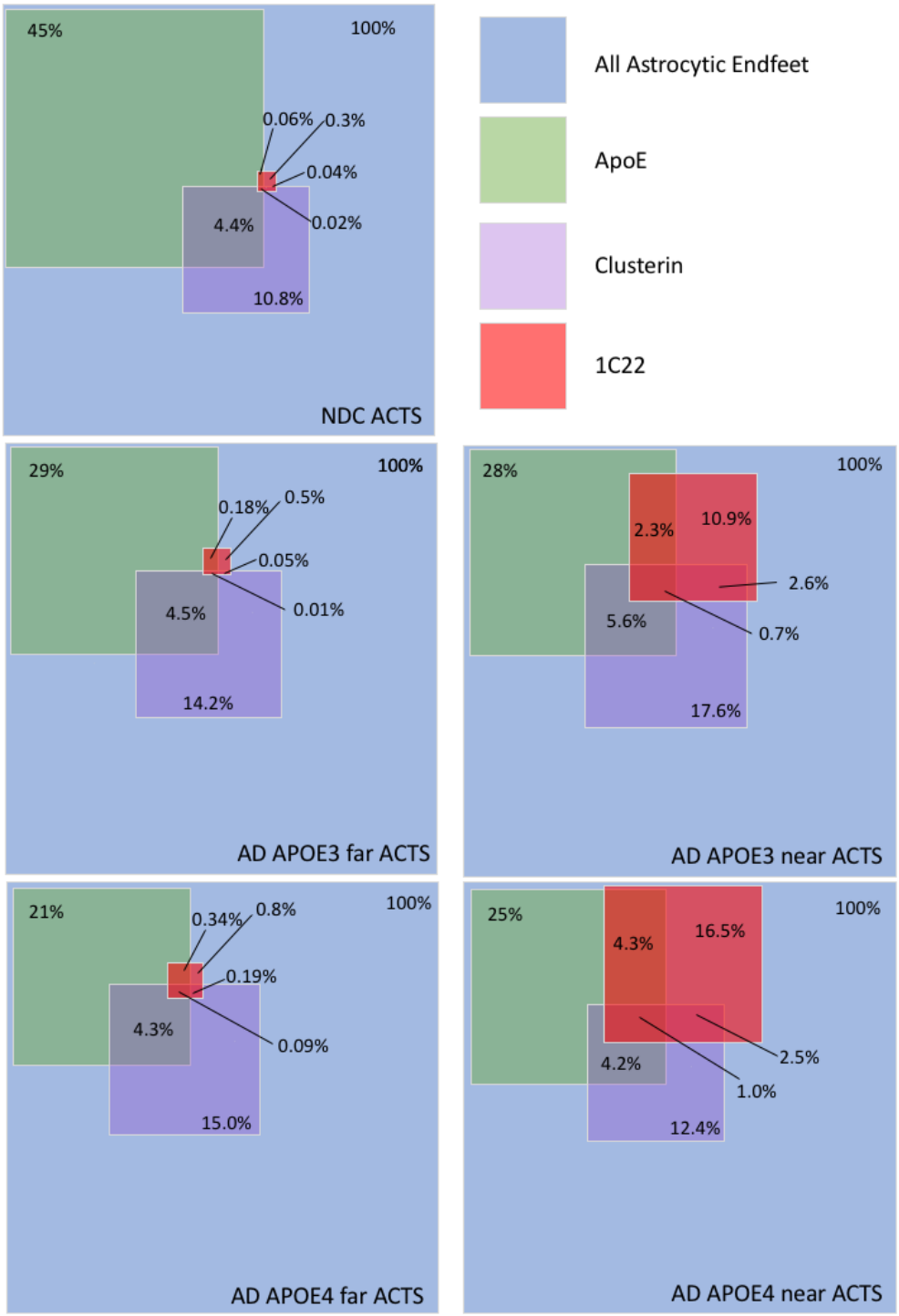

Figure 5.15: Euler diagram of ACTS co-localization with ApoE, Clusterin, and 1C22. Blue boxes represent 100% of the ACTS for that condition and area of overlap with other colored boxes (green for ApoE, purple for Clusterin, and red for Aβ stained using 1C22) represent the percent of ACTS that co-localize with that or those markers. Numbers represent the percent of total ACTSco-localizing with that marker, for example 45% of ACTS in a control condition colocalize with ApoE.

6 A novel human cell model of Aβ mediated synapse loss

6.1 Background and Aims

Model systems provide an excellent opportunity to discover the effects of proteins as they allow for manipulation of targets under controlled conditions. Human induced pluripotent stem cells (iPSC) allow for the reprogramming of cells to neurons from both patients and healthy controls (Takahashi *et al.*, 2007). These cells provide scientists with a human system that can easily be manipulated and iPSC-derived neurons particularly from familial AD cases are used widely to study pathological processes in AD (Arber *et al.*, 2017). This is beneficial as, as seen in chapter 3, mouse models of AD do not replicate many aspects of the disease and studying humanized proteins in a murine system can be complicated by the presence of endogenous murine proteins. However, neurons derived from iPSCs have a developmental phenotype and many of the genes associated with AD are not transcribed until later in development necessitating long culture times (Sposito *et al.*, 2015).

Chapter 3 and chapter 5 showed increased synaptic Aβ correlates with areas of synaptic loss. Other studies have shown that when oligomeric Aβ (oAβ) is applied to rodent primary culture, oAβ is synaptotoxic in low concentrations and neurotoxic in higher concentrations (Ferreira and Bigio, 2011). However while the exact species of oAβ that are synaptotoxic in disease is still an area of study and debate, it is clear that different oAβ species have different effects on cell culture systems (Lesne, 2014). oAβ extracted from AD human brain has been shown to cause learning and memory deficits when injected into animals and reductions in LTP in slices (Barry *et al.*, 2011; Borlikova *et al.*, 2013). When probed using western blot and chromatography smaller oligomers found in the soluble fraction of human brain extract were found to be more neuroactive than larger oligomers (Yang *et al.*, 2017).

The chapter aims to combine these two systems to

- Develop a novel cell model using Aβ derived from human AD brains and human iPSCs
- Test the effect of knocking down Clusterin on Aβ mediated synapse loss in this new model

6.2 Methods

6.2.1 Immunohistochemistry

Cortical neurons derived from human iPSCs from an individual with an *APOE* ε3/4 genotype and no known cognitive or neurological disorders were grown to 8 weeks as described in 2.7.3. Human brain extract, experimental control or aCSF (media control) was added to the cells and well volume was brought up to 500µl with +BDNF/GDNF media. After 48 hours cells were fixed using 4% PFA for 20 minutes at room temperature. Cells were stained as described in 2.7.6 using the antibodies table 6.1. Images (Figure 6.1) were taken on a Leica DM6 CS upright microscope with a TCS SP8 confocal platform and 5-10 images per well were analysed using custom cell profiler pipelines (appendix 3). Synaptic puncta were only counted if they overlapped with MAP2 and the number of synaptic puncta per µm of MAP2 positive dendrites was calculated for each well. An average synaptic density was generated for all aCSF control wells and each experimental well was compared with that average to generate the percent of control.

Table 6.2: Antibodies used in cell culture immunohistochemistry

Target	Host	Concentration (mg/ml)	Wavelength	Catalogue number
Map2	Guinea Pig	0.001	-	188 004
Synaptophysin	Mouse	0.002	-	ab8049
PSD95	Rabbit	0.001	-	D27E11
Guinea-pig IgG	Goat	0.0014	488	706-545-148
Mouse IgG	Goat	0.0007	Cy3	ab97035
Rabbit IgG	Goat	0.0007	Cy5	ab97077

Table 6.2: Antibodies used in cell culture western blots

Target	Host	Dilution	Catalogue number
Beta-actin	Mouse	1:1000	ab8226
Clusterin	Rabbit	1:1000	Sc-8354

Linear regression analysis was used to analyse the effect of Aβ concentration on synapse loss and one-way-ANOVA with Tukeys post-hoc test was used to analyse the results of Aβ mock immune depleted and immune depleted experiment and the siRNA experiments.

6.2.2 Western blotting

Cells were incubated with siRNA for 72 hours as described in 2.7.4 before being lysed with lysis buffer (50 mmol/L Tris [pH 7.5], 1.5% SDS, and 2 mmol/L DTT) and protein assayed. Western blotting was performed on cell lysates as described in 2.2.2 using the antibodies described in table 6.2. Students t-test was used to compare the two groups.

6.3 Results

6.3.1 Aβ derived from AD human brain but not NDC human brain causes synapse loss

8 week old cortical neurons derived from human iPSCs were challenged with brain extract derived from AD or NDC post-mortem tissue. Analysis of confocal images (Figure 6.1) of these cells show when AD brain extract is added there is strong correlation between the concentration of Aβ and the amount of synapse loss for both presynapses (R^2=0.5796, F(1,24) = 33.09, p<0.0001) and postsynapses (R^2=0.7767, F(1,24) = 83.46, p<0.0001) (Figure 6.2). The highest concentration of Aβ tested here was 0.651ng/ml which caused ~30% loss of synaptic puncta. However, NDC brain extract treated in the same way does not show any correlation between Aβ concentration and synaptic loss (presynapses: R^2=0.1123, F(1,10) = 1.265, n.s., postsynapses: R^2=0.0013, F(1,10) = 0.0129, n.s.) (Figure 6.2).

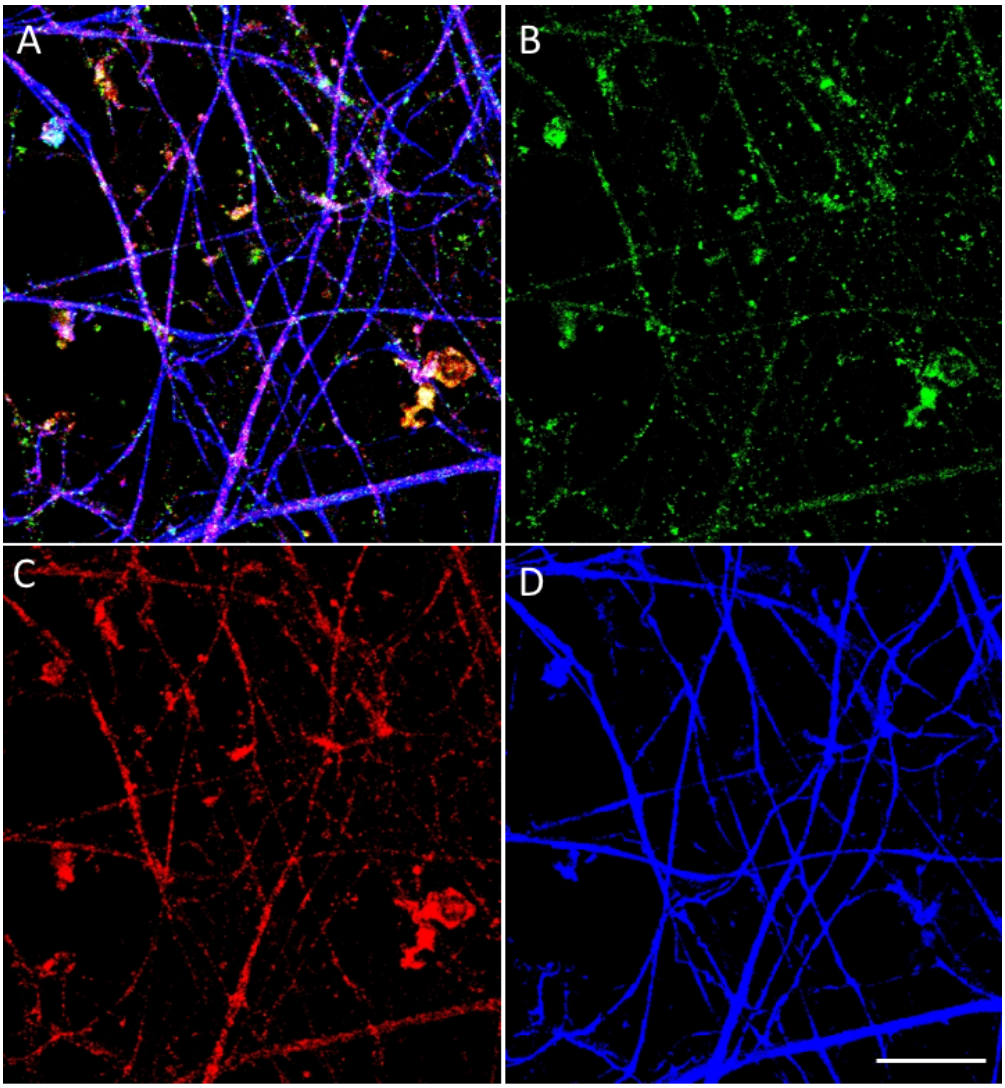

Figure 6.1: Representative images of iPSC. iPSC (A) were stained with synaptophysin (B) for presynapses, PSD95 (C) for postsynapses and MAP2 (D) to label dendrites. Scale bar is 20μm

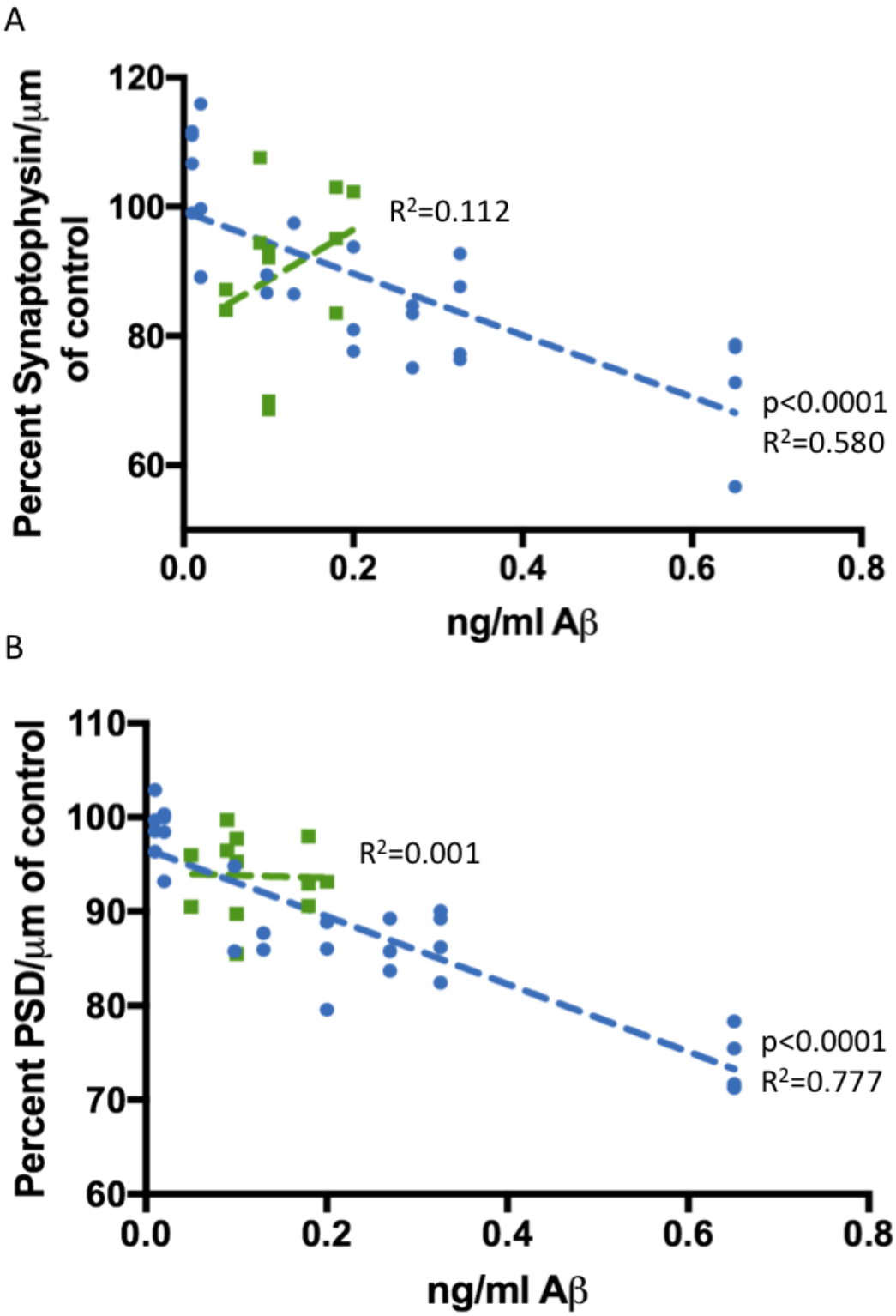

Figure 6.2: Synaptic loss with Aβ addition is concentration dependent. Linear regression analysis shows a significant interaction between the amount of Aβ added to the well and the number of synaptic puncta per μm of dendrite expressed as a percent of control wells for the same plate down when AD brain extract (blue) is added but not when NDC brain extract (green) is added for both presynapses (A) and postsynapses (B).

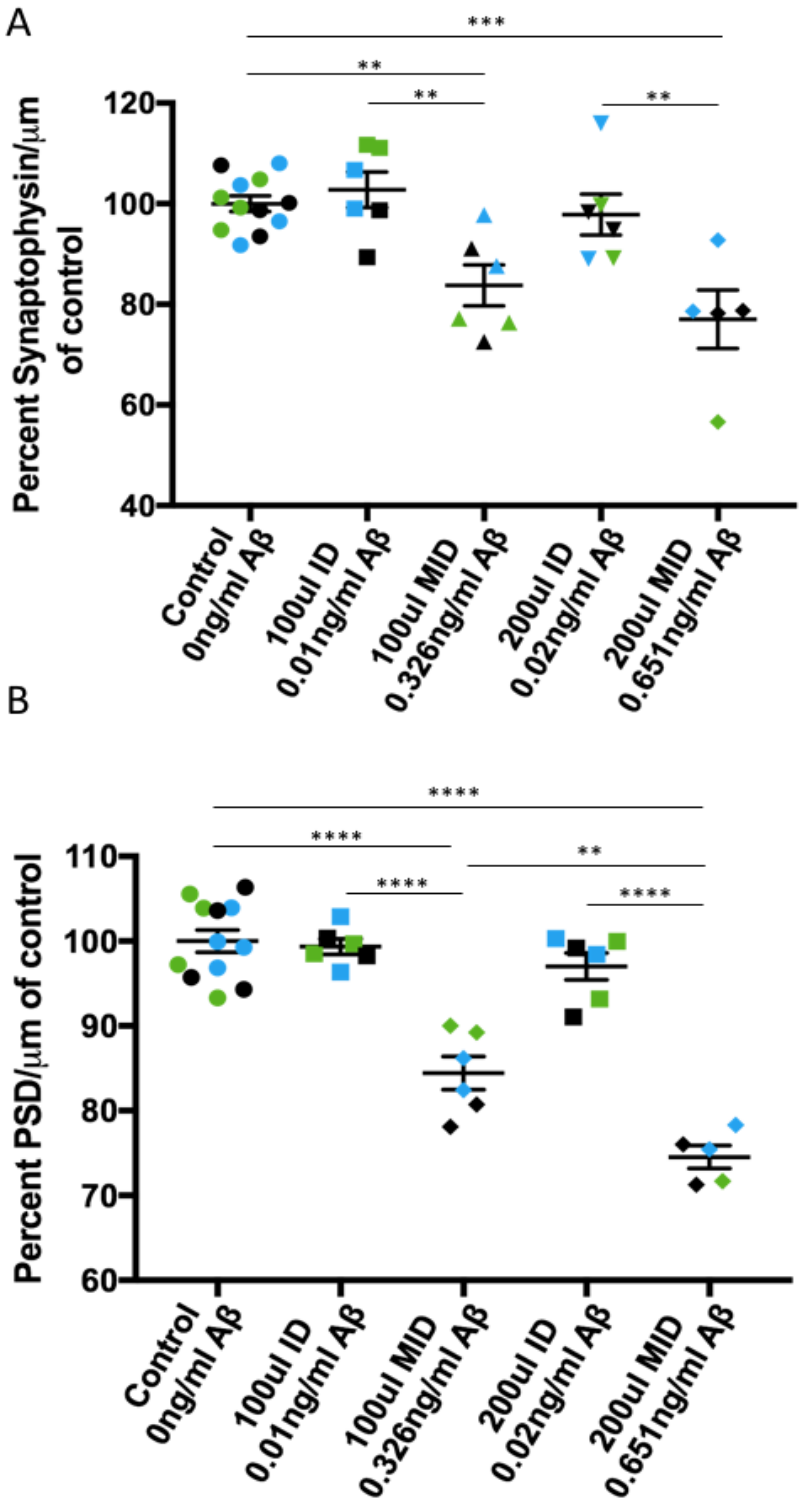

Figure 6.3: Immunodepletion of Aβ ameliorates the effects of AD brain extract on synapse loss.

There is a significant loss of synapses in wells treated with mock immunodepleted (MID) brain extract but not in wells treated with immunodepleted (ID) brain extract for both presynapses (A) and postsynapses (B). Colors indicate wells from the same plate down. (** $p<0.01$, *** $p<0.001$, **** $p<0.0001$).

6.3.2 Aβ is necessary for the synaptotoxic effect of AD human brain extract in iPSCs

To ensure that it is the Aβ content of AD brain extract that is causing synaptic loss, brain extract was immune depleted (ID) of Aβ. Brain extract treated with 4G8, an anti-Aβ antibody, and protein A agarose beads was prepared alongside mock immune depleted (MID) brain extract which was treated with pre-immune sera and beads. Incubation of MID extract with cells showed a significant loss of synaptic puncta compared with controls for presynapses (one-way ANOVA ($F(4,30)= 9.776$, $p<0.0001$) Tukeys post-hoc for 100μl MID $p=0.0076$ and 200μl MID $p=0.0003$) and postsynapses (one-way ANOVA ($F(4,30)= 47.91$, $p<0.0001$) Tukeys post-hoc for 100μl MID $p<0.0001$ and 200μl MID $p<0.0001$) (Figure 6.3). However, incubation with ID extract did not cause a loss of synapses when compared with controls.

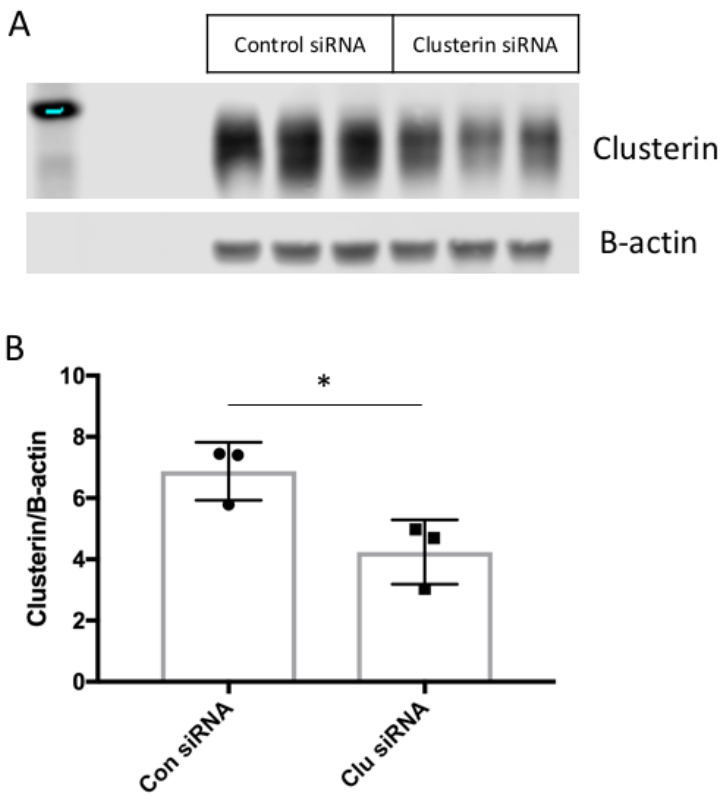

Figure 6.4: siRNA knocks down Clusterin expression in IPS cells. Analysis of cell homogenate by western blot (A) shows a significant ~30% decrease in Clusterin in cells treated with clusterin siRNA compared with control siRNA after 96 hours (B). (* $p<0.05$)

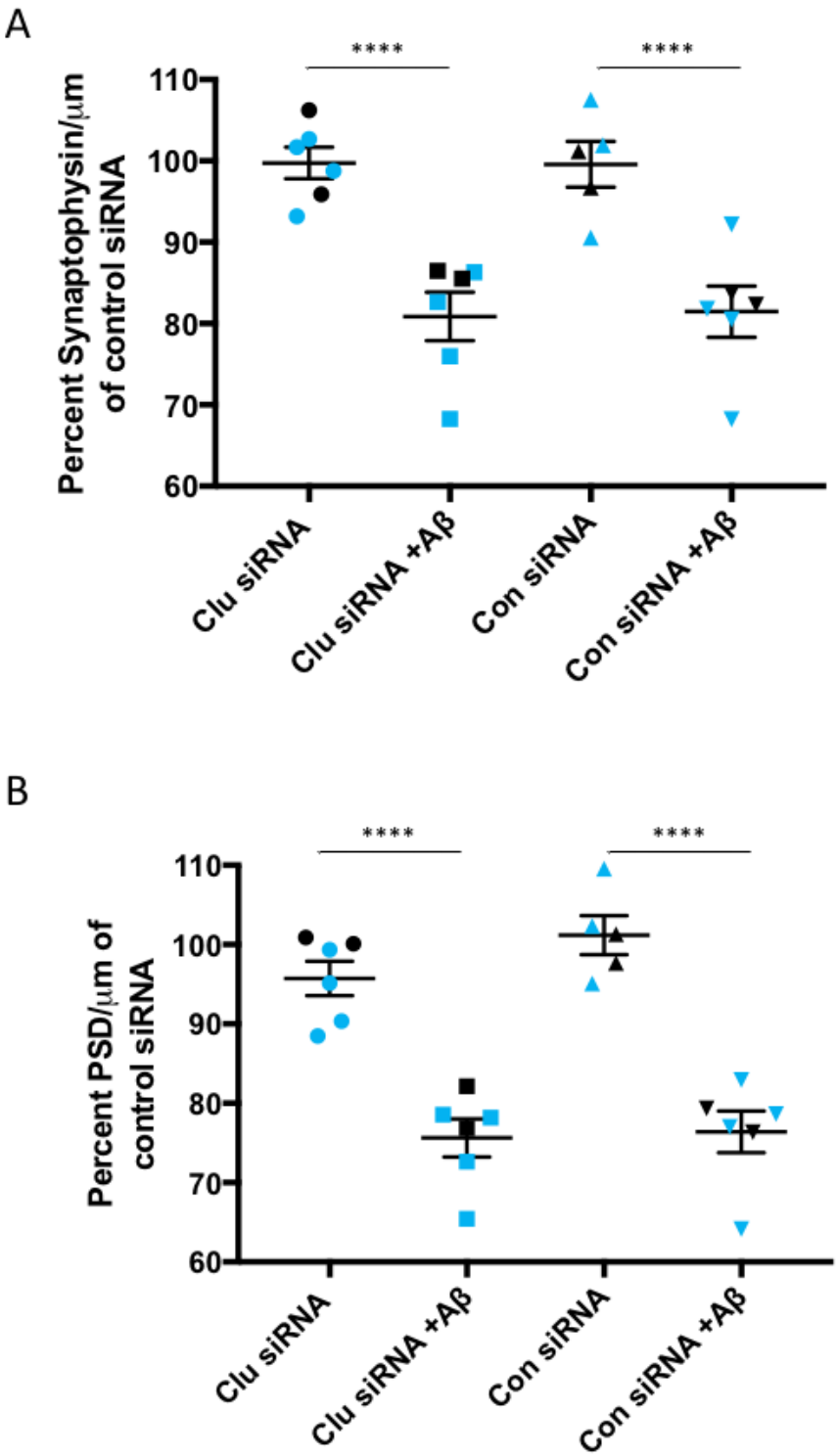

Figure 6.5: Knock down of Clusterin expression by siRNA does not change the effect of AD human brain extract on synapse loss. Human brain extract causes a significant loss of both pre-synapse (A) and postsynapses (B) but knock down of Clusterin with siRNA does not change the amount of synaptic loss. Colors indicate wells from the same plate down. (** $p<0.01$, *** $p<0.001$, **** $p<0.0001$).

6.3.3 Knock down of Clusterin does not affect the synaptotoxic effect of AD human brain extract

To investigate if knock down of Clusterin would have an effect on the synaptotoxic effects of Aβ at the synapse in this model, siRNA was used to knock down Clusterin by ~30% as assessed by western blot (t-test, $t(4)=3.234$, $p=0.0318$)(Figure 6.4). Cells incubated with AD brain extract showed a significant loss of synapses compared with those incubated with aCSF for both presynapses (one-way ANOVA ($F(3,19)= 14.87$, $p<0.0001$) Tukeys post-hoc Clu siRNA v Clu siRNA+AD $p=0.0005$ and Con siRNA v Con siRNA+AD $p=0.0009$) and postsynapse (one-way ANOVA ($F(3,19)= 28.83$, $p<0.0001$) Tukeys post-hoc Clu siRNA v Clu siRNA+AD $p<0.0001$ and Con siRNA v Con siRNA+AD $p<0.0001$) but there was no difference between cells with Clusterin knocked down and those incubated with a control siRNA (Figure 6.5).

6.4 Discussion

The benefits of an all human system

This chapter presents a new model of oAβ induced synaptotoxicity using cortical neurons derived from human iPSCs and oAβ extracted from AD post-mortem tissue. The cortical neurons used here are derived from control human iPSCs with no known neurological defects. Neurons grown using the protocol used show synaptic puncta (Figure 6.1) and functional synaptic connections (Bilican *et al.*, 2014) 5 weeks after differentiation from neural precursor cells negating the need for complicated immunopanning techniques (Nieweg *et al.*, 2015) . Using these cells as a model allows for the development of an entirely human based model of the early stages of synaptic loss in sporadic AD. The model presented here has a number of both benefits and drawbacks some of which will be enumerated here.

The study of a human disease in an all human system has obvious benefits to understanding the role of various proteins in pathology especially in a disease as

complex as AD. Studies in rodent primary culture have been very valuable in revealing a multitude of diverse and occasionally contradictory downstream effects of oAβ on neurons (Hiruma 2003, Shankar 2007). However, which of these effects is applicable to humans is still an important question and neurons derived from human iPSCs provide an in vitro approach to study these effects. iPSCs are also particularly important for diseases in which no causal genetic link is established but many risk factors are involved such as sAD. The generation of iPSC lines from individuals with high risk genetic polymorphisms such as *APOE* ε4/4 could aid in our understanding of how these risk factors increase risk of disease both individually and in concert with each other. The power of iPSC technology has recently increased due to the discovery of the CRISPR/Cas9 system which allows for easier manipulation of the iPSC genome. This enables the creation of isogenic controls for these high risk factors or familial mutations (Zhang *et al.*, 2014).

The use of oAβ derived from human post-mortem brain also provides this model with an increased relevance to disease. The exact species of oAβ that is toxic in AD is unknown and different species and sizes of oAβ are known to have different levels of toxicity at the synapse (Ono *et al.*, 2009; Roychaudhuri *et al.*, 2009). By using oAβ found in post-mortem AD cases in the model it can be assumed that the disease relevant species are present. This is important for a number of reasons not least of which is that oAβ from human brain appears to be more neurotoxic than synthetic oAβ. Others have shown that oAβ derived from the human brain is in a conformation that makes it highly potent in inducing neuronal changes in a way that synthetic oligomers are not (Jin *et al.*, 2011). In this model the concentrations used are in the pM range which is much closer to the pathological concentration found in AD (Lue *et al.*, 1999). Studies using synthetic oAβ often use in excess of 10nM to achieve synaptotoxic effects (Deleglise *et al.*, 2014). This has important implications for therapeutics directed against oligomeric species of Aβ as those directed against synthetic oligomers might have less of an effect than those directed against pathologically important ones.

Finally, this model reduces the impact on animals and animal welfare of scientific research. Although there are many questions that can be answered only through animal research, scientists have an ethical responsibility to ensure that the minimum number of animals possible are used in research. This model represents a replacement of a previously rodent based model with no loss of scientific merit.

Drawbacks of this system

There are also many limitations of this model although it is worth mentioning that many of these are limitations of cell culture in general and thus also apply to rodent primary culture. These of course include that cells in a dish are not cognitively aware and thus the cognitive effects of AD can not be tested using in vitro models. However, a major limitation of this model compared with other in vitro systems is that iPSCs are inherently developmental in nature (Patani *et al.*, 2012; Camp *et al.*, 2015). In a disease primarily of aging, cells expressing proteins mainly associated with early development do not express many of the proteins associated with AD (Sposito *et al.*, 2015). Rodent neurons reach a level of maturity quicker in a culture dish and thus do not require as long an incubation period to become functionally mature. The cells studied in this chapter do have all the synaptic machinery required for functionally active synapses after 5 weeks in culture and to the best our knowledge the synaptic machinery needed for synapse denegation is in place by 8 weeks in culture (Bilican *et al.*, 2014; Livesey *et al.*, 2014). However new protocols are being developed which generate cortical neurons from iPSCs which are more developmentally mature and it will be interesting to see what these cells do in a system similar to the one described here (Vera *et al.*, 2016; Qi *et al.*, 2017).

Neuronal cultures also intentionally contain low concentrations of glial cells. Glial cells have been shown to play an important role in the pathology and synaptotoxicity of AD (Garwood *et al.*, 2011). Glia are also important for cell development and studies have shown that co-culturing iPSC derived neurons with astrocytes or even conditioned media from astrocytes increases the speed of

development of functional synapses (Tang *et al.*, 2013; Odawara *et al.*, 2014). Future experiments using this model could investigate the effects of co-culturing these cells with human astrocytes to see what effect that might have. This would be particularly interesting in regards to ApoE and Clusterin as there is some evidence that the cell these proteins are derived from makes a difference to their physiology.

The effect of Clusterin knock down on the toxic effect of oAβ at the synapse

Proteomic analysis of synaptoneurosomes in chapter 4 indicated that Clusterin was up-regulated in the synapse in AD cases. In depth analysis of the synapse using the high-resolution imaging technique, array tomography, in chapter 5 confirmed this increase in Clusterin in both presynapses and postsynapses. Further-more, array tomography found that 15% of the synapses near plaques that contained Clusterin also contained oAβ indicating a link between these two proteins that might mirror the link between ApoE and oAβ. However further investigation of the role of Clusterin on the synaptic effects mediated by Aβ is required to understand the interaction between these proteins in AD.

Killick *et al.* showed in 2014 that knock out of Clusterin in rat primary neurons prevented the neurotoxic effects of exogenous Aβ addition however the synaptic effects of this Aβ addition were not mentioned (Killick *et al.*, 2014). To investigate the effects of Clusterin on oAβ induced synaptotoxcity, Clusterin was knocked down by 30% in human iPSC derived cortical neurons (Figure 6.4) and oAβ derived from human brain was added. In the absence of AD brain extract knock down of Clusterin did not change the number of synaptic puncta per μm of dendrite when compared to a control siRNA. Application of human derived oAβ caused a 20-25% decrease in the number of synaptic puncta per μm of dendrite for both presynapses and postsynapses. However, Clusterin knock down by siRNA did not change the amount of synaptic loss with the addition of brain extract (Figure 6.5).

Due to the observations of Killick *et al.* the expectation was that knock down of Clusterin would prevent against synaptic loss however this was not the observed result (Killick *et al.*, 2014). It is possible that this is due to the differences in the level of knock down of Clusterin, as here Clusterin is knocked down by ~30% (Figure 6.4) rather than fully silenced. Full knock down of Clusterin in this model would help elucidate the effect of Clusterin in oAβ induced synaptotoxicity, as would increasing the concentration of Clusterin. Cascella *et al.* showed that incubating oAβ with Clusterin prior to incubating it with cells reduced the amount of fibrillisation of Aβ and thus the toxic effect on neurons (Cascella *et al.*, 2013). However, this experiment did not look at the effect of an increase in intracellular Clusterin or the downstream signalling cascades such an increase might cause. Killick *et al.* showed that an increase in intracellular Clusterin causes an increase in Dkk1 and Wnt which then causes neuron death. Interrupting this cascade both at Clusterin and at Dkk1 prevented neuron death implicating this pathway further in AD (Killick *et al.*, 2014). Manipulation of other players in this pathway particularly dkk1 and dkk3, which was found to be altered in AD in chapter 4 could help increase knowledge about the role of this pathway in synaptic toxicity in AD (Purro *et al.*, 2014; Bruggink *et al.*, 2015).

7 Discussion

7.1 Overview of results

In this thesis, synapse degeneration and dysfunction in AD were investigated using multiple methods and models as well as post mortem tissue from AD and NDC cases. In particular the following research questions were addressed.

1) Does the expression of wild type human tau in a mouse model of fAD affect Aβ mediated synaptic loss?

Chapter 3 shows that in the APP/PS1 model of AD, expression of full-length wild type human tau increased the size of Aβ plaques and the number of dystrophic neurites associated with plaques. However, these mice did not show any increase in plaque associated synapse loss or neurons loss compared with APP/PS1 mice.

2) What are the protein changes that occur in the synapse in post mortem AD cases compared with controls and how does an *APOE* ε4 allele affect those changes?

Chapter 4 shows that AD has a profound effect on the synaptic proteome by comparing AD and NDC post mortem cases using unbiased label-free LC/MS-MS. IPA analysis indicated that the protein networks that were most affected in AD were endocytosis, exocytosis, cell morphology, and mitochondrial function. Further-more *APOE* genotype has a significant effect on some of these pathways most especially in regards to lipid metabolism and cellular homeostasis.

3) How does an *APOE* ε4 allele affect the synaptic density of presynapses, postsynapses, and astrocytic end feet in AD, and what effect does it have on the synaptic co-localization of Clusterin, Aβ, and ApoE?

Chapter 5 shows using array tomography that there is a decrease in the synaptic density of synaptic puncta near plaques in AD cases compared with NDC. AD cases with an *APOE* ε4 allele show a further decrease in synaptic density both near and

far from plaques. These cases also show an increase in Clusterin and Aβ compared to cases without an *APOE* ε4 allele and indicate a relationship between Clusterin and Aβ at the synapse.

4) Does Aβ isolated from post mortem brain cause synaptic loss in cortical neurons derived from human iPSCs?

Chapter 6 shows a clear loss of synapses in cortical neurons derived from human iPSCs when Aβ extracted from human post mortem is added. This loss of synapses correlates with the concentration of Aβ added and did not occur when NDC brain extract or AD brain extract immunodepleted of Aβ was added.

7.2 The synapse and AD

Synapses are incredibly complicated and diverse structures crucial to the creation and maintenance of memory and loss of these structures is though to underlie the symptoms in several neurodegenerative disease including AD (Moreno and Mallucci, 2010). In fact, in AD the greatest correlate of the cognitive decline seen in the disease is synaptic loss placing synaptic loss at the centre of disease pathogenesis (Selkoe *et al.*, 2012). Preventing the loss of synapses, which in AD is associated with oligomeric species of Aβ and tau, is likely of therapeutic benefit(Shankar *et al.*, 2008; Guerrero-Muñoz *et al.*, 2015). Indeed, studies in the related field of prion diseases show that preventing synaptic loss in mouse models of scrapie prevents clinical disease even in the presence of toxic protein accumulation (Moreno *et al.*, 2013). This thesis therefore focuses on uncovering the effect of AD and the toxic proteins associated with AD on proteins and protein networks within the synapse in an effort to further understand how this contributes to synaptic dysfunction and death in AD.

The interaction of Tau and Aβ at the synapse

The work shown here shows that expression of wild type tau did not exacerbate Aβ mediated synapses loss. Previous studies in this area have shown that tau is

necessary for the effects of Aβ induced memory loss, LTP deficits, and synaptic death and therefore it was surprising that increasing the level of non-mutant tau had no effect on synaptic loss (Roberson *et al.*, 2007, 2011; Shipton *et al.*, 2011). This indicates that endogenous mouse tau is necessary and sufficient to cause the synaptic loss associated with Aβ. These studies together would indicate that this places tau dysfunction downstream of Aβ accumulation at the synapse but upstream of synaptic death. However other studies have shown that pathological species of tau are detrimental to the synapse indicating that tau can cause synaptic dysfunction in the absence of Aβ (Lasagna-Reeves *et al.*, 2011).

It is clear that the interaction between tau and Aβ at the synapse still requires further investigation. An interesting line of further study would be to express Aβ and human tau in a mouse tau knockout mouse to investigate this interaction in the absence of mouse tau. Indeed there is evidence that endogenous mouse tau effects the pathogenicity of mutated human tau in a mouse model and it is possible that the same is true of wild type tau (Ando *et al.*, 2011; Wegmann *et al.*, 2015). A limitation of this study would be that although there would then be no interference of mouse tau, the kinases that phosphorylate tau would still be murine in nature. It is known that hyper-phosphorylation of tau is an early feature in AD and a recent study has indicated that phospho-tau is increased in Aβ positive synapses in AD (Bilousova *et al.*, 2016). Gotz *et al.* review the importance of phosphorylation of tau in human disease and expressing humanized kinases along side Aβ and hTau in a mouse model would be an interesting path for further study (Götz *et al.*, 2010).

Another potential follow up study would be to investigate the interaction between Aβ and tau using an human iPSC culture based model similar to that described in chapter 6. A benefit of this system would be that all proteins expressed would be human in nature and and yet a major limitation of this model is that all 6 isoforms of tau are not expressed until late in development necessitating long culture times (Sposito *et al.*, 2015). New protocols might make this approach more possible by reducing the amount of time required for neurons to reach a more developmentally

mature state although it is currently unknown what effect this has on the proteins related to AD (Vera *et al.*, 2016; Qi *et al.*, 2017).

The role of synaptic protein changes in AD

To further understand the synaptic dysfunction that occurs in AD, proteomics was used on post mortem tissue from AD and NDC cases. By isolating the synapse this study increased our understanding of which proteins and pathways are involved in synaptic dysfunction while minimising the effect of other subcellular compartments and cell types. As trafficking is known to be disrupted in AD it is important to consider the effects of protein location as well abundance (Encalada and Goldstein, 2014). Mitochondrial transport in particular is known to be affected in AD and this study adds to that knowledge by indicating that many of the proteins involved in energy production in the mitochondria are affected in the AD synapse (Sheng and Cai, 2012; Cai and Tammineni, 2017). Dysfunction of the mitochondria is known to occur early in AD pathogenesis and represents an area of potential therapeutic development. In particular PITRM1, an enzyme found in the mitochondria and known to degrade Aβ is shown to be reduced in AD cases (Alikhani *et al.*, 2011). It is possible that reduced PITRM1 lessens the ability of mitochondria in AD to degrade Aβ leading to mitochondrial dysfunction and synaptic death. This protein and others discovered in this study merit further investigation as mitochondrial dysfunction can be a trigger for apoptosis and other groups have shown that protecting mitochondria in mouse models of AD can prevent against synaptic dysfunction and loss.

This study also found that proteins involved in the immune system and neuroinflammation are dysregulated in the AD synapse. Microglia and astrocytes are known to play a large role in synaptic function both in health and disease. Indeed, recent evidence has indicated that the complement system of innate immunity, particularly complement components C1q and C3, are involved in synaptic death in AD (Hong *et al.*, 2016; Shi *et al.*, 2017). This study shows that other proteins in this cascade including complement component C4, HLA-1, and Clusterin are all increased at the

synapse in AD presenting innate immunity as an attractive area for further study and therapeutic intervention. Clusterin also functions as a modulator of cellular homeostasis and has been found to act through Dkk1 and Wnt to cause neuronal death in the presence of Aβ (Killick *et al.*, 2014). Wnt signalling has already been proposed as a therapeutic target in AD and is known to be involved in synaptic maintenance and Aβ mediated synapse loss (Purro *et al.*, 2012; Dickins and Salinas, 2013; Wan *et al.*, 2014). Although Dkk1 was not found in this dataset, the closely related Dkk3 was, adding evidence to the importance of this pathway in synaptic dysfunction in AD.

The effect of ApoE on synaptic proteins changes

The *APOE* ε4 allele is the strongest genetic risk factor for AD increasing not only the risk of AD but also the rate of cognitive decline. *APOE* genotype also affects the cognitive ability of elderly people in the absence of AD indicating that *APOE* might affect synaptic protein composition in the absence and presence of AD (Deary *et al.*, 2004). The effects of *APOE* genotype on the synaptic proteome in the absence of AD are relatively small and highlights proteins involved in endocytosis and exocytosis indicating that differences in the lipid binding properties of the different ApoE isoforms might affect the stability or composition of the lipid bilayer in old age (Alberts *et al.*, 2002; Zhong and Weisgraber, 2009).

The affects on the synaptic proteome of an *APOE* ε4 genotype in the presence of AD are more numerous and could indicate proteins which contribute to that increased risk or rate of cognitive decline seen in APOE4 cases. Here Clusterin is found to be increased in the presence of ApoE4 and AD, a relationship that is confirmed using array tomography. Array tomography also showed that Clusterin and Aβ were more likely to be found together in the synapse of *APOE* ε4 carriers compared with *APOE* ε3/3 individuals and that this coincided with an decrease in synaptic density in these cases. However knock down of Clusterin in a cell culture model of Aβ mediated synapse loss did not affect the loss synapses so it remains to be seen if this increase in Clusterin at the synapse plays a detrimental or a protective role.

Array tomography also revealed that an *APOE* ε4 allele in AD was associated with a decrease in synaptic density not only near plaques but also far from plaques when compared with AD APOE3 cases. The synaptic density of APOE3 cases far from plaques returned to APOE3 NDC levels and so a question remains as to whether the density observed far from plaques in AD APOE4 cases is the density of APOE4 NDCs or if the synaptic loss in AD APOE4 cases occurs both near and far from plaques. To answer this question would require samples not currently available but would aid enormously in understanding the mechanisms by which an *APOE* ε4 allele affects synaptic health and loss. Interestingly this study also found that the astrocytic component of the tripartite synapse (ACTS) was reduced in AD cases with an *APOE* ε4 allele and again it is unknown how and why this might contribute to disease. However, astrocytes are known to be important in the maintenance of the synapse and pathogenesis of AD and it would be a fascinating area for further study as protecting the ACTS could also have an enormous therapeutic benefit (Talantova *et al.*, 2013; Phillips *et al.*, 2014).

The experiments presented in this thesis indicate that the study of a disease as heterogeneous and complex as AD requires investigation from multiple angles through the use of many models and techniques. The study of post-mortem tissue is immensely valuable in allowing study of disease in the human condition. This then allows for the formation of new hypothesises about the effect that dysregulation of certain proteins and processes have on disease. However, to test these hypothesises requires models of disease which allow for manipulation of one or more proteins under controlled conditions. The results described in this thesis demonstrate that AD has a profound impact on the protein content of the synapse and that further understanding of the effects of these protein changes using both animal and cell culture models may contribute to the development of novel therapies for AD.

8 References

Agosta, F. *et al.* (2009) 'Apolipoprotein E epsilon4 is associated with disease-specific effects on brain atrophy in Alzheimer's disease and frontotemporal dementia.', *Proceedings of the National Academy of Sciences of the United States of America*, 106(6), pp. 2018–22.

Ahmed, T. *et al.* (2014) 'Cognition and hippocampal synaptic plasticity in mice with a homozygous tau deletion', *Neurobiology of Aging*. Elsevier Ltd, 35(11), pp. 2474–2478.

Alberts, B. *et al.* (2002) *Molecular Biology of the Cell, 4th edition*, *Garland Science*.

Alikhani, N. *et al.* (2011) 'Decreased proteolytic activity of the mitochondrial amyloid-β degrading enzyme, {PreP} peptidasome, in Alzheimer's disease brain mitochondria.', *Journal of Alzheimer's disease : JAD*, 27(1), pp. 75–87.

Allsop, D. *et al.* (1986) 'Monoclonal antibodies raised against a subsequence of senile plaque core protein react with plaque cores, plaque periphery and cerebrovascular amyloid in Alzheimer's disease', *Neuroscience Letters*, 68(2), pp. 252–256.

Alzforum (2017) *ALZFORUM*.

AlzGene (2017) *AlzGene*.

Alzheimer, A., Stelzmann, R. A., Schnitzlein, H. N. and Murtagh, F. R. (1907) 'An english translation of alzheimer's 1907 paper, {ü}ber eine eigenartige erkankung der hirnrinde', *Clin Anat*, 8(6).

Alzheimer, A., Stelzmann, R. A., Schnitzlein, H. N. and Murtagh, F. R. (1995) 'An English translation of Alzheimer's 1907 paper, "Uber eine eigenartige Erkankung der Hirnrinde".', *Clinical anatomy (New York, N.Y.)*, 8(6), pp. 429–31.

Anderson, R. *et al.* (1998) 'Behavioural, physiological and morphological analysis of a line of apolipoprotein E knockout mouse.', 85(1), pp. 93–110.

Ando, K. *et al.* (2011) 'Accelerated human mutant tau aggregation by knocking out murine tau in a transgenic mouse model', *American Journal of Pathology*. American Society for Investigative Pathology, 178(2), pp. 803–816.

Ando, K. *et al.* (2013) 'Clathrin adaptor CALM/PICALM is associated with neurofibrillary tangles and is cleaved in Alzheimer's brains', *Acta Neuropathologica*. Springer-Verlag, 125(6), pp. 861–878.

Andreev, V. P. *et al.* (2012) 'Label-free quantitative LC-MS proteomics of Alzheimer's disease and normally aged human brains.', *Journal of proteome research*, 11(6), pp. 3053–67.

Arber, C., Lovejoy, C. and Wray, S. (2017) 'Stem cell models of Alzheimer's disease: progress and challenges', *Alzheimer's Research & Therapy*. Alzheimer's Research & Therapy, 9(1), p. 42.

Augustine, G. J., Santamaria, F. and Tanaka, K. (2003) 'Local calcium signaling in neurons.', *Neuron*, 40(2), pp. 331–46.

Bal, M. *et al.* (2013) 'Reelin Mobilizes a VAMP7-Dependent Synaptic Vesicle Pool and Selectively Augments Spontaneous Neurotransmission', *Neuron*. Elsevier Inc., 80(4), pp. 934–946.

Bales, K. R. *et al.* (1997) 'Lack of apolipoprotein E dramatically reduces amyloid β-peptide deposition', *Nature Genetics*, 17(3), pp. 263–264.

Ballatore, C., Lee, V. M.-Y. and Trojanowski, J. Q. (2007) 'Tau-mediated neurodegeneration in Alzheimer's disease and related disorders', *Nature Reviews Neuroscience*, 8(9), pp. 663–672.

Bantscheff, M., Lemeer, S., Savitski, M. M. and Kuster, B. (2012) 'Quantitative mass spectrometry in proteomics: Critical review update from 2007 to the present', *Analytical and Bioanalytical Chemistry*, pp. 939–965.

Barry, A. E. *et al.* (2011) 'Alzheimer's disease brain-derived amyloid-β-mediated inhibition of LTP in vivo is prevented by immunotargeting cellular prion protein.', *The Journal of neuroscience : the official journal of the Society for Neuroscience*, 31(20), pp. 7259–7263.

Basu, J. *et al.* (2005) 'A minimal domain responsible for Munc13 activity', *Nature Structural & Molecular Biology*, 12(11), pp. 1017–1018.

Bayés, À. *et al.* (2014) 'Human post-mortem synapse proteome integrity screening for proteomic studies of postsynaptic complexes', *Molecular Brain*, 7(1), p. 88.

Bayés, A. and Grant, S. G. N. (2009) 'Neuroproteomics: understanding the molecular organization and complexity of the brain', *Nature Reviews Neuroscience*, 10(9), pp. 635–646.

Beffert, U. *et al.* (2002) 'Reelin-mediated signaling locally regulates protein kinase B/Akt and glycogen synthase kinase 3β', *Journal of Biological Chemistry*, 277(51), pp. 49958–49964.

Begcevic, I. *et al.* (2013) 'Semiquantitative proteomic analysis of human hippocampal tissues from Alzheimer's disease and age-matched control brains.', *Clinical proteomics*, 10(1), p. 5.

Beharry, C. *et al.* (2014) 'Tau-induced neurodegeneration: mechanisms and targets', *Neurosci Bull*, 30(2), pp. 346–358.

Bell, R. D. *et al.* (2006) 'Transport pathways for clearance of human Alzheimer's amyloid β-peptide and apolipoproteins E and J in the mouse central nervous system', *Journal of Cerebral Blood Flow & Metabolism*, 27(5), pp. 909–18.

Bennett, M., Calakos, N. and Scheller, R. (1992) 'Syntaxin: a synaptic protein implicated in docking of synaptic vesicles at presynaptic active zones', *Science*, 257(5067), pp. 255–259.

Bernardinelli, Y., Muller, D. and Nikonenko, I. (2014) 'Astrocyte-synapse structural plasticity', *Neural Plasticity*, pp. 1–13.

Bertram, L. and Tanzi, R. E. (2008) 'Thirty years of Alzheimer's disease genetics: the implications of systematic meta-analyses'.

Bilican, B. *et al.* (2014) 'Physiological normoxia and absence of EGF is required for the long-term propagation of anterior neural precursors from human pluripotent cells', *PLoS ONE*, 9(1).

Billings, L. M. *et al.* (2005) 'Intraneuronal Aβ Causes the Onset of Early Alzheimer's Disease-Related Cognitive Deficits in Transgenic Mice', *Neuron*, 45(5), pp. 675–688.

Bilousova, T., Miller, C. A., Poon, W. W. and Vinters, H. V (2016) 'Synaptic Amyloid-β Oligomers Precede {p-Tau} and Differentiate High Pathology Control Cases'.

Bliss, T. V. P. and Lømo, T. (1973) 'Long-lasting potentiation of synaptic transmission in the dentate area of the anaesthetized rabbit following stimulation of the perforant path', *The Journal of Physiology*, 232(2), pp. 331–356.

Borlikova, G. G. *et al.* (2013) 'Alzheimer brain-derived amyloid β-protein impairs synaptic remodeling and memory consolidation', *Neurobiology of Aging*, 34(5), pp. 1315–1327.

Bosch, C. *et al.* (2016) 'Reelin Regulates the Maturation of Dendritic Spines, Synaptogenesis and Glial Ensheathment of Newborn Granule Cells', *Cerebral Cortex*, 26(11), pp. 4282–4298.

Braak, H. and Braak, E. (1991) 'Neuropathological stageing of Alzheimer-related changes.', 82(4), pp. 239–259.

Braak, H. and Braak, E. (1995) 'Staging of Alzheimer's disease-related neurofibrillary changes.',

16(3), pp. 271–284.

Branco, T. and Staras, K. (2009) 'The probability of neurotransmitter release: variability and feedback control at single synapses', *Nature Reviews Neuroscience*. Nature Publishing Group, 10(5), pp. 373–383.

Brinkmalm, A. *et al.* (2015) 'Explorative and targeted neuroproteomics in Alzheimer's disease', *Biochimica et Biophysica Acta (BBA) - Proteins and Proteomics*. Elsevier B.V., pp. 1–10.

Brown, M. R., Sullivan, P. G. and Geddes, J. W. (2006) 'Synaptic mitochondria are more susceptible to Ca2+ overload than nonsynaptic mitochondria', *Journal of Biological Chemistry*, 281(17), pp. 11658–11668.

Bruggink, K. A. *et al.* (2015) 'Dickkopf-related protein 3 is a potential Aβ-associated protein in Alzheimer's Disease', *Journal of Neurochemistry*, 134(6), pp. 1152–1162.

Buddhala, C., Hsu, C.-C. and Wu, J.-Y. (2009) 'A novel mechanism for GABA synthesis and packaging into synaptic vesicles', *Neurochemistry International*, 55(1–3), pp. 9–12.

Burdick, D. *et al.* (1992) 'Assembly and aggregation properties of synthetic Alzheimer's A4/beta amyloid peptide analogs.', *Journal of Biological &*.

Busche, M. A. *et al.* (2012) 'Critical role of soluble amyloid- for early hippocampal hyperactivity in a mouse model of Alzheimer's disease', *Proceedings of the National Academy of Sciences*, 109(22), pp. 8740–8745.

Caesar, I. and Gandy, S. (2012) 'Evidence that an APOE ε4 "double whammy" increases risk for Alzheimer's disease', *BMC Medicine*. BioMed Central, 10(1), p. 36.

Cai, Q. and Tammineni, P. (2017) 'Mitochondrial Aspects of Synaptic Dysfunction in Alzheimer's Disease.', *Journal of Alzheimer's disease : JAD*. NIH Public Access, 57(4), pp. 1087–1103.

Cajal, S. R. Y. (1894) 'The Croonian Lecture: La Fine Structure des Centres Nerveux', *Proceedings of the Royal Society of London*, 55(331–335), pp. 444–468.

de Calignon, A. *et al.* (2012) 'Propagation of tau pathology in a model of early Alzheimer's disease.', *Neuron*, 73(4), pp. 685–97.

Cam, J. A. *et al.* (2004) 'The low density lipoprotein receptor-related protein 1B retains beta-amyloid precursor protein at the cell surface and reduces amyloid-beta peptide production.', *The Journal of biological chemistry*, 279(28), pp. 29639–46.

Cam, J. a, Zerbinatti, C. V, Li, Y. and Bu, G. (2005) 'Rapid endocytosis of the low density lipoprotein receptor-related protein modulates cell surface distribution and processing of the beta-amyloid precursor protein.', *The Journal of biological chemistry*, 280(15), pp. 15464–15470.

Camp, J. G. *et al.* (2015) 'Human cerebral organoids recapitulate gene expression programs of fetal neocortex development', *Proceedings of the National Academy of Sciences*, p. 201520760.

Carpenter, A. E. *et al.* (2006) 'CellProfiler: image analysis software for identifying and quantifying cell phenotypes.', *Genome biology*, 7(10), p. R100.

Carrillo-Mora, P., Luna, R. and Colín-Barenque, L. (2014) 'Amyloid beta: multiple mechanisms of toxicity and only some protective effects?', *Oxidative medicine and cellular longevity*. Hindawi, 2014, p. 795375.

Cascella, R. *et al.* (2013) 'Extracellular chaperones prevent Aβ42-induced toxicity in rat brains', *Biochimica et Biophysica Acta (BBA) - Molecular Basis of Disease*. Elsevier B.V., 1832(8), pp.

1217–1226.

Castellano, J. M. *et al.* (2011) 'Human apoE isoforms differentially regulate brain amyloid-β peptide clearance.', *Science Translational Medicine*, 3(89), p. 89ra57-89ra57.

Castillo, P. E. *et al.* (2002) 'RIM1α is required for presynaptic long-term potentiation', *Nature*, 415(6869), pp. 327–330.

Cenini, G. *et al.* (2014) 'An investigation of the molecular mechanisms engaged before and after the development of Alzheimer disease neuropathology in Down syndrome: A proteomics approach', *Free Radical Biology and Medicine*, 76, pp. 89–95.

Cesca, F., Baldelli, P., Valtorta, F. and Benfenati, F. (2010) 'The synapsins: key actors of synapse function and plasticity.', *Progress in neurobiology*, 91(4), pp. 313–48.

Chakroborty, S. *et al.* (2012) 'Early Presynaptic and Postsynaptic Calcium Signaling Abnormalities Mask Underlying Synaptic Depression in Presymptomatic Alzheimer's Disease Mice', *Journal of Neuroscience*, 32(24), pp. 8341–8353.

Chang, R. Y. K., Nouwens, A. S., Dodd, P. R. and Etheridge, N. (2013) 'The synaptic proteome in Alzheimer's disease', *Alzheimer's & Dementia*. The Alzheimer's Association, 9(5), pp. 499–511.

Chater, T. E. and Goda, Y. (2014) 'The role of AMPA receptors in postsynaptic mechanisms of synaptic plasticity.', *Frontiers in cellular neuroscience*. Frontiers Media SA, 8, p. 401.

Chen, Y. (2005) 'Reelin Modulates NMDA Receptor Activity in Cortical Neurons', *Journal of Neuroscience*, 25(36), pp. 8209–8216.

Chen, Y., Durakoglugil, M. S., Xian, X. and Herz, J. (2010) 'ApoE4 reduces glutamate receptor function and synaptic plasticity by selectively impairing ApoE receptor recycling', *Proceedings of the National Academy of Sciences*, 107(26), pp. 12011–12016.

Chevaleyre, V., Takahashi, K. A. and Castillo, P. E. (2006) 'ENDOCANNABINOID-MEDIATED SYNAPTIC PLASTICITY IN THE CNS', *Annual Review of Neuroscience*. Annual Reviews, 29(1), pp. 37–76.

Choi, S. H. *et al.* (2014) 'A three-dimensional human neural cell culture model of Alzheimer's disease', *Nature*, 515(7526), pp. 274–278.

Chung, W. S., Allen, N. J. and Eroglu, C. (2015) 'Astrocytes control synapse formation, function, and elimination', *Cold Spring Harbor Perspectives in Biology*. NIH Public Access, 7(9), p. a020370.

Cole, G. M. and Ard, M. D. (2000) 'Influence of lipoproteins on microglial degradation of Alzheimer's amyloid beta-protein', *Microscopy Research and Technique*, pp. 316–324.

Collingridge, G. L., Peineau, S., Howland, J. G. and Wang, Y. T. (2010) 'Long-term depression in the CNS', *Nature Reviews Neuroscience*, 11(7), pp. 459–473.

Contractor, A., Mulle, C. and Swanson, G. T. (2011) 'Kainate receptors coming of age: milestones of two decades of research.', *Trends in neurosciences*. NIH Public Access, 34(3), pp. 154–63.

Coppola, G. *et al.* (2012) 'Evidence for a role of the rare p.A152T variant in MAPT in increasing the risk for FTD-spectrum and Alzheimer's diseases', *Human Molecular Genetics*. Oxford University Press, 21(15), pp. 3500–3512.

Corder, E. H. *et al.* (1994) 'Protective effect of apolipoprotein E type 2 allele for late onset Alzheimer disease.', *Nature genetics*, 7(2), pp. 180–184.

Corder, E. H., Saunders, A. M. and Strittmatter, W. J. (1993) 'Gene dose of apolipoprotein E type

4 allele and the risk of Alzheimer's disease in late onset families'.

Cordero-Llana, O. *et al.* (2011) 'Clusterin secreted by astrocytes enhances neuronal differentiation from human neural precursor cells', *Cell Death and Differentiation*. Nature Publishing Group, 18(5), pp. 907–913.

Cousin, M. A. and Robinson, P. J. (2001) 'The dephosphins: Dephosphorylation by calcineurin triggers synaptic vesicle endocytosis', *Trends in Neurosciences*, pp. 659–665.

Crimins, J. L. *et al.* (2013) 'The intersection of amyloid β and tau in glutamatergic synaptic dysfunction and collapse in Alzheimer's disease.', 12(3), pp. 757–763.

Deane, R. *et al.* (2008) 'apoE isoform – specific disruption of amyloid β peptide clearance from mouse brain', *The Journal of Clinical Investigation*, 118(12), pp. 4002–4013.

Deary, I. J. *et al.* (2004) 'Apolipoprotein e gene variability and cognitive functions at age 79: a follow-up of the Scottish mental survey of 1932.', *Psychology and aging*, 19(2), pp. 367–71.

DeKosky, S. T. *et al.* (1990) 'Synapse loss in frontal cortex biopsies in Alzheimer's disease: correlation with cognitive severity.', *Annals of neurology*, 27(5), pp. 457–464.

DeKosky, S. T., Scheff, S. W. and Styren, S. D. (1996) 'Structural Correlates of Cognition in Dementia: Quantification and Assessment of Synapse Change', *Neurodegeneration*, 5(4), pp. 417–421.

Deleglise, B. *et al.* (2014) 'B-Amyloid Induces a Dying-Back Process and Remote Trans-Synaptic Alterations in a Microfluidic-Based Reconstructed Neuronal Network.', *Acta neuropathologica communications*, 2, p. 145.

DeMattos, R. B. *et al.* (2004) 'ApoE and Clusterin Cooperatively Suppress A?? Levels and Deposition: Evidence that ApoE Regulates Extracellular A?? Metabolism In Vivo', *Neuron*, 41(2), pp. 193–202.

Dementia Statistics Hub (2017) *Prevalence | Dementia Statistics Hub*.

Desikan, R. S. *et al.* (2014) 'The Role of Clusterin in Amyloid-β–Associated Neurodegeneration', *JAMA Neurology*. NIH Public Access, 71(2), p. 180.

Dickins, E. M. and Salinas, P. C. (2013) 'Wnts in action: from synapse formation to synaptic maintenance', *Frontiers in Cellular Neuroscience*. Frontiers Media SA, 7, p. 162.

Dickstein, D. L. *et al.* (2010) 'Role of vascular risk factors and vascular dysfunction in Alzheimer's disease.', *The Mount Sinai journal of medicine, New York*. NIH Public Access, 77(1), pp. 82–102.

Dieterich, D. C. and Kreutz, M. R. (2016) 'Proteomics of the Synapse – A Quantitative Approach to Neuronal Plasticity', *Molecular & Cellular Proteomics*, 15(2), pp. 368–381.

Dietschy, J. M. and Turley, S. D. (2004) 'Thematic review series: Brain Lipids. Cholesterol metabolism in the central nervous system during early development and in the mature animal', *Journal of lipid research*, 45(8), pp. 1375–1397.

Djogo, N. *et al.* (2013) 'Adhesion molecule L1 binds to amyloid beta and reduces Alzheimer's disease pathology in mice.', *Neurobiology of disease*, 56, pp. 104–15.

Dong, H. K., Gim, J.-A., Yeo, S. H. and Kim, H.-S. (2017) 'Integrated late onset Alzheimer's disease (LOAD) susceptibility genes: Cholesterol metabolism and trafficking perspectives', *Gene*, 597, pp. 10–16.

Donovan, L. E. *et al.* (2012) 'Analysis of a membrane-enriched proteome from postmortem human brain tissue in Alzheimer's disease', *Proteomics - Clinical Applications*, 6(3–4), pp.

201–211.

Dorey, E. *et al.* (2014) 'Apolipoprotein E, amyloid-beta, and neuroinflammation in Alzheimer's disease', *Neuroscience Bulletin*, pp. 317–330.

Dragicevic, N. *et al.* (2010) 'Mitochondrial amyloid-beta levels are associated with the extent of mitochondrial dysfunction in different brain regions and the degree of cognitive impairment in Alzheimer's transgenic mice.', *Journal of Alzheimer's disease : JAD*. Edited by X. Zhu et al., 20 Suppl 2(s2), pp. S535-50.

Du, H. *et al.* (2010) 'Early deficits in synaptic mitochondria in an Alzheimer's disease mouse model.', *Proceedings of the National Academy of Sciences of the United States of America*. National Academy of Sciences, 107(43), pp. 18670–5.

Du, H., Guo, L. and Yan, S. S. (2012) 'Synaptic Mitochondrial Pathology in Alzheimer's Disease', *Antioxidants & Redox Signaling*, 16(12), pp. 1467–1475.

Eckert, A., Nisbet, R., Grimm, A. and Götz, J. (2014) 'March separate, strike together - Role of phosphorylated TAU in mitochondrial dysfunction in Alzheimer's disease', *Biochimica et Biophysica Acta - Molecular Basis of Disease*, pp. 1258–1266.

Encalada, S. E. and Goldstein, L. (2014) 'Biophysical Challenges to Axonal Transport: {Motor-Cargo} Deficiencies and Neurodegeneration', 43(1), pp. 141–169.

Espeseth, T. *et al.* (2008) 'Accelerated age-related cortical thinning in healthy carriers of apolipoprotein E epsilon 4.', *Neurobiology of aging*, 29(3), pp. 329–40.

Fabelo, N. *et al.* (2014) 'Altered lipid composition in cortical lipid rafts occurs at early stages of sporadic Alzheimer's disease and facilitates {APP/BACE1} interactions.', 35(8), pp. 1801–1812.

Fabre, S. F. *et al.* (2001) 'Clinic-based cases with frontotemporal dementia show increased cerebrospinal fluid tau and high apolipoprotein E epsilon4 frequency, but no tau gene mutations.', *Experimental neurology*, 168(2), pp. 413–8.

Fagan, A. M. *et al.* (1998) 'Evidence for normal aging of the septo-hippocampal cholinergic system in {apoE} (-/-) mice but impaired clearance of axonal degeneration products following injury.', 151(2), pp. 314–325.

Farfel, J. M. *et al.* (2016) 'Association of APOE with tau-tangle pathology with and without β-amyloid', *Neurobiology of Aging*, 37, pp. 19–25.

Ferreira, A. and Bigio, E. (2011) 'Calpain-mediated tau cleavage: a mechanism leading to neurodegeneration shared by multiple tauopathies.', *Molecular Medicine*, 17(7–8), p. 1.

Fiandaca, M. S., Mapstone, M. E., Cheema, A. K. and Federoff, H. J. (2014) 'The critical need for defining preclinical biomarkers in Alzheimer's disease', *Alzheimer's and Dementia*, 10(3 SUPPL.), pp. S196–S212.

Fleisher, A. S. *et al.* (2013) 'Apolipoprotein E ε4 and age effects on florbetapir positron emission tomography in healthy aging and Alzheimer disease', *Neurobiology of Aging*. Elsevier Inc., 34(1), pp. 1–12.

Frerking, M., Malenka, R. C. and Nicoll, R. A. (1998) 'Synaptic activation of kainate receptors on hippocampal interneurons', *Nature Neuroscience*, 1(6), pp. 479–486.

Frost, B., Jacks, R. L. and Diamond, M. I. (2009) 'Propagation of Tau misfolding from the outside to the inside of a cell', *Journal of Biological Chemistry*, 284(19), pp. 12845–12852.

Fryer, J. D. *et al.* (2005) 'The low density lipoprotein receptor regulates the level of central

nervous system human and murine apolipoprotein E but does not modify amyloid plaque pathology in PDAPP mice', *Journal of Biological Chemistry*, 280(27), pp. 25754–25759.

Gandy, S. *et al.* (1994) '{APP} processing, A -amyloidogenesis, and the pathogenesis of Alzheimer's disease', 15(2), pp. 253–256.

Gao, C., Tronson, N. C. and Radulovic, J. (2013) 'Modulation of behavior by scaffolding proteins of the post-synaptic density.', *Neurobiology of learning and memory*. NIH Public Access, 105, pp. 3–12.

Garai, K. *et al.* (2014) 'The Binding of Apolipoprotein E to Oligomers and Fibrils of Amyloid-β Alters the Kinetics of Amyloid Aggregation', *Biochemistry*, 53(40), pp. 6323–6331.

Garwood, C. J. *et al.* (2011) 'Astrocytes are important mediators of Aβ-induced neurotoxicity and tau phosphorylation in primary culture', *Cell Death and Disease*, 2(6), p. e167.

Gassmann, M. and Bettler, B. (2012) 'Regulation of neuronal GABAB receptor functions by subunit composition', *Nature Reviews Neuroscience*, 13(6), pp. 380–394.

Gerber, S. H. *et al.* (2008) 'Conformational Switch of Syntaxin-1 Controls Synaptic Vesicle Fusion', *Science*, 321(5895), pp. 1507–1510.

Giannakopoulos, P., Herrmann, F. R. and Bussiere, T. (2003) 'Tangle and neuron numbers, but not amyloid load, predict cognitive status in Alzheimer's disease'.

Glenner, G. G. and Wong, C. W. (1984) 'Alzheimer's disease: initial report of the purification and characterization of a novel cerebrovascular amyloid protein. 1984.', *Biochemical and Biophysical Research Communications*, 425(3), pp. 885–890.

Goedert, M. *et al.* (1989) 'Cloning and sequencing of the {cDNA} encoding an isoform of microtubule-associated protein tau containing four tandem repeats: differential expression of tau protein {mRNAs} in human brain.', 8(2), pp. 393–399.

Goedert, M. and Jakes, R. (1990) 'Expression of separate isoforms of human tau protein: correlation with the tau pattern in brain and effects on tubulin polymerization.', 9(13), pp. 4225–4230.

Goedert, M. and Jakes, R. (2005) 'Mutations causing neurodegenerative tauopathies'.

Gordon-Weeks, P. R. and Fournier, A. E. (2014) 'Neuronal cytoskeleton in synaptic plasticity and regeneration', *Journal of Neurochemistry*, 129(2), pp. 206–212.

Götz, J. *et al.* (2010) 'Animal models reveal role for tau phosphorylation in human disease', *Biochimica et Biophysica Acta*, 1802(10), pp. 860–871.

Greger, I. H., Khatri, L., Kong, X. and Ziff, E. B. (2003) 'AMPA receptor tetramerization is mediated by Q/R editing.', *Neuron*, 40(4), pp. 763–74.

Grootendorst, J., Bour, A., Vogel, E. and Kelche, C. (2005) 'Human {apoE} targeted replacement mouse lines: {h-apoE4} and {h-apoE3} mice differ on spatial memory performance and avoidance behavior'.

Grundke-Iqbal, I. *et al.* (1986) 'Microtubule-associated protein tau. A component of Alzheimer paired helical filaments.', *The Journal of biological chemistry*, 261(13), pp. 6084–9.

Guerrero-Muñoz, M. J., Gerson, J. and Castillo-Carranza, D. L. (2015) 'Tau Oligomers: The Toxic Player at Synapses in Alzheimer's Disease', *Frontiers in Cellular Neuroscience*, 9, p. 464.

Guillot-Sestier, M.-V. and Town, T. (2013) 'Innate Immunity in Alzheimer's Disease: A Complex Affair', *CNS & Neurological Disorders - Drug Targets*, 12(5), pp. 593–607.

Guntupalli, S., Widagdo, J. and Anggono, V. (2016) 'Amyloid-β-Induced Dysregulation of AMPA

Receptor Trafficking.', *Neural plasticity*. Hindawi, 2016, p. 3204519.

Hallermann, S. *et al.* (2010) 'Bassoon Speeds Vesicle Reloading at a Central Excitatory Synapse', *Neuron*, 68(4), pp. 710–723.

Hamilton, A. *et al.* (2014) 'Metabotropic glutamate receptor 5 knockout reduces cognitive impairment and pathogenesis in a mouse model of Alzheimer's disease', *Molecular Brain*, 7(1), p. 40.

Han, H. Y. *et al.* (2013) '???? and ??1 Integrins Mediate A??-Induced Neurotoxicity in Hippocampal Neurons via the FAK Signaling Pathway', *PLoS ONE*, 8(6), pp. 1–7.

Han, J., Pluhackova, K. and Böckmann, R. A. (2017) 'The multifaceted role of SNARE proteins in membrane fusion', *Frontiers in Physiology*.

Hardy, J. and Higgins, G. (1992) 'Alzheimer's disease: the amyloid cascade hypothesis', 256(5054), pp. 184–185.

Harold, D. *et al.* (2009) 'Genome-wide association study identifies variants at CLU and PICALM associated with Alzheimer's disease', *Nature Genetics*, 41(10), pp. 1088–1093.

Harris, J. A. *et al.* (2012) 'Human P301L-Mutant Tau Expression in Mouse Entorhinal-Hippocampal Network Causes Tau Aggregation and Presynaptic Pathology but No Cognitive Deficits', *PLoS ONE*. Edited by T. Ikezu, 7(9), p. e45881.

Hashimoto, M. *et al.* (2012) 'Analysis of microdissected neurons by 18O mass spectrometry reveals altered protein expression in Alzheimer's disease', *Journal of Cellular and Molecular Medicine*, 16(8), pp. 1686–1700.

Hatters, D. M., Budamagunta, M. S., Voss, J. C. and Weisgraber, K. H. (2005) 'Modulation of apolipoprotein E structure by domain interaction: Differences in lipid-bound and lipid-free forms', *Journal of Biological Chemistry*. American Society for Biochemistry and Molecular Biology, 280(40), pp. 34288–34295.

Hazell, A. S. *et al.* (2010) 'Loss of astrocytic glutamate transporters in Wernicke encephalopathy', *GLIA*, 58(2), pp. 148–156.

Hebb, D. O. (1949) *The Organization of Behavior: A Neuropsychological Theory*. Edited by J. W. & Sons. New York.

Heneka, M. T. *et al.* (2015) 'Neuroinflammation in Alzheimer's disease.', 14(4), pp. 388–405.

Henstridge, C. M. *et al.* (2015) 'Post-mortem brain analyses of the Lothian Birth Cohort 1936: extending lifetime cognitive and brain phenotyping to the level of the synapse', *Acta Neuropathologica Communications*, 3(1), p. 53.

Hernandez, F., Lucas, J. J. and Avila, J. (2013) 'GSK3 and tau: two convergence points in Alzheimer's disease.', *Journal of Alzheimer's disease : JAD*, 33 Suppl 1, pp. S141-4.

Hiesberger, T. *et al.* (1999) 'Direct binding of Reelin to VLDL receptor and ApoE receptor 2 induces tyrosine phosphorylation of Disabled-1 and modulates tau phosphorylation', *Neuron*, 24(2), pp. 481–489.

Hiroki, S. (2017) 'APP Mouse Models for Alzheimer's Disease Preclinical Studies', *EMBO*, 11(2), pp. 109–117.

Hirota, Y. *et al.* (2015) 'Reelin receptors ApoER2 and VLDLR are expressed in distinct spatiotemporal patterns in developing mouse cerebral cortex', *Journal of Comparative Neurology*, 523(3), pp. 463–478.

Holtzman, D. M., Herz, J. and Bu, G. (2012) 'Apolipoprotein E and Apolipoprotein E Receptors:

Normal Biology and Roles in Alzheimer Disease', 2(3), p. a006312.

Hong, S. *et al.* (2016) 'Complement and microglia mediate early synapse loss in Alzheimer mouse models.', *Science*, 352(6286), pp. 712–6.

Hoover, B. R. *et al.* (2010) 'Tau mislocalization to dendritic spines mediates synaptic dysfunction independently of neurodegeneration.', *Neuron*, 68(6), pp. 1067–81.

Horváth, A. *et al.* (2016) 'Epileptic Seizures in Alzheimer Disease', *Alzheimer Disease & Associated Disorders*, 30(2), pp. 186–192.

Huang, D. W., Sherman, B. T. and Lempicki, R. A. (2008) 'Systematic and integrative analysis of large gene lists using DAVID bioinformatics resources', *Nature Protocols*, 4(1), pp. 44–57.

Huang, D. W., Sherman, B. T. and Lempicki, R. A. (2009) 'Bioinformatics enrichment tools: paths toward the comprehensive functional analysis of large gene lists', *Nucleic Acids Research*, 37(1), pp. 1–13.

Huang, Y.-W., Zhou, B., Wernig, M. and Südhof, T. C. (2017) '{ApoE2,} {ApoE3,} and {ApoE4} Differentially Stimulate {APP} Transcription and Aβ Secretion'.

Hutton, M. (2000) 'Molecular genetics of chromosome 17 tauopathies', *Neurobiology of Aging*, 21, p. 285.

Huynh, T.-P. V, Davis, A. A., Ulrich, J. D. and Holtzman, D. M. (2017) 'Apolipoprotein E and Alzheimer Disease: The influence of apoE on amyloid-β and other amyloidogenic proteins.', *Journal of lipid research*, p. jlr.R075481.

Imtiaz, B., Tolppanen, A., Kivipelto, M. and Soininen, H. (2014) 'Future directions in Alzheimer's disease from risk factors to prevention', *Biochemical Pharmacology*. Elsevier Inc., 88(4), pp. 661–670.

Ingelsson, M. *et al.* (2004) 'Early Aβ accumulation and progressive synaptic loss, gliosis, and tangle formation in {AD} brain', 62(6), pp. 925–931.

Iqbal, K., Liu, F. and Gong, C.-X. (2016) 'Tau and neurodegenerative disease: the story so far', 12(1).

Ittner, L. M. and Götz, J. (2011) 'Amyloid-β and tau--a toxic pas de deux in Alzheimer's disease.', 12(2), pp. 65–72.

Jackson, R. J. *et al.* (2016) 'Human tau increases amyloid β plaque size but not amyloid β-mediated synapse loss in a novel mouse model of Alzheimer's disease.', *The European journal of neuroscience*. Edited by G. Mallucci, 44(12), pp. 3056–3066.

Jamain, S. *et al.* (2003) 'Mutations of the X-linked genes encoding neuroligins NLGN3 and NLGN4 are associated with autism', *Nature Genetics*, 34(1), pp. 27–29.

Jameson, L. *et al.* (1980) 'Inhibition of microtubule assembly by phosphorylation of microtubule-associated proteins.', 19(11), pp. 2472–2479.

Jayaraman, A. and Pike, C. J. (2014) 'Alzheimer's disease and type 2 diabetes: multiple mechanisms contribute to interactions.', *Current diabetes reports*. NIH Public Access, p. 476.

Jiang, Q. *et al.* (2008) 'ApoE Promotes the Proteolytic Degradation of Aβ', *Neuron*, 58(5), pp. 681–693.

Jin, M. *et al.* (2011) 'Soluble amyloid beta-protein dimers isolated from Alzheimer cortex directly induce Tau hyperphosphorylation and neuritic degeneration.', *Proceedings of the National Academy of Sciences of the United States of America*. National Academy of Sciences, 108(14), pp. 5819–24.

de Jong, A. P. and Verhage, M. (2009) 'Presynaptic signal transduction pathways that modulate synaptic transmission', *Current Opinion in Neurobiology*, 19(3), pp. 245–253.

Jongbloed, W. *et al.* (2015) 'Clusterin Levels in Plasma Predict Cognitive Decline and Progression to Alzheimer's Disease', *Journal of Alzheimer's Disease*, 46(4), pp. 1103–1110.

Jonsson, T. *et al.* (2012) 'A mutation in APP protects against Alzheimer's disease and age-related cognitive decline', *Nature*, 488(7409), pp. 96–99.

Jonsson, T. *et al.* (2013) 'Variant of TREM2 Associated with the Risk of Alzheimer's Disease', *New England Journal of Medicine*, 368(2), pp. 107–116.

Junge, H. J. *et al.* (2004) 'Calmodulin and Munc13 Form a Ca2+ Sensor/Effector Complex that Controls Short-Term Synaptic Plasticity', *Cell*, 118(3), pp. 389–401.

Jurado, S., Biou, V. and Malenka, R. C. (2010) 'A calcineurin/AKAP complex is required for NMDA receptor–dependent long-term depression', *Nature Neuroscience*, 13(9), pp. 1053–1055.

Kaeser, P. S. *et al.* (2011) 'RIM proteins tether Ca2+ channels to presynaptic active zones via a direct PDZ-domain interaction', *Cell*, 144(2), pp. 282–295.

Kanaan, N. M. *et al.* (2011) 'Pathogenic Forms of Tau Inhibit Kinesin-Dependent Axonal Transport through a Mechanism Involving Activation of Axonal Phosphotransferases', *Journal of Neuroscience*, 31(27), pp. 9858–9868.

Kandel, E. R. *et al.* (2012) *Principles of Neural Science*. 5th edn. New York: McGraw-Hill, Health Professions Division.

Karch, C. M. and Goate, A. M. (2015) 'Alzheimer's disease risk genes and mechanisms of disease pathogenesis.', *Biological psychiatry*, 77(1), pp. 43–51.

Karran, E., Mercken, M. and Strooper, B. (2011) 'The amyloid cascade hypothesis for Alzheimer's disease: an appraisal for the development of therapeutics.', 10(9), pp. 698–712.

Kay, K. R. *et al.* (2013) 'Studying synapses in human brain with array tomography and electron microscopy.', *Nature protocols*. Nature Publishing Group, a division of Macmillan Publishers Limited. All Rights Reserved., 8(7), pp. 1366–1380.

Kayed, R. and Lasagna-Reeves, C. A. (2012) 'Molecular mechanisms of amyloid oligomers toxicity', *Advances in Alzheimer's Disease*, 3, pp. 67–78.

Ke, Y. D. *et al.* (2012) 'Lessons from tau-deficient mice.', 2012, p. 873270.

Kidd, M. (1963) 'Paired helical filaments in electron microscopy of Alzheimer's disease.', *Nature*, 197, pp. 192–3.

Killick, R. *et al.* (2014) 'Clusterin regulates β-amyloid toxicity via Dickkopf-1-driven induction of the {wnt–PCP–JNK} pathway', *Molecular psychiatry*. Nature Publishing Group, 19(1), pp. 88–98.

Kim, J. *et al.* (2007) 'A~40 Inhibits Amyloid Deposition In Vivo', 27(3), pp. 627–633.

Kivipelto, M. *et al.* (2001) 'Midlife vascular risk factors and Alzheimer's Disease in later life: Longitudinal, population based study', *Bmj*, 322(June), pp. 1447–1451.

Kivipelto, M. *et al.* (2013) 'The Finnish Geriatric Intervention Study to Prevent Cognitive Impairment and Disability (FINGER): Study design and progress', *Alzheimer's and Dementia*, 9(6), pp. 657–665.

Klein, W. L. (2013) 'Synaptotoxic amyloid-β oligomers: a molecular basis for the cause, diagnosis, and treatment of Alzheimer's disease?', *Journal of Alzheimer's disease : JAD*, 33 Suppl 1, pp. S49-65.

Klemann, C. J. H. M. and Roubos, E. W. (2011) 'The gray area between synapse structure and function-Gray's synapse types I and II revisited', *Synapse*, 65(11), pp. 1222–1230.

Koch-Brandt, C. and Morgans, C. (1996) 'Clusterin: a role in cell survival in the face of apoptosis?', *Progress in molecular and subcellular biology*, 16, pp. 130–49.

Koffie, R. M. *et al.* (2009) 'Oligomeric amyloid beta associates with postsynaptic densities and correlates with excitatory synapse loss near senile plaques.', *Proceedings of the National Academy of Sciences of the United States of America*, 106(10), pp. 4012–7.

Koffie, R. M. *et al.* (2012) 'Apolipoprotein E4 effects in Alzheimer's disease are mediated by synaptotoxic oligomeric amyloid-β.', *Brain : a journal of neurology*, 135(Pt 7), pp. 2155–68.

Koffie, R. M. R. *et al.* (2011) 'Alzheimer's disease: synapses gone cold.', *Molecular neurodegeneration*, 6(1), p. 63.

Koistinaho, M. *et al.* (2004) 'Apolipoprotein E promotes astrocyte colocalization and degradation of deposited amyloid-beta peptides.', *Nature medicine*, 10(7), pp. 719–726.

Kopeikina, K. J. *et al.* (2011) 'Tau accumulation causes mitochondrial distribution deficits in neurons in a mouse model of tauopathy and in human Alzheimer's disease brain.', *The American journal of pathology*, 179(4), pp. 2071–82.

Kopeikina, K. J. *et al.* (2013) 'Tau causes synapse loss without disrupting calcium homeostasis in the rTg4510 model of tauopathy', *PLoS ONE*, 8(11), pp. 1–8.

Kopeikina, K. J., Hyman, B. T. and Spires-Jones, T. L. (2012) 'Soluble forms of tau are toxic in Alzheimer's disease', *Translational neuroscience*, 3(3), pp. 223–233.

Kowal, R. C. *et al.* (1990) 'Opposing effects of apolipoprotein E and C on lipoprotein binding to low density lipoprotein receptor-related protein.', *J.Biol.Chem.*, 265(18), pp. 10771–10779.

Kuchibhotla, K. V, Lattarulo, C. R., Hyman, B. T. and Bacskai, B. J. (2009) 'Synchronous Hyperactivity and Intercellular Calcium Waves in Astrocytes in Alzheimer Mice', *Science*, 323(5918), pp. 1211–1215.

Kuijlaars, J. *et al.* (2016) 'Sustained synchronized neuronal network activity in a human astrocyte co-culture system', *Sci Rep*, 6(1), p. 36529.

Kümmel, D. *et al.* (2011) 'Complexin cross-links prefusion SNAREs into a zigzag array', *Nature Structural & Molecular Biology*. Nature Publishing Group, 18(8), pp. 927–933.

Lacor, P. N. *et al.* (2007) 'Abeta oligomer-induced aberrations in synapse composition, shape, and density provide a molecular basis for loss of connectivity in Alzheimer's disease.', *The Journal of neuroscience : the official journal of the Society for Neuroscience*, 27(4), pp. 796–807.

Lamb, B. T. *et al.* (1997) 'Altered metabolism of familial Alzheimer's disease-linked amyloid precursor protein variants in yeast artificial chromosome transgenic mice.', *Human molecular genetics*, 6(9), pp. 1535–1541.

Lane-Donovan, C. *et al.* (2016) 'Genetic Restoration of Plasma ApoE Improves Cognition and Partially Restores Synaptic Defects in ApoE-Deficient Mice', *Journal of Neuroscience*, 36(39), pp. 10141–10150.

Lasagna-Reeves, C. a *et al.* (2011) 'Tau oligomers impair memory and induce synaptic and mitochondrial dysfunction in wild-type mice', *Molecular Neurodegeneration*. BioMed Central Ltd, 6(1), p. 39.

Lawson, L. J., Perry, V. H., Dri, P. and Gordon, S. (1990) 'Heterogeneity in the distribution and

morphology of microglia in the normal adult mouse brain.', 39(1), pp. 151–170.
Leshchyns'ka, I. and Sytnyk, V. (2016) 'Synaptic Cell Adhesion Molecules in Alzheimer's Disease.', *Neural plasticity*. Hindawi Publishing Corporation, 2016, p. 6427537.
Lesne, S. (2014) 'Toxic oligomer species of amyloid-β in Alzheimer's disease, a timing issue', *Swiss Medical Weekly*, 144.
Li, X. *et al.* (2014) 'Clusterin in Alzheimer's disease: A player in the biological behavior of amyloid-beta', *Neuroscience Bulletin*, 30(1), pp. 162–168.
Li, Y. C. and Kavalali, E. T. (2017) 'Synaptic Vesicle-Recycling Machinery Components as Potential Therapeutic Targets', *Pharmacological Reviews*, 69(2), pp. 141–160.
Li, Y. J. *et al.* (2004) 'Apolipoprotein E controls the risk and age at onset of Parkinson disease.', *Neurology*, 62(11), pp. 2005–9.
Liao, M.-C. *et al.* (2016) 'Single-Cell Detection of Secreted Aβ and sAPPα from Human IPSC-Derived Neurons and Astrocytes', *The Journal of Neuroscience*, 36(5), pp. 1730–1746.
Lidström, a M. *et al.* (1998) 'Clusterin (apolipoprotein J) protein levels are increased in hippocampus and in frontal cortex in Alzheimer's disease.', *Experimental neurology*, 154(154), pp. 511–521.
Lim, Y. Y. *et al.* (2014) 'APOE and BDNF polymorphisms moderate amyloid β-related cognitive decline in preclinical Alzheimer's disease.', *Molecular psychiatry*. Nature Publishing Group, 20(August), pp. 1–7.
Lin, M. T. *et al.* (2002) 'High aggregate burden of somatic mtDNA point mutations in aging and Alzheimer's disease brain.', *Human molecular genetics*, 11(2), pp. 133–45.
Lindwall, G. and Cole, R. D. (1984) 'Phosphorylation affects the ability of tau protein to promote microtubule assembly.', 259(8), pp. 5301–5305.
Liu, L. *et al.* (2012) 'Trans-synaptic spread of tau pathology in vivo', *PLoS ONE*, 7(2), pp. 1–9.
Liu, Q. *et al.* (2007) 'Amyloid Precursor Protein Regulates Brain Apolipoprotein E and Cholesterol Metabolism through Lipoprotein Receptor LRP1', *Neuron*, 56(1), pp. 66–78.
Livesey, M. R. *et al.* (2014) 'Maturation of AMPAR composition and the GABAAR reversal potential in hPSC-derived cortical neurons.', *The Journal of neuroscience : the official journal of the Society for Neuroscience*, 34(11), pp. 4070–5.
Lombardo, S. and Maskos, U. (2015) 'Role of the nicotinic acetylcholine receptor in Alzheimer's disease pathology and treatment', *Neuropharmacology*, 96(Pt B), pp. 255–262.
Lue, L.-F. *et al.* (1999) 'Soluble Amyloid B Peptide Concentration as a Predictor of Synaptic Change in Alzheimer's Disease', *AMerican Journal of Pathology*, 155(3), pp. 853–862.
Luna-Munoz, J. *et al.* (2013) 'Phosphorylation of Tau Protein Associated as a Protective Mechanism in the Presence of Toxic, C-Terminally Truncated Tau in Alzheimer's Disease', in *Understanding Alzheimer's Disease*. InTech, p. 89.
Ly, C. V. and Verstreken, P. (2006) 'Mitochondria at the Synapse', *The Neuroscientist*, 12(4), pp. 291–299.
Ma, Q.-L. *et al.* (2014) 'Loss of MAP function leads to hippocampal synapse loss and deficits in the Morris Water Maze with aging.', *The Journal of neuroscience : the official journal of the Society for Neuroscience*, 34(21), pp. 7124–36.
Mably, A. J. *et al.* (2015) 'Anti-Aβ antibodies incapable of reducing cerebral Aβ oligomers fail to attenuate spatial reference memory deficits in J20 mice', *Neurobiology of Disease*, 82, pp.

372–384.

Machulda, M. M. *et al.* (2011) 'Effect of APOE ε4 status on intrinsic network connectivity in cognitively normal elderly subjects.', *Archives of neurology*, 68(9), pp. 1131–6.

Mahley, R. W. (1988) 'Apolipoprotein E: cholesterol transport protein with expanding role in cell biology'.

Mahley, R. W. and Rall, S. C. (2000) 'Apolipoprotein E: Far More Than a Lipid Transport Protein', *Annual Review of Genomics and Human Genetics*, 1(1), pp. 507–537.

Mak, A. C. Y. *et al.* (2014) 'Effects of the Absence of Apolipoprotein E on Lipoproteins, Neurocognitive Function, and Retinal Function', *JAMA Neurology*, 71(10), p. 1228.

Malm, T. M., Jay, T. R. and Landreth, G. E. (2015) 'The evolving biology of microglia in Alzheimer's disease.', 12(1), pp. 81–93.

Maloney, J. A. *et al.* (2014) 'Molecular mechanisms of Alzheimer disease protection by the A673T allele of amyloid precursor protein', *Journal of Biological Chemistry*, 289(45), pp. 30990–31000.

Manavalan, A. *et al.* (2013) 'Brain site-specific proteome changes in aging-related dementia', *Experimental & Molecular Medicine*. Nature Publishing Group, 45(9), p. e39.

Mandrekar, S. *et al.* (2009) 'Microglia mediate the clearance of soluble Abeta through fluid phase macropinocytosis', *J Neurosci*, 29(13), pp. 4252–4262.

Masliah, E., Terry, R. D., DeTeresa, R. M. and Hansen, L. A. (1989) 'Immunohistochemical quantification of the synapse-related protein synaptophysin in Alzheimer disease', *Neuroscience Letters*, 103(2), pp. 234–239.

Matsubara, E., Frangione, B. and Ghiso, J. (1995) 'Characterization of apolipoprotein J-Alzheimer's A beta interaction.', *The Journal of biological chemistry*, 270(13), pp. 7563–7.

Matsunaga, W., Shirokawa, T. and Isobe, K. (2003) 'Specific uptake of Abeta1-40 in rat brain occurs in astrocyte, but not in microglia.', *Neuroscience letters*, 342(1–2), pp. 129–31.

Mauch, D. H., Nägler, K., Schumacher, S. and Göritz, C. (2001) '{CNS} synaptogenesis promoted by glia-derived cholesterol'.

Maximov, A. *et al.* (2009) 'Complexin controls the force transfer from SNARE complexes to membranes in fusion.', *Science (New York, N.Y.)*. Howard Hughes Medical Institute, 323(5913), pp. 516–21.

Mazanetz, M. P. and Fischer, P. M. (2007) 'Untangling tau hyperphosphorylation in drug design for neurodegenerative diseases', 6(6).

McArthur, S. *et al.* (2010) 'Annexin A1: A Central Player in the Anti-Inflammatory and Neuroprotective Role of Microglia', *The Journal of Immunology*. Europe PMC Funders, 185(10), pp. 6317–6328.

Micheva, K. D. and Smith, S. J. (2007) 'Array tomography: a new tool for imaging the molecular architecture and ultrastructure of neural circuits.', *Neuron*, 55(1), pp. 25–36.

Miners, J. S., Clarke, P. and Love, S. (2017) 'Clusterin levels are increased in Alzheimer's disease and influence the regional distribution of A β', *Brain Pathology*, 27(3), pp. 305–313.

Montagna, E., Dorostkar, M. M. and Herms, J. (2017) 'The Role of APP in Structural Spine Plasticity.', *Frontiers in molecular neuroscience*. Frontiers Media SA, 10, p. 136.

Moreira, P. I. *et al.* (2010) 'Mitochondrial dysfunction is a trigger of Alzheimer's disease pathophysiology', *Biochimica et Biophysica Acta (BBA) - Molecular Basis of Disease*. Elsevier

B.V., 1802(1), pp. 2–10.

Moreno, J. A. *et al.* (2013) 'Oral Treatment Targeting the Unfolded Protein Response Prevents Neurodegeneration and Clinical Disease in Prion-Infected Mice', *Science Translational Medicine*, 5(206), p. 206ra138-206ra138.

Moreno, J. A. and Mallucci, G. R. (2010) 'Dysfunction and recovery of synapses in prion disease: implications for neurodegeneration.', *Biochemical Society transactions*, 38(2), pp. 482–7.

Morris, J. C. *et al.* (2010) 'APOE predicts amyloid-beta but not tau Alzheimer pathology in cognitively normal aging', *Annals of Neurology*, 67(1), pp. 122–131.

Moya-Alvarado, G., Gershoni-Emek, N., Perlson, E. and Bronfman, F. C. (2016) 'Neurodegeneration and Alzheimer's disease (AD). What Can Proteomics Tell Us About the Alzheimer's Brain?', *Molecular & Cellular Proteomics*, 15(2), pp. 409–425.

Mukherjee, K. *et al.* (2010) 'Piccolo and bassoon maintain synaptic vesicle clustering without directly participating in vesicle exocytosis', *Proceedings of the National Academy of Sciences*, 107(14), pp. 6504–6509.

Mukherjee, S. and Manahan-Vaughan, D. (2013) 'Role of metabotropic glutamate receptors in persistent forms of hippocampal plasticity and learning.', *Neuropharmacology*, 66, pp. 65–81.

Mulder, S. D., Veerhuis, R., Blankenstein, M. A. and Nielsen, H. M. (2012) 'The effect of amyloid associated proteins on the expression of genes involved in amyloid-?? clearance by adult human astrocytes', *Experimental Neurology*. Elsevier Inc., 233(1), pp. 373–379.

Musunuri, S. *et al.* (2013) 'Quanti fi cation of the Brain Proteome in Alzheimer ' s Disease Using Multiplexed Mass Spectrometry', *Journal of proteome research*.

Musunuri, S. *et al.* (2014) 'Quantification of the brain proteome in Alzheimer's disease using multiplexed mass spectrometry', *Journal of Proteome Research*, 13(4), pp. 2056–2068.

Nabavi, S. *et al.* (2013) 'Metabotropic NMDA receptor function is required for NMDA receptor-dependent long-term depression', *Proceedings of the National Academy of Sciences*, 110(10), pp. 4027–4032.

Nakajima, C. *et al.* (2013) 'Low density lipoprotein receptor-related protein 1 (LRP1) modulates N-methyl-D-aspartate (NMDA) receptor-dependent intracellular signaling and NMDA-induced regulation of postsynaptic protein complexes', *Journal of Biological Chemistry*, 288(30), pp. 21909–21923.

Newman, S. F. *et al.* (2007) 'An increase in S-glutathionylated proteins in the Alzheimer's disease inferior parietal lobule, a proteomics approach', *Journal of Neuroscience Research*, 85(7), pp. 1506–1514.

Nickerson, D. A. (2000) 'Sequence Diversity and Large-Scale Typing of SNPs in the Human Apolipoprotein E Gene', *Genome Research*, 10(10), pp. 1532–1545.

Nieland, T. J. F. *et al.* (2014) 'High Content Image Analysis Identifies Novel Regulators of Synaptogenesis in a High-Throughput RNAi Screen of Primary Neurons', *PLoS ONE*. Edited by L. Mei. Public Library of Science, 9(3), p. e91744.

Nieweg, K. *et al.* (2015) 'Alzheimer's disease-related amyloid-β induces synaptotoxicity in human iPS cell-derived neurons', *Cell Death and Disease*, 6(4), p. e1709.

Nuutinen, T., Suuronen, T., Kauppinen, A. and Salminen, A. (2009) 'Clusterin: A forgotten player in Alzheimer's disease', *Brain Research Reviews*, pp. 89–104.

Oakley, H. *et al.* (2006) 'Intraneuronal beta-Amyloid Aggregates, Neurodegeneration, and Neuron Loss in Transgenic Mice with Five Familial Alzheimer's Disease Mutations: Potential Factors in Amyloid Plaque Formation', *Journal of Neuroscience*, 26(40), pp. 10129–10140.

Odawara, A. *et al.* (2014) 'Long-term electrophysiological activity and pharmacological response of a human induced pluripotent stem cell-derived neuron and astrocyte co-culture.', *Biochemical and Biophysical Research Communications*, 443(4), pp. 1176–1181.

Oddo, S. *et al.* (2003) 'Triple-transgenic model of Alzheimer's disease with plaques and tangles: intracellular Abeta and synaptic dysfunction.', 39(3), pp. 409–421.

Ohkubo, N. *et al.* (2003) 'Apolipoprotein E and Reelin ligands modulate tau phosphorylation through an apolipoprotein E receptor/disabled-1/glycogen synthase kinase-3beta cascade.', *The FASEB journal : official publication of the Federation of American Societies for Experimental Biology*, 17(2), pp. 295–297.

Okada, Y., Yamazaki, H., Sekine-Aizawa, Y. and Hirokawa, N. (1995) 'The neuron-specific kinesin superfamily protein KIF1A is a unique monomeric motor for anterograde axonal transport of synaptic vesicle precursors.', *Cell*, 81(5), pp. 769–80.

Ono, K., Condron, M. M. and Teplow, D. B. (2009) 'Structure-neurotoxicity relationships of amyloid beta-protein oligomers.', *Proceedings of the National Academy of Sciences of the United States of America*. National Academy of Sciences, 106(35), pp. 14745–50.

Opazo, P., Sainlos, M. and Choquet, D. (2012) 'Regulation of AMPA receptor surface diffusion by PSD-95 slots', *Current Opinion in Neurobiology*, 22(3), pp. 453–460.

Osborn, L. M., Kamphuis, W., Wadman, W. J. and Hol, E. M. (2016) 'Astrogliosis: An integral player in the pathogenesis of Alzheimer's disease'.

Oyler, G. A. *et al.* (1989) 'The identification of a novel synaptosomal-associated protein, SNAP-25, differentially expressed by neuronal subpopulations', *Journal of Cell Biology*, 109(6 I), pp. 3039–3052.

Pang, Z. P. *et al.* (2006) 'A Gain-of-Function Mutation in Synaptotagmin-1 Reveals a Critical Role of Ca2+-Dependent Soluble N-Ethylmaleimide-Sensitive Factor Attachment Protein Receptor Complex Binding in Synaptic Exocytosis', *Journal of Neuroscience*, 26(48), pp. 12556–12565.

Paolicelli, R. C. *et al.* (2011) 'Synaptic Pruning by Microglia Is Necessary for Normal Brain Development', *Science*, 333(6048), pp. 1456–1458.

Pardo, C. A. and Eberhart, C. G. (2007) 'The neurobiology of autism', in *Brain Pathology*, pp. 434–447.

Park, S. A., Ahn, S. Il and Gallo, J.-M. (2016) 'Tau mis-splicing in the pathogenesis of neurodegenerative disorders', *BMB Reports*. Korean Society for Biochemistry and Molecular Biology, 49(8), pp. 405–413.

Pastor, P. *et al.* (2015) 'MAPT H1 Haplotype is Associated with Late-Onset Alzheimer's Disease Risk in APOE ε4 Noncarriers: Results from the Dementia Genetics Spanish Consortium', *Journal of Alzheimer's Disease*, 49(2), pp. 343–352.

Patani, R. *et al.* (2012) 'Investigating the utility of human embryonic stem cell-derived neurons to model ageing and neurodegenerative disease using whole-genome gene expression and splicing analysis', *Journal of Neurochemistry*, 122(4), pp. 738–751.

Pawley, J. and Pawley, J. B. (2006) 'Handbook Of Biological Confocal Microscopy', *Handbook Of Biological Confocal Microscopy*, (August), p. 985.

Peineau, S. *et al.* (2007) 'LTP Inhibits LTD in the Hippocampus via Regulation of GSK3β', *Neuron*, 53(5), pp. 703–717.

Perez-Nievas, B. G. *et al.* (2013) 'Dissecting phenotypic traits linked to human resilience to Alzheimer's pathology.', *Brain : a journal of neurology*, 136(Pt 8), pp. 2510–26.

Peric, A. and Annaert, W. (2015) 'Early etiology of Alzheimer's disease: tipping the balance toward autophagy or endosomal dysfunction?', *Acta neuropathologica*. Springer, 129(3), pp. 363–81.

Perl, D. P. (2010) 'Neuropathology of Alzheimer's Disease', 77(1), pp. 32–42.

Peters, O. *et al.* (2009) 'Astrocyte function is modified by alzheimer's disease-like pathology in aged mice', *Journal of Alzheimer's Disease*, 18(1), pp. 177–189.

Phillips, E. C. *et al.* (2014) 'Astrocytes and neuroinflammation in Alzheimer's disease.', *Biochemical Society transactions*, 42(5), pp. 1321–5.

Pickett, E. K. *et al.* (2017) 'Spread of tau down neural circuits precedes synapse and neuronal loss in the rTgTauEC mouse model of early Alzheimer's disease', *Synapse*, 71(6), pp. 1–8.

Piehowski, P. D. *et al.* (2013) 'Sources of Technical Variability in Quantitative LC–MS Proteomics: Human Brain Tissue Sample Analysis', *Journal of Proteome Research*, 12(5), pp. 2128–2137.

Pievani, M. *et al.* (2011) 'APOE4 is associated with greater atrophy of the hippocampal formation in Alzheimer's disease', *NeuroImage*, 55(3), pp. 909–919.

Pihlaja, R. *et al.* (2011) 'Multiple cellular and molecular mechanisms Are involved in human Aβ clearance by transplanted adult astrocytes', *Glia*. Wiley Subscription Services, Inc., A Wiley Company, 59(11), pp. 1643–1657.

Pike, C. J. (2017) 'Sex and the development of Alzheimer's disease.', 95(1–2), pp. 671–680.

Pitas, R. E. *et al.* (1987) 'Astrocytes synthesize apolipoprotein E and metabolize apolipoprotein E-containing lipoproteins.', 917(1), pp. 148–161.

Pooler, A. M. *et al.* (2013) 'Tau-amyloid interactions in the rTgTauEC model of early Alzheimer's disease suggest amyloid-induced disruption of axonal projections and exacerbated axonal pathology', *Journal of Comparative Neurology*, 521(18), pp. 4236–4248.

Pooler, A. M. *et al.* (2015) 'Amyloid accelerates tau propagation and toxicity in a model of early Alzheimer's disease.', 3, p. 14.

Pooler, A. M., Noble, W. and Hanger, D. P. (2014) 'A role for tau at the synapse in Alzheimer's disease pathogenesis', *Neuropharmacology*, 76, pp. 1–8.

Prince, M. *et al.* (2015) 'World Alzheimer Report 2015: The Global Impact of Dementia - An analysis of prevalence, incidence, cost and trends', *Alzheimer's Disease International*, p. 84.

Purro, S. A., Dickins, E. M. and Salinas, P. C. (2012) 'The secreted Wnt antagonist Dickkopf-1 is required for amyloid β-mediated synaptic loss.', *The Journal of neuroscience : the official journal of the Society for Neuroscience*, 32(10), pp. 3492–8.

Purro, S. A., Galli, S. and Salinas, P. C. (2014) 'Dysfunction of Wnt signaling and synaptic disassembly in neurodegenerative diseases', *Journal of Molecular Cell Biology*, pp. 75–80.

Qi, Y. *et al.* (2017) 'Combined small-molecule inhibition accelerates the derivation of functional cortical neurons from human pluripotent stem cells', *Nature Biotechnology*, 35(2), pp. 154–163.

Rankin, C. A., Sun, Q. and Gamblin, T. C. (2007) 'Tau phosphorylation by GSK-3β promotes tangle-like filament morphology', *Molecular Neurodegeneration*, 2(1), p. 12.

Rebeck, G. W. *et al.* (1993) 'Apolipoprotein E in sporadic Alzheimer's disease: Allelic variation and receptor interactions', *Neuron*, 11(4), pp. 575–80.

Reiman, E. M. *et al.* (2004) 'Functional brain abnormalities in young adults at genetic risk for late-onset Alzheimer's dementia.', *Proceedings of the National Academy of Sciences of the United States of America*, 101(1), pp. 284–9.

Renner, M. *et al.* (2010) 'Deleterious Effects of Amyloid β Oligomers Acting as an Extracellular Scaffold for mGluR5', *Neuron*. Elsevier Ltd, 66(5), pp. 739–754.

Riddell, D. R. *et al.* (2008) 'Impact of Apolipoprotein E (ApoE) Polymorphism on Brain ApoE Levels', *Journal of Neuroscience*, 28(45), pp. 11445–11453.

Rizo, J. and Xu, J. (2015) 'The Synaptic Vesicle Release Machinery'.

Roberson, E. D. *et al.* (2007) 'Reducing endogenous tau ameliorates amyloid beta-induced deficits in an Alzheimer's disease mouse model.', 316(5825), pp. 750–754.

Roberson, E. D., Halabisky, B. and Yoo, J. W. (2011) '{Amyloid-β/Fyn–induced} synaptic, network, and cognitive impairments depend on tau levels in multiple mouse models of Alzheimer's disease'.

Robinson, M., Lee, B. Y. and Hane, F. T. (2017) 'Recent Progress in Alzheimer's Disease Research, Part 2: Genetics and Epidemiology', *Journal of Alzheimer's Disease*. IOS Press, 57(2), pp. 317–330.

Rocher, A. B. *et al.* (2010) 'Structural and functional changes in tau mutant mice neurons are not linked to the presence of NFTs', *Experimental Neurology*. Elsevier Inc., 223(2), pp. 385–393.

Rodríguez-Moreno, A. and Lerma, J. (1998) 'Kainate receptor modulation of GABA release involves a metabotropic function.', *Neuron*, 20(6), pp. 1211–8.

Rodríguez-Moreno, A. and Sihra, T. S. (2011) 'Metabotropic Actions of Kainate Receptors in the Control of Glutamate Release in the Hippocampus', in. Springer, Boston, MA, pp. 39–48.

Roses, A. D. (1996) 'Apolipoprotein E alleles as risk factors in Alzheimer's disease.', *Annual review of medicine*, 47, pp. 387–400.

Roychaudhuri, R., Yang, M., Hoshi, M. M. and Teplow, D. B. (2009) 'Amyloid beta-protein assembly and Alzheimer disease.', *The Journal of biological chemistry*. American Society for Biochemistry and Molecular Biology, 284(8), pp. 4749–53.

Rozas, J. L., Paternain, A. V and Lerma, J. (2003) 'Noncanonical signaling by ionotropic kainate receptors.', *Neuron*, 39(3), pp. 543–53.

Rushworth, J. V, Griffiths, H. H., Watt, N. T. and Hooper, N. M. (2013) 'Prion protein-mediated toxicity of amyloid-β oligomers requires lipid rafts and the transmembrane LRP1.', *The Journal of biological chemistry*, 288(13), pp. 8935–51.

Sanhueza, M. and Lisman, J. (2013) 'The CaMKII/NMDAR complex as a molecular memory.', *Molecular brain*. BioMed Central, 6, p. 10.

Santos, M. S., Li, H. and Voglmaier, S. M. (2009) 'Synaptic vesicle protein trafficking at the glutamate synapse.', *Neuroscience*. NIH Public Access, 158(1), pp. 189–203.

Sarvestany, A. A. *et al.* (2014) 'Label-Free Quantitative Proteomic Pro fi ling Identi fi es Disruption of Ubiquitin Homeostasis As a Key Driver of Schwann Cell Defects in Spinal Muscular Atrophy', *J Proteome Res*.

Schiepers, O. J. G. *et al.* (2012) 'APOE E4 status predicts age-related cognitive decline in the ninth decade: longitudinal follow-up of the Lothian Birth Cohort 1921', *Molecular Psychiatry*.

Nature Publishing Group, 17(3), pp. 315–324.
Schindelin, J. *et al.* (2012) 'Fiji: an open-source platform for biological-image analysis.', 9(7), pp. 676–682.
Schlicker, E. and Feuerstein, T. (2017) 'Human presynaptic receptors', *Pharmacology and Therapeutics*. Elsevier Inc., pp. 1–21.
Schneider, A. *et al.* (2008) 'Flotillin-Dependent Clustering of the Amyloid Precursor Protein Regulates Its Endocytosis and Amyloidogenic Processing in Neurons', *Journal of Neuroscience*, 28(11), pp. 2874–2882.
Schoch, S. *et al.* (2002) 'RIM1α forms a protein scaffold for regulating neurotransmitter release at the active zone', *Nature*, 415(6869), pp. 321–326.
Schonberger, S. J. *et al.* (2001) 'Proteomic analysis of the brain in Alzheimer ' s disease : Molecular phenotype of a complex disease process', *Proteomics*, pp. 1519–1528.
Scott, R. (2007) 'Use-dependent control of presynaptic calcium signalling at central synapses', *Journal of Anatomy*. Wiley-Blackwell, 210(6), p. 642.
Sekar, A. *et al.* (2016) 'Schizophrenia risk from complex variation of complement component 4', *Nature*. NIH Public Access, 530(7589), pp. 177–183.
Selkoe, D., Mandelkow, E. and Holtzman, D. (2012) 'Deciphering alzheimer disease', *Cold Spring Harbor Perspectives in Medicine*, 2(1).
Sepulcre, J. *et al.* (2016) 'In Vivo Tau, Amyloid, and Gray Matter Profiles in the Aging Brain', *Journal of Neuroscience*. Society for Neuroscience, 36(28), pp. 7364–7374.
Shankar, G. M. *et al.* (2007) 'Natural Oligomers of the Alzheimer Amyloid-β Protein Induce Reversible Synapse Loss by Modulating an NMDA-Type Glutamate Receptor-Dependent Signaling Pathway', *J Neurosci*, 27(11), pp. 2866–2875.
Shankar, G. M. *et al.* (2010) 'Isolation of Low-n Amyloid β-Protein Oligomers from Cultured Cells, CSF, and Brain', in *Methods in Molecular Biology*, pp. 33–44.
Shankar, G. M., Li, S., Mehta, T. H. and A, G.-M. (2008) 'Amyloid-β protein dimers isolated directly from Alzheimer's brains impair synaptic plasticity and memory'.
Sharaf, A. *et al.* (2013) 'ApoER2 and VLDLr Are Required for Mediating Reelin Signalling Pathway for Normal Migration and Positioning of Mesencephalic Dopaminergic Neurons', *PLoS ONE*. Edited by R. Homayouni, 8(8), p. e71091.
Sheng, Z.-H. and Cai, Q. (2012) 'Mitochondrial transport in neurons: impact on synaptic homeostasis and neurodegeneration.', *Nature reviews Neuroscience*. NIH Public Access, 13(2), pp. 77–93.
Shi, L. *et al.* (2014) 'Cumulative effects of the ApoE genotype and gender on the synaptic proteome and oxidative stress in the mouse brain', *The International Journal of Neuropsychopharmacology*, 17(11), pp. 1863–1879.
Shi, Q. *et al.* (2017) 'Complement C3 deficiency protects against neurodegeneration in aged plaque-rich APP/PS1 mice.', *Science translational medicine*, 9(392), pp. 1–14.
Shipton, O. A., Leitz, J. R. and Dworzak, J. (2011) 'Tau protein is required for amyloid β-induced impairment of hippocampal long-term potentiation'.
Šimić, G. *et al.* (2016) 'Tau Protein Hyperphosphorylation and Aggregation in Alzheimer's Disease and Other Tauopathies, and Possible Neuroprotective Strategies', 6(1).
Small, S. a and Duff, K. (2008) 'Linking Abeta and tau in late-onset Alzheimer's disease: a dual

pathway hypothesis.', *Neuron*, 60(4), pp. 534–42.

Smart, T. G. and Paoletti, P. (2012) 'Synaptic neurotransmitter-gated receptors.', *Cold Spring Harbor perspectives in biology*. Cold Spring Harbor Laboratory Press, 4(3).

Smith, S. M., Renden, R. and von Gersdorff, H. (2008) 'Synaptic vesicle endocytosis: fast and slow modes of membrane retrieval', *Trends in Neurosciences*, 31(11), pp. 559–568.

Snyder, E. M. *et al.* (2005) 'Regulation of NMDA receptor trafficking by amyloid-β', *Nature Neuroscience*, 8(8), pp. 1051–1058.

Soldano, A. and Hassan, B. A. (2014) 'Beyond pathology: APP, brain development and Alzheimer's disease', *Current Opinion in Neurobiology*, pp. 61–67.

Southam, K. A., Vincent, A. J. and Small, D. H. (2016) 'Do Microglia Default on Network Maintenance in Alzheimer's Disease?', *Journal of Alzheimer's Disease*, 51(3), pp. 657–669.

Spires-Jones, T. L., Attems, J. and Thal, D. R. (2017) 'Interactions of pathological proteins in neurodegenerative diseases', *Acta Neuropathologica*. Springer Berlin Heidelberg, pp. 187–205.

Spires-Jones, T. L. and Hyman, B. T. (2014) 'The intersection of amyloid beta and tau at synapses in Alzheimer's disease.', *Neuron*. Elsevier Inc., 82(4), pp. 756–71.

Sposito, T. *et al.* (2015) 'Developmental regulation of tau splicing is disrupted in stem cell-derived neurons from frontotemporal dementia patients with the 10 + 16 splice-site mutation in MAPT', *Human Molecular Genetics*, 24(18), pp. 5260–5269.

Stauch, K. L., Purnell, P. R. and Fox, H. S. (2014) 'Quantitative Proteomics of Synaptic and Nonsynaptic Mitochondria: Insights for Synaptic Mitochondrial Vulnerability', *Journal of Proteome Research*, 13(5), pp. 2620–2636.

Steardo, L. *et al.* (2015) 'Does neuroinflammation turn on the flame in Alzheimer's disease? Focus on astrocytes.', 9, p. 259.

Stephen, R., Hongisto, K., Solomon, A. and Lönnroos, E. (2017) 'Physical Activity and Alzheimer's Disease: A Systematic Review', *The Journals of Gerontology Series A: Biological Sciences and Medical Sciences*. American Psychiatric Association, Washington DC, 13(6), p. 251.

Stevens, B. *et al.* (2007) 'The Classical Complement Cascade Mediates CNS Synapse Elimination', *Cell*, 131(6), pp. 1164–1178.

Stevens, D. R. *et al.* (2005) 'Identification of the Minimal Protein Domain Required for Priming Activity of Munc13-1', *Current Biology*, 15(24), pp. 2243–2248.

Stone, D. J. *et al.* (1998) 'Increased synaptic sprouting in response to estrogen via an apolipoprotein E-dependent mechanism: implications for Alzheimer's disease.', 18(9), pp. 3180–3185.

Stoothoff, W. *et al.* (2009) 'Differential effect of three-repeat and four-repeat tau on mitochondrial axonal transport', *Journal of Neurochemistry*, 111(2), pp. 417–427.

Sudhof, T. C. (2012) 'Calcium Control of Neurotransmitter Release', *Cold Spring Harbor Perspectives in Biology*. Cold Spring Harbor Laboratory Press, 4(1), pp. a011353–a011353.

Südhof, T. C. (2008) 'Neuroligins and neurexins link synaptic function to cognitive disease', *Nature*, 455(7215), pp. 903–911.

Südhof, T. C. (2012) 'The Presynaptic Active Zone', *Neuron*, 75(1), pp. 11–25.

Südhof, T. C. (2013) 'Neurotransmitter release: the last millisecond in the life of a synaptic vesicle.', *Neuron*. NIH Public Access, 80(3), pp. 675–90.

Sultana, R. *et al.* (2007) 'Proteomics analysis of the Alzheimer's disease hippocampal proteome.', *Journal of Alzheimer's disease : JAD*, 11(2), pp. 153–64.

Sun, X., Chen, W.-D. D. and Wang, Y.-D. D. (2015) '{β-Amyloid:} the key peptide in the pathogenesis of Alzheimer's disease.', 6, p. 221.

Sunderland, T. *et al.* (2004) 'Cerebrospinal fluid β-amyloid1–42 and tau in control subjects at risk for Alzheimer's disease: The effect of APOE ε4 allele', *Biological Psychiatry*, 56(9), pp. 670–676.

Sweet, R. A. *et al.* (2016) '{APOE*4} genotype is associated with altered levels of glutamate signaling proteins and synaptic co-expression networks in the prefrontal cortex in mild to moderate Alzheimer disease.', *Molecular & cellular proteomics : MCP*, 15(7), pp. 1–32.

Tai, H.-C. *et al.* (2012) 'The synaptic accumulation of hyperphosphorylated tau oligomers in Alzheimer disease is associated with dysfunction of the ubiquitin-proteasome system.', *The American journal of pathology*, 181(4), pp. 1426–35.

Tai, L. M. *et al.* (2015) '{APOE-modulated} Aβ-induced neuroinflammation in Alzheimer's disease: current landscape, novel data, and future perspective', 133(4), pp. 465–488.

Takahashi, K. *et al.* (2007) 'Induction of Pluripotent Stem Cells from Adult Human Fibroblasts by Defined Factors', *Cell*, 131(5), pp. 861–872.

Takuma, H., Tomiyama, T., Kuida, K. and Mori, H. (2004) 'Amyloid beta peptide-induced cerebral neuronal loss is mediated by caspase-3 in vivo.', *Journal of neuropathology and experimental neurology*, 63(3), pp. 255–261.

Talantova, M. *et al.* (2013) 'A induces astrocytic glutamate release, extrasynaptic NMDA receptor activation, and synaptic loss', *Proceedings of the National Academy of Sciences*, 110(27), pp. E2518–E2527.

Tang, S. J. and Schuman, E. M. (2002) 'Protein synthesis in the dendrite', *Philosophical Transactions of the Royal Society B: Biological Sciences*, 357(1420), pp. 521–529.

Tang, X. *et al.* (2013) 'Astroglial cells regulate the developmental timeline of human neurons differentiated from induced pluripotent stem cells', *Stem Cell Research*, 11(2), pp. 743–757.

Tanzi, R. E. (2012) 'The genetics of Alzheimer disease.', *Cold Spring Harbor perspectives in medicine*, 2(10), p. a006296.

Tarasoff-Conway, J. M. *et al.* (2015) 'Clearance systems in the brain—implications for Alzheimer disease', *Nature Reviews Neurology*, 11(4), pp. 457–470.

Terry, R. D. *et al.* (1991) 'Physical basis of cognitive alterations in Alzheimer's disease: synapse loss is the major correlate of cognitive impairment.', 30(4), pp. 572–580.

Thevenaz, P., Ruttimann, U. E. and Unser, M. (1998) 'A pyramid approach to subpixel registration based on intensity', *IEEE Transactions on Image Processing*, 7(1), pp. 27–41.

Tiraboschi, P. *et al.* (2004) 'Impact of APOE genotype on neuropathologic and neurochemical markers of Alzheimer disease', *Neurology*, 62(11), pp. 1977–1983.

Tokumaru, H. *et al.* (2001) 'SNARE complex oligomerization by synaphin/complexin is essential for synaptic vesicle exocytosis', *Cell*, 104(3), pp. 421–432.

Tomiyama, T. *et al.* (2010) 'A Mouse Model of Amyloid Oligomers: Their Contribution to Synaptic Alteration, Abnormal Tau Phosphorylation, Glial Activation, and Neuronal Loss In Vivo', *Journal of Neuroscience*, 30(14), pp. 4845–4856.

Tremblay, M.-È. *et al.* (2011) 'The Role of Microglia in the Healthy Brain', 31(45), pp. 16064–

16069.

Trimble, W. S., Cowan, D. M. and Scheller, R. H. (1988) 'VAMP-1: a synaptic vesicle-associated integral membrane protein.', *Proceedings of the National Academy of Sciences of the United States of America*, 85(12), pp. 4538–42.

Trinidad, J. C. *et al.* (2012) 'Global Identification and Characterization of Both O -GlcNAcylation and Phosphorylation at the Murine Synapse', *Molecular & Cellular Proteomics*, 11(8), pp. 215–229.

Tsuji, T. *et al.* (2002) 'Proteomic Profiling and Neurodegeneration in Alzheimer ' s Disease', *Neurochemical Research*, 27(10), pp. 1245–1253.

Tyrrell, J. *et al.* (2001) 'Dementia in people with Down's syndrome', *International Journal of Geriatric Psychiatry*, 16(12), pp. 1168–1174.

Ueno, M. *et al.* (2013) 'Layer V cortical neurons require microglial support for survival during postnatal development.', *Nature neuroscience*. Nature Publishing Group, 16(5), pp. 543–51.

Ulery, P. G. *et al.* (2000) 'Modulation of -Amyloid Precursor Protein Processing by the Low Density Lipoprotein Receptor-related Protein (LRP): EVIDENCE THAT LRP CONTRIBUTES TO THE PATHOGENESIS OF ALZHEIMER'S DISEASE', *Journal of Biological Chemistry*, 275(10), pp. 7410–7415.

Vázquez-Higuera, J. L. *et al.* (2009) 'Genetic Interaction between Tau and the Apolipoprotein e Receptor LRP1 Increases Alzheimer's Disease Risk', *Dementia and Geriatric Cognitive Disorders*, 28(2), pp. 116–120.

Vera, E., Bosco, N. and Studer, L. (2016) 'Generating Late-Onset Human iPSC-Based Disease Models by Inducing Neuronal Age-Related Phenotypes through Telomerase Manipulation', *Cell Reports*, 17(4), pp. 1184–1192.

Vincent, A. J., Gasperini, R., Foa, L. and Small, D. H. (2010) 'Astrocytes in Alzheimer's disease: Emerging roles in calcium dysregulation and synaptic plasticity', *Journal of Alzheimer's Disease*, pp. 699–714.

Vithlani, M., Terunuma, M. and Moss, S. J. (2011) 'The Dynamic Modulation of GABAA Receptor Trafficking and Its Role in Regulating the Plasticity of Inhibitory Synapses', *Physiological Reviews*, 91(3), pp. 1009–1022.

Völgyi, K. *et al.* (2015) 'Synaptic mitochondria: a brain mitochondria cluster with a specific proteome.', *Journal of Proteomics*. Elsevier B.V., 120, pp. 142–157.

Wahrle, S. E. *et al.* (2004) 'ABCA1 is required for normal central nervous system apoE levels and for lipidation of astrocyte-secreted apoE', *Journal of Biological Chemistry*, 279(39), pp. 40987–40993.

Wahrle, S. E. *et al.* (2008) 'Overexpression of ABCA1 reduces amyloid deposition in the PDAPP mouse model of Alzheimer disease', *Journal of Clinical Investigation*, 118(2), pp. 671–682.

Walsh, D. M. *et al.* (2002) 'Naturally secreted oligomers of amyloid β protein potently inhibit hippocampal long-term potentiation in vivo', 416(6880), pp. 535–539.

Wan, W. *et al.* (2014) 'The role of Wnt signaling in the development of alzheimer's disease: A potential therapeutic target?', *BioMed Research International*, pp. 1–9.

Wang, C., Wilson, W. A., Moore, S. D. and Mace, B. E. (2005) 'Human {apoE4-targeted} replacement mice display synaptic deficits in the absence of neuropathology'.

Wang, Q. *et al.* (2008) 'Alpha v integrins mediate beta-amyloid induced inhibition of long-term

potentiation.', 29(10), pp. 1485–1493.
Wang, Y. L. and Zhang, C. X. (2017) 'Putting a brake on synaptic vesicle endocytosis', *Cellular and Molecular Life Sciences*. Springer International Publishing, pp. 2917–2927.
Wang, Z. *et al.* (2017) 'Human brain-derived Aβ oligomers bind to synapses and disrupt synaptic activity in a manner that requires APP.', *The Journal of neuroscience : the official journal of the Society for Neuroscience*.
Wegmann, S. *et al.* (2015) 'Removing endogenous tau does not prevent tau propagation yet reduces its neurotoxicity.', *The EMBO journal*, 34(24), pp. 3028–3041.
Weingarten, Lockwood, A. H., Hwo, S. Y. and Kirschner, M. W. (1975) 'A protein factor essential for microtubule assembly.', 72(5), pp. 1858–1862.
Weisgraber, K. H. (1990) 'Apolipoprotein E distribution among human plasma lipoproteins: role of the cysteine-arginine interchange at residue 112.', *Journal of lipid research*, 31(8), pp. 1503–1511.
Wilson, N. R. *et al.* (2005) 'Presynaptic Regulation of Quantal Size by the Vesicular Glutamate Transporter VGLUT1', *Journal of Neuroscience*, 25(26), pp. 6221–6234.
Wright, S. *et al.* (2007) 'Alpha2beta1 and alphaVbeta1 integrin signaling pathways mediate amyloid-beta-induced neurotoxicity.', *Neurobiology of aging*, 28(2), pp. 226–37.
Wu, H. Y. *et al.* (2010) 'Amyloid β induces the morphological neurodegenerative triad of spine loss, dendritic simplification, and neuritic dystrophies through calcineurin activation', *The Journal of …*.
Wu, L.-G., Ryan, T. A. and Lagnado, L. (2007) 'Modes of Vesicle Retrieval at Ribbon Synapses, Calyx-Type Synapses, and Small Central Synapses', *Journal of Neuroscience*, 27(44), pp. 11793–11802.
Wyss-Coray, T. *et al.* (2003) 'Adult mouse astrocytes degrade amyloid-β in vitro and in situ', *Nature Medicine*, 9(4), pp. 453–457.
Xia, M. *et al.* (2016) 'The Binding Receptors of Aβ: an Alternative Therapeutic Target for Alzheimer's Disease', *Molecular Neurobiology*. Springer US, 53(1), pp. 455–471.
Yagi, T. *et al.* (2011) 'Modeling familial Alzheimer's disease with induced pluripotent stem cells', *Human Molecular Genetics*, 20(23), pp. 4530–4539.
Yang, T. *et al.* (2017) 'Large Soluble Oligomers of Amyloid β-Protein from Alzheimer Brain Are Far Less Neuroactive Than the Smaller Oligomers to Which They Dissociate', *The Journal of Neuroscience*. Society for Neuroscience, 37(1), pp. 152–163.
Yang, X. *et al.* (2010) 'Complexin clamps asynchronous release by blocking a secondary Ca(2+) sensor via its accessory α helix.', *Neuron*. Howard Hughes Medical Institute, 68(5), pp. 907–20.
Yu, J. T. and Tan, L. (2012) 'The role of clusterin in Alzheimer's disease: Pathways, pathogenesis, and therapy', *Molecular Neurobiology*, pp. 314–326.
Zacchi, P., Antonelli, R. and Cherubini, E. (2014) 'Gephyrin phosphorylation in the functional organization and plasticity of GABAergic synapses', *Frontiers in Cellular Neuroscience*, 8, p. 103.
Zahid, S., Oellerich, M., Asif, A. R. and Ahmed, N. (2014) 'Differential expression of proteins in brain regions of alzheimer's disease patients', *Neurochemical Research*, 39(1), pp. 208–215.
Zhang, F., Wen, Y. and Guo, X. (2014) 'CRISPR/Cas9 for genome editing: progress, implications

and challenges', *Human Molecular Genetics*, 23(R1), pp. R40–R46.

Zhang, H. *et al.* (2005a) 'Clusterin inhibits apoptosis by interacting with activated Bax.', *Nature cell biology*, 7(9), pp. 909–15.

Zhang, H. *et al.* (2005b) 'Clusterin inhibits apoptosis by interacting with activated Bax.', *Nature cell biology*, 7(9), pp. 909–915.

Zhao, N., Liu, C. C., Qiao, W. and Bu, G. (2017) 'Apolipoprotein E, Receptors, and Modulation of Alzheimer's Disease', *Biological Psychiatry*. Elsevier.

Zhong, N. and Weisgraber, K. H. (2009) 'Understanding the association of apolipoprotein E4 with Alzheimer disease: Clues from its structure', *Journal of Biological Chemistry*. American Society for Biochemistry and Molecular Biology, pp. 6027–6031.

Zhou, J. *et al.* (2013) 'Proteomic analysis of postsynaptic density in Alzheimer's Disease', *Clinica Chimica Acta*, 420, pp. 62–68.

Zhou, L. *et al.* (2017) 'Tau association with synaptic vesicles causes presynaptic dysfunction', *Nature Communications*. Nature Publishing Group, 8(May), p. 15295.

Zhou, M. *et al.* (2016) 'APOE4 Induces Site-Specific Tau Phosphorylation Through Calpain-CDK5 Signaling Pathway in EFAD-Tg Mice.', *Current Alzheimer research*, 13(9), pp. 1048–55.

Zlokovic, B. V (2011) 'Neurovascular pathways to neurodegeneration in Alzheimer's disease and other disorders.', *Nature reviews. Neuroscience*. NIH Public Access, 12(12), pp. 723–38.

9 Appendices

Appendix 1: Analysis scripts and macros used for array tomography in Chapter 3

Image J Macros

Jackson, Rosemary. (2017). An Investigation of Synaptic Dysfunction in Alzheimer's Disease - Chapter 3 - Thresholding Macros, [dataset]. University of Edinburgh, Deanery of Biomedical Sciences. **http://dx.doi.org/10.7488/ds/2133.**

MatLab Scripts

Jackson, Rosemary. (2017). An Investigation of Synaptic Dysfunction in Alzheimer's Disease - Chapter 3 - Matlab Scripts, [dataset]. University of Edinburgh, Deanery of Biomedical Sciences. **http://dx.doi.org/10.7488/ds/2134.**

Appendix 2: Full list of proteins identified by LC-MS/MS

Entry	Gene names	Protein name
V9HW43	HEL-S-102	Epididymis secretory protein Li 102
H0YEX9	JAM2	Junctional adhesion molecule B
B4DW11	CLU	Clusterin
B3KS70	DKK3	Dickkopf-related protein 3
E9PHR9	PLSCR4	Phospholipid scramblase
P0C0L4	C4A	Complement C4-A
A0A0A0MRG2	APP	Amyloid beta A4 protein
Q59G10		Aldehyde dehydrogenase 1 family, member L1 variant
P07305	H1F0	Histone H1.0
Q9NR45	NANS	Sialic acid synthase
A0A024QZ62	hCG_1998851	HCG1998851, isoform CRA_c
A0A024R0L6	PAFAH1B3	Platelet-activating factor acetylhydrolase, isoform Ib, gamma subunit 29kDa, isoform CRA_a
Q9H936	SLC25A22	Mitochondrial glutamate carrier 1
E5KNY5	LRPPRC	Leucine-rich PPR-motif containing protein
P12273	PIP	Prolactin-inducible protein
Q68E00	DKFZp686G2045	Uncharacterized protein DKFZp686G2045
B2RBR9		cDNA, FLJ95650, highly similar to Homo sapiens karyopherin
B4DVJ0		Glucose-6-phosphate isomerase
A0A024R6Z0	DYNC1LI2	Dynein, cytoplasmic 1, light intermediate chain 2, isoform CRA_a
V9HWI3	HEL-S-130P	Cathepsin D
V9HWC3	HEL-S-1a	Epididymis secretory sperm binding protein Li 1a
Q9UBB6	NCDN	Neurochondrin
Q92561	PHYHIP	Phytanoyl-CoA hydroxylase-interacting protein
V9HWG1	HEL-S-134P	Epididymis secretory sperm binding protein Li 134P
B4DY09	ILF2	Interleukin enhancer-binding factor 2
P82909	MRPS36	28S ribosomal protein S36, mitochondrial
A0A024QZQ2	PSAP	Prosaposin
Q5ST80	FLOT1	FLOT1
I1VE20	SEC22B	SEC22 vesicle trafficking protein B

Q9BQ69	MACROD1	O-acetyl-ADP-ribose deacetylase MACROD1
Q5T9B7	AK1	Adenylate kinase isoenzyme 1
Q8N135	LGI4	Leucine-rich repeat LGI family member 4
Q6MZW0	DKFZp686J11235	Uncharacterized protein DKFZp686J11235
E7EVA0	MAP4	Microtubule-associated protein
Q8N450	FSD1L	FSD1-like protein
V9HWI0	HEL-S-165	Epididymis secretory protein Li 6
H7C286	NAGK	N-acetyl-D-glucosamine kinase
Q5D862	FLG2	Filaggrin-2
G5E9L9	DCLK2	Doublecortin and CaM kinase-like 2, isoform CRA_c
A0A024R228	HNRPK	Heterogeneous nuclear ribonucleoprotein K, isoform CRA_d
V9HW35	HEL-S-55	Epididymis secretory protein Li 55
A0A0A0MS54	PRKACB	cAMP-dependent protein kinase catalytic subunit beta
B4DPZ3		cDNA FLJ53290, highly similar to Cytoplasmic dynein 1 intermediate chain 2
A0A024R6Q1	EIF5	Eukaryotic translation initiation factor 5, isoform CRA_b
Q15818	NPTX1	Neuronal pentraxin-1
Q9NZT1	CALML5	Calmodulin-like protein 5
B3KXB8		cDNA FLJ45106 fis, clone BRAWH3033293, highly similar to Synaptopodin
Q9UHG2	PCSK1N	ProSAAS
P60880	SNAP25	Synaptosomal-associated protein 25
P11216	PYGB	Glycogen phosphorylase, brain form
G3V295	PSMA6	Proteasome subunit alpha type
Q15149	PLEC	Plectin
Q6UWP8	SBSN	Suprabasin
Q9NSD9	FARSB	Phenylalanine--tRNA ligase beta subunit
D3DVQ1	LETM1	Leucine zipper-EF-hand containing transmembrane protein 1, isoform CRA_a
B4DSF0		cDNA FLJ56734, moderately similar to Sepiapterin reductase
Q6IB54	ATP5J	ATP synthase-coupling factor 6, mitochondrial
Q9Y3D6	FIS1	Mitochondrial fission 1 protein
H7C0R7	CYB5R1	NADH-cytochrome b5 reductase 1
A0A0A0MT83	IVD	Isovaleryl-CoA dehydrogenase, mitochondrial
A0A087X2B5	BSG	Basigin

Q5U0A0		Proteasome subunit alpha type
Q5VU08	ADD3	Adducin 3
B3KXD3		cDNA FLJ45230 fis, clone BRCAN2021325, highly similar to Carboxypeptidase E
A0A024R6U7	GPR56	G protein-coupled receptor 56 isoform 1
B4DIZ1	ERMN	Ermin
P25311	AZGP1	Zinc-alpha-2-glycoprotein
A0PJJ9	GGT7	GGT7 protein
G4XXL9	CYCS	Cytochrome c
X5D2M8	MVP	Major vault protein isoform A
P0DOY2	IGLC2	Immunoglobulin lambda constant 2
P0DOY3	IGLC3	Immunoglobulin lambda constant 3
B5BU38	ANXA1	Annexin
A0FGR8	ESYT2	Extended synaptotagmin-2
A0A024R050	SLC1A3	Amino acid transporter
A8K288		cDNA FLJ76322
Q6FHU2	PGAM1	Phosphoglycerate mutase
A0A024R5Z7	ANXA2	Annexin
E9PN17	ATP5L	ATP synthase subunit g, mitochondrial
O60262	GNG7	Guanine nucleotide-binding protein G
P01834	IGKC	Immunoglobulin kappa constant
B7Z5V0		cDNA FLJ53647, highly similar to Four and a half LIM domains protein 1
B1AKZ4	PEA15	Phosphoprotein enriched in astrocytes 15, isoform CRA_a
Q9UG16		Uncharacterized protein DKFZp564P0562
E9PKZ0	RPL8	60S ribosomal protein L8
Q7Z7M4	SOD2	Superoxide dismutase
A0A024RB59	PDE1B	Phosphodiesterase
Q9UDT6	CLIP2	CAP-Gly domain-containing linker protein 2
A0A087WZH7		Deleted.
A0A0A0MS47	OPALIN	Opalin
P04632	CAPNS1	Calpain small subunit 1
Q59EU3		Dematin variant
G3V582	GPHN	Gephyrin
A0A090N7T9	SCRN1	Secernin 1

Q6ICQ8	ARHG	ARHG protein
V9HWJ1	HEL-S-64p	Glutathione synthetase
A0A0A0MRT6	ABI1	Abl interactor 1
Q96JE9	MAP6	Microtubule-associated protein 6
P05556	ITGB1	Integrin beta-1
Q9Y3P9	RABGAP1	Rab GTPase-activating protein 1
Q6FG42	NDUFA7	NDUFA7 protein
A0A0A0MSS8	AKR1C3	Aldo-keto reductase family 1 member C3
A0A024R9G4	FAM49B	Family with sequence similarity 49, member B, isoform CRA_a
B4DH37		cDNA FLJ53760, highly similar to Syntaxin-7
Q27J81	INF2	Inverted formin-2
G3XAL9	SLC12A2	Solute carrier family 12
A8K6I6		cDNA FLJ75092, highly similar to Homo sapiens golgi associated, gamma adaptin ear containing, ARF binding protein 3
Q53ES7		Myelin associated glycoprotein isoform a variant
Q6IBC4	NDUFS6	NADH dehydrogenase [ubiquinone] iron-sulfur protein 6, mitochondrial
A0A087WXX9	PRKAA2	Non-specific serine/threonine protein kinase
A0A024RDD7	RUFY3	RUN and FYVE domain containing 3, isoform CRA_a
B2R9S4		cDNA, FLJ94534, highly similar to Homo sapiens capping protein
O95373	IPO7	Importin-7
A0A024R652	MTHFD1	Methylenetetrahydrofolate dehydrogenase
Q0QF37	MDH2	Malate dehydrogenase
Q5HYI7	MTX3	Metaxin-3
Q5VZU9	TPP2	Tripeptidyl-peptidase 2
B4DV94		cDNA FLJ58285, highly similar to Homo sapiens pre-B-cell leukemia transcription factor interacting protein 1
A0A024R1A3	UBE1	Testicular secretory protein Li 63
A0A024R2U9	APEH	N-acylaminoacyl-peptide hydrolase, isoform CRA_b
A0A024R1Y6	PALM	Paralemmin, isoform CRA_a
A8K3J4	CA14	Carbonic anhydrase XIV, isoform CRA_d
A5YM53	ITGAV	ITGAV protein
Q8NFZ8	CADM4	Cell adhesion molecule 4
A0A024R2Q3	CTNNB1	Catenin
A0A024R0G8	SIRT2	Sirtuin
Q9BX67	JAM3	Junctional adhesion molecule C

A0A024R882	STOM	Stomatin, isoform CRA_a
D1MGQ2	HBA2	Alpha-2 globin chain
Q9H444	CHMP4B	Charged multivesicular body protein 4b
B4DFG7		cDNA FLJ59862, highly similar to Claudin-11
P46109	CRKL	Crk-like protein
A0A024RAK9	HAPLN1	Hyaluronan and proteoglycan link protein 1, isoform CRA_a
O15540	FABP7	Fatty acid-binding protein, brain
O00194	RAB27B	Ras-related protein Rab-27B
P49006	MARCKSL1	MARCKS-related protein
D3DRP5	C9orf19	Chromosome 9 open reading frame 19, isoform CRA_a
A0A024R1J3	CDC42EP1	CDC42 effector protein
Q6FIE5	PHP14	PHP14 protein
Q07954	LRP1	Prolow-density lipoprotein receptor-related protein 1
J3QTA6	CHCHD6	MICOS complex subunit
P49773	HINT1	Histidine triad nucleotide-binding protein 1
Q6A1A2	PDPK2P	Putative 3-phosphoinositide-dependent protein kinase 2
B2R7P8		cDNA, FLJ93545, highly similar to Homo sapiens 5-aminoimidazole-4-carboxamide ribonucleotide formyltransferase/IMP cyclohydrolase
Q96PY5	FMNL2	Formin-like protein 2
A7E294		Deleted.
B4DKF8	PSD3	PH and SEC7 domain-containing protein 3
Q6FHF7	RABGGTA	RABGGTA protein
Q5VVD0	RPL11	Ribosomal protein L11, isoform CRA_b
J3KR44	OTUB1	Ubiquitin thioesterase
B0YJA4	THY1	Thy-1 cell surface antigen, isoform CRA_a
P02689	PMP2	Myelin P2 protein
J3KQ32	OLA1	Obg-like ATPase 1
J9ZVQ3	APOE	Apolipoprotein E
H3BPK3	HAGH	Hydroxyacylglutathione hydrolase, mitochondrial
Q8TAS0		ATP synthase subunit gamma
C9J6B0	MADD	MAP kinase-activating death domain protein
A0A024R7A8	AKR1B1	Aldo-keto reductase family 1, member B1
H7C5H4		Deleted.

A8K5W7		cDNA FLJ75180, highly similar to Homo sapiens mitochondrial isoleucine tRNA synthetase, mRNA
B4DH07		cDNA FLJ53321, highly similar to Homo sapiens pitrilysin metallopeptidase 1
V9HW71	HEL-S-107	Endoplasmic reticulum resident protein 29
P48047	ATP5O	ATP synthase subunit O, mitochondrial
B3KXN4		cDNA FLJ45763 fis, clone N1ESE2000698, highly similar to WD repeat protein 1
B4DFL3		cDNA FLJ56661, highly similar to Proteasome subunit beta type 4
Q8WYJ5		Protein kinase C inhibitor-2
D6RJ96	HSPA4L	Heat shock 70 kDa protein 4L
B2R673		Dihydrolipoamide acetyltransferase component of pyruvate dehydrogenase complex
Q6IBR2	FARSLA	FARSLA protein
B4DFP1		cDNA FLJ51818, highly similar to Phosphoglucomutase-1
B4E184		cDNA FLJ53267, highly similar to Optineurin
Q9ULP0	NDRG4	Protein NDRG4
Q5SYC1	CLVS2	Clavesin-2
A0A024R713	DLD	Dihydrolipoyl dehydrogenase
A8K3D0		cDNA FLJ75185
X2L7S8	HLA-A	MHC class I antigen
B9A067	IMMT	MICOS complex subunit MIC60
A0A024QZ77	EFHD2	EF-hand domain family, member D2, isoform CRA_a
A8K1Z2		Glycerol-3-phosphate dehydrogenase
A0A024QZV0	hCG_1811539	HCG1811539, isoform CRA_b
A0A024R5U5	ADAM10	ADAM metallopeptidase domain 10, isoform CRA_b
P80723	BASP1	Brain acid soluble protein 1
Q9H598	SLC32A1	Vesicular inhibitory amino acid transporter
Q9BPU6	DPYSL5	Dihydropyrimidinase-related protein 5
A0A024RBI7	GLTP	Glycolipid transfer protein, isoform CRA_a
C9JTE0	MOG	Myelin-oligodendrocyte glycoprotein
B5MCX3	Sep2	Septin-2
A0A024R561	HRASLS3	HRAS-like suppressor 3, isoform CRA_a
Q5HYD7	DKFZp686K101	Phosphoinositide phospholipase C
Q9UIU0	CACNA2D1	Dihydropyridine receptor alpha 2 subunit
A0A024R5M3	CTTN	Cortactin, isoform CRA_c
O00217	NDUFS8	NADH dehydrogenase [ubiquinone] iron-sulfur protein 8, mitochondrial

O43181	NDUFS4	NADH dehydrogenase [ubiquinone] iron-sulfur protein 4, mitochondrial
J3QRN6	MYO1D	Unconventional myosin-Id
P09417	QDPR	Dihydropteridine reductase
B5ME97	Sep10	Septin 10, isoform CRA_c
Q9BRX8	FAM213A	Redox-regulatory protein FAM213A
B4DHY8	TSFM	Elongation factor Ts, mitochondrial
B3KM48		cDNA FLJ10286 fis, clone HEMBB1001384, highly similar to COP9 signalosome complex subunit 4
B4DE76		cDNA FLJ57507, highly similar to Ran-specific GTPase-activating protein
K7EN45	PIN1	Peptidyl-prolyl cis-trans isomerase
B7Z2L1		cDNA FLJ55775, highly similar to Growth-arrest-specific protein 7
Q0VGA5	SARS	SARS protein
Q5TZC3	PACSIN1	Protein kinase C and casein kinase substrate in neurons 1, isoform CRA_a
Q16658	FSCN1	Fascin
B2R747		cDNA, FLJ93281, highly similar to Homo sapiens calcium/calmodulin-dependent protein kinase IV
Q9Y2Q0	ATP8A1	Phospholipid-transporting ATPase IA
A0A024R4V4	MLC1	Megalencephalic leukoencephalopathy with subcortical cysts 1, isoform CRA_a
Q9Y2A7	NCKAP1	Nck-associated protein 1
B4DDF7		cDNA FLJ53296, highly similar to Serine/threonine-protein phosphatase 2A 65 kDa regulatory subunit A alpha isoform
A0A024R1T5	CNP	2',3'-cyclic-nucleotide 3'-phosphodiesterase
D3DU87	CASKIN1	CASK interacting protein 1, isoform CRA_a
O75947	ATP5H	ATP synthase subunit d, mitochondrial
C9J0K6	SRI	Sorcin
B4DFR2		cDNA FLJ59194, moderately similar to Dynein light chain 2A, cytoplasmic
B4DY96		cDNA FLJ55769, highly similar to Trifunctional enzyme subunit beta, mitochondrial
Q9NQC3	RTN4	Reticulon-4
B2CIS9	CASP14	Caspase 14, apoptosis-related cysteine peptidase
B4DV69		cDNA FLJ55312, highly similar to Homo sapiens neuronal guanine nucleotide exchange factor
A0A024R3X7	HSPE1	Heat shock 10kDa protein 1
G5EA42	TMOD2	Tropomodulin 2
P17568	NDUFB7	NADH dehydrogenase [ubiquinone] 1 beta subcomplex subunit 7
A0A087WYS1	UGP2	UTP--glucose-1-phosphate uridylyltransferase
Q6FHJ5	SCAMP3	Secretory carrier-associated membrane protein
Q9HCC0	MCCC2	Methylcrotonoyl-CoA carboxylase beta chain, mitochondrial

A0A024R138	GPD1	Glycerol-3-phosphate dehydrogenase [NAD
A0A024R151	SLC44A1	Solute carrier family 44, member 1, isoform CRA_a
A0A024RAE4	CDC42	Cell division cycle 42
A0A024R9D7	DECR1	2,4-dienoyl CoA reductase 1, mitochondrial, isoform CRA_b
B3KTR0	SNTA1	Syntrophin, alpha 1
Q6UWR	ENPP6	Ectonucleotide pyrophosphatase/phosphodiesterase family member 6
A0A0A6YYG9	ARPC4-TTLL3	Protein ARPC4-TTLL3
Q53YD7	EEF1G	EEF1G protein
H3BMU1	IST1	IST1 homolog
B7Z7G4		cDNA FLJ60939, highly similar to NAD-dependent deacetylase sirtuin-3, mitochondrial
A0A087WUQ6	GPX1	Glutathione peroxidase
A0A087WTI3	NDUFS7	NADH dehydrogenase [ubiquinone] iron-sulfur protein 7, mitochondrial
P09497	CLTB	Clathrin light chain B
Q9UBI6	GNG12	Guanine nucleotide-binding protein G
B2RB32		Alpha-1,4 glucan phosphorylase
A0A024R5Q7	ADSS	Adenylosuccinate synthetase isozyme 2
Q5JPE4	DKFZp667O202	Vacuolar protein sorting-associated protein 29
A4D2P0	RAC1	Ras-related C3 botulinum toxin substrate 1
Q0QER2	IDH1	Isocitrate dehydrogenase 1
Q15111	PLCL1	Inactive phospholipase C-like protein 1
V9HVZ6	HEL-68	Epididymis luminal protein 68
V9HWE3	HEL-S-11	Carbonic anhydrase I, isoform CRA_a
Q7L1I2	SV2B	Synaptic vesicle glycoprotein 2B
Q02790	FKBP4	Peptidyl-prolyl cis-trans isomerase FKBP4
Q15435	PPP1R7	Protein phosphatase 1 regulatory subunit 7
A0A024R1S8	LASP1	LIM and SH3 protein 1, isoform CRA_b
A0A024R4N0	hCG_1640809	HCG1640809, isoform CRA_b
A0A024R573	ASRGL1	Asparaginase like 1, isoform CRA_a
P45954	ACADSB	Short/branched chain specific acyl-CoA dehydrogenase, mitochondrial
P23297	S100A1	Protein S100-A1
B4DG82		cDNA FLJ61094, highly similar to Rap guanine nucleotide exchange factor 2
V9HW74	HEL-117	Ubiquitin carboxyl-terminal hydrolase
A0A0A0MRN6		Deleted.

C9JDV8	NIPSNAP1	Protein NipSnap homolog 1
A4D1N4	CHCHD3	MICOS complex subunit
Q53HB8		Oligodendrocyte myelin glycoprotein variant
Q7Z3Z9	L1CAM	L1 cell adhesion molecule
P49327	FASN	Fatty acid synthase
P24752	ACAT1	Acetyl-CoA acetyltransferase, mitochondrial
I3L4A1	CHMP6	Charged multivesicular body protein 6
B7Z4M3		Adenylyl cyclase-associated protein
B4DVZ8		Leukotriene A
B4DVV3		cDNA FLJ53218, highly similar to Homo sapiens SAC1 suppressor of actin mutations 1-like
Q14CZ8	HEPACAM	Hepatocyte cell adhesion molecule
Q8N2F6	ARMC10	Armadillo repeat-containing protein 10
Q6IBA0	NDUFS5	NADH dehydrogenase
Q13057	COASY	Bifunctional coenzyme A synthase
A0A024R2E9	ATG7	ATG7 autophagy related 7 homolog
P62760	VSNL1	Visinin-like protein 1
A0A024RA49	ANLN	Anillin, actin binding protein
B4DY28		cDNA FLJ61189, highly similar to Cysteine and glycine-rich protein 1
A5YM72	CARNS1	Carnosine synthase 1
B2RD40		cDNA, FLJ96442, highly similar to Homo sapiens copine II
A0A024RCC9	NAP1L4	Nucleosome assembly protein 1-like 4, isoform CRA_b
O60245	PCDH7	Protocadherin-7
B4DIF5		cDNA FLJ55687, highly similar to Cell cycle control protein 50A
H3BPF6	PFDN5	Prefoldin subunit 5
Q6PUV4	CPLX2	Complexin-2
B0AZL9		cDNA, FLJ79459, highly similar to Synaptotagmin-12
P51970	NDUFA8	NADH dehydrogenase [ubiquinone] 1 alpha subcomplex subunit 8
B2R4A2		Cytochrome b-c1 complex subunit 7
A0A024RBK8	RASAL1	RAS protein activator like 1
A0A024RCB7	CD81	Tetraspanin
Q8N145	LGI3	Leucine-rich repeat LGI family member 3
Q13011	ECH1	Delta
C9JHV9	PTK2B	Protein-tyrosine kinase 2-beta

A0A024R040	OXCT1	Succinyl-CoA:3-ketoacid-coenzyme A transferase
Q5SRR8	DDAH2	N
B2R7M1		V-type proton ATPase subunit
Q14240	EIF4A2	Eukaryotic initiation factor 4A-II
Q9NQE9	HINT3	Histidine triad nucleotide-binding protein 3
A0A024R7U9	ATP6V1H	ATPase, H+ transporting, lysosomal 50/57kDa, V1 subunit H, isoform CRA_a
Q9NZN3	EHD3	EH domain-containing protein 3
C9J634	PDHB	Pyruvate dehydrogenase E1 component subunit beta
O95168	NDUFB4	NADH dehydrogenase [ubiquinone] 1 beta subcomplex subunit 4
Q14008	CKAP5	Cytoskeleton-associated protein 5
X5D7J0	KIF1A	Kinesin family member 1A isoform A
Q6FHM9	CD59	CD59 antigen, complement regulatory protein, isoform CRA_b
V9HW77	HEL-211	Epididymis luminal protein 211
A0A024RCM3	hCG_2005638	DDX39B
J3QRD1	ALDH3A2	Fatty aldehyde dehydrogenase
A0A0A0MRI2	SNX6	Sorting nexin
P21281	ATP6V1B2	V-type proton ATPase subunit B, brain isoform
H0YFA4	CRIP2	Cysteine-rich protein 2
B4DH44		cDNA FLJ52538, highly similar to Dual specificity mitogen-activated proteinkinase kinase 4
B3KSI4		cDNA FLJ36348 fis, clone THYMU2007025, highly similar to TRANSKETOLASE
Q6PI78	TMEM65	Transmembrane protein 65
B1AKK2	DDAH1	Dimethylarginine dimethylaminohydrolase 1, isoform CRA_b
P16152	CBR1	Carbonyl reductase [NADPH] 1
Q8N5M8	PHGDH	PHGDH protein
C9J1E1	BLVRA	Biliverdin reductase A
A8K8U1		cDNA FLJ77762, highly similar to Homo sapiens cullin-associated and neddylation-dissociated 1
O15079	SNPH	Syntaphilin
Q02413	DSG1	Desmoglein-1
A0A024RAB5	RAP1GA1	RAP1, GTPase activating protein 1, isoform CRA_b
B4DQR1	FLJ10769	cDNA FLJ55241
A0A087X1H6		Deleted.
B4DW81		cDNA FLJ58863, highly similar to Protein NipSnap3A
P12532	CKMT1A	Creatine kinase U-type, mitochondrial

B4DF38		cDNA FLJ52123, highly similar to Platelet-activating factor acetylhydrolase IB alpha subunit
Q9HBH5	RDH14	Retinol dehydrogenase 14
A0A0B4J2C3	TPT1	Translationally-controlled tumor protein
B4DE91		cDNA FLJ55534, highly similar to 4-trimethylaminobutyraldehyde dehydrogenase
Q9UID3	VPS51	Vacuolar protein sorting-associated protein 51 homolog
Q5U058	GAP43	Growth associated protein 43
B4DXX8		cDNA FLJ55545, highly similar to Zinc transporter 3
A0A024RD41	RAB23	RAB23, member RAS oncogene family, isoform CRA_a
C9J8Z4	IGSF8	Immunoglobulin superfamily member 8
Q99250	SCN2A	Sodium channel protein type 2 subunit alpha
O43678	NDUFA2	NADH dehydrogenase [ubiquinone] 1 alpha subcomplex subunit 2
B3KM74		cDNA FLJ10425 fis, clone NT2RP1000326, highly similar to Metaxin-2
Q53HV2		Chaperonin containing TCP1, subunit 7
B4DN50		Gap junction protein
B3KSQ7	DBN1	Drebrin 1, isoform CRA_d
B4DEJ3		cDNA FLJ51798, highly similar to Guanine nucleotide-binding protein G
K7ELW0	PARK7	Protein DJ-1
B8ZZQ6	PTMA	Prothymosin alpha
A0A024RDY9	ARHGEF7	Rho guanine nucleotide exchange factor
I4AY87	MIF	Macrophage migration inhibitory factor
A0A0A0MTP9	FAIM2	Protein lifeguard 2
A0A024R1I3	PDXP	Pyridoxal
Q8N6I2	ICAM5	ICAM5 protein
D3DNI2	PFN2	Profilin
A0A024R1U4	RAB5C	RAB5C, member RAS oncogene family, isoform CRA_a
Q7Z4X2		Neuronal protein
Q9H1V8	SLC6A17	Sodium-dependent neutral amino acid transporter SLC6A17
A0A024R2G0	SLC6A1	Transporter
H7BXE5		Deleted.
P14415	ATP1B2	Sodium/potassium-transporting ATPase subunit beta-2
Q9NS69	TOMM22	Mitochondrial import receptor subunit TOM22 homolog
U3KQ07	C12orf57	Protein C10
A0A024RB09	RAB5B	RAB5B, member RAS oncogene family, isoform CRA_a

B4DHR1		cDNA FLJ53009, highly similar to Calreticulin
A0A024R0E5	CAPZA1	Capping protein
A0A024R9Z0	NDUFA4	NADH dehydrogenase
A0A024R9D3	RPL30	Ribosomal protein L30, isoform CRA_b
A0A024R7M3	CSPG3	Chondroitin sulfate proteoglycan 3
Q9NZZ3	CHMP5	Charged multivesicular body protein 5
H0UI06	COX7A2	Cytochrome c oxidase subunit 7A2, mitochondrial
P49411	TUFM	Elongation factor Tu, mitochondrial
D3DP78	DARS	Aspartyl-tRNA synthetase, isoform CRA_b
P30050	RPL12	60S ribosomal protein L12
Q9Y6C9	MTCH2	Mitochondrial carrier homolog 2
P49419	ALDH7A1	Alpha-aminoadipic semialdehyde dehydrogenase
Q96QK1	VPS35	Vacuolar protein sorting-associated protein 35
A0A024R1Z6	VAT1	Vesicle amine transport protein 1 homolog
Q99714	HSD17B10	3-hydroxyacyl-CoA dehydrogenase type-2
Q9BZV1	UBXN6	UBX domain-containing protein 6
Q96QE2	SLC2A13	Proton myo-inositol cotransporter
Q01650	SLC7A5	Large neutral amino acids transporter small subunit 1
A2A274	ACO2	Aconitate hydratase, mitochondrial
A1YVW6	PRNP	Major prion protein
Q9NZQ3	NCKIPSD	NCK-interacting protein with SH3 domain
B4DJE7		cDNA FLJ52595, highly similar to Medium-chain specific acyl-CoA dehydrogenase, mitochondrial
A0A024R4B3	NDUFA10	NADH dehydrogenase [ubiquinone] 1 alpha subcomplex subunit 10, mitochondrial
P30084	ECHS1	Enoyl-CoA hydratase, mitochondrial
B2RAH7		cDNA, FLJ94921, highly similar to Homo sapiens prolyl endopeptidase
Q9Y2I8	WDR37	WD repeat-containing protein 37
Q8TBG9	SYNPR	Synaptoporin
Q5QNZ2	ATP5F1	ATP synthase F
B5MCD7	SYNGR1	Synaptogyrin-1
Q8TF61	FBXO41	F-box only protein 41
B3KTR3		Chloride intracellular channel protein
Q2VYF8		Lysophospholipase-like protein
A0A0A0MRE6	WDR47	WD repeat-containing protein 47

B4DJ44		cDNA FLJ54716, highly similar to Target of Myb protein 1
A0A024R4X9	SULT4A1	Sulfotransferase
Q9C0D0	PHACTR1	Phosphatase and actin regulator 1
J3KPX7	PHB2	Prohibitin-2
V9HW21	HEL-76	Epididymis luminal protein 76
A8K607		cDNA FLJ76855, highly similar to Homo sapiens exportin 7
A0A024RC87	RNH1	Ribonuclease/angiogenin inhibitor 1, isoform CRA_a
A0A087X165	SRCIN1	SRC kinase-signaling inhibitor 1
Q9UK22	FBXO2	F-box only protein 2
B1ANH5	GUK1	Guanylate kinase
B7Z899		Aminopeptidase
A0A024R640	AGPAT5	1-acylglycerol-3-phosphate O-acyltransferase 5
A0A024R0K3	BCKDHA	Branched chain keto acid dehydrogenase E1, alpha polypeptide, isoform CRA_a
H3BQ06		Uncharacterized protein
A0A087WT45	GRIPAP1	GRIP1-associated protein 1
E5RJR5	SKP1	S-phase kinase-associated protein 1
V9HWA6	HEL32	Epididymis luminal protein 32
O43236	Sep4	Septin-4
B2RCU8		cDNA, FLJ96301, highly similar to Homo sapiens limbic system-associated membrane protein
P62877	RBX1	E3 ubiquitin-protein ligase RBX1
H0YLU7	ETFA	Electron transfer flavoprotein subunit alpha, mitochondrial
A0A024R814	RPL7	Ribosomal protein L7, isoform CRA_a
A0A024R702	CGI-38	Brain specific protein, isoform CRA_a
M0R210	RPS16	40S ribosomal protein S16
V9HW96	HEL-S-100n	Chaperonin containing TCP1, subunit 2
A0A024R371	ARL6IP5	PRA1 family protein
P30049	ATP5D	ATP synthase subunit delta, mitochondrial
Q14643	ITPR1	Inositol 1,4,5-trisphosphate receptor type 1
V9HWE0	HEL-S-7	Annexin
Q8N5J2	MINDY1	Ubiquitin carboxyl-terminal hydrolase MINDY-1
A0A024R3X4	HSPD1	Heat shock 60kDa protein 1
B7Z5A7		cDNA FLJ57557, highly similar to Solute carrier family 2, facilitated glucose transporter member 3
P43155	CRAT	Carnitine O-acetyltransferase

C9JKM9	XPO1	Exportin-1
A4D1U3	SSBP1	Single-stranded DNA binding protein 1
Q8TET0	FLJ00095	FLJ00095 protein
Q53Y06	ATP6V1E1	ATPase, H+ transporting, lysosomal 31kDa, V1 subunit E isoform 1
Q1JQ76	RPL10A	Ribosomal protein
A0A024R830	IMPA1	Inositol-1-monophosphatase
P14854	COX6B1	Cytochrome c oxidase subunit 6B1
A0A087WYB4	STOML2	Stomatin-like protein 2, mitochondrial
H3BU31	RPL4	60S ribosomal protein L4
Q6IB76	NDUFV2	NDUFV2 protein
K7EKU3	FXYD7	FXYD domain-containing ion transport regulator 7
A0A024R222	PSAT1	Phosphoserine aminotransferase
A0A024R520	SYT7	Synaptotagmin VII, isoform CRA_b
Q9NQ66	PLCB1	1-phosphatidylinositol 4,5-bisphosphate phosphodiesterase beta-1
B7Z2F8		cDNA FLJ59320, highly similar to Tyrosine-protein phosphatase non-receptor type5
Q9GZV7	HAPLN2	Hyaluronan and proteoglycan link protein 2
K7EPN1	ROGDI	Protein rogdi homolog
A6NF51	BPNT1	3'
A0A024R230	NTRK2	Tyrosine-protein kinase receptor
Q9Y3F4	STRAP	Serine-threonine kinase receptor-associated protein
Q9UNS2	COPS3	COP9 signalosome complex subunit 3
B2RBN7		cDNA, FLJ95607, highly similar to Homo sapiens breast carcinoma amplified sequence 3
O60268	KIAA0513	Uncharacterized protein KIAA0513
A0A024RBB7	NAP1L1	Nucleosome assembly protein 1-like 1, isoform CRA_a
H0YK42	SNX1	Sorting nexin-1
A0A087WW77	LLGL1	Lethal
A0A087WXB0	SCAMP1	Secretory carrier-associated membrane protein
A0A0A0MRJ6	PCMT1	Protein-L-isoaspartate O-methyltransferase
A0A024R4S1	EPN1	Epsin 1, isoform CRA_a
Q8NHG7	SVIP	Small VCP/p97-interacting protein
A0A024RB32	PTGES3	Prostaglandin E synthase 3
A0A024R884	TNC	Tenascin C

B2R5T5	PRKAR1A	Protein kinase, cAMP-dependent, regulatory, type I, alpha
Q8N3F0	MTURN	Maturin
Q4J6C6	PREPL	Prolyl endopeptidase-like
A2A2D0	STMN1	Stathmin
A0A024RBA9	RAB21	RAB21, member RAS oncogene family, isoform CRA_a
A0A024RAD8	ALDH4A1	Aldehyde dehydrogenase 4 family, member A1, isoform CRA_a
J3QT77	PON2	Serum paraoxonase/arylesterase 2
A0A024RBP6	CAMKK2	Calcium/calmodulin-dependent protein kinase kinase 2, beta, isoform CRA_b
B3KTN5		cDNA FLJ38538 fis, clone HCHON2001407, highly similar to LanC-like protein 2
A0A024R5P0	PAK1	p21/Cdc42/Rac1-activated kinase 1
A0A024R7G6	EPS15L1	Epidermal growth factor receptor pathway substrate 15-like 1, isoform CRA_a
B4DZF8		Serine/threonine-protein phosphatase 2A activator
P14621	ACYP2	Acylphosphatase-2
Q07960	ARHGAP1	Rho GTPase-activating protein 1
A0A024RD97	SLC4A4	Anion exchange protein
A0A024R0C3	NNT	Nicotinamide nucleotide transhydrogenase, isoform CRA_a
D3YTA9	PPP3R1	Calcineurin subunit B type 1
Q53R19	ARPC2	Arp2/3 complex 34 kDa subunit
Q5JR94	RPS8	40S ribosomal protein S8
B2R960		cDNA, FLJ94230, highly similar to Homo sapiens thioredoxin-like 1
A0A024R6S1	DNAJA2	DnaJ
A8KA83		cDNA FLJ78586, highly similar to Homo sapiens VAMP
A0A024RD93	PAICS	Phosphoribosylaminoimidazole carboxylase, phosphoribosylaminoimidazole succinocarboxamide synthetase, isoform CRA_c
Q96ID5	IGSF21	Immunoglobulin superfamily member 21
B2R5W6		cDNA, FLJ92661, highly similar to Homo sapiens microtubule-associated protein, RP/EB family, member 3
P38606	ATP6V1A	V-type proton ATPase catalytic subunit A
B4E325		cDNA FLJ54048, highly similar to 55 kDa erythrocyte membrane protein
H7BY35	RYR2	Ryanodine receptor 2
B4DEQ0		cDNA FLJ59482, highly similar to Electron transfer flavoprotein-ubiquinone oxidoreductase, mitochondrial
G3V4P8	GMFB	Glia maturation factor beta
B3KY04		cDNA FLJ46506 fis, clone THYMU3030752, highly similar to BTB/POZ domain-containing protein KCTD12
Q9UNE7	STUB1	E3 ubiquitin-protein ligase CHIP
A0A0A0MS51	GSN	Gelsolin

P41208	CETN2	Centrin-2
F8WF69	CLTA	Clathrin light chain
V9HWC7	HEL-S-128m	Epididymis secretory sperm binding protein Li 128m
A0A087X0T8	CADM1	Cell adhesion molecule 1
Q9HCH3	CPNE5	Copine-5
A4D1X5	ELMO1	Engulfment and cell motility 1
Q9Y2J0	RPH3A	Rabphilin-3A
B3KM34		cDNA FLJ10132 fis, clone HEMBA1003046, highly similar to Mitochondrial-processing peptidase subunit beta, mitochondrial
Q9P0J0	NDUFA13	NADH dehydrogenase [ubiquinone] 1 alpha subcomplex subunit 13
Q6IB11	PGRMC1	PGRMC1 protein
A0A024R240	GNAQ	Guanine nucleotide binding protein
J3KN10		Deleted.
Q0VAS5	HIST1H4H	Histone H4
B4DJ12		cDNA FLJ58355, highly similar to Tyrosine-protein phosphatase non-receptor type 23
A0A024RAP3	CSPG2	Chondroitin sulfate proteoglycan 2
A0A024QZM6	SEC24C	SEC24 related gene family, member C
Q7Z6L0	PRRT2	Proline-rich transmembrane protein 2
P48066	SLC6A11	Sodium- and chloride-dependent GABA transporter 3
A0A024R331	CAMKV	CaM kinase-like vesicle-associated, isoform CRA_c
A0A024RDG1	VDP	Vesicle docking protein p115, isoform CRA_a
P09496	CLTA	Clathrin light chain A
F8W7Q4	FAM162A	Protein FAM162A
A0A024RAS8	HEBP1	Heme binding protein 1, isoform CRA_a
H0Y390	MACF1	Microtubule-actin cross-linking factor 1, isoforms 1/2/3/5
Q9Y6M9	NDUFB9	NADH dehydrogenase [ubiquinone] 1 beta subcomplex subunit 9
Q96A00	PPP1R14A	Protein phosphatase 1 regulatory subunit 14A
A0A0A1HAN9		H.sapiens ras-related Hrab5 protein
B2RCM3		cDNA, FLJ96158, highly similar to Homo sapiens calpain 2,
A0A024R475	CUL3	Cullin 3, isoform CRA_a
A0A024QZ30	SDHA	Succinate dehydrogenase [ubiquinone] flavoprotein subunit, mitochondrial
O14495	PLPP3	Phospholipid phosphatase 3
A0A024R9U3	OCIAD1	OCIA domain containing 1, isoform CRA_a
P13073	COX4I1	Cytochrome c oxidase subunit 4 isoform 1, mitochondrial

A0A024RAZ7	HNRPA1	Heterogeneous nuclear ribonucleoprotein A1, isoform CRA_b
O00408	PDE2A	cGMP-dependent 3',5'-cyclic phosphodiesterase
A0A024R2P0	RPSA	40S ribosomal protein SA
A0A024R5F4	CPT1A	Carnitine palmitoyltransferase 1A
A0A024R104	CNTN1	Contactin 1, isoform CRA_a
B4DH45		cDNA FLJ53322, highly similar to Homo sapiens sorbin and SH3 domain containing 1
E5RH77	RPS14	40S ribosomal protein S14
P09382	LGALS1	Galectin-1
Q15907	RAB11B	Ras-related protein Rab-11B
O94919	ENDOD1	Endonuclease domain-containing 1 protein
A0A024QZD1	RPL18	Ribosomal protein L18, isoform CRA_c
A0A024R4E2	TARDBP	TAR DNA binding protein, isoform CRA_b
A0A024R2M6	ACAA1	Acetyl-Coenzyme A acyltransferase 1
Q5VWJ9	SNX30	Sorting nexin-30
P22695	UQCRC2	Cytochrome b-c1 complex subunit 2, mitochondrial
X1WI28	RPL10	60S ribosomal protein L10
H0YCJ7	RPS3	40S ribosomal protein S3
B2R6A3		Na
G3V1M7	ACADVL	Very long-chain-specific acyl-CoA dehydrogenase, mitochondrial
A0A024R9W8	SLC30A9	Solute carrier family 30
Q9Y512	SAMM50	Sorting and assembly machinery component 50 homolog
Q53G72		B-cell receptor-associated protein 31 variant
Q9UBV8	PEF1	Peflin
Q6PUJ7	HEL-215	Epididymis luminal protein 215
D3DVA5	ARHGEF2	Rho/rac guanine nucleotide exchange factor
B2R6C4		Receptor expression-enhancing protein
B4DDU6		cDNA FLJ50442, highly similar to T-complex protein 1 subunit epsilon
I3L1P8	SLC25A11	Mitochondrial 2-oxoglutarate/malate carrier protein
P25786	PSMA1	Proteasome subunit alpha type-1
B7Z3H2		cDNA FLJ53370, highly similar to Mus musculus cytoplasmic FMR1 interacting protein 2
G3XHN4	CADM2	Cell adhesion molecule 2 isoform 4
A0A024R1Q8	RPL23	Ribosomal protein L23, isoform CRA_b
B7Z3Y2		cDNA FLJ51879, highly similar to Prenylcysteine oxidase

Q96FE5	LINGO1	Leucine-rich repeat and immunoglobulin-like domain-containing nogo receptor-interacting protein 1
P56134	ATP5J2	ATP synthase subunit f, mitochondrial
A4D1I7	DNCI1	Dynein, cytoplasmic 1, intermediate chain 1, isoform CRA_e
Q6LES2	ANXA4	Annexin
O00429	DNM1L	Dynamin-1-like protein
Q8N126	CADM3	Cell adhesion molecule 3
A0A024R6I3	TMED10	Testicular tissue protein Li 206
Q5SZK4	WASF1	Wiskott-Aldrich syndrome protein family member 1
A0A024R3M7	NRGN	Neurogranin
B5BU41	CAMK1	Calcium/calmodulin-dependent protein kinase I
Q9UQ03	CORO2B	Coronin-2B
Q08AL8	ADAM22	ADAM metallopeptidase domain 22
H0YB26	CPNE3	Copine-3
A0A024RB99	SHMT2	Serine hydroxymethyltransferase
Q14894	CRYM	Ketimine reductase mu-crystallin
A0A024RBE8	SLC25A3	Solute carrier family 25
B4DKX6		cDNA FLJ53584, highly similar to Desmoplakin
Q8TC12	RDH11	Retinol dehydrogenase 11
Q9UBQ7	GRHPR	Glyoxylate reductase/hydroxypyruvate reductase
A0A024R9B7	COX6C	Cytochrome c oxidase subunit VIc, isoform CRA_a
Q53FM7		NADH dehydrogenase
I3L4C2	BAIAP2	Brain-specific angiogenesis inhibitor 1-associated protein 2
V9HW44	HEL-S-303	Epididymis secretory protein Li 303
A8K761	NDUFB10	NADH dehydrogenase
O00186	STXBP3	Syntaxin-binding protein 3
Q9NUP9	LIN7C	Protein lin-7 homolog C
B4DUX0		cDNA FLJ60167, highly similar to Cytosolic acyl coenzyme A thioester hydrolase
B2R4D5		Actin-related protein 2/3 complex subunit 3
A0A024R1I8	SYN3	Synapsin III, isoform CRA_f
A0A024R0E2	CSDE1	Cold shock domain containing E1, RNA-binding, isoform CRA_a
B3KM95		Phosphatidate cytidylyltransferase
B4DJB4		Isocitrate dehydrogenase [NAD] subunit, mitochondrial
Q7Z759	CCT8	CCT8 protein

B4DID5	TALDO1	Transaldolase 1, isoform CRA_c
A0A024RCN6	VARS	VARS
Q7Z4S6	KIF21A	Kinesin-like protein KIF21A
Q68CN5	DKFZp686D17136	Uncharacterized protein DKFZp686D17136
A0A024RCT2	VPS52	Vacuolar protein sorting 52
B2R995		Malic enzyme
C9JFZ1	SYNJ1	Synaptojanin-1
A0A024R4G1	LRRC47	Leucine rich repeat containing 47, isoform CRA_a
H9NIL8	GABBR2	Gamma-aminobutyric acid
Q08722	CD47	Leukocyte surface antigen CD47
H3BP57	MPI	Mannose-6-phosphate isomerase
H3BUX2	CYB5B	Cytochrome b5 type B
A0A024QZ63	hCG_27198	HCG27198, isoform CRA_c
Q06AH7	TF	Transferrin
A0A024RB16	FAM62A	Family with sequence similarity 62
A0A087WWT1	SDHB	Succinate dehydrogenase [ubiquinone] iron-sulfur subunit, mitochondrial
P63215	GNG3	Guanine nucleotide-binding protein G
E9PMA0	AIFM1	Apoptosis-inducing factor 1, mitochondrial
Q9H0Q0	FAM49A	Protein FAM49A
Q8N6T3	ARFGAP1	ADP-ribosylation factor GTPase-activating protein 1
Q6U841	SLC4A10	Sodium-driven chloride bicarbonate exchanger
Q3B7A7	GART	Trifunctional purine biosynthetic protein adenosine-3 [Includes: Phosphoribosylamine--glycine ligase
A0A024R6R7	MT3	Metallothionein
U3KPS5	TPI1	Triosephosphate isomerase
B3KNR9		cDNA FLJ30276 fis, clone BRACE2002736, highly similar to Fructosamine-3-kinase
C9JUG7	CAPZA2	F-actin-capping protein subunit alpha-2
D3DUG9	USP14	Ubiquitin specific peptidase 14
Q4W4Y1	DRIP4	Dopamine receptor interacting protein 4
A0A024R7F1	PRKCSH	Protein kinase C substrate 80K-H, isoform CRA_a
H0Y2W2	ATAD3A	ATPase family AAA domain-containing protein 3A
B3KU62		cDNA FLJ39243 fis, clone OCBBF2008283, highly similar to Protein NDRG1

Q6LET3	HPRT1	HPRT1 protein
A0A024R0L5	GSK3A	Glycogen synthase kinase 3 alpha, isoform CRA_a
B3KQT9		Protein disulfide-isomerase
B2R5S3		cDNA, FLJ92597, highly similar to Homo sapiens NFS1 nitrogen fixation 1
I6L8B7	FABP5	Fatty acid-binding protein, epidermal
B4DV28		cDNA FLJ54170, highly similar to Cytosolic nonspecific dipeptidase
Q9H1Z4	WDR13	WD repeat-containing protein 13
A0A024RDL1	CCT6A	Chaperonin containing TCP1, subunit 6A
Q9UIW2	PLXNA1	Plexin-A1
Q96L92	SNX27	Sorting nexin-27
Q9NP72	RAB18	Ras-related protein Rab-18
E5KLJ5	OPA1	Dynamin-like 120 kDa protein, mitochondrial
P15882	CHN1	N-chimaerin
A0A087WW40	SH3GLB1	Endophilin-B1
A8MWU7	GABRG2	Gamma-aminobutyric acid receptor subunit gamma-2
P23526	AHCY	Adenosylhomocysteinase
Q53X12		V-type proton ATPase subunit a
P53677	AP3M2	AP-3 complex subunit mu-2
M0R1L2	PGLS	6-phosphogluconolactonase
E5RHG6	TBCA	Tubulin-specific chaperone A
A8K4V2		cDNA FLJ75930, highly similar to Homo sapiens NADH dehydrogenase
H0Y2P0	CD44	CD44 antigen
Q6P587	FAHD1	Acylpyruvase FAHD1, mitochondrial
A0A024R745	NDUFA5	NADH dehydrogenase
A0A024RBR4	HIP1R	Huntingtin interacting protein 1 related, isoform CRA_a
B2RAY1		cDNA, FLJ95184, highly similar to Homo sapiens signal transducing adaptor molecule
A0A024R683	ATP6V1D	ATPase, H+ transporting, lysosomal 34kDa, V1 subunit D, isoform CRA_a
B3KQJ0		cDNA FLJ90530 fis, clone NT2RP4002187, highly similar to Homo sapiens hydroxysteroid
H0YKT8	PSMA4	Proteasome subunit beta type
J3KTF8	ARHGDIA	Rho GDP-dissociation inhibitor 1
A6NP24	CRYZ	Quinone oxidoreductase
Q6FHM4	COX5B	COX5B protein

Q9UL26	RAB22A	Ras-related protein Rab-22A
B4DM97		cDNA FLJ55002, highly similar to Alpha-centractin
Q59FC3		G protein-coupled receptor kinase interactor 1 variant
A0A024R6C9	DLST	Dihydrolipoamide S-succinyltransferase
A8CDT9		MYO5A variant protein
Q5VZ30	GAD2	Glutamate decarboxylase 2
B4DM84		cDNA FLJ60694, highly similar to Deubiquitinating protein VCIP135
B4DMM4		cDNA FLJ60304, highly similar to Rab GTPase-binding effector protein 1
A0A024R798	SLC44A2	Choline transporter-like protein 2 isoform 2
Q8N111	CEND1	Cell cycle exit and neuronal differentiation protein 1
A0A024R5C5	PC	Pyruvate carboxylase
Q9UJD0	RIMS3	Regulating synaptic membrane exocytosis protein 3
Q6FHY4	NAPG	N-ethylmaleimide-sensitive factor attachment protein, gamma, isoform CRA_b
A0A024RC33	MAPRE2	Microtubule-associated protein, RP/EB family, member 2, isoform CRA_a
B1AHR1	Sept3	Neuronal-specific septin-3
B3KNN7		cDNA FLJ30049 fis, clone ADRGL1000033, highly similar to 26S proteasome non-ATPase regulatory subunit 3
Q8N2K0	ABHD12	Monoacylglycerol lipase ABHD12
A0A0B4J2A4	ACAA2	3-ketoacyl-CoA thiolase, mitochondrial
E5RIY1	PPP2R2A	Serine/threonine-protein phosphatase 2A 55 kDa regulatory subunit B alpha isoform
Q6IPH7	RPL14	RPL14 protein
B2RDW1	RPS27A	Epididymis luminal protein 112
H3BNX8	COX5A	Cytochrome c oxidase subunit 5A, mitochondrial
B4DPP0		cDNA FLJ51032, highly similar to CD9 antigen
A0A024R6W0	GOT2	Aspartate aminotransferase
P31689	DNAJA1	DnaJ homolog subfamily A member 1
Q99426	TBCB	Tubulin-folding cofactor B
S4R435	RPS10-NUDT3	RPS10-NUDT3 readthrough
A8YXX4	PIG59	Glutamine synthetase
B7Z792		cDNA FLJ53932, highly similar to NADH-ubiquinone oxidoreductase 49 kDa subunit, mitochondrial
Q2VPJ0	FOLH1	FOLH1 protein
P42263	GRIA3	Glutamate receptor 3
V9HWC9	HEL-S-44	Superoxide dismutase [Cu-Zn]
A0A087WY55	VTA1	Chromosome 6 open reading frame 55, isoform CRA_b

Q9Y2Z4	YARS2	Tyrosine--tRNA ligase, mitochondrial
Q9BST9	RTKN	Rhotekin
A0A087WWT8	GDAP1L1	Ganglioside-induced differentiation-associated protein 1-like 1
F8WAV2	GABBR1	Gamma-aminobutyric acid type B receptor subunit 1
P17987	TCP1	T-complex protein 1 subunit alpha
A0A0A0MRI6		Deleted.
B4E1E2		cDNA FLJ61530, highly similar to Hepatocyte growth factor-regulated tyrosine kinase substrate
B4DZX1		cDNA FLJ53892, highly similar to Pantothenate kinase 4
R4GNH3	PSMC3	26S proteasome regulatory subunit 6A
A0A024R159	HSDL2	Hydroxysteroid dehydrogenase like 2, isoform CRA_c
B2RB13		cDNA, FLJ95253, highly similar to Homo sapiens acyl-CoA synthetase long-chain family member 6
Q2NLC8	GSTK1	GSTK1 protein
A0A024RCR6	BAT3	BAG6
A0A024QZT9	NQO2	NAD
P10768	ESD	S-formylglutathione hydrolase
B3KWF8		cDNA FLJ43009 fis, clone BRTHA2015406, highly similar to BR serine/threonine-protein kinase 1
B2RBS8		cDNA, FLJ95666, highly similar to Homo sapiens albumin
J3KS22	DCXR	L-xylulose reductase
Q59HA9		Glutamate [NMDA] receptor subunit epsilon 2 variant
Q9NPJ3	ACOT13	Acyl-coenzyme A thioesterase 13
C9J826	JUP	Junction plakoglobin
P07954	FH	Fumarate hydratase, mitochondrial
Q7Z6G3	NECAB2	N-terminal EF-hand calcium-binding protein 2
V9HWF4	HEL-S-68p	Phosphoglycerate kinase
B2RDY9		Adenylyl cyclase-associated protein
J3KR97	TBCD	Tubulin-specific chaperone D
E5KRK5	NDUFS1	Mitochondrial NADH-ubiquinone oxidoreductase 75 kDa subunit
Q14DD4	STXBP5	Syntaxin binding protein 5
Q14204	DYNC1H1	Cytoplasmic dynein 1 heavy chain 1
Q0QEN7	ATP5B	ATP synthase subunit beta
H0YI72	ANKS1B	Ankyrin repeat and sterile alpha motif domain-containing protein 1B
A0A024QZN9	VDAC2	Voltage-dependent anion channel 2, isoform CRA_a

E9PQQ8	AK5	Adenylate kinase isoenzyme 5
A0A024RDE1	SPARCL1	SPARC-like 1
E9PF63	ROCK2	Rho-associated protein kinase 2
Q8TBT6		Uncharacterized protein
A0A024R896	SH3GLB2	SH3-domain GRB2-like endophilin B2, isoform CRA_a
Q14257	RCN2	Reticulocalbin-2
P05165	PCCA	Propionyl-CoA carboxylase alpha chain, mitochondrial
B4DH47		cDNA FLJ53769, highly similar to Homo sapiens nebulette
B2RCK1		Voltage-dependent calcium channel gamma subunit
A0A024RA98	PADI2	Peptidyl arginine deiminase, type II, isoform CRA_a
B7Z582		Annexin
Q15120	PDK3	[Pyruvate dehydrogenase
B4YAH7	ALDH2	ALDH2
Q8TEA8	DTD1	D-tyrosyl-tRNA
A0A024R4E3	KCNAB2	Potassium voltage-gated channel, shaker-related subfamily, beta member 2, isoform CRA_a
E9PR44	CRYAB	Alpha-crystallin B chain
Q5T8U3	RPL7A	60S ribosomal protein L7a
E7EPC8	CTNND2	Catenin delta-2
B2RB06		cDNA, FLJ95242, highly similar to Homo sapiens L-3-hydroxyacyl-Coenzyme A dehydrogenase, short chain
Q08AM6	VAC14	Protein VAC14 homolog
A0A024RDY0	RANBP5	RAN binding protein 5, isoform CRA_d
B2RDG9		cDNA, FLJ96603, highly similar to Homo sapiens actin-related protein 10 homolog
B4DVZ9		cDNA FLJ61177, highly similar to Phosphatidylinositol-4-phosphate 5-kinasetype-1 gamma
A0A024R3Z5	LANCL1	LanC lantibiotic synthetase component C-like 1
G3V0I5	NDUFV1	NADH dehydrogenase [ubiquinone] flavoprotein 1, mitochondrial
A0A024R977	ARL8A	ADP-ribosylation factor-like 8A, isoform CRA_a
A0A024R118	METTL7A	Methyltransferase like 7A, isoform CRA_a
H3BQI7	HSDL1	Inactive hydroxysteroid dehydrogenase-like protein 1
Q9UBB4	ATXN10	Ataxin-10
J3QSB4	RPL13	60S ribosomal protein L13
E9PCG9	BDH1	D-beta-hydroxybutyrate dehydrogenase, mitochondrial
A8K132		cDNA FLJ75476, highly similar to Homo sapiens glutaminase
Q7Z4W8		Heparin-binding protein HBp15

B7Z766		cDNA FLJ54564, highly similar to 150 kDa oxygen-regulated protein
D6RAS9	RASGRF2	Ras-specific guanine nucleotide-releasing factor 2
Q09470	KCNA1	Potassium voltage-gated channel subfamily A member 1
A0A0A0MRU0	MPP2	MAGUK p55 subfamily member 2
A0A024RCG3	CARS	Cysteinyl-tRNA synthetase, isoform CRA_a
E7EP65	ABI2	Abl interactor 2
A8K651		cDNA FLJ75700, highly similar to Homo sapiens complement component 1, q subcomponent binding protein
P61160	ACTR2	Actin-related protein 2
F8VRD8	NDUFA12	NADH dehydrogenase [ubiquinone] 1 alpha subcomplex subunit 12
Q8WXF7	ATL1	Atlastin-1
Q9NVH1	DNAJC11	DnaJ homolog subfamily C member 11
A0A024R231	GDA	Guanine deaminase, isoform CRA_b
A8K143		cDNA FLJ75342, highly similar to Homo sapiens solute carrier family 12,
B3KRM2		Serine/threonine-protein phosphatase
J3QRS3	MYL12A	Myosin regulatory light chain 12A
A0A0A0MTJ9	NCEH1	Neutral cholesterol ester hydrolase 1
A5PLQ8	C6orf174	C6orf174 protein
I6TRR8		SND1-BRAF fusion
Q9UJW0	DCTN4	Dynactin subunit 4
A0A024RAI1	ACTR3	ARP3 actin-related protein 3 homolog
Q6ZMI0	PPP1R21	Protein phosphatase 1 regulatory subunit 21
S4R305	DNAJC6	Putative tyrosine-protein phosphatase auxilin
H0YH82	CS	Citrate synthase, mitochondrial
B4E1Q7		cDNA FLJ57294, highly similar to Lipoamide acyltransferase component of branched-chain alpha-keto acid dehydrogenase complex, mitochondrial
A0A024R611	CORO1A	Coronin
P17174	GOT1	Aspartate aminotransferase, cytoplasmic
H3BNQ7	ABAT	4-aminobutyrate aminotransferase, mitochondrial
V9HW33	HEL-S-5a	Epididymis secretory sperm binding protein Li 5a
B3KX11		T-complex protein 1 subunit gamma
D3DP75	RAB3GAP1	RAB3 GTPase activating protein subunit 1
P81605	DCD	Dermcidin
A0A024R497	ACSL3	Acyl-CoA synthetase long-chain family member 3, isoform CRA_a

A0A024R7B7	CDC37	CDC37 cell division cycle 37 homolog
B3KW21		cDNA FLJ41945 fis, clone PLACE6019676, highly similar to Coatomer subunit gamma
B2R514		cDNA, FLJ92300, Homo sapiens COP9 subunit 6
E5KSU5	TFAM	Mitochondrial transcription factor A
G3V113	UBE2V2	Ubiquitin-conjugating enzyme E2 variant 2
Q96IX5	USMG5	Up-regulated during skeletal muscle growth protein 5
A0A024RBS2	RPLP0	60S acidic ribosomal protein P0
A0A087WT44	HMOX2	Heme oxygenase 2
P08247	SYP	Synaptophysin
B4DRV2	SUCLA2	Succinate--CoA ligase [ADP-forming] subunit beta, mitochondrial
P23677	ITPKA	Inositol-trisphosphate 3-kinase A
Q2NLC9	PURA	PURA protein
K7EQQ3	KRT9	Keratin, type I cytoskeletal 9
B4DZP5		cDNA FLJ51165, highly similar to DNA damage-binding protein 1
O15240	VGF	Neurosecretory protein VGF [Cleaved into: Neuroendocrine regulatory peptide-1
Q8N573	OXR1	Oxidation resistance protein 1
P25686	DNAJB2	DnaJ homolog subfamily B member 2
C9JF17	APOD	Apolipoprotein D
B2R9M7		Protein kinase C epsilon type
Q6NX51	EXOC4	Exocyst complex component 4
B4DG62		cDNA FLJ56506, highly similar to Hexokinase-1
A0A087WUW9	ARL15	ADP-ribosylation factor-like protein 15
P31930	UQCRC1	Cytochrome b-c1 complex subunit 1, mitochondrial
Q9Y639	NPTN	Neuroplastin
B3KS36		cDNA FLJ35376 fis, clone SKMUS2004044, highly similar to Homo sapiens ribosomal protein L3
A4D1U5	FLJ10842	Multiple substrate lipid kinase, isoform CRA_a
A0A024R156	hCG_1994888	Guanine nucleotide-binding protein subunit gamma
B3KSI7		cDNA FLJ36374 fis, clone THYMU2008185, highly similar to Xaa-Pro aminopeptidase 1
P47985	UQCRFS1	Cytochrome b-c1 complex subunit Rieske, mitochondrial
O94772	LY6H	Lymphocyte antigen 6H
A0A096LNH5	LOC102724023	Uncharacterized protein
A0A024R4Q8	RPS5	Ribosomal protein S5, isoform CRA_a

P78357	CNTNAP1	Contactin-associated protein 1
A0A024R4X0	CYB5R3	NADH-cytochrome b5 reductase
A0A087WXS7	ASNA1	ATPase ASNA1
Q6LAP8		Mitochondrial citrate transport protein
A0A024R9M9	CHP	Calcium binding protein P22, isoform CRA_a
Q6FGP0	MRAS	MRAS protein
P55327	TPD52	Tumor protein D52
B4DM22		cDNA FLJ53357, highly similar to 26S proteasome non-ATPase regulatory subunit 2
J3KSJ8	PPP1R1B	Protein phosphatase 1 regulatory subunit 1B
Q9P2U7	SLC17A7	Vesicular glutamate transporter 1
P28074	PSMB5	Proteasome subunit beta type-5
V9HVZ4	HEL-S-162eP	Glyceraldehyde-3-phosphate dehydrogenase
Q59F93		Glutamate receptor, ionotropic, AMPA 2 variant
Q05DH1	PSMA7	Proteasome subunit alpha type
A8K4K9		cDNA FLJ76169
A0A024R9I0	ATP6V1C1	V-type proton ATPase subunit C
Q9P2R3	ANKFY1	Rabankyrin-5
H0Y9Y4	RPS3A	40S ribosomal protein S3a
Q9UPV7	PHF24	PHD finger protein 24
B7Z2Z8		T-complex protein 1 subunit delta
B2R6S5	CMPK	UMP-CMP kinase
Q53HB3		Proteasome 26S ATPase subunit 1 variant
Q9C040	TRIM2	Tripartite motif-containing protein 2
Q8N9R8	SCAI	Protein SCAI
A0A024RCR2	GNL1	GNL1
A8KAK1		cDNA FLJ77398, highly similar to Homo sapiens UDP-glucose ceramide glucosyltransferase-like 1, transcript variant 2, mRNA
A0A024R4Z9	SBF1	SET binding factor 1, isoform CRA_a
A0A023QZ25	COX2	Cytochrome c oxidase subunit 2
P07737	PFN1	Profilin-1
Q92823	NRCAM	Neuronal cell adhesion molecule
Q7RTP6	MICAL3	[F-actin]-methionine sulfoxide oxidase MICAL3
Q9NQR4	NIT2	Omega-amidase NIT2
Q5TH30	NDRG3	NDRG family member 3, isoform CRA_c

Q5SQQ7	CAMK1D	Calcium/calmodulin-dependent protein kinase ID, isoform CRA_b
P16389	KCNA2	Potassium voltage-gated channel subfamily A member 2
Q9BYB0	SHANK3	SH3 and multiple ankyrin repeat domains protein 3
B4DDH8		cDNA FLJ55184, highly similar to Homo sapiens leukocyte receptor cluster
B2R7T8		cDNA, FLJ93598, highly similar to Homo sapiens capping protein
J3KPJ3	CAMKK1	Calcium/calmodulin-dependent protein kinase kinase 1
A0A024R4D1	COPS8	COP9 constitutive photomorphogenic homolog subunit 8
K7EMT4		Uncharacterized protein
Q15084	PDIA6	Protein disulfide-isomerase A6
Q8NBX0	SCCPDH	Saccharopine dehydrogenase-like oxidoreductase
E5RHW4	ERLIN2	Erlin-2
Q6DHX1	C2CD2L	C2CD2L protein
B1AKC9	EPHB2	Ephrin type-B receptor 2
D9IAI1	PEBP1	Epididymis secretory protein Li 34
A3KLL5	ATP1B1	Sodium/potassium-transporting ATPase subunit beta
Q53FW2		Phosphoribosyl pyrophosphate synthetase 1 variant
A0A024R8B2	FREQ	Frequenin homolog
Q3ZCU5	DLG4	DLG4 protein
D6W648	hCG_2004001	HCG2004001, isoform CRA_b
O43765	SGTA	Small glutamine-rich tetratricopeptide repeat-containing protein alpha
A0A087WUK0		Deleted.
S4R371	FABP3	Fatty acid-binding protein, heart
B3KTX4		cDNA FLJ38923 fis, clone NT2NE2011823, highly similar to Dynactin subunit 2
V9HW90	HEL-75	Epididymis luminal protein 75
P49588	AARS	Alanine--tRNA ligase, cytoplasmic
Q9UMB8		EEN-2B-L3
Q8N335	GPD1L	Glycerol-3-phosphate dehydrogenase 1-like protein
A0A024RCH0	TCEAL6	Transcription elongation factor A
Q8TBX8	PIP4K2C	Phosphatidylinositol 5-phosphate 4-kinase type-2 gamma
A0A024QZN7	C10orf70	Chromosome 10 open reading frame 70, isoform CRA_b
Q15323	KRT31	Keratin, type I cuticular Ha1
P56556	NDUFA6	NADH dehydrogenase [ubiquinone] 1 alpha subcomplex subunit 6
P13639	EEF2	Elongation factor 2

Q53G58		Coronin
P51149	RAB7A	Ras-related protein Rab-7a
Q3ZCW5	SUCLG2	Succinate-CoA ligase subunit beta
B4DQG5		cDNA FLJ54122, highly similar to Cytosol aminopeptidase
A0A024R9W7	TMEM33	Transmembrane protein 33, isoform CRA_a
V9HWB9	HEL-S-133P	L-lactate dehydrogenase
A0A0A0MTP4	DLGAP1	Disks large-associated protein 1
A0A024R0Q7	PPP5C	Serine/threonine-protein phosphatase
B3KR70		cDNA FLJ33764 fis, clone BRCOC2000360, highly similar to Vacuolar ATP synthase subunit S1
P38117	ETFB	Electron transfer flavoprotein subunit beta
B2R659		cDNA, FLJ92803, highly similar to Homo sapiens hydroxysteroid
P36405	ARL3	ADP-ribosylation factor-like protein 3
A0A087X2G1	DDX1	ATP-dependent RNA helicase DDX1
B5BUI8	DUSP3	Dual specificity phosphatase 3
B4DDD8	HARS	Histidine--tRNA ligase, cytoplasmic
P23368	ME2	NAD-dependent malic enzyme, mitochondrial
Q53F18		Homer 1 variant
O00232	PSMD12	26S proteasome non-ATPase regulatory subunit 12
Q6PCE3	PGM2L1	Glucose 1,6-bisphosphate synthase
A0A024RC42	CDH2	Cadherin 2, type 1, N-cadherin
Q9P1U1	ACTR3B	Actin-related protein 3B
A8YXX5	PIG60	Cell proliferation-inducing protein 60
O15075	DCLK1	Serine/threonine-protein kinase DCLK1
Q75L23	PSMC2	Uncharacterized protein PSMC2
A0A087WYR3	TPD52L2	Tumor protein D54
B0AZS5		Kinesin-like protein
Q17RE6	TXNRD2	TXNRD2 protein
A0A024R9C1	PABPC1	Polyadenylate-binding protein
F8W9T3	SNX4	Sorting nexin-4
A0A024R6G4	ALDH6A1	Aldehyde dehydrogenase 6 family, member A1, isoform CRA_b
P0CG29	GSTT2	Glutathione S-transferase theta-2
D3DWV9	hCG_2004980	Isocitrate dehydrogenase [NAD] subunit, mitochondrial
B4DSZ1		cDNA FLJ54877, highly similar to Syntaxin-12

A8K486		Peptidyl-prolyl cis-trans isomerase
A0A0A0MRK6	MTX1	Metaxin 1, isoform CRA_b
E3W994	CLASP2	CLIP-associating protein 2
P52306	RAP1GDS1	Rap1 GTPase-GDP dissociation stimulator 1
Q68D91	MBLAC2	Metallo-beta-lactamase domain-containing protein 2
B3KM80	NCL	Nucleolin, isoform CRA_c
A8K9B2		cDNA FLJ76725, highly similar to Homo sapiens L-2-hydroxyglutarate dehydrogenase
B4DPJ2		Annexin
Q7Z6L1	TECPR1	Tectonin beta-propeller repeat-containing protein 1
A0A024R904	CACYBP	Calcyclin binding protein, isoform CRA_a
A0A024R3D8	DLAT	Acetyltransferase component of pyruvate dehydrogenase complex
Q6ZMF1		cDNA FLJ23967 fis, clone HEP16652, highly similar to Golgi apparatus protein 1
Q4KMQ8	CTBP1	C-terminal binding protein 1
A0A0A0MQZ2	SYNGAP1	Ras/Rap GTPase-activating protein SynGAP
Q59F90		Brevican isoform 1 variant
A0A024R6N2	CDC42BPB	CDC42 binding protein kinase beta
A0A024QZ42	PDCD6	HCG1985580, isoform CRA_c
F1DSG4	AQP4	Aquaporin 4 transcript variant a
Q86YB0	GPM6A	Glycoprotein M6A
Q53TB0	PDE1A	Uncharacterized protein PDE1A
O95886	DLGAP3	Disks large-associated protein 3
B4DG51		cDNA FLJ61110, highly similar to Hippocalcin-like protein 4
A0A087WXI1		Deleted.
E7EV41	SLC8A1	Sodium/calcium exchanger 1
A0A087WW66	PSMD1	26S proteasome non-ATPase regulatory subunit 1
H0YB09	C14orf159	D-glutamate cyclase, mitochondrial
D3DU10	hCG_1810810	HCG1810810, isoform CRA_b
Q9UPR5	SLC8A2	Sodium/calcium exchanger 2
B4DL86		6-phosphogluconate dehydrogenase, decarboxylating
O75323	NIPSNAP2	Protein NipSnap homolog 2
Q8TF44	C2CD4C	C2 calcium-dependent domain-containing protein 4C
I3L397	EIF5A	Eukaryotic translation initiation factor 5A

F5GWE5	PITPNA	Phosphatidylinositol transfer protein alpha isoform
Q8IY17	PNPLA6	Neuropathy target esterase
E7EX90	DCTN1	Dynactin subunit 1
Q2VPA0	LONP1	Lon protease homolog
H0Y7A7	CALM2	Calmodulin-2
M0R366	FSD1	Fibronectin type III and SPRY domain-containing protein 1
G3V1V0	MYL6	Myosin light polypeptide 6
P27824	CANX	Calnexin
A2A2U1	SLC1A2	Amino acid transporter
Q8IXI2	RHOT1	Mitochondrial Rho GTPase 1
Q6IAL5	SUCLG1	Succinate--CoA ligase [ADP/GDP-forming] subunit alpha, mitochondrial
P45974	USP5	Ubiquitin carboxyl-terminal hydrolase 5
A8K4W5		cDNA FLJ76813, highly similar to Homo sapiens acetyl-Coenzyme A acetyltransferase 2
I3L0N3	NSF	Vesicle-fusing ATPase
A0A024R9U8	HUWE1	HECT, UBA and WWE domain containing 1, isoform CRA_c
Q6PK82	AP3D1	AP3D1 protein
V9HW80	HEL-S-70	Epididymis luminal protein 220
D3DUJ0	AFG3L2	AFG3 ATPase family gene 3-like 2
A0A024RBV7	GPM6B	Glycoprotein M6B, isoform CRA_b
B4DH16		cDNA FLJ54709, highly similar to Methylcrotonoyl-CoA carboxylase subunit alpha, mitochondrial
B3KNG8		cDNA FLJ14579 fis, clone NT2RM4001203, highly similar to Rab3 GTPase-activating protein non-catalytic subunit
Q8N4C8	MINK1	Misshapen-like kinase 1
Q96HU8	DIRAS2	GTP-binding protein Di-Ras2
B3KPZ2		cDNA FLJ32487 fis, clone SKNSH1000002, highly similar to Prostaglandin E synthase 2
A0A024RA75	HIBADH	3-hydroxyisobutyrate dehydrogenase
A0A024R3J8	FXYD6	FXYD domain containing ion transport regulator 6, isoform CRA_a
Q9Y4E6	WDR7	WD repeat-containing protein 7
E9KL44		Epididymis tissue sperm binding protein Li 14m
B4DM67		cDNA FLJ59343, highly similar to Exportin-2
A0A024R3W8	ADAM23	ADAM metallopeptidase domain 23, isoform CRA_a
Q8TB36	GDAP1	Ganglioside-induced differentiation-associated protein 1
Q13825	AUH	Methylglutaconyl-CoA hydratase, mitochondrial
H0YG16	KLC1	Kinesin light chain 1

Q59HE2		Ornithine aminotransferase variant
A0A090N7T7	CNTNAP2	Contactin associated protein-like 2
Q9UKU7	ACAD8	Isobutyryl-CoA dehydrogenase, mitochondrial
P29992	GNA11	Guanine nucleotide-binding protein subunit alpha-11
A0A087X0K9	TJP1	Tight junction protein ZO-1
A0A087WZN1	IDH3B	Isocitrate dehydrogenase [NAD] subunit, mitochondrial
Q92845	KIFAP3	Kinesin-associated protein 3
B2R7L2		Annexin
Q53XM7	VAPB	VAMP
D3DRG7	DPYSL4	Dihydropyrimidinase-like 4, isoform CRA_a
B7Z7U9		cDNA FLJ50917, highly similar to Propionyl-CoA carboxylase beta chain, mitochondrial
B4DRK5		cDNA FLJ59584, highly similar to Mitochondrial-processing peptidase alpha subunit, mitochondrial
A0A024R5R9	GNB5	Guanine nucleotide binding protein
A0A024RCA7	RPLP2	Ribosomal protein, large, P2, isoform CRA_a
A0A024R6W4	LIN10	Lin-10 homolog
A0A024R0M6	TIMM50	Translocase of inner mitochondrial membrane 50 homolog
Q8N987	NECAB1	N-terminal EF-hand calcium-binding protein 1
A0A024R9P6	FAM82C	Family with sequence similarity 82, member C, isoform CRA_a
A0A024R1T9	ACLY	ATP-citrate synthase
B4DJ30		cDNA FLJ61290, highly similar to Neutral alpha-glucosidase AB
A8K7A4		Methionine adenosyltransferase 2 subunit beta
F6X2W2		Deleted.
B7Z4Z4		cDNA FLJ51918, highly similar to Peroxisomal membrane protein PEX14
Q96ES0	KIAA1468	KIAA1468 protein
A0A024RE27	FAHD2A	Fumarylacetoacetate hydrolase domain containing 2A, isoform CRA_a
Q9NUJ1	ABHD10	Mycophenolic acid acyl-glucuronide esterase, mitochondrial
A0A087WWM6	PRODH	Proline dehydrogenase
B3KWK1	CPNE6	Copine VI
A0A024R9A4	DDX3Y	DEAD
F5GYF7	COPS7A	COP9 signalosome complex subunit 7a
Q59FT7		Mitogen-activated protein kinase kinase kinase 7 interacting protein 1 isoform alpha variant
O94819	KBTBD11	Kelch repeat and BTB domain-containing protein 11

V9HWF2	HEL-S-32	Malate dehydrogenase
O43761	SYNGR3	Synaptogyrin-3
A8K690		cDNA FLJ76863, highly similar to Homo sapiens stress-induced-phosphoprotein 1
A0A024R8Q0	Sep-09	Septin 9, isoform CRA_b
X5D299	ALDH5A1	Aldehyde dehydrogenase 5 family member A1 isoform A
A9UEZ4	BCR/ABL	BCR/ABL fusion protein isoform X1
A0A024R7P2	FKBP8	Peptidylprolyl isomerase
P24588	AKAP5	A-kinase anchor protein 5
B4DP80	APOA1BP	NAD
J3KPF3	SLC3A2	4F2 cell-surface antigen heavy chain
A0A024R452	EPHA4	EPH receptor A4, isoform CRA_a
Q4L233	FREP1	Brain-specific protein p25 alpha, isoform CRA_b
O95970	LGI1	Leucine-rich glioma-inactivated protein 1
B2R491	RPS4X	40S ribosomal protein S4
O43617	TRAPPC3	Trafficking protein particle complex subunit 3
A0A024RDQ0	HSPH1	Heat shock 105kDa/110kDa protein 1, isoform CRA_a
Q9NQ79	CRTAC1	Cartilage acidic protein 1
O15083	ERC2	ERC protein 2
A0A024QZK8	HNRPH3	Heterogeneous nuclear ribonucleoprotein H3
B4DNB9		cDNA FLJ53069, highly similar to AP-2 complex subunit mu-1
F5GXJ9	ALCAM	CD166 antigen
A2A3R5	RPS6	40S ribosomal protein S6
A0A024R048	FLJ30596	NAD kinase 2, mitochondrial
Q7L0J3	SV2A	Synaptic vesicle glycoprotein 2A
A0A024R5V2	DMXL2	Dmx-like 2, isoform CRA_c
P16615	ATP2A2	Sarcoplasmic/endoplasmic reticulum calcium ATPase 2
B8XPJ7	COMT	Soluble catechol-O-methyltransferase
P54577	YARS	Tyrosine--tRNA ligase, cytoplasmic
J3QRY4	PSMD11	26S proteasome non-ATPase regulatory subunit 11
I3L3U6	P4HB	Protein disulfide-isomerase
P59768	GNG2	Guanine nucleotide-binding protein G
A0A024RB41	hCG_2016482	HCG2016482, isoform CRA_b

Appendix 3: Analysis scripts and macros used for array tomography in Chapter 5

Image J Macros

Jackson, Rosemary. (2017). An Investigation of Synaptic Dysfunction in Alzheimer's Disease - Chapter 5 - Thresholding Macros, [dataset]. University of Edinburgh, Deanery of Biomedical Sciences. **http://dx.doi.org/10.7488/ds/2135.**

Matlab Scripts

Jackson, Rosemary. (2017). An Investigation of Synaptic Dysfunction in Alzheimer's Disease - Chapter 5 - Matlab Scripts, [dataset]. University of Edinburgh, Deanery of Biomedical Sciences. **http://dx.doi.org/10.7488/ds/2136.**

Appendix 4: Analysis scripts and macros used for synapse quantification in Chapter 6

Image J Macros

Jackson, Rosemary. (2017). An Investigation of Synaptic Dysfunction in Alzheimer's Disease - Chapter 6 - Image J Macros, [dataset]. University of Edinburgh, Deanery of Biomedical Sciences. **http://dx.doi.org/10.7488/ds/2131.**

Cell Profiler Pipeline

Jackson, Rosemary. (2017). An Investigation of Synaptic Dysfunction in Alzheimer's Disease - Chapter 6 - Cell Profiler Pipeline, [dataset]. University of Edinburgh, Deanery of Biomedical Sciences**. http://dx.doi.org/10.7488/ds/2132.**

Appendix 5: Publications

Jackson RJ, Herrmann AG, Llavero M, Burr K, Johnson M, Henstridge CM, Lamont DJ, Wishart TM, Chandran S, Spires-Jones TL. Changes in the synaptic proteome in Alzheimer's disease indicate a role for Clusterin and ApoE4 in synapse degeneration. (In Prep)

Hesse R, von Einem B, Wagner F, Schwanzar D, **Jackson RJ**, Föhr K, Lausser L, Kroker KS, Proepper C, Walther P, Kestler HA, Spires-Jones TL, Boeckers T, Rosenbrock H, von Arnim CAF. sAPPβ and sAPPα increase structural complexity and synapse morphology in primary hippocampal neurons by altering Ca2+ homeostasis and CREB1-signaling (2017) Neurobiology of Disease (manuscript submitted)

Wang Z, **Jackson RJ**, Hong W, Taylor W, Moreno A, Liu W, Li S, Frosch M, Young-Pearse T, Slutsky I, Spires-Jones T, Walsh D. Human brain-derived Aβ oligomers bind to synapses and disrupt synaptic activity in a manner that requires APP (2017) Journal of Neuroscience (2017) Dec 6;37(49):11947-11966. doi: 10.1523/JNEUROSCI.2009-17.2017

Ritchie DL, Adlard P, Peden AH, Lowrie S, Le Grice M, Burns K, **Jackson RJ**, Yull H, Keogh MJ, Wei W, Chinnery PF, Head MW, Ironside JW. Amyloid-β accumulation in the CNS in human growth hormone recipients in the UK (2017) *Acta. Neuropathol*;134(2):221-240. doi: 10.1007/s00401-017-1703-0.

Zhou L, McInnes J, Wierda K, Holt M, Herrmann AG, **Jackson RJ**, Wang YC, Swerts J, Beyens J, Miskiewicz K, Vilain S, Dewachter I, Moechars D, De Strooper B, Spires-Jones TL, De Wit J, Verstreken P. Tau association with synaptic vesicles causes presynaptic dysfunction (2017) *Nat. Commun.* 11;8:15295 doi: 10.1038/ncomms15295.

Jackson RJ, Rudinskiy N, Herrmann AG, Croft S, Kim JM, Petrova V, Ramos-Rodriguez JJ, Pitstick R, Wegmann S, Garcia-Alloza M, Carlson GA, Hyman BT, Spires-Jones TL. Human tau increases amyloid β plaque size but not amyloid β-mediated synapse loss in a novel mouse model of Alzheimer's disease. (2016) *Eur J Neurosc.* 44(12):3056-3066 doi: 10.1111/ejn.13442

Henstridge CM, **Jackson RJ**, Kim JM, Herrmann AG, Wright AK, Harris SE, Bastin ME, Starr JM, Wardlaw J, Gillingwater, Smith C, McKenzie CA, Cox SR, Deary IJ, Spires-Jones TL. Post-mortem brain analyses of the Lothian Birth Cohort 1936: extending lifetime cognitive and brain phenotyping to the level of the synapse. (2015) *Acta Neuropathol Commun*. **4(**3)53. doi: 10.1186/s40478-015-0232-0.

Walden M, Edwards JM, Dziewulska AM, Bergmann R, Saalbach G, Kan SY, Miller OK, Weckener M, **Jackson RJ**, Shirran SL, Botting CH, Florence GJ, Rohde M, Banfield MJ, Schwarz-Linek U. An internal thioester in a pathogen surface protein mediates covalent host binding. (2015) *Elife* doi: 10.7554/eLife.06638.